Contract No:

This document was prepared in conjunction with work accomplished under Contract No. DE-AC09-08SR22470 with the U.S. Department of Energy (DOE) Office of Environmental Management (EM).

Disclaimer:

WSRC-TR-2002-00128

Characteristics of the Melt-Dilute Form of Aluminum-Based Spent Nuclear Fuel

Savannah River Technology Center
Strategic Materials Technology Department
Materials Technology Section

Publication Date: March 2002

Westinghouse Savannah River Company
Savannah River Site
Aiken, SC 29808

This document was prepared in connection with work done under Contract No. DE-AC09-96SR18500 with the U. S. Department of Energy

DISCLAIMER

DOCUMENT: WSRC-TR-2002-00128

TITLE: Characteristics of the Melt-Dilute Form of Aluminum-Based Spent Nuclear Fuel

TASK: Qualification TTP SRTC-MTS-2001-2035, Revision 1

APPROVALS

Date: _____

D. W. Vinson, Author
Materials Applications & Process Technology
SRTC-MATERIALS TECHNOLOGY SECTION

Date: _____

T. M. Adams, Author
Materials Applications & Process Technology
SRTC-MATERIALS TECHNOLOGY SECTION

Date: _____

A. J. Duncan, Author
Materials Applications & Process Technology
SRTC-MATERIALS TECHNOLOGY SECTION

Date: _____

S. Y. Lee, Author
Engineering Modeling and Simulation
SRTC-ENGINEERING DEVELOPMENT SECTION

Date: _____

A. W. Serkiz, Technical Editor
SCUREF-MATERIALS TECHNOLOGY SECTION

Date: _____

H. B. Peacock, Jr., Technical Review
Materials Applications & Process Technology
SRTC-MATERIALS TECHNOLOGY SECTION

Date: _____

W. F. Swift, Technical Review
NMMD-NUCLEAR MATERIALS TRANSPORT SECTION

Date: _____

R. L. Sindelar, Manager
Materials Applications & Process Technology
SRTC-MATERIALS TECHNOLOGY SECTION

Date: _____

N. C. Iyer, Manager
SRTC-MATERIALS TECHNOLOGY SECTION

Date: _____

H. M. Brooks, Customer
Strategic Planning and Integration
NMMD-MGR. INTEGRATION SECTION

Table of Contents

List of Figures

List of Tables

Table of Acronyms

ANL	Argonne National Laboratory
AMR	Analysis/Model Report
AP	Administrative procedure
ASM	American Society for Metals
ASME	American Society of Mechanical Engineers
ASTM	American Society for Testing and Materials
ATP	Alternate Treatment Program
BPVC	Boiler and Pressure Vessel Code
BSC	Bechtel SAIC Company, LLC
CFD	Computational Fluid Mechanics
CFR	Code of Federal Regulations
CRWMS	Civilian Radioactive Waste Management System
DHLW	Defense High-level Radioactive Waste
DOE	U.S. Department of Energy
DOT	U.S. Deapartment of Transportation
DRR	Domestic Research Reactor
DWPF	Defense Waste Processing Facility
EBR	Experimental Breeder Reactor
EDM	Electronic Discharge Machine
EDS	Energy Dispersive Spectroscopy
EIS	Environmental Impact Statement
EPA	Environmental Protection Agency
ERR	Elk River Reactor
FCC	Face centered cubic
FEP	Features, events, and processes
FM	Fissionable material
FRR	Foreign Research Reactor
Gr	Grashof Number (dimensionless)
HEU	Highly-enriched uranim
HFBR	High Flux Beam Reactor
HWCTR	Heavy Water Components Test Reactor
ICPES	Inductively Coupled Plasma Electron Spectroscopy
ID	Inner Diameter
IP	Intrusion Process
J-13	Designated composition of well water
K	Thermal conductivity (W/m-K)
k_{eff}	Effective neutron multiplication factor
kW	Kilowatts thermal

LA	License Application
LEU	Low-enriched uranium
M&O	Management and Operating Contractor
MCNP	Monte Carlo particle transport code
MD	Melt Dilute
MD-SNF	Melt-Dilute Spent Nuclear Fuel
MEU	Medium-enriched uranium
MGR	Monitored Geologic Repository
MTR	Materials Test Reactor
NG	Nuclear grade
NRC	U.S. Nuclear Regulatory Commission
OCRWM	Office of Civilian Radioactive Management
OIC	Other internal components
OD	Outer diameter
PA	Performance Assessment
PNNL	Pacific Northwest National Laboratory
QARD	Quality Assurance Requirements and Description
Re	Reynolds Number (dimensionless)
RW	Radioactive Waste
SDD	System Description Document
SEM	Scanning Electron Microscopy
SNF	Spent nuclear fuel
SRS	Savannah River Site
SS	Stainless steel
TSPA	Total System Performance Assement
UNS	Unified Numbering System
Vol%	Volume %
WASRD	Waste Acceptance System Requirement Document
WF	Waste Form
WP	Waste package
wt%	Weight %
YMP	Yucca Mountain Project

ES.1.0 EXECUTIVE SUMMARY

Melt-dilute treatment technology for aluminum-based spent nuclear fuel (Al-SNF) is being developed at Savannah River Site (SRS) for ultimate disposal of these fuels in the Monitored Geologic Repository (MGR).[1] This alternative for disposition has been selected as the preferred alternative and the U. S. DOE has issued a Record of Decision following the Environmental Impact Statement process.[2] [i] The proposed codisposal repository waste package will be designed to codispose a centrally positioned canister containing the melt-dilute SNF form surrounded by several borosilicate glass logs of defense high-level waste (DHLW). Figure ES.1 illustrates the envisioned emplacement of several waste packages in the geologic repository.

This report documents the information base for the melt-dilute SNF form needed for submittal of a license application for the repository to the U.S. Nuclear Regulatory Commission (NRC). The National Spent Fuel Program will use the information in this report to compile the information base for all DOE-SNF and transmit to the DOE Office of Civilian Radioactive Waste Management (DOE-OCRWM or DOE-RW). The DOE-RW is the agency that will actually submit the license application.

The information in this report is assembled from results of testing and analysis completed to-date that followed the quality assurance program controls established for the repository.[3] At this time the final design specifications for the codisposal waste package (WP) and for the melt-dilute SNF form have not been established. Thus the findings reported would have to be updated and be validated prior to submission of a license application (LA) or during the actual licensing period.

This report describes: the present envisioned codisposal waste package, the melt-dilute SNF form metallurgical composition, WP criticality evaluations which address interim criticality limits, decay heat estimates, thermal analyses of the WP placed in the expected repository conditions, and codisposal WP shielding analyses.

The technical information in this report, and referenced reports, can be applied to show that the proposed disposal configuration of the melt-dilute for aluminum-based SNF can meet the current requirements for the MGR, based on the waste disposal system in the *Waste Acceptance System Requirements Document* (WASRD). The road-ready packages must also meet U.S. Department of Transportation (DOT) and NRC regulations that govern shipment of nuclear materials as provided in 10 CFR 71. Modeling of the long-term behavior of the Al-SNF forms is part of a performance assessment (PA) of the repository conducted by OCRWM to ensure compliance with 10 CFR 63 and EPA dose and ground water standards. Shipment and PA requirements have been incorporated into the disposal system requirements and are not discussed directly in this report.

The proposed codisposal waste package design for the melt-dilute SNF form is summarized in Section 2.0. Key information and compliance with major disposal system requirements are summarized below.

---

[i] As of December 2001, the program to develop and implement the melt-dilute treatment technology was suspended as directed by DOE-SR. The U. S. DOE Office of Environmental Management is revisiting the disposition alternatives. For the purpose of this report, the melt-dilute treatment of aluminum-based spent nuclear fuel for repository disposal is assumed

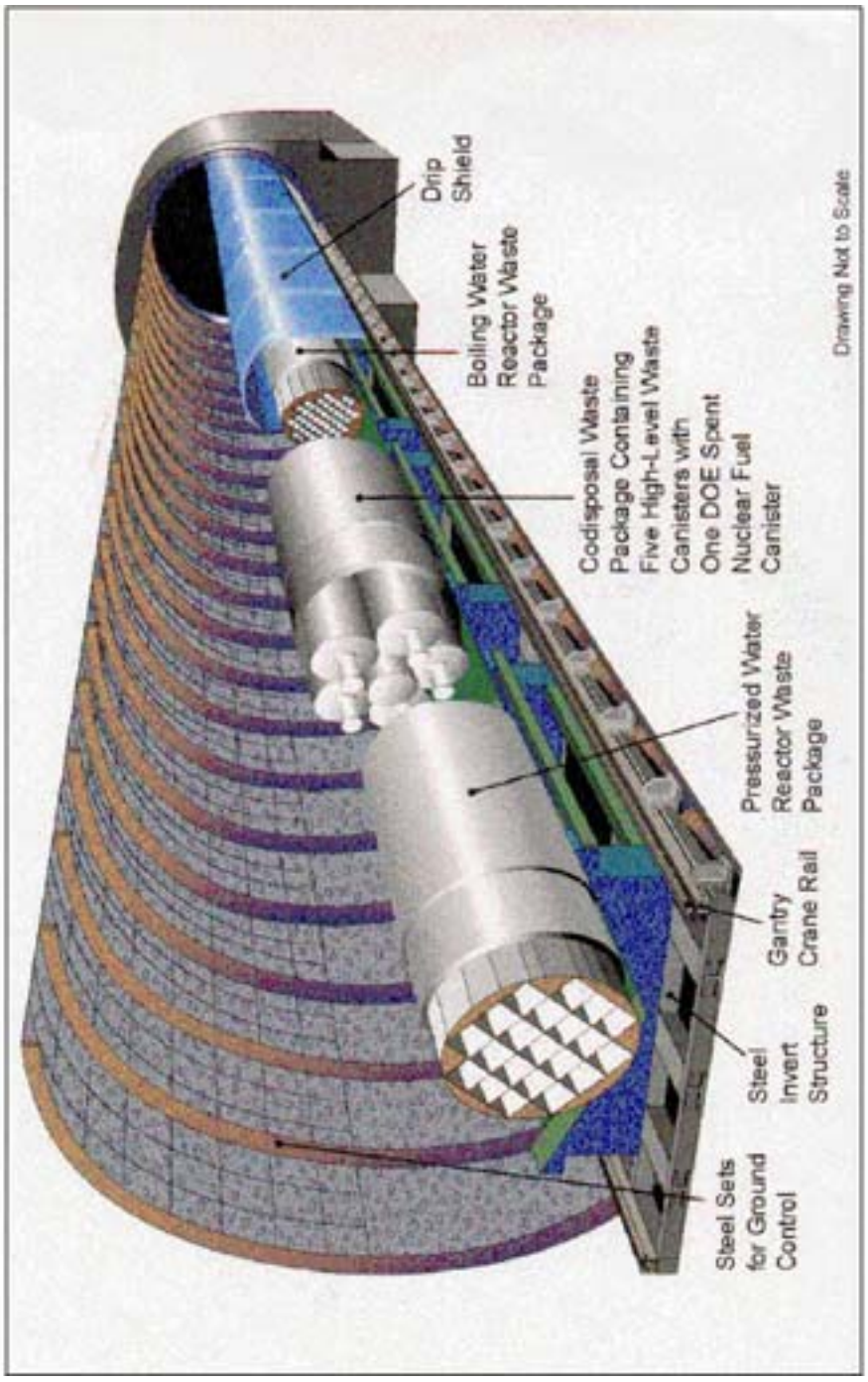

Figure ES.1 Schematic Illustration of the Emplacement Drift, with Cutaway Views of Different Waste Packages

ES.1.1 Material Characterization of Melt-Dilute Form of Al-Based SNF

ES.1.1.1 Physical Characteristics

The melt-dilute SNF form consists of a casting from melting Al-SNF assemblies that results in an alloy containing an aluminum matrix with UAl_x phases diluted with depleted uranium to reduce enrichment to below 20% ^{235}U.

ES.1.1.2 Metallurgical Characteristics

The overall composition of these ingots is based on the nominal eutectic composition of Al-13.2 weight percent U. The uranium is nearly all contained in a UAl_4 phase. Minor amounts of neutron-absorbing materials such as gadolinium and/or hafnium are also added for criticality control in amounts up to a total of 3 weight percent. Gadolinium additions tend to concentrate in the UAl_4 phase. Hafnium additions tend to concentrate with aluminum in a $(U, Hf)Al_3$ phase with or without trace quantities of gadolinium. Thus, the gadolinium is expected to stay closely associated with fissile uranium in the UAl_4 phase as the MD-SNF form degrades, providing an additional barrier against the solubility facilitated removal of gadolinium from a degraded waste package.

ES.1.2 Codisposal Waste Package Criticality Analysis

A criticality analysis was performed using the NRC-approved methodology in Reference 4. The worst-case bias, calculated from MCNP simulations of experiments described in Reference 5 includes a bias in the method of calculation and the uncertainty in the experiments. The interim critical limit of 0.93, as specified in the *Waste Acceptance Systems Requirements Document*, was applied to the WP criticality calculations reported in Section 1.0.

Three-dimensional Monte Carlo criticality calculations, for all anticipated intact- and degraded-mode configurations using DOE specified degradation scenarios, show that the requirement of $k_{eff}+2\sigma$ values less than or equal to the interim critical limit of 0.93 is satisfied for the MD codisposal package if at least 7.5% of the original Gd loading (394.2 g) remains mixed with the fissile material. In the alternate MD ingot composition, Hf remains in the DOE SNF canister or waste package under all degraded conditions, thereby preventing a critical condition even if all Gd is removed from the degraded system.

Conversely, the distribution of hafnium makes its release from the waste package more heterogeneous than Gd and may make the hafnium more susceptible to release from the MD-SNF form by corrosion. However, the relative insolubility of hafnium (as compared to Gd, U and Al) should prevent it from being removed from the waste package prematurely.

ES.1.3 Corrosion/Dissolution of Melt-Dilute SNF Form

Dissolution rates of radionuclides from both irradiated Al-SNF and unirradiated UAl alloys were measured under repository-relevant conditions. The irradiated fuels had dissolution rates at 25 °C that ranged from approximately 0.2 $mgU/m^2/day$ ($mgU/m^2/d$) for all the fuels in nominal J-13 to 30-100 $mgU/m^2/d$ in a nitric acid solution. Dissolution rates for radionuclides such as Cs, Sr, and Pu were approximately the same as the U dissolution rate over the duration of the test. The unirradiated alloys had dissolution rates ranging from 0.2 $mgU/m^2/d$ in nominal J-13 at 25 °C to 200-400 $mgU/m^2/d$ in low pH J-13 at 90 °C.

ES.1.4 Decay Heat Estimates

The development of the source term for decay heat of aluminum-based research reactor spent fuel assemblies per single assembly and the melt-dilute form per DOE canister, is described in Section 6.0. Bounding and nominal design source term values for use in thermal analyses of waste packages are developed.

The WASRD[6] specifies that thermal heat loads shall not exceed 1,970 watts for the DOE SNF and 2,540 watts for the DHLW packaged within the codisposal waste package at time of acceptance into the CRWMS. These decay heat calculations estimate that a DOE canister containing the melt-dilute form will have a heat load of less than 3,500 thermal watts.

ES.1.5 Codisposal Waste Package Thermal Analysis

The engineering viability of disposal of spent nuclear fuel in a geologic repository requires a thermal analysis to provide the expected temperature history of the fuel waste forms within the disposal package. Calculated temperatures are used to demonstrate compliance with criteria for waste acceptance into the Monitored Ground Repository (MGR) and also to assess the chemical and physical behavior of the waste form within the codisposal Waste Package (WP).

A thermal analysis of the codisposal WP was performed to estimate temperature conditions when such a package was positioned in an emplacement drift tunnel. A peak temperature criterion of 350 °C specified in the latest revision of the WASRD is applied to the MD-SNF form.

The analyses show that a helium-filled codisposal WP containing one Al-SNF canister and five Defense High-Level Waste (DHLW) glass logs having a 16 years cooling time, can satisfy a thermal design criteria for MD/SNF peak temperature criterion, $T_{max} \leq 350$ °C, under the reference boundary conditions. In addition, these analyses show that average temperature of the WP decays close to geologic ambient temperature at about 2000 years of storage time after emplacement in a repository drift tunnel. These analyses are summarized in Section 7.0.

ES.1.6 Waste Package Shielding Analysis

The Disposal Container Handling System, the Waste Emplacement/Retrieval System, and the Performance Confirmation Emplacement Drift Monitoring System acceptance criterion requires that the dose rate at all external surfaces of a disposal waste package to be 1,450 rem/h or less.

Shielding calculations for the proposed codisposal waste package (reported in Section 8.0) estimate a maximum surface level dose level of less than 200 rem/h which is considerably less than 1,450 rem/h. In addition this value is well below a 10^4 rad/h value which has been shown to represent the onset of corrosion of materials used in the fabrication of waste packages when subjected to environments expected at the Yucca Mountain site.[7]

ES.1.7 References

[1] Adams, T. M., ***"Technology Development Program Plan,"*** WSRC-TR-2000-00237 (July 2000).

[2] **Savannah River Site Spent Nuclear Fuel Management Final Environmental Impact Statement**. USDOE-Savannah River Operations Office, DOE/EIS-0279 (2000).

[3] ***"Quality Assurance Requirements and Description (QARD),"*** DOE/RW-0333P, Revision 10 (April 27, 2000).

[4] ***"Disposal Criticality Analysis Methodology Topical Report,"*** YMP/TR-004Q, Rev. 01. Las Vegas, Nevada: Yucca Mountain Site Characterization Office. ACC: MOL.20001214.0001 (2000).

[5] ***"Evaluation of Codisposal Viability for Melt and Dilute DOE-Owned Fuel,"*** Bechtel SAIC Report TDR-EDC-NU-000006, Rev. 0 (July 2001).

[6] ***"Waste Acceptance Systems Requirements Document,"*** Revision 04G (March 2001).

[7] Shoesmith, D.W. and King, F., ***"The Effects of Gamma Radiation on the Corrosion of Candidate Materials for the Fabrication of Nuclear Waste Package,"*** AECL-11999. Pinawa, Manitoba, Canada: Atomic Energy of Canada Limited. ACC: MOL.19990311.0212.Shoesmith (1998).

This Page Intentionally Left Blank

1.0 INTRODUCTION

The United States Department of Energy (DOE) has selected the Savannah River Site (SRS) as the location to consolidate aluminum-clad, aluminum-based spent nuclear fuel (Al-SNF) from foreign and domestic research reactors (FRR and DRR, respectively) through the Environmental Impact Statement (EIS) process.[1-3] These SNF elements are either in service, being stored in water basins or in dry storage casks at other reactor sites, or have been transferred to SRS and are presently being stored in water basins.

Approximately 20 metric tons heavy metal of aluminum-based spent nuclear fuel, or approximately 18,000 assemblies, is being consolidated at the Savannah River Site. A significant portion of this Al-SNF contains highly enriched uranium. Appendix A identifies the inventory of the FRR/DRR Al-SNF that is presently at or is expected to be received at the Savannah River Site.

The goal of the SRS Aluminum Spent Nuclear Fuel Alternate Treatment Technology Program (ATP) is to develop and implement technology for the non-reprocessing alternatives which entails treatment and storage of the Al-SNF in a road-ready package that meets the requirements for disposal in the Monitored Geologic Repository (MGR). The melt-dilute treatment alternative was selected as the preferred alternative through the Environmental Impact Statement process[4] and approved by the DOE record of Decision.[5] Receipt, treatment, storage, and packaging of the Al-SNF are expected to continue over the next four decades and extend beyond the shutdown of the reprocessing facilities at SRS.

Development and licensing of the facilities of the MGR or the federal repository for ultimate disposal of commercial SNF, defense high level waste (DHLW), and DOE-owned SNF is the responsibility of the Office of Civilian Radioactive Waste Management (OCRWM) of DOE. The present schedule calls for a licensing application for the disposal of these SNF forms in the proposed repository at Yucca Mountain to be submitted during 2004. The purpose of this report is to compile an information base for the melt-dilute SNF form for Al-SNF that is needed to prepare the license application.

The subsequent sections of this report describe: the proposed designs for a disposable canister and the waste package, the melt-dilute Al-SNF formulations being considered, and the acceptability of the DOE-owned SNF for interim dry storage at SRS. The road-ready packages must also meet DOT and NRC regulations that govern shipment of nuclear materials as provided in 10 CFR 71. Modeling of the long-term behavior of the Al-SNF forms is part of a performance assessment (PA) of the repository conducted by OCRWM to ensure compliance with EPA dose and groundwater standards as directed in 10 CFR 63. Shipping and PA requirements are not discussed directly in this report.

The purpose of this report is to document findings of research and development activities and analysis that will form the scientific bases necessary to ensure qualification of an appropriate Al-SNF form for the repository and submittal of a license application to the U.S. Nuclear Regulatory Commission. This report describes the codisposal waste package (WP), the melt-dilute metallurgy, WP criticality evaluations, decay heat estimates of the proposed SNF, repository relevant thermal analyses, codisposal WP shielding analyses

.

1.1 References

[1] **Final Environmental Impact Statement, Interim Management of Nuclear Materials.** DOE (U.S. Department of Energy), DOE/EIS-0220, Savannah River Operations Office, Aiken, South Carolina (1995).

[2] **Final Environmental Impact Statement, Proposed Nuclear Weapons Non-Proliferation Policy Concerning Foreign Research Reactor Spent Nuclear Fuel.** DOE (U.S. Department of Energy), DOE/EIS-0218F, Assistant Secretary for Environmental Management, Washington, DC (1995).

[3] **DOE-Owned Spent Nuclear Fuel Technology Integration Plan.** DOE/SNF/PP-002, Rev. 1, Idaho National Engineering Laboratory (May 1996).

[4] **Savannah River Site Spent Nuclear Fuel Management Final Environmental Impact Statement.** USDOE-Savannah River Operations Office, DOE/EIS-0279 (2000).

[5] **Record of Decision for the Savannah River Site Spent Nuclear Fuel Management Final Environmental Impact Statement.** USDOE-Savannah River Operations Office, 61 FR 69085 (August 7, 2000).

2.0 CODISPOSAL WASTE PACKAGE DESCRIPTION AND DESIGN ASSUMPTIONS

The following subsections describe the proposed codisposal waste package design for the DOE SNF that contains the melt-dilute SNF form. The configuration, materials, and dimensions are those that were used in the criticality evaluation in Section 1.0. The thermal analysis used the same inputs except that the waste package internal structure (basket and support tube) were ignored.

2.1 Codisposal Waste Package Overview

The codisposal waste package for melt-dilute ingots contains five DHLW glass canisters and one DOE SNF canister loaded with three to six melt-dilute ingots. The 5-DHLW/DOE SNF-short waste package design is based on the Site Recommendation design.[1] The shell materials of the waste package are typical of those used for commercial SNF waste packages. The waste package design consists of two concentric cylindrical shells. The inner shell is a 50-mm-thick cylinder of stainless steel 316 NG (nuclear grade). The outer shell is composed of 25 mm of high-nickel alloy ASTM B 575 (Alloy 22). The outside diameter of the waste package is 2,030 mm and the length of the inside cavity is 3,040 mm which is designed to accommodate five Savannah River Site (SRS) 3-m-long DHLW glass canisters as shown in Figure 2.1. Figure 2.2 provides structural details for the codisposal WP shown in Figure 2.1. The lid of the inner shell is 80-mm thick. The outer shell flat bottom lid is 25-mm thick and the outer shell flat closure lid is 10-mm thick. Table 2.1 summarizes the dimensions and materials of the waste package.

The DOE SNF canister is placed into a 31.75-mm-thick carbon steel (ASTM A 516 Grade 70) support tube with a nominal outer diameter of 565 mm. The support tube is connected to the inside wall of the waste package by a web-like structure of carbon steel (ASTM A 516 Grade 70) basket plates to support five long DHLW glass canisters, as shown in Figure 2.1. The support tube and the plates are 3,030-mm long.

Table 2.1 Codisposal Waste Package Dimensions and Material Specifications

Component	Material	Parameter	Dimension (mm)
Outer barrier shell	ASTM B 575 (Alloy 22)	Thickness	25
		Outer diameter	2,030
Inner barrier shell	SS 316 NG	Thickness	50
		Inner length	3,040
Top and bottom outer barrier lids	ASTM B 575 (Alloy 22)	Thickness	25
Closure lid (only at the top)	ASTM B 575 (Alloy 22)	Thickness	10
Top and bottom inner barrier lids	SS 316 NG	Thickness	80
Gap between the top inner and closure lids	Air	Thickness	30
Gap between the top outer and closure lids	Air	Thickness	30
Gap between the bottom inner and outer lids	Air	Thickness	70
Support tube	ASTM A 516 Grade 70	Outer diameter	565
		Inner diameter	501.5
		Length	3,030

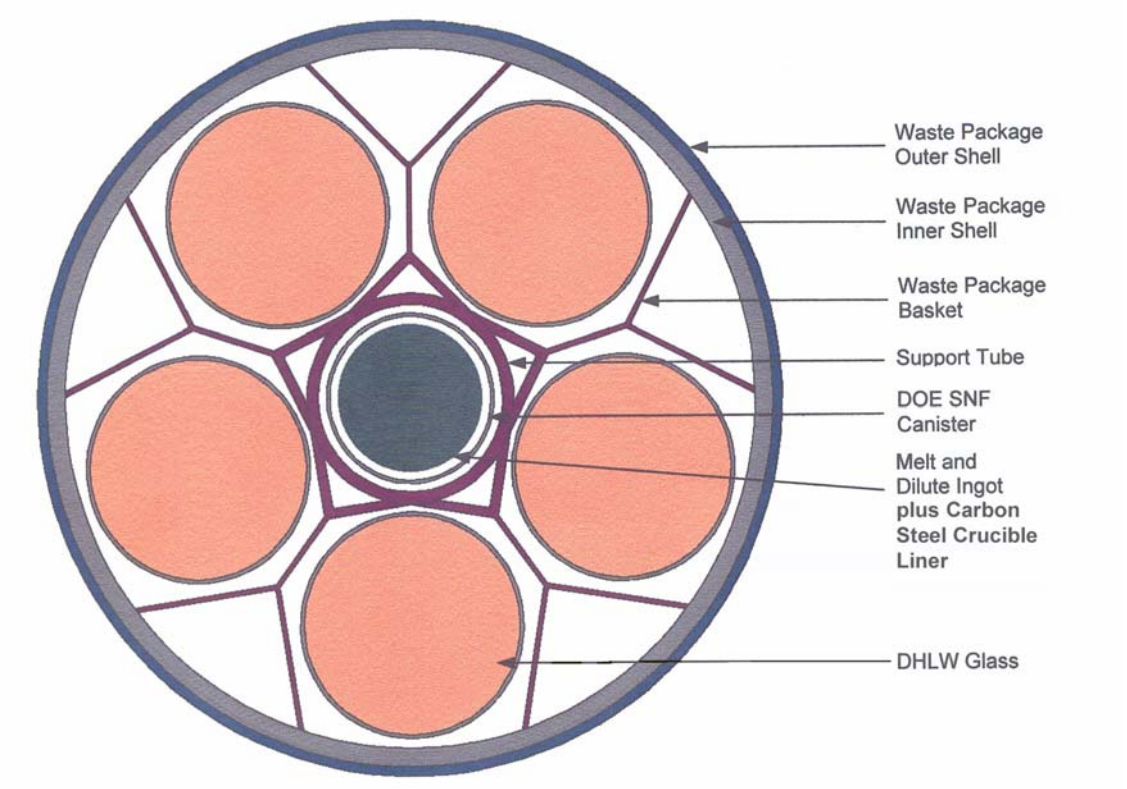

Figure 2.1 Cross-section View of the "As-Loaded" 5-DHLW/DOE Waste Package Containing Melt-Dilute Ingots

2.2 High-Level Waste Glass Pour Canisters

The SRS Defense Waste Processing Facility (DWPF) high-level waste canister, as shown in Figure 2.3, is a cylindrical stainless steel (SS) (Type 304L) shell. The outer diameter of the cylindrical stainless steel shell is approximately 610-mm, it has a wall thickness of 9.525-mm and a nominal length of 3,000 mm.[1] The flanged head and neck of the canister is 225.6-mm high. DHLW glass occupies approximately 85% of the volume of the canister. The glass weight is 1,682 kg and the approximate total loaded weight of the canister is 2,182 kg.[2] The nominal dimensions of the canister are used for the analyses. The maximum heat generation from a single canister is 752 W at the time of loading.[1] The geometry and material specifications for DHLW glass canisters are given in Table 2.2.

Table 2.2 Geometry and Material Specifications for DHLW Glass Canisters[1]

Component	Material	Parameter	Value
SRS 3-m Canister	SS 304L	Outer diameter	610 mm
		Total weight of canister and glass	2,182 kg
		Fill volume of glass in canister	85%
		Wall thickness	9.525 mm
		Length	3,000 mm

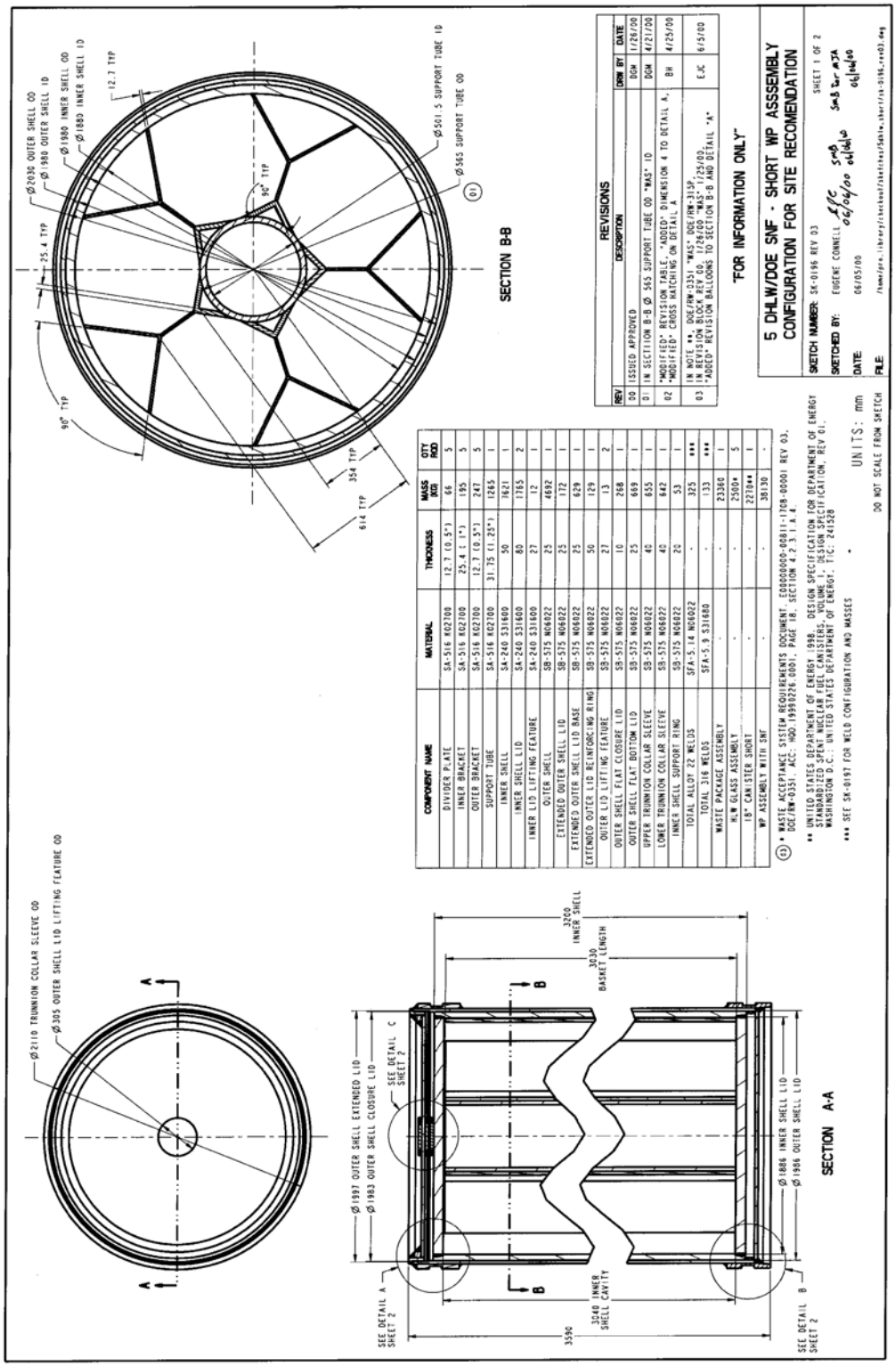

Figure 2.2 5 DHLW/DOE SNF Short WP Assembly Configuration for Site Recommendation

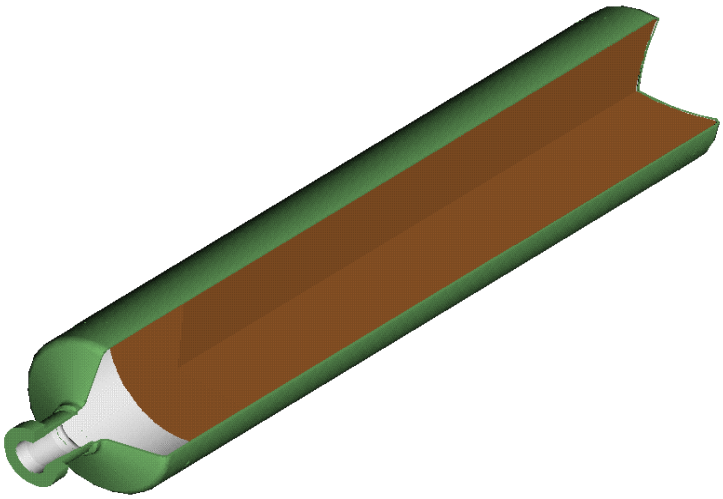

Figure 2.3 High-Level Waste Glass Pour Canister

2.3 DOE Standardized SNF Canister

The conceptual design for the standardized 18-in.-OD DOE SNF canister is taken from Reference 1. The canister is a right circular cylinder of stainless steel (Type 316L) with an outer diameter of 457 mm and a wall thickness 9.525 mm. The minimum internal length of the canister is 2,540 mm and the nominal overall length is 2,999 mm. In order to maximize the MD ingot volume, an internal length of 2,575 mm is used, consistent with previous calculations. There is a curved carbon-steel impact plate, 50-mm thick, at the top and bottom boundaries of the canister. The maximum loaded weight of the canister is 2,270 kg.[1] A drawing of the canister is shown in Figure 2.4 The DOE standardized SNF canister will contain three to six MD ingots, depending on the dimensions of the individual ingots as described in Section 2.4.

2.4 Melt-Dilute SNF Ingots

The MD ingots are homogeneous monolithic cylinders composed primarily of a U-Al alloy. These ingots will range in height from 381.0 to 762.0 mm (15 to 30 in.) and will be contained in a plain carbon steel crucible liner (e.g. Grade A516). This liner will be standardized at approximately to 508.0 to 762.0 mm (20 to 30 in) in height. The crucible liner will have a maximum OD of 393.7 to 419.1 mm (15.5-16.5 in) and a thickness of up to 12.5 mm (0.5 in).

The OD and thickness of the crucible liner assumed in a given configuration will provide the OD of the MD ingot. The mass of a MD ingot will be limited by the dimensions of the crucible liner and will vary to accommodate different size Al-SNF assemblies. The density of the melt-dilute ingot will be approximately 2.7-3.0 g/cm^3, and the ingot will have a porosity of between 5 and 10%. The ingot composition is 13.2±5 wt% uranium, enriched at less than 20 wt% ^{235}U and 0.5 wt% gadolinium metal, with the balance of the ingot being aluminum. Silicate and oxide Al-based SNF forms will result in the presence of 2 wt% Si and 3 wt% Ca in the MD-SNF form, respectively. Figure 2.4 illustrates a “surrogate” ingot fabricated to demonstrate the melt-dilute process. Figure 2.5 presents a plan view of the 18-in OD standardized SNF canister.

Figure 2.4 Surrogate MD-SNF Ingot Produced in an Induction Furnace without Carbon Steel Liner

2.5 Material Compositions

The chemical compositions of the materials of WP construction and that of DHLW glass are provided in the following Tables 2.3 through 2.7. The isotopic content of fission and activation products of the melt-dilute SNF form is provided in Table A.8 of Appendix A.

Table 2.3 Chemical Composition of ASTM B 575 (Alloy 22) (Universal Numbering System [UNS] N06022) for Waste Package[3]

Element	Composition (wt%)	Value Used (wt%)
Carbon (C)	0.015 (max)	0.015
Manganese (Mn)	0.50 (max)	0.50
Silicon (Si)	0.08 (max)	0.08
Chromium (Cr)	20.0 - 22.5	21.25
Molybdenum (Mo)	12.5 - 14.5	13.5
Cobalt (Co)	2.50 (max)	2.50
Tungsten (W)	2.5 - 3.5	3.00
Vanadium (V)	0.35 (max)	0.35
Iron (Fe)	2.0 - 6.0	4.00
Phosphorus (P)	0.02 (max)	0.02
Sulfur (S)	0.02 (max)	0.02
Nickel (Ni)	Balance	54.765
Density = 8.69 g/cm^3		

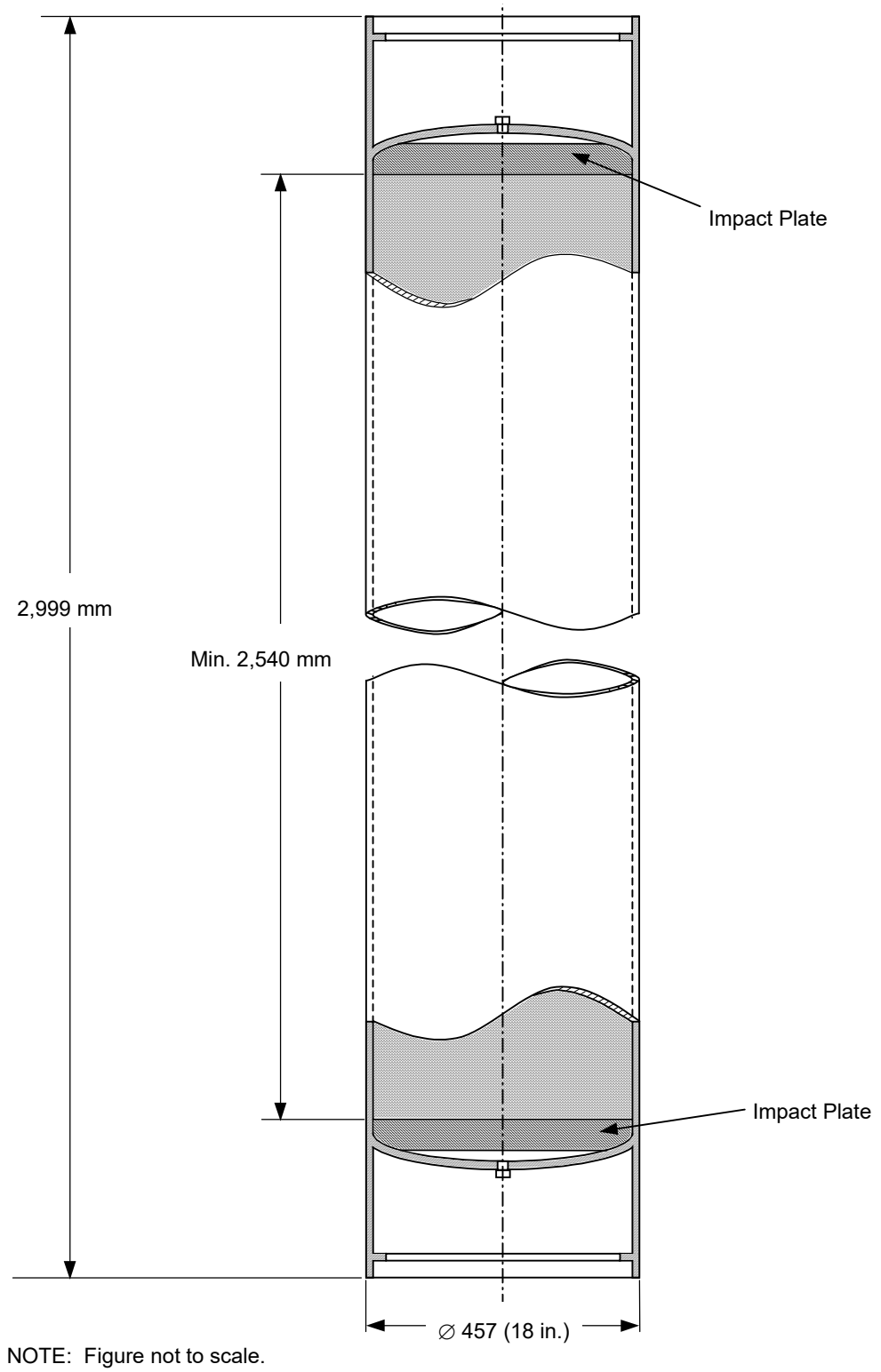

Figure 2.5 Plan View of the 18-in OD Standardized SNF Canister[2]

Table 2.4 Chemical Composition of ASTM A 516 Grade 70 Carbon Steel (UNS K02700) for Crucible Liner[4-5]

Element	Composition[4] (wt%)	Value Used (wt%)
Carbon (C)	0.28 (max)	0.28
Manganese (Mn)	0.79-1.30	1.045
Phosphorus (P)	0.035 (max)	0.035
Sulfur (S)	0.035 (max)	0.035
Silicon (Si)	0.13-0.45	0.29
Iron (Fe)	Balance	98.325
Density[5] = 7.85 g/cm^3		

Table 2.5 Chemical Composition of Stainless Steel Type 304L (UNS S30403) for Spacers/Grids in Waste Package[6-7]

Element	Composition[6] (wt%)	Value Used (wt%)
Carbon (C)	0.03 (max)	0.03
Manganese (Mn)	2.00 (max)	2.00
Phosphorus (P)	0.045 (max)	0.045
Sulfur (S)	0.03 (max)	0.03
Silicon (Si)	0.75 (max)	0.75
Chromium (Cr)	18.00 - 20.00	19.00
Nickel (Ni)	8.00 - 12.00	10.00
Nitrogen (N)	0.10	0.10
Iron (Fe)	Balance	68.045
Density[7] = 7.94 g/cm^3		

Table 2.6 Chemical Composition of Stainless Steel Type 316L (UNS S31603) for DOE Cansiter[7-8]

Element	Composition[8] (wt%)	Value Used (wt%)
Carbon (C)	0.03 (max)	0.03
Manganese (Mn)	2.00 (max)	2.00
Phosphorus (P)	0.045 (max)	0.045
Sulfur (S)	0.03 (max)	0.03
Silicon (Si)	1.00 (max)	1.00
Chromium (Cr)	16.00 - 18.00	17.00
Nickel (Ni)	10.00 - 14.00	12.00
Molybdenum (Mo)	2.00 - 3.00	2.50
Nitrogen (N)	0.00	0.10*
Iron (Fe)	Balance	65.295
Density[7] = 7.98 g/cm^3		

* This value is consistent with previous releases of Reference 8. However, the amount is negligible and does not affect the results of the criticality calculations in Section 1.0

Table 2.7 Chemical Composition of SRS HLW Glass[9-10]

Element/Isotope	Composition[9] (wt %)	Element/Isotope	Composition[a] (wt %)
O	4.4770E+01	Ni	7.3490E-01
U-234	3.2794E-04	Pb	6.0961E-02
U-235	4.3514E-03	Si	2.1888E+01
U-236	1.0415E-03	Th	1.8559E-01
U-238	1.8666E+00	Ti	5.9676E-01
Pu-238	5.1819E-03	Zn	6.4636E-02
Pu-239	1.2412E-02	B-10	5.9176E-01
Pu-240	2.2773E-03	B-11	2.6189E+00
Pu-241	9.6857E-04	Li-6	9.5955E-02
Pu-242	1.9168E-04	Li-7	1.3804E+00
Cs-133	4.0948E-02	F	3.1852E-02
Cs-135	5.1615E-03	Cu	1.5264E-01
Ba-137	1.1267E-01	Fe	7.3907E+00
Al	2.3318E+00	K	2.9887E+00
S	1.2945E-01	Mg	8.2475E-01
Ca	6.6188E-01	Mn	1.5577E+00
P	1.4059E-02	Na	8.6284E+00
Cr	8.2567E-02	Cl	1.1591E-01
Ag	5.0282E-02		
Maximum Density[10] at 25 °C = 2.85 g/cm^3			

2.6 References

[1] ***"Design Analysis for the Defense High-Level Waste Disposal Container."*** ANL-DDC-ME-000001 REV 00. Las Vegas, Nevada: CRWMS M&O. ACC: MOL.20000627.0254 (2000).

[2] ***"Defense High Level Waste Disposal Container System Description Document,"*** SDD-DDC-SE-000001 REV 01 ICN 01. Las Vegas, Nevada: Bechtel SAIC Company. URN-0921 (2001).

[3] ASTM B 575-97, ***"Standard Specification for Low-Carbon Nickel-Molybdenum-Chromium, Low-Carbon Nickel-Chromium-Molybdenum, Low-Carbon Nickel-Chromium-Molybdenum-Copper and Low-Carbon Nickel-Chromium-Molybdenum-Tungsten Alloy Plate, Sheet, and Strip,"*** West Conshohocken, Pennsylvania: American Society for Testing and Materials. TIC: 241816 (1998).

[4] ASTM A 516/A 516M – 90, ***"Standard Specification for Pressure Vessel Plates, Carbon Steel, for Moderate- and Lower-Temperature Service,"*** Philadelphia, Pennsylvania: American Society for Testing and Materials. TIC: 240032 (1991).

[5] ASTM A 20/A20M-99a, ***"Standard Specification for General Requirements for Steel Plates for Pressure Vessels,"*** West Conshohocken, Pennsylvania: American Society of Testing and Materials. TIC: 247403 (1999).

[6] ASTM A 240/ A 240M-99b, ***"Standard Specification for Heat-Resisting Chromium and Chromium-Nickel Stainless Steel Plate, Sheet, and Strip for Pressure Vessels,"*** West Conshohocken, Pennsylvania: American Society for Testing and Materials. TIC: 248529 (2000).

[7] ASTM G 1-90, ***"Standard Practice for Preparing, Cleaning, and Evaluating Corrosion Test Specimens,"*** West Conshohocken, Pennsylvania: American Society for Testing and Materials. TIC: 238771 (1999).

[8] ASTM A 276-00, ***"Standard Specification for Stainless and Heat-Resisting Steel Bars and Shapes,"*** West Conshohocken, Pennsylvania: American Society for Testing and Materials. TIC: 248098 (2000).

[9] ***"DOE SRS HLW Glass Chemical Composition,"*** BBA000000-01717-0210-00038 REV 00. Las Vegas, Nevada: CRWMS M&O. ACC: MOL.19990215.0397 (1999).

[10] Stout, R.B. and Leider, H.R., eds., ***"Preliminary Waste Form Characteristics Report,"*** Version 1.0. Livermore, California: Lawrence Livermore National Laboratory. ACC: MOL.19940726.0118 (1991).

This Page Intentionally Left Blank

3.0 MICROSTRUCTURAL CHARACTERIZATION OF THE MD-SNF FORM

The melt-dilute treatment technology consolidates fuel assemblies by a melting/casting process in which depleted uranium is added to reduce enrichment below 20% ^{235}U. The product of this treatment is a uranium-aluminum alloy. Criticality analyses have shown that minor amounts of neutron-absorbing materials are needed to demonstrate criticality control (i.e., maintain $k_{eff} < 0.95$) for the melt-dilute spent nuclear fuel (MD-SNF) form with 20% ^{235}U enrichment. Therefore, it is necessary to demonstrate process and performance compatibility of neutron absorbing materials in the MD-SNF form. This section describes the metallurgical/microstructural characteristics of the MD form with a focus on the process compatibility of neutron absorbing materials for the uranium-aluminum alloy fuels.

The overall volume is reduced, criticality control is improved, and the issue of proliferation is eliminated by using the melt-dilute treatment to reduce the uranium enrichment to below 20%.

3.1 Criticality Control of the Melt-Dilute SNF Form

Criticality control in waste packages for disposal at Yucca Mountain is discussed in detail in Section 1.0. Results of criticality analyses[1] indicate a need for neutron absorbing materials in the WP to preclude the possibility of achieving a critical configuration within the WP. The current melt-dilute process provides for the addition of up to three percent of neutron absorbing materials by weight to the MD-SNF form. The current melt-dilute process provides for the addition of up to three percent of neutron absorbing materials by weight to the MD-SNF form. Gadolinium and hafnium are the neutron absorbing materials selected for use in the melt-dilute process as described in the following section.

3.1.1 Neutron Absorber Options and Considerations

Candidate melt-dilute/neutron absorber systems include melt-dilute plus gadolinium, melt-dilute plus hafnium, and melt-dilute plus gadolinium and hafnium. These systems have been selected based upon thermal neutron absorption cross-section and upon geochemical considerations. The specific compositions have not been established; however it is anticipated that less than 1% by weight of neutron-absorbing species in the melt-dilute form is required to maintain criticality control.

Gadolinium has been selected due to its high neutron absorption cross-section. The solubility of gadolinium metal may become a concern over geologic times as it has the potential for being selectively removed from a waste package while leaving behind fissile uranium. However, gadolinium metal has the potential for forming a less soluble oxide, gadolinia (Gd_2O_3), or even an insoluble phosphate, $GdPO_4$, as the MD-SNF form degrades in expected repository environments. Gadolinia has been used in transport/shipment casks as a criticality control material. In addition, gadolinia provides improved solubility characteristics over gadolinium metal. The phosphate form of gadolinium, gadolinium-phosphate ($GdPO_4$), would provide significant neutron absorbing capacity while exhibiting desirable geochemical characteristics. Unfortunately, $GdPO_4$ is not commercially available at this time. Gadolinia and gadolinium-phosphate are not currently being pursued for melt-dilute criticality control since gadolinium readily alloys with aluminum and uranium and can be readily integrated into the MD-SNF form.

Hafnium is attractive metallurgically. In its pure form, hafnium is extremely corrosion resistant and is relatively insoluble over a wide pH range. However, the thermal neutron absorption cross-section of hafnium (106 barns) is significantly lower than that of gadolinium (48800 barns). Hafnium has been selected due to its modest neutron absorption cross-section in combination with its relative insolubility. The hafnium loading required to preclude criticality over geologic times in the proposed repository is many times that of gadolinium.

The ideal melt-dilute/neutron absorber system is one that will utilize a combination of gadolinium, for its very large neutron cross-section and alloying characteristics, and hafnium, for its insolubility. This combination will provide optimum neutron absorption and solubility characteristics to allow for the demonstration of criticality control of the MD-SNF form over geologic times. The final neutron absorber will be decided by processing conditions and criticality calculations for each waste form.

3.1.2 Melt Dilute/Neutron Absorber System

Because the primary constituents of the aluminum-based SNF assemblies are uranium and aluminum, the MD-SNF form will be based on neutron absorber additions to the binary uranium-aluminum system (see Figure 3.1). The majority of Al-SNF assemblies are comprised of an enriched uranium-aluminum alloy in an aluminum matrix with aluminum cladding. This section represents the demonstration of a melt-dilute SNF form for these uranium-aluminum alloy based fuels. MD-SNF forms of the silicide and oxide based fuels will also be based on the binary uranium-aluminum system with small additions of other components (i.e., Si and oxides other than uranium). Figure 3.1 illustrates the region of interest involved for the melt-dilute process with the use of the uranium-aluminum phase diagram. The MD-SNF form will be comprised, primarily of UAl_4 and Al, shown by the shaded region in Figure 3.1. In the binary system, the solidification is shown to occur as a eutectic transformation, i.e. a liquid transforming on cooling to UAl_4 and Al phases. This transformation occurs at approximately 13.2 wt% U and 642 °C. The aluminum phase is a disordered face centered cubic (FCC) structure, while the UAl_4 phase is an ordered intermetallic phase, based on an orthorhombic structure. Deviation from 13.2 wt% U will cause either primary Al or UAl_4 to form in conjunction with this eutectic microstructure. If the composition contains more than 15.5 to 16 wt% U, primary UAl_3 (cubic $L1^2$ structure) will form followed by a transformation to UAl_4 by a peritectic reaction. Both the UAl_3 and UAl_4 phases are commonly observed to form in a faceted manner, which leads to irregularly shaped phase boundaries in the alloy system.

Ternary additions to the alloy can also cause the composition to deviate from the simple two-phase field. To accommodate additional constituents, the composition of each phase in the melt may change or new phases may form. Figures 3.2 and 3.3 are the phase diagrams for the aluminum-gadolinium and aluminum-hafnium systems, respectively. When comparing these two diagrams to the U-Al phase diagram, similar phases may be observed. Specifically, Figure 3.2 shows the existence of a $GdAl_4$ and a $GdAl_3$ phase and Figure 3.3 shows a $HfAl_3$ phase. Although the $GdAl_3$ and $HfAl_3$ phases exhibit different structures than their uranium counterpart, the $GdAl_4$ phase is isomorphous with the UAl_4 phase. Thus, from a preliminary examination of the phase diagrams and crystal structures for the aluminum-rich intermetallic phases in the three binary alloys systems, the neutron absorber additions can be expected to exhibit the following behavior: 1) partitioning to the UAl_x intemetallic phases or 2) formation of a unique ternary phase with uranium. For either case uranium will be colocated with a neutron absorbing species which will provide effective criticality control.

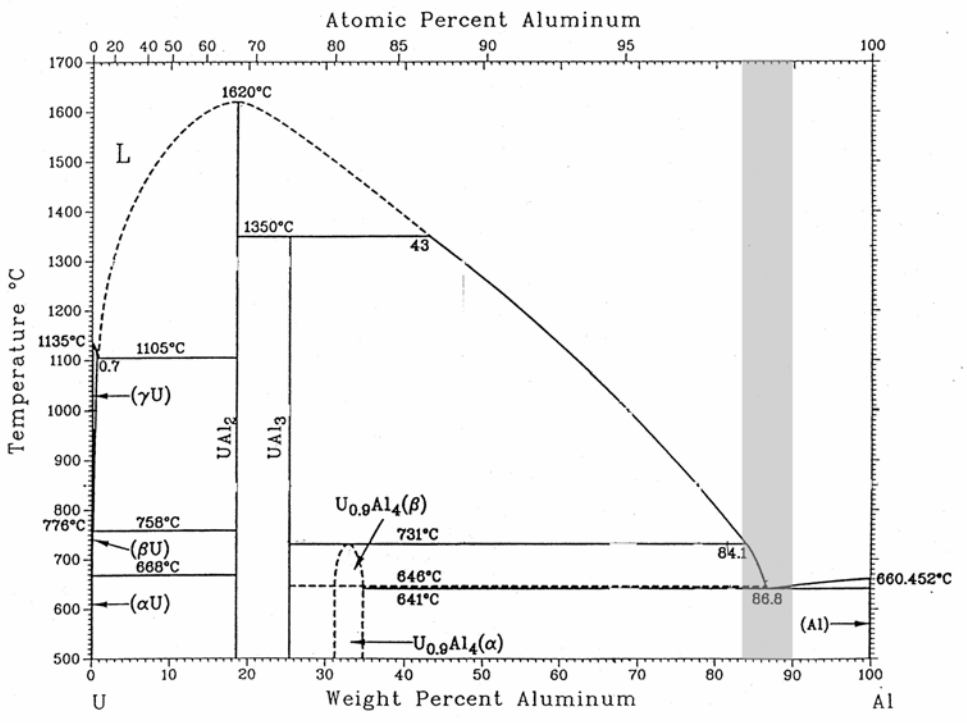

Figure 3.1 Uranium-Aluminum Phase Diagram

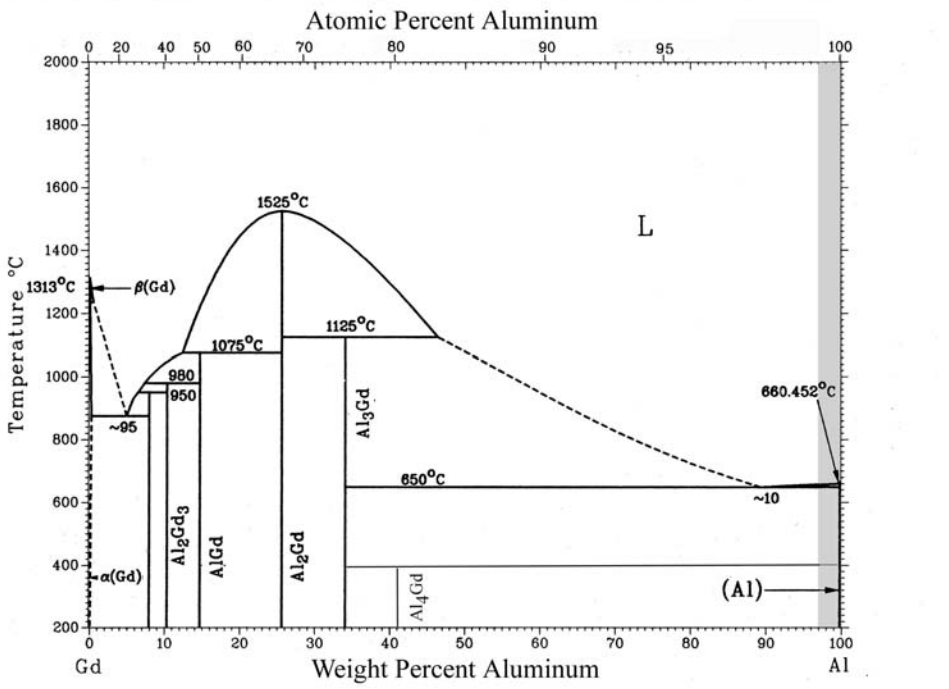

Figure 3.2 Gadolinium-Aluminum Phase Diagram

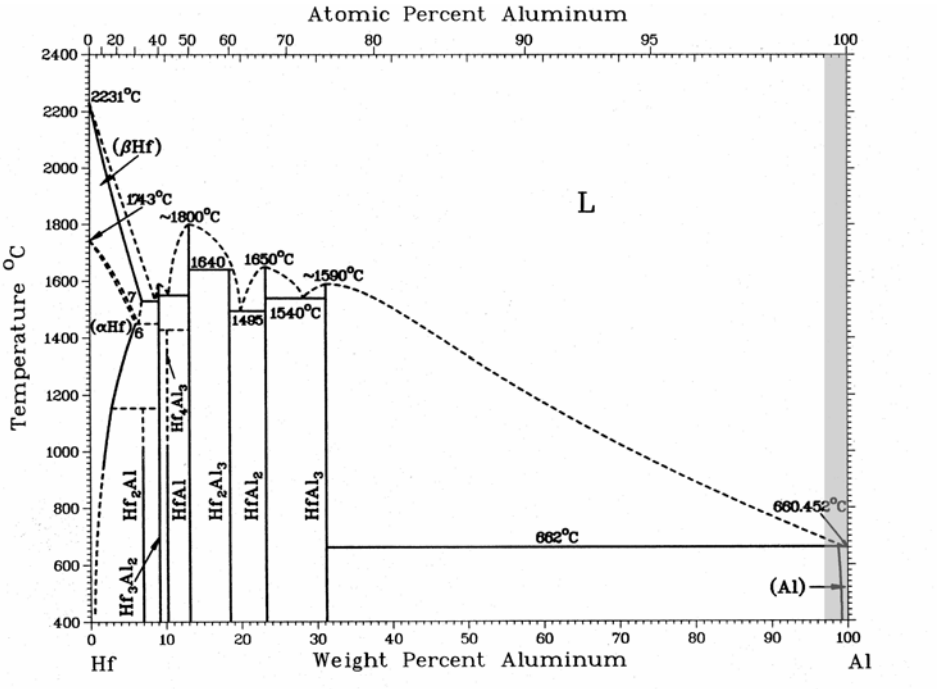

Figure 3.3 Hafnium-Aluminum Phase Diagram

3.1.3 The Melt-Dilute/Neutron Absorber System Fabrication

The Al-SNF assemblies are typically fabricated using enriched uranium and aluminum alloy, with an aluminum alloy cladding. During reactor service, fission products are produced within the assemblies. The relatively small quantities of fission products by mass, however, are not expected to significantly alter the microstructure of the MD-SNF form from a simply binary mixture of uranium and aluminum. Therefore, a surrogate fuel assembly fabricated using depleted-uranium and aluminum has been developed to simulate the behavior and characteristics of actual MD-SNF. These surrogate fuel assemblies are melted and alloyed with additional aluminum to obtain a near eutectic composition (~13.2 percent by weight U in Al). Neutron absorber materials are added (in levels of 1.5 to 3 wt%) during the melt-dilute treatment to produce samples used in the compatibility program, as necessary. These levels are higher than expected for the MD-SNF but allow for easy detection in phase segregation and degradation studies.

Neutron absorber doped aluminum-uranium alloys were prepared using a commercial grade 1100 Al alloy, reactor grade depleted uranium and 99.9% purity gadolinium and hafnium. These alloys were prepared using an induction casting furnace (see Figure 3.4) operated at approximately 25 kW. The alloys were melted in graphite crucibles at melt temperatures of 850 °C. The melting procedure for these alloys involved melting approximately 8380 gms of 1100 Al alloys followed by induction stirring during which additions of depleted uranium (≈ 1320 grams) and neutron absorber (Gd/Hf ≈ 300 grams) were made. The melt was induction stirred for 3 minutes. The alloys were reheated to 850 °C at which time furnace power was shut-off and the melts were allowed to furnace cool. Samples were cut from the 6 inch × 10 inch solidified ingot (see Figure 3.5) using a wire EDM and characterization was performed using light optical microscopy, x-ray diffraction, and scanning electron microscopy with EDS.

Figure 3.4 Induction Furnace Used to Produce Surrogate MD-SNF Ingots

Figure 3.5 Surrogate MD-SNF Ingot Produced in the Induction Furnace

3.2 Melt-Dilute/Neutron Absorber System Microstructure

3.2.1 Microstructure of Binary Uranium Aluminum Alloys

The general microstructure of the MD-SNF form is that of a simple binary eutectic. The eutectic composition is usually reported as 13.2 wt% U but deviation from this value is common because of the nature of solidification in a faceted/non-faceted eutectic microstructure. The eutectic composition is observed to be sensitive to cooling rate or impurity level, and hence, will not be the same under varying processing conditions.[2] If the melt composition deviates slightly from the eutectic composition, the microstructure will form primary Al or UAl_4 followed by the formation of a eutectic between regions of the primary phase. An example of this microstructure is presented in Figure 3.6. In SEM micrographs, UAl_x phases appear as light phases contrasted to the dark appearance of the aluminum matrix. In this figure, blocky primary UAl_4 is observed surrounded by a layer of the aluminum phase and then a coupled eutectic of Al + UAl_4. From this microstructure, we can discern that the actual composition of the alloy is higher in uranium content than the eutectic composition (i.e., hypereutectic). The presence of an intermediate aluminum layer between the primary phase and the eutectic region is common in faceted systems and results from the sluggish growth kinetics of the faceted UAl_4 phase in the coupled eutectic.[2]

In some cases the composition may vary enough (> 15.5 wt. % U) or impurities can change the microstructure such that other UAl_x phases form. In Figure 3.7a, the UAl_x phases are surrounded by an Al matrix in a binary U-Al alloy that has iron (Fe) as its primary impurity. Figure 3.7b presents the x-ray map that indicates the presence of uranium. Higher uranium density leads to lighter appearance in the x-ray map. These figures suggest the presence of two separate uranium-containing phases. The phases are UAl_3 and UAl_4. The UAl_3 phase appears as the lighter of the two phases due to its enriched uranium content. In this particular case, the UAl_4 phase also contains Fe (see Figure 3.8) in solid solution while no iron was observed in the UAl_3 or the Al. Iron is a common impurity in commercial grade aluminum and is expected to be present in the MD-SNF form.

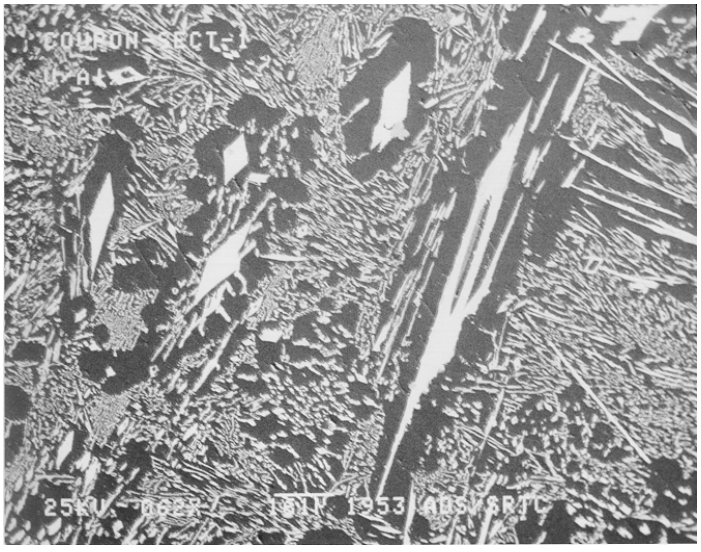

Figure 3.6 General Microstructure of the Binary U-Al MD-SNF Form

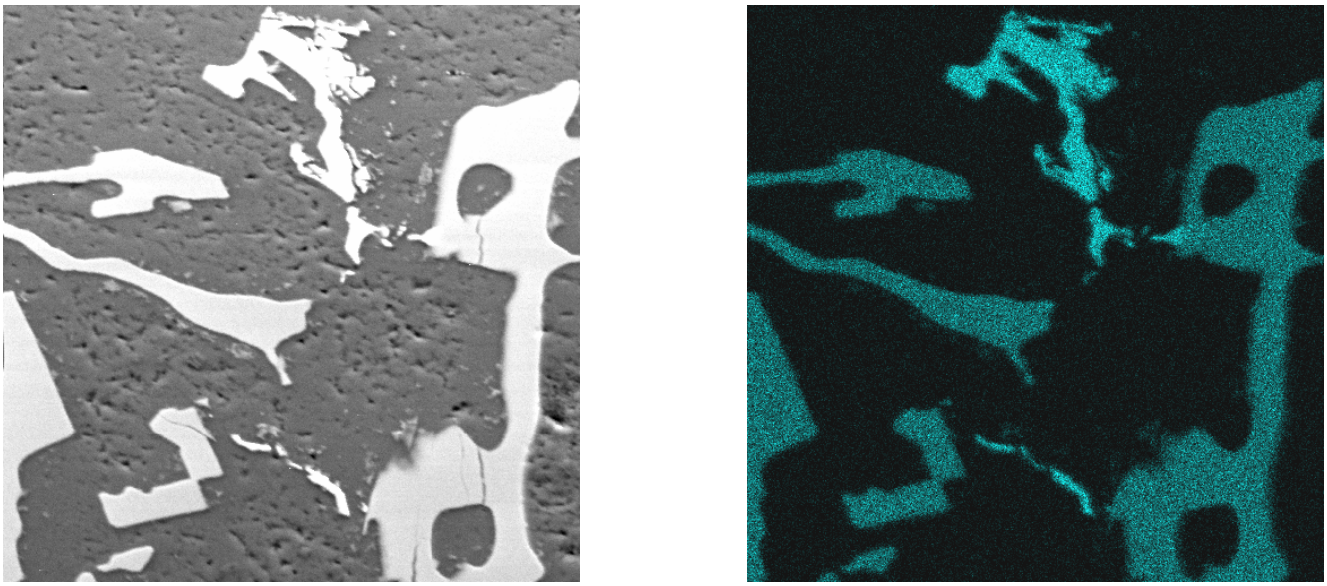

(a) (b)

Figure 3.7 Back-Scattered Electron Micrograph (a) and a X-ray Map of Uranium in the Same Region (b) of the Surrogate MD-SNF Form

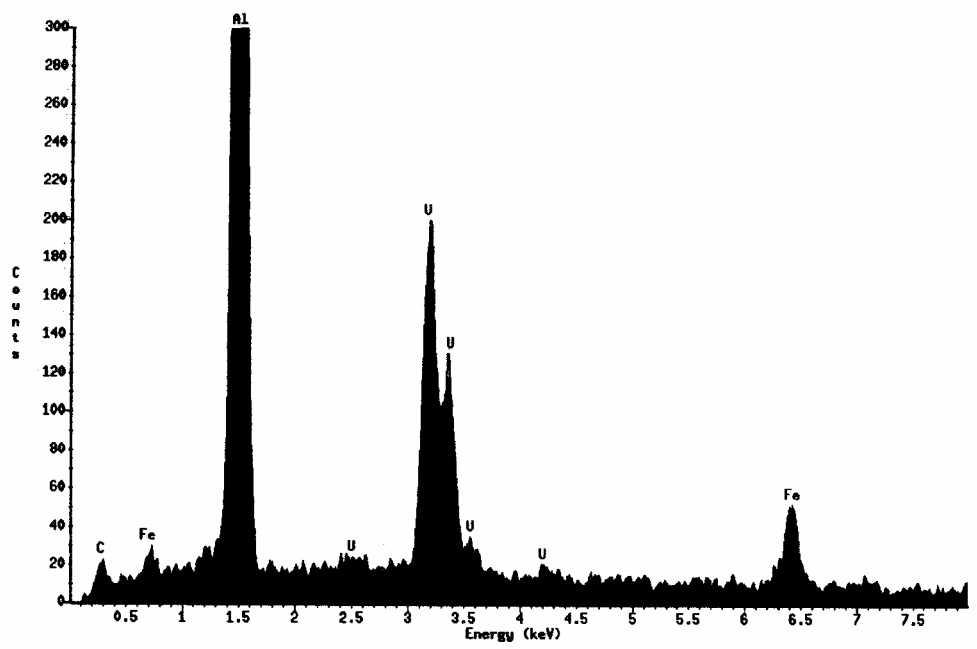

Figure 3.8 An Energy Dispersive Spectroscopy (EDS) Scan of the UAl_4 Phase Observed in Figure 3.7 (right side) Showing Iron in Solid Solution

3.2.2 Microstructure of Uranium, Aluminum and Gadolinium Alloys

The addition of gadolinium in amounts up to a total of three percent by weight, to the MD-SNF form does not substantially alter the microstructure of the form. An example of this microstructure is observed in Figure 3.9. A comparison of Figure 3.9 with Figure 3.6 shows the microstructures with and without gadolinium additions are similar. Once again, large blocky UAl_4 phases are surrounded by a thin aluminum layer followed by a eutectic of Al + UAl_4. No UAl_3 is observed in this sample (either by SEM analysis or by x-ray diffraction). The detailed illustration of microstructure and elemental partitioning of this alloy are presented in Figures 3.10 and 3.11, respectively. Figure 3.10 shows a high magnification SEM micrograph of the UAl_4 + Al eutectic. Figure 3.11a presents the x-ray map that indicates the presence of uranium within the MD-SNF form, while Figure 3.11b presents the x-ray map indicating gadolinium location. A comparison of these figures shows that the gadolinium added to the melt-dilute form collocates with the uranium present in the UAl_4 phase.

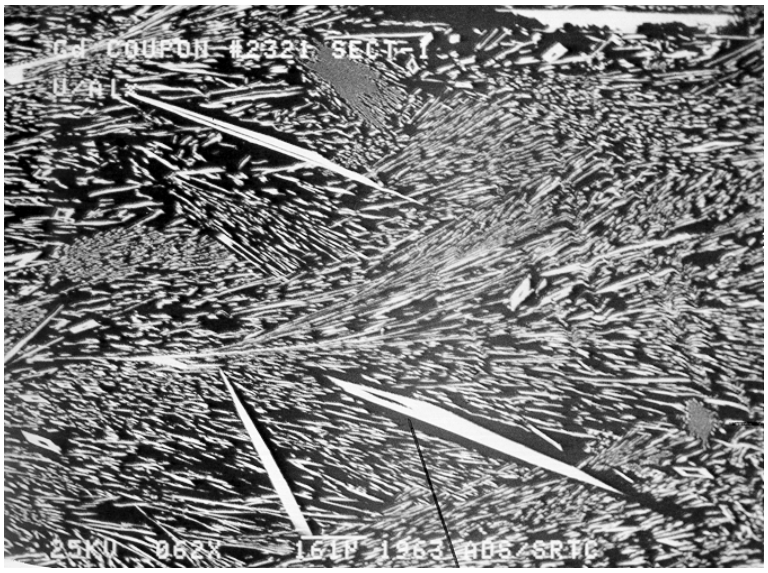

Figure 3.9 General Microstructure of the Binary U-Al MD-SNF Form with 3% Gd by Weight

3.2.3 Microstructure of Uranium, Aluminum and Hafnium Alloys

The microstructure of the melt-dilute SNF form with an addition of 3% hafnium by weight is presented in Figures 3.12 and 3.13. In Figure 3.12, bright, blocky particles are surrounded by dark gray regions of aluminum dendrites, followed by light gray areas of simple eutectic. Figure 3.13 illustrates the partitioning of elements in this alloy with Energy Dispersive Spectroscopy (EDS) scans from each region of the microstructure presented. These EDS scans clearly show that the bright blocky particles contain the majority of the hafnium, as well as significant levels of uranium and aluminum. This phase was identified as a hafnium containing (U, Hf)Al_3 solid solution by x-ray diffraction. Adjacent to these blocky phases is the binary form of UAl_3 (i.e., almost no Hf) along with pure aluminum dendrites. Both of these phases are observed to contain almost no hafnium. Finally, the light gray regions of the UAl_4 + Al coupled eutectic surround these regions. An EDS scan of the UAL_4 phase in the eutectic region show no hafnium present.

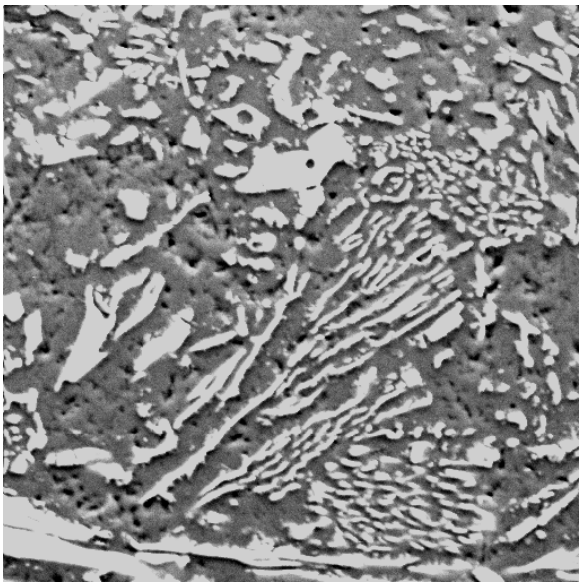

Figure 3.10 Back-Scattered Electron Micrograph of the Surrogate MD-SNF Form with 3% Gd by Weight

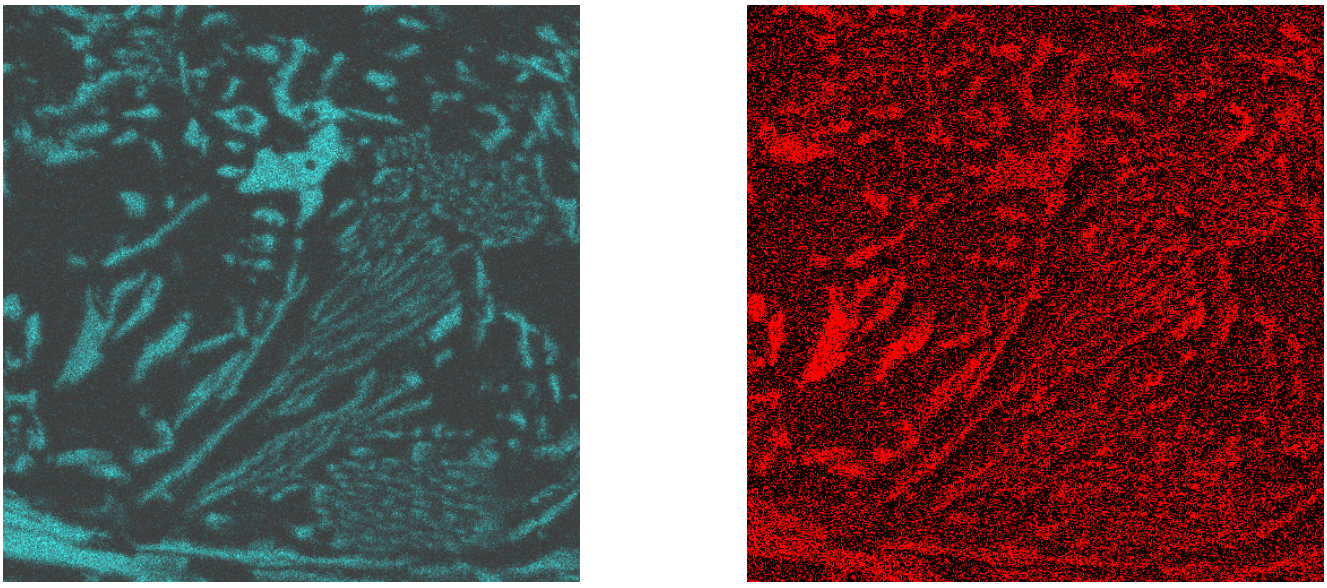

(a) (b)

Figure 3.11 X-Ray map of Uranium (a) and of Gadolinium (b) in the Surrogate MD-SNF Form with 3% Gd by Weight

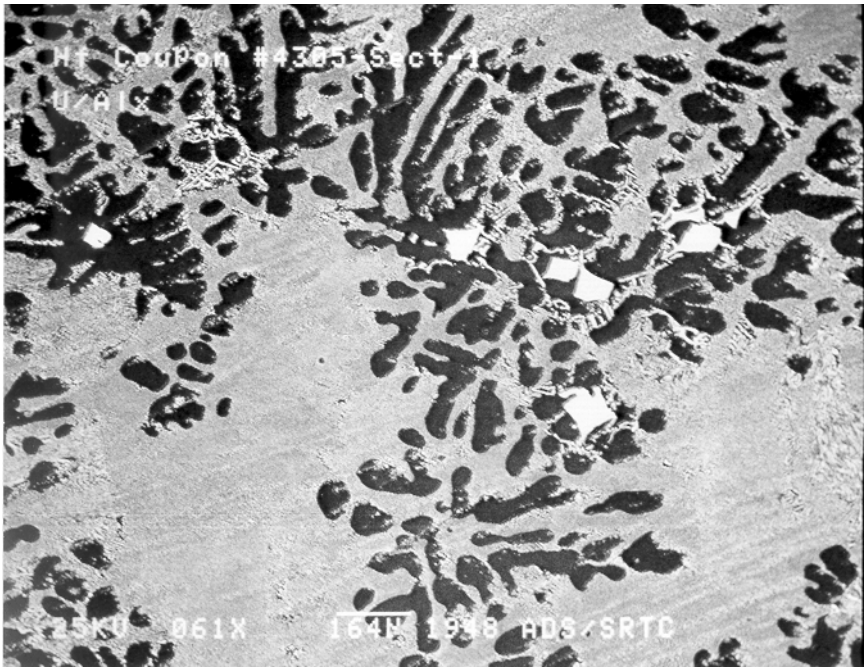

Figure 3.12 SEM Photomicrograph of the Surrogate MD-SNF Form with 3% Hf by Weight

From these figures, it is evident that the hafnium added to the melt-dilute SNF form is located primarily in a (U, Hf)Al_3 phase, as opposed to the orthorhombic UAl_4. Once the hafnium partitions to this phase, a mixture of binary UAl_3 and aluminum dendrites nucleate at the solid/liquid interface prior to the coupled eutectic of UAl_4 + Al. The presence of this intermediate layer between the primary phase and the eutectic region is a result of sluggish growth kinetics of the faceted UAl_4 phase in the coupled eutectic.

3.2.4 Microstructure of Uranium, Aluminum, Gadolinium and Hafnium Alloys

The microstructure of the melt-dilute form with an addition of 1.5 % gadolinium and 1.5 % hafnium (by weight) is presented in Figure 3.14. The microstructure in this alloy closely resembles the microstructure in the U-Al + Hf alloy with the exception of a new phase present. In addition to the primary blocky (U, Hf)Al_3 phase (exemplified in Figure 3.12), a binary $HfAl_3$ phase is observed. Figure 3.15 illustrates the partitioning of the elements in this alloy with EDS scans from specific phases of the microstructure presented. In this figure, the presence of a binary $HfAl_3$ phase, a (U, Hf)Al_3 phase, a (U,Gd)Al_4 phase, and an Al phase are all observed by their EDS spectra. From these figures, it is apparent that a binary $HfAl_3$ phase nucleates heterogeneously from the liquid followed by blocky (U, Hf)Al_3 phases at the solid-liquid interface. An intermediate layer of aluminum dendrites then form before the UAl_4 + Al coupled eutectic. From the EDS scan of the (U, Hf)Al_3 phase, small levels of Gd can be observed to be present in this phase. However, Gd preferentially partitions to the UAl_4 phase and Hf preferentially partitions to both (U, Hf)Al_3 type phases. No binary UAl_3 was observed in this alloy which suggests a different liquidus path than that of the U-Al + Hf alloy.

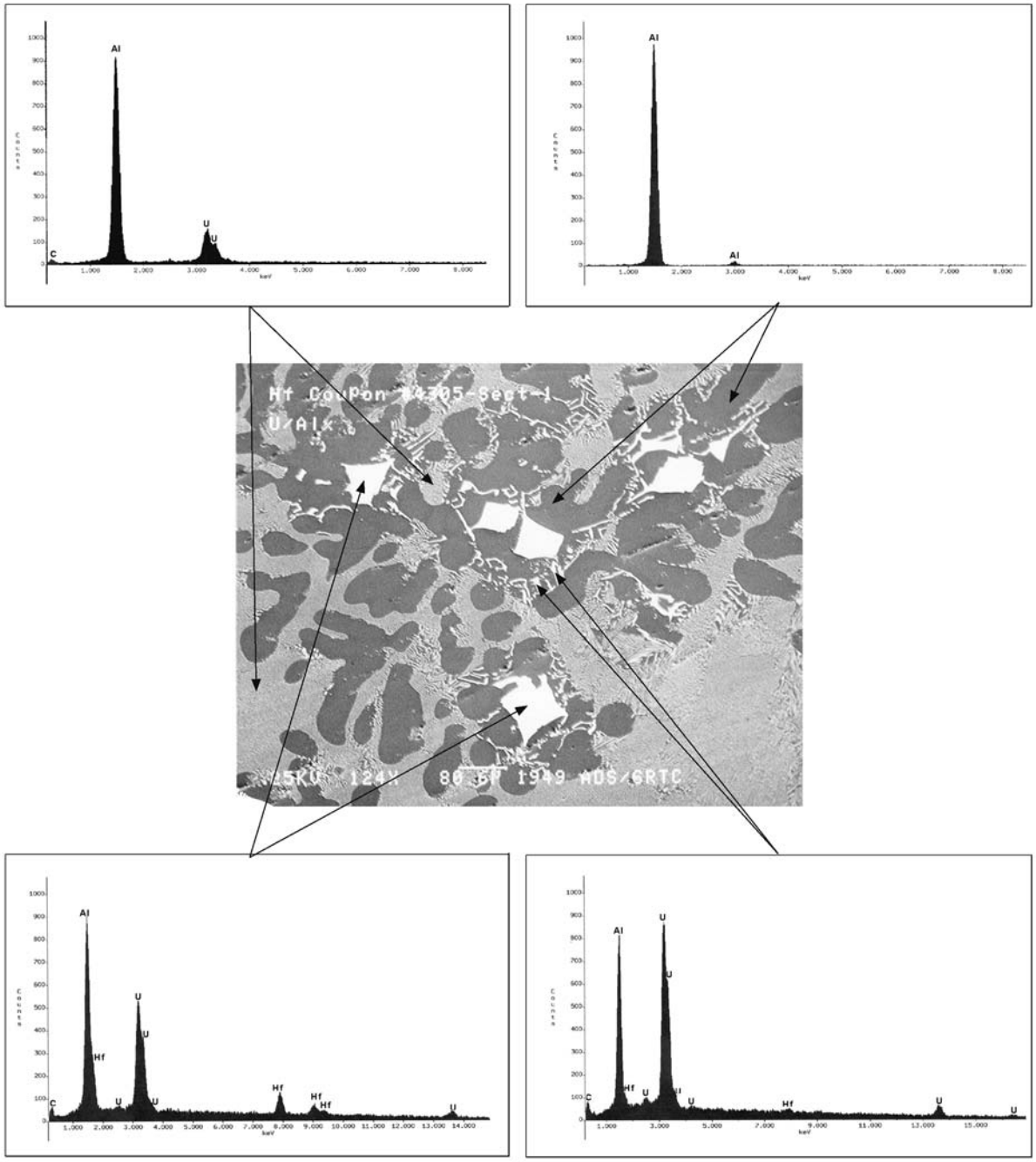

Figure 3.13 Detailed Microstructure of the U-Al System with 3% Hf by Weight along with EDS Scans of Individual Phases

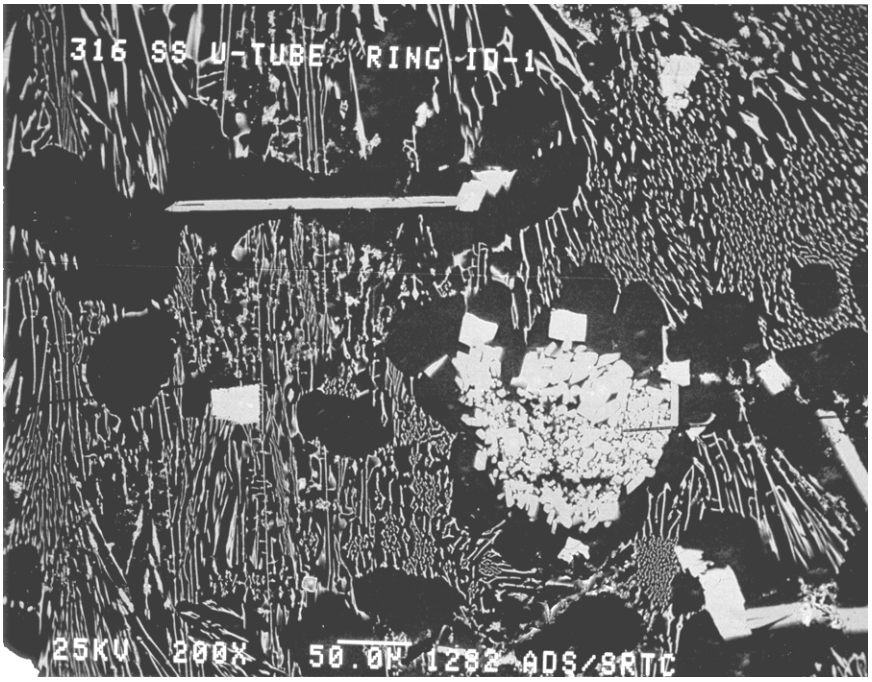

Figure 3.14 SEM Photomicrograph of the Surrogate MD-SNF Form with 1.5% Gd and 1.5% Hf by Weight

3.3 Summary

Uranium-aluminum melt-dilute SNF form surrogates can be fabricated with Gd and Hf neutron absorbers integral to the microstructure. The microstructures of the MD form surrogates with gadolinium and hafnium neutron absorbers were metallurgically characterized. Gadolinium additions tend to concentrate in the UAl_4 phase that is more corrosion resistant than the bulk MD-SNF form. Therefore, the gadolinium is expected to stay closely associated with fissile uranium in the UAl_4 phase as the MD-SNF form degrades, providing an additional barrier against the solubility facilitated removal of gadolinium from the waste package. Hafnium additions tend to concentrate with aluminum in a $(U, Hf)Al_3$ phase with or without trace quantities of gadolinium. This makes the distribution of Hf in the waste package more heterogeneous than Gd and may make the hafnium more susceptible to release from the MD-SNF form by corrosion. However, the relative insolubility of hafnium would prevent it from being removed from the waste package. The combination of gadolinium and hafnium for criticality control provides an ideal microstructure and phase distribution for a suitable MD-SNF form. It is recommended to verify the process additions of Gd and Hf, and the resultant microstructures using spent nuclear fuel.

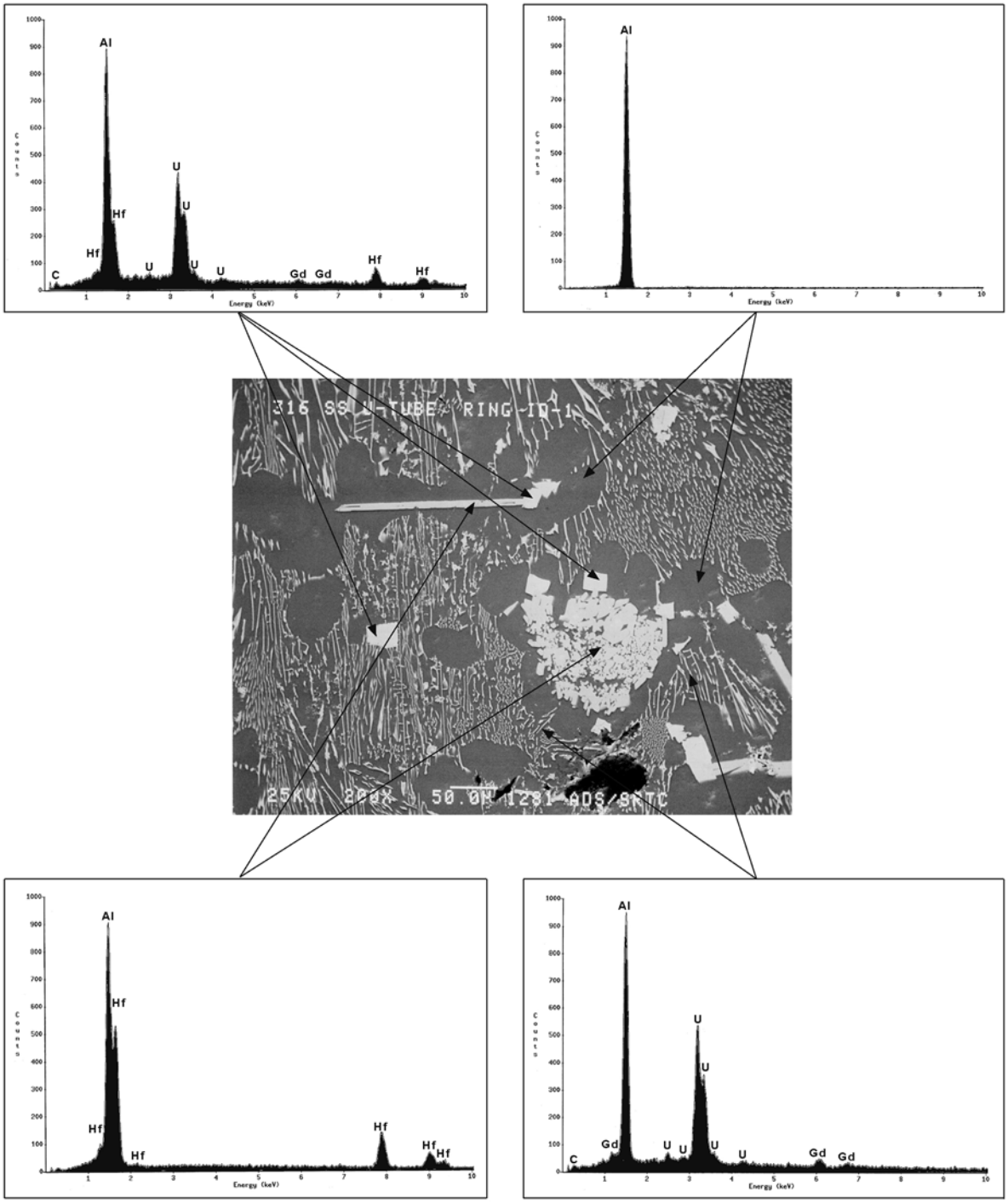

Figure 3.15 SEM Photomicrograph of the Surrogate MD-SNF Form with 1.5% Gd and 1.5% Hf by Weight along with EDS Scans of Individual Phases

3.4 References

[1] ***"Evaluation of Codisposal Viability for Melt and Dilute DOE-Owned Fuel,"*** Bechtel SAIC Report TDR-EDC-NU-000006, Rev. 0 (July 2001).

[2] Munitz, A., Zenou, V. Y., Dahan, I., Cotler, C., and Nechama, E., ***"Solidification Characteristics of Slowly Cooled Aluminum-Uranium Alloys,"*** Israel Materials Engineering Conference, 5th Edition, pp. 371-382 (1991).

4.0 CRITICALITY EVALUATION

4.1 Codisposal Waste Package Criticality Overview

Criticality analyses have been performed by the DOE-Office of Civilian Radioactive Waste Management (RW) according to the ***Disposal Criticality Analysis Methodology Topical Report***.[1] This report had been submitted to the U.S. Nuclear Regulatory Commission as part of the pre-license exchange of information. The methodology provides guidance for analyzing the geochemical and physical processes that can breach the waste package and degrade the waste forms as well as the intact and degraded component criticality analyses. Addenda to the topical report will be required to establish the critical limit for the DOE SNF types once sufficient critical benchmarks are identified and run.

The codisposal waste package is comprised of one 18-inch-outer diameter DOE standardized SNF canister containing the melt-dilute ingots, surrounded by five defense high-level radioactive waste (DHLW) glass canisters as shown in Figure 4.1. This waste package design was subjected to degradation scenarios comprised of a combination of features, events, and processes (FEPs) that could result in the degraded configurations shown and evaluated for potential criticality. The assessment of the criticality potential of the waste package involves (i) degradation scenarios analyses; (ii) geochemistry analysis; and (iii) criticality analysis of postulated degraded waste form configurations and chemical composition.

This criticality section summarizes detailed analyses and findings reported in References 2-3, which can be referred to for additional information as needed. The results show that the proposed melt-dilute SNF form containing gadolinium and/or hafnium as neutron absorbers will maintain subcriticality and that the interim repository subcriticality criterion $k_{eff} + 2\sigma \leq 0.93$ can be met.[i]

4.2 Codisposal Waste Package Degradation Assumptions

Degradation scenarios comprise a combination of features, events, and processes that result in degraded configurations to be evaluated for criticality. A configuration is defined by a set of parameters characterizing the amount and physical arrangement, at a specific location, of the materials that can significantly affect criticality (e.g., fissile materials, neutron absorbing materials, reflecting materials, and moderators). The variety of possible configurations is best understood by grouping them into classes. A configuration class is a set of similar configurations whose composition and geometry is defined by specific parameters that distinguish one class from another. Within a configuration class, the values of configuration parameters may vary over a given range.

---

[i] The criterion of $k_{eff} + 2\sigma \leq 0.93$ has been used in calculations performed in preparation of the subject document. This value has been derived as unity (critical) less the sum of a five percent margin (10 CFR 60.131(h)) and estimates for calculational bias, and the uncertainty of the experiments used to validate the method of calculation. That is, k_{eff} + uncertainty + bias + margin = 1; where uncertainty = 2σ, bias = 0.02, and margin = 0.05. The estimates of bias and bias-uncertainty are taken as the worst-case values calculated from the MCNP simulations of the validation experiments. These estimates will be confirmed at a later time.

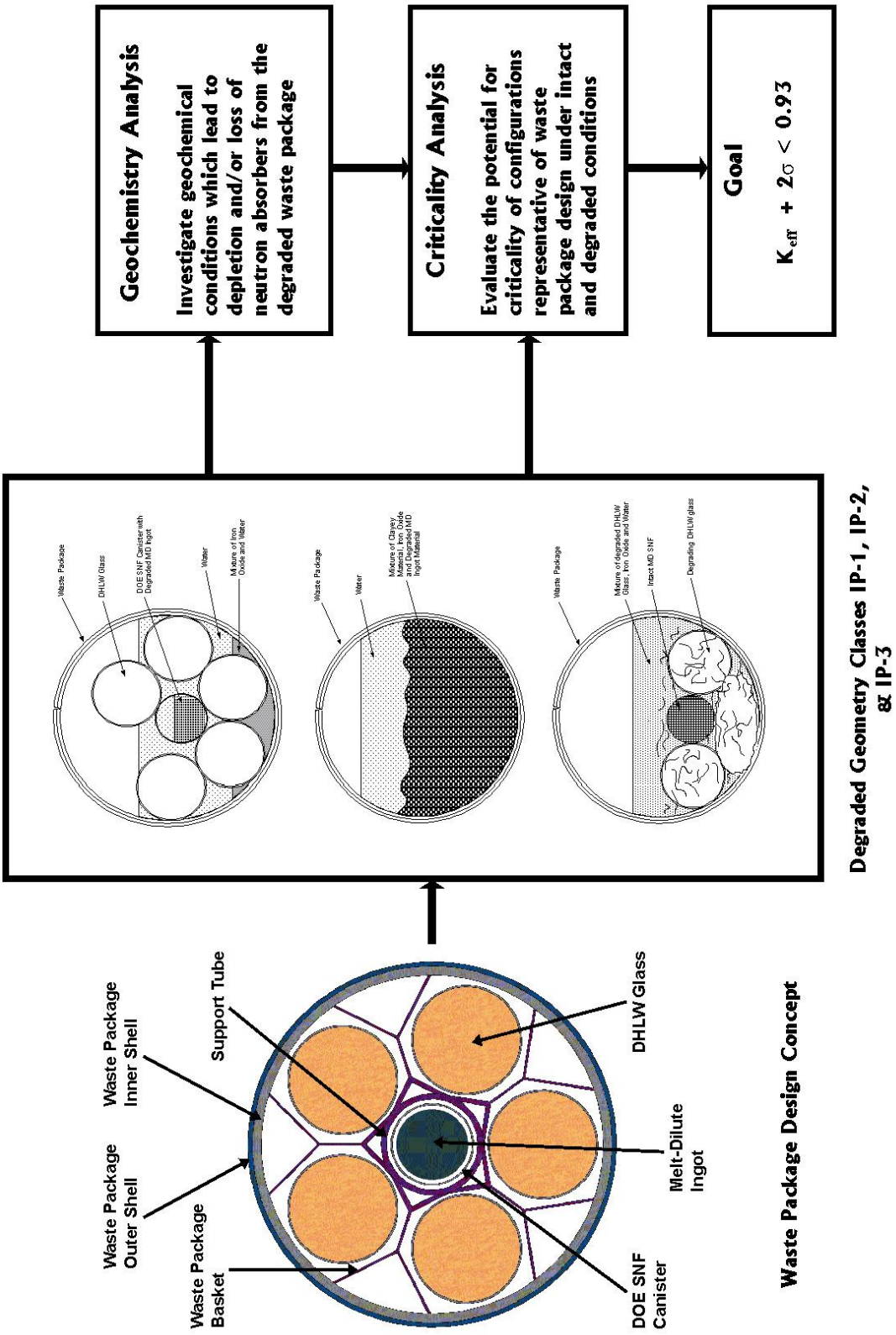

Figure 4.1 Criticality Analysis Logic Diagram

A master scenario list and set of configuration classes relating to internal criticality is given in Reference 1. A logic diagram that illustrates the disposal site postulated water intrusion that can result in degradation of waste package, waste form, and/or fissile materials is presented in

Figure 4.2. This coupled event logic tree was developed by a process that involved workshops and peer review. The comprehensive evaluation of disposal package criticality for any waste form must include variations of such standard scenarios and configurations to ensure that no credible degradation scenario is neglected.

When the waste package is breached only on the top, water flowing into the waste package collects and fills the waste package and provides water for moderation to potentially increase the probability of criticality. Further, after a few hundred years of steady dripping, the water can overflow through the hole on the top of the waste package and flush out any dissolved degradation products.

When the waste package breach occurs on the bottom as well as the top, the water can flow through the waste package. This group of scenarios allows the soluble degradation products to be removed more quickly, but does not directly provide water for moderation. Criticality is possible, however, if the waste package fills with corrosion products that can retain water of hydration and/or plug any holes in the bottom of the waste package while fissile material is retained. Silica released by the degrading high-level waste glass may form clay with enough water of hydration to support criticality.

4.2.1 Application of Standard Scenarios to Melt-Dilute Ingots

The MD ingots are encased in a thin carbon steel crucible liner and fit into the MD disposal canister. Neutron absorber material is metallurgic ally incorporated into the Al-SNF during the casting of the ingots. Therefore, neither separation nor loss of neutron absorber material is possible while the SF stays intact. This means that some separation mechanisms, such as differential settling of particles having different densities are not applicable to MD-SNF. Such differences from the "standard" scenarios have been accounted for in the degradation and criticality analyses performed. The following configuration classes were utilized for criticality calculations performed.

IP-1: The configurations resulting from IP-1 scenarios involve the MD ingots degrading before other internal components (OICs) and depend on the degradation rates of the various materials selected for such OICs. The ingot degradation rate is judged to be 4.8×10^{-12} mol·cm^{-2}·s^{-1} versus the lower rate for SS components of 2.5×10^{-14} mol·cm^{-2}·s^{-1}. Carbon steel has a degradation rate of 1.8×10^{-11} mol·cm^{-2}·s^{-1}. Therefore, the degradation of the carbon steel basket and the ingot materials while the stainless steel and DHLW glass components remaining intact is possible. Since there is no basket structure within the DOE SNF canister containing the MD-SNF ingots, configuration variations within the DOE SNF canister are limited. Possible variations are configurations with partial or total degradations of the components outside the DOE SNF canister. The DOE SNF canister falling to the bottom of the WP, near the end of this sequence, could leave layers of degradation products in the WP surrounding a partially degraded DOE SNF canister shell is such an example (see Figure 4.3).

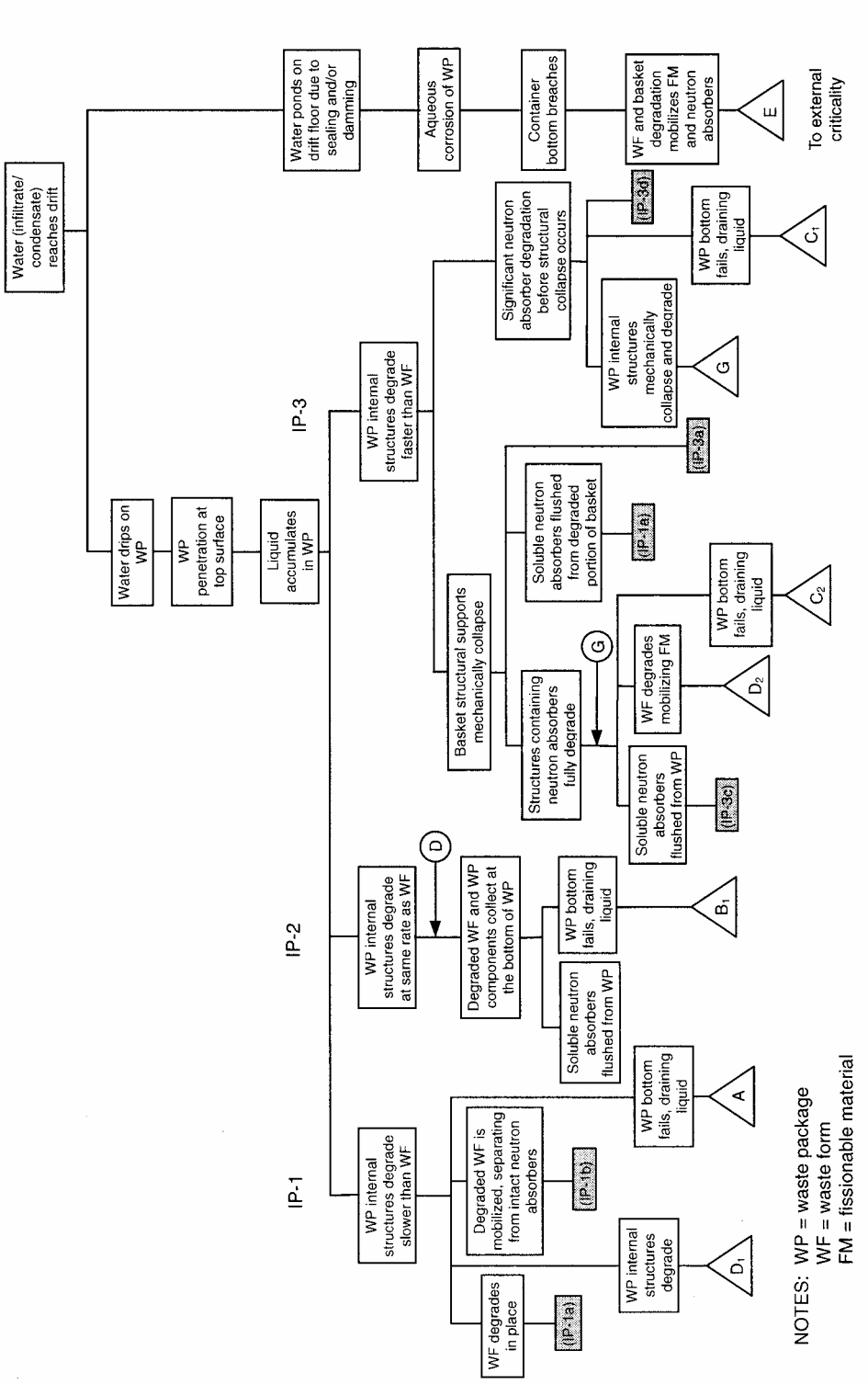

Figure 4.2 Internal Criticality Master Scenarios

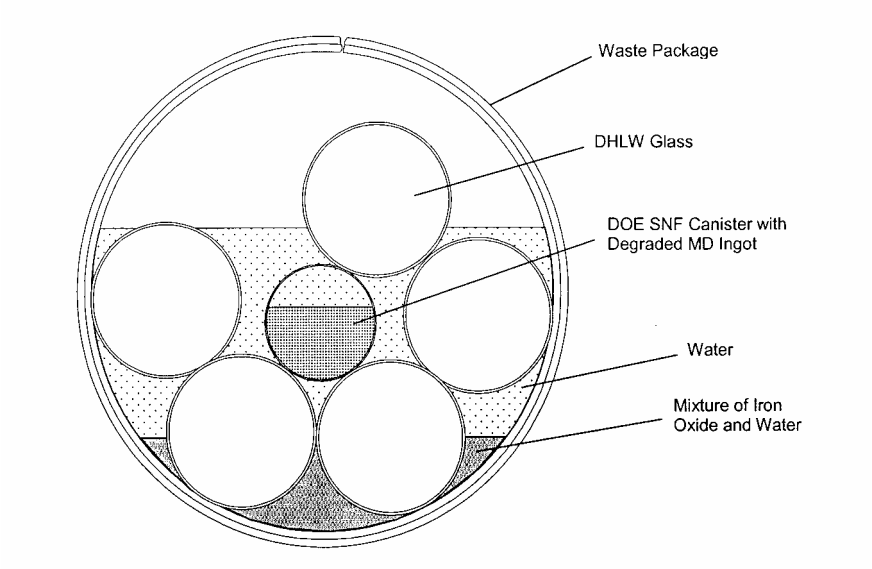

Figure 4.3 Conceptual Sketch of Waste Package for Degradation Scenario IP-1

IP-2: In the configurations resulting from IP-2 scenario, the SNF may degrade simultaneously with the other components in the WP if the environmental conditions favor glass degradation rates that are comparable to ingot and steel degradation rates. Figure 4.4 is such an example. In this scenario the gradual degradation of the various constituents could result in a configuration where higher density material collects at the bottom of the waste package while lower density material stays on top. The potential for criticality could be significant if the neutron absorber (Gd as $GdPO_4$ – the most likely mineral to form) enters into solution and is flushed out of the WP while the fissile material is in a geometry favorable to criticality. Because the Gd is integral to the MD ingots, this would require complete degradation of the ingots. Potential Gd loss due to geochemical phenomena is discussed in Section 4.3.

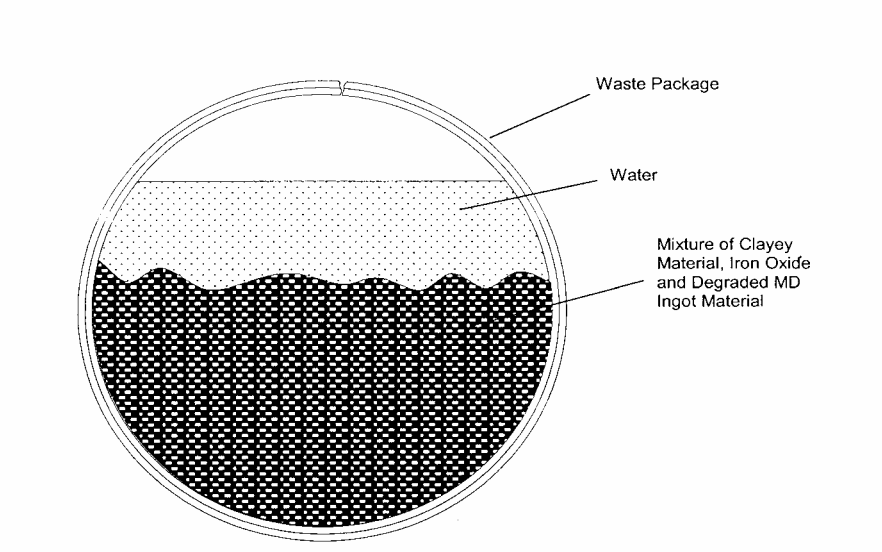

Figure 4.4 Conceptual Sketch of Waste Package for Degradation Scenario IP-2

IP-3: Application of configurations resulting from the IP-3 scenario for DOE SNF degrading after OICs postulates that the ingots have a low degradation rate and the 316L stainless steel of the DOE SNF canister have substantially lower rates than the 304L stainless steel of the DHLW canisters, along with high degradation rates for the DHLW glass. In this configuration the ingots collect at the bottom of the WP while surrounded by degradation products (e.g., clayey material). As long as the ingots are intact there is no possibility for criticality since the neutron absorber is maintained. Loss of the neutron absorber, Gd, entering into solution due to the formation of $GdPO_4 \cdot H_2O$, then being flushed out of the WP while the fissile material is in a favorable criticality geometry has been considered. Flushing out of the neutron absorber also requires that water over-flows through the hole in the top of the WP.

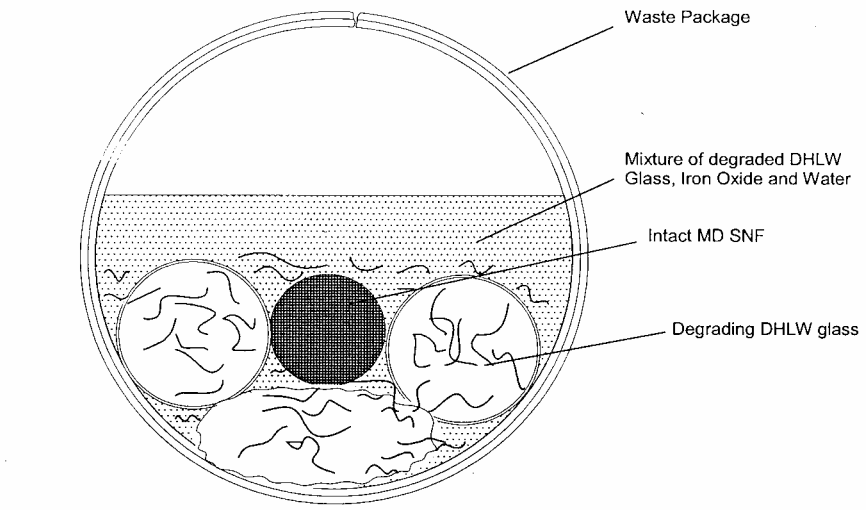

Figure 4.5 Conceptual Sketch of WP for Degradation Scenario IP-3

Other degradation scenarios, designated as IP-4, IP-5 and IP-6 in Reference 1, that allow for water flow-through require a top and bottom breach in the waste package. However, for these scenarios to lead to potential critical configurations there must be some plugging of the hole(s) in the bottom, so that water can accumulate to provide neutron moderation. In addition, geochemistry calculations assume that a material does not get flushed out unless it is in solution. Therefore, the resulting configurations are the same as the configurations for the top breach only cases (IP-1, IP-2 and IP-3).

4.2.2 Degradation Scenarios Used to Formulate Criticality Models

Configuration classes resulting from degradation scenario IP-1, in which the SNF degrades before the other internal components (OICs):

IP-1-A: SNF degraded, DOE SNF canister and internal supporting structure not degraded.
IP-1-B: SNF degraded, DOE SNF canister and supporting structure partially degraded.
IP-1-C: All WP components degraded.

Configuration classes resulting from degradation scenario IP-2, in which WP components degrade concurrently with the SNF:

IP-2-A: All WP components degraded.

Configuration classes resulting from degradation scenario IP-3, in which the SNF degrades after the OICs:

IP-3-A: Degraded DOE SNF canister internal structure; intact SNF and DOE SNF canister shell; degraded WP basket structure and HLW glass canister(s).
IP-3-B: Degraded WP basket structure, HLW glass canister(s), and DOE SNF canister; intact SNF.
IP-3-C: All WP components degraded.

When the waste package breach occurs on the bottom as well as the top, water can flow through and allow more rapid removable of soluble degradation products as well as the water. Criticality could be possible if corrosion products that retain water would plug the bottom breach and water retention commenced. However, such scenarios would revert to those identified above and have not been separately analyzed.

Variations of configurations with the DOE SNF canister degraded and intact SNF accumulated at the WP bottom with partial or total degradation of WP components have been considered in formulating criticality models and these are discussed further in Section 4.4.

4.3 Geochemistry Analysis Methods & Considerations

*4.3.1 **Computer Software***

Geochemistry analyses were performed using the EQ3/6 Version 7.2bLV geochemistry software package in the solid-centered flow-through mode. The information regarding the code and its use for the degradation and geochemistry analysis is documented in Reference 4.

A principal objective of the geochemistry calculations was to assess the chemical circumstances that could lead to removal of neutron absorbing materials (mainly Gd) from a waste package containing MD ingots (Al-SNF) and DHLW glass, while fissile materials (^{235}U) remain behind. Such circumstances could increase the probability of a nuclear criticality occurrence within the waste package. EQ6 reaction path calculations were carried out to span the range of possible system behavior and to assess the specific and coupled effects of MD ingots degradation, steel corrosion, DHLW glass degradation, and fluid influx rate on U mobilization. Corrosion product accumulation was examined as well. The results of these geochemistry calculations have been used to develop representative criticality models.

*4.3.2 **Geochemistry Analysis Methodology***

The method used for these analyses involves eight steps as described below:

1) Use the basic EQ3/6 capability to trace the progress of reactions as the chemistry evolves, including estimating the concentrations of material remaining in solution as well as the composition of precipitated solids. EQ3 is used to determine a starting fluid composition for EQ6 calculations; it does not simulate reaction progress.

2) Evaluate available data on the range of dissolution rates for the materials involved to be used as material/species input for each time step.

3) Use the "solid-centered flow-through" mode in EQ6. In this mode, an increment of aqueous "feed" solution is added continuously to the waste-package system, and a like volume of the existing solution is removed. This mode simulates a continuously stirred tank reactor.

4) Determine the concentrations of fissile material in solution as a function of time (from the output of EQ6 simulated reaction times up to ~ 6×10^5 years).

5) Calculate the amount of fissile material released from the waste package as a function of time (which, thereby, reduces the chance of criticality within the waste package).

6) Determine the concentrations of neutron absorbers (most importantly Gd) in solution as a function of time (from the output of EQ6 over times up to ~ 6×10^5 years).

7) Calculate the amount of neutron absorbing materials retained within the waste package as a function of time.

8) Calculate the composition and amounts of solids (e.g. precipitated minerals or corrosion products and un-reacted waste package materials).

4.3.3 Geochemistry Degradation Calculations and Results

The calculations begin using selected representative values from known ranges for composition, amounts, surface areas, and reaction rates of the various components of the MD waste packages. The input to EQ6 includes the composition of J-13 well water, a rate of influx to the waste package that corresponds to suitably chosen percolation rates into a drift, and a drip rate into the waste package, which is also the flow rate out of the waste package. In some cases, the degradation of the waste package is divided into stages (e.g., degradation of the DHLW glass before breach of the DOE SNF canister and exposure of the ingot material to the water). The EQ6 outputs include the compositions and amounts of solid products and the solution composition.

Table 4.1 illustrates representative analysis cases that explore the different sequences of degradation: a) degrading the glass first and then the ingots, b) the ingots first and then the glass, or c) degrading the glass and ingots together, etc.

The results shown in this illustrative table, as well as most EQ6 runs, showed that in majority of the cases investigated more than 80% of the Gd will remain in the waste package. However, the two-stage scenario exposing the MD ingots first followed by the glass has the potential for higher Gd removal from the waste package.

In addition, geochemical sensitivity analyses investigating the influence $GdPO_4 \cdot H_2O$ formation and certain iron minerals identified have shown that, under certain EQ6/3 modeling assumptions, significant loss of Gd could occur. These calculations are discussed next.

Table 4.1 Cases Varying the Sequence of Degradation

md02_01	Maximum volume of ingots that fit in a DOE SNF canister with a minimum ingot liner thickness (1 mm). 2 stage run: Degrade glass and then expose ingots. High glass and drip rates, low ingot and SS rates.				
	Reactant Fully Degraded	**Time (years)**	**pH**	**% Gd Remaining**	**% U Remaining**
	Glass	14,839	8.81	100.00%	55.85%
	Ingots	535,140	7.82	99.48%	22.91%
	WP Liner	601,360	7.83	99.41%	19.53%
	End	633,780	8.05	99.26%	17.94%
md02_02	Maximum volume of ingots that fit in a DOE can with a minimum ingot liner thickness (1 mm). 2 stage run: Degrade glass and then expose ingots. Stage 1: high glass and drip rates, low Ingot and SS rates. Stage 2: change to high stainless rate and low drip rate (causes a low pH in the second stage).				
	Reactant Fully Degraded	**Time (years)**	**pH**	**% Gd Remaining**	**% U Remaining**
	Glass	14,839	8.81	100.00%	55.85%
	Ingots	16,721	7.02	100.00%	55.79%
	WP Liner	44,545	5.32	99.59%	55.68%
	End	634,170	7.90	99.54%	54.03%
md02_03	Maximum volume of ingots that fit in a DOE can with a minimum ingot liner thickness (1 mm). 2 stage run: Degrade ingots and then expose glass. Low glass rate, mean drip rate, high ingot and SS rates.				
	Reactant Fully Degraded	**Time (years)**	**pH**	**% Gd Remaining**	**% U Remaining**
	Ingots	1,506	5.44	77.35%	96.69%
	WP Liner	30,091	5.75	77.21%	96.42%
	Glass	229,650	8.68	77.21%	0.00%
	End	633,820	8.07	77.06%	0.00%
md02_06	Maximum volume of ingots that fit in a DOE can with a minimum ingot liner thickness (1 mm). Ingots and glass degrade together, low glass rate, mean SS and drip rates, low ingot rate.				
	Reactant Fully Degraded	**Time (years)**	**pH**	**% Gd Remaining**	**% U Remaining**
	WP Liner	60,134	5.85	100.00%	99.97%
	Glass	248,180	8.67	100.00%	29.17%
	Ingots	519,930	8.07	99.62%	19.09%
	End	633,800	8.07	99.37%	18.44%

4.3.3.1 Impact of Suppression of $GdPO_4 \cdot 10H_2O$ Formation

The suppression of formation of a mineral is an option available in EQ6 software code. Although the formation of $GdPO_4 \cdot 10H_2O$, is judged the most likely Gd mineral compound to be formed, such formation was artificially suppressed in two cases, to study the sensitivity of loss of Gd and/or retention of U. The results of such sensitivity calculations are shown in Table 4.2.

Because the formation of $GdPO_4 \cdot 10H_2O$ was mathematically suppressed, the mineral $GdOHCO_3$ forms instead of $GdPO_4 \cdot 10H_2O$. The conservative two-stage case md02_03 retains 77% of the initial Gd content with the formation of $GdPO_4 \cdot 10H_2O$. However, with $GdPO_4 \cdot 10H_2O$ formation suppressed, all Gd is predicted to be lost (md02-03). This case demonstrates a strong sensitivity of Gd retention to $GdPO_4 \cdot 10H_2O$ formation under the unlikely event of the ingots degrading in the absence of the glass plus the complete suppression of $GdPO_4 \cdot 10H_2O$ formation. Thermodynamic data indicate that $GdPO_4 \cdot 10H_2O$ will form, and since formation of this mineral is key to retaining the neutron absorber Gd, consideration should be given to subject the geochemistry reasons for suppressing such formation to peer review. This can be accomplished by a detailed analysis of the experiments on which the data is based to show applicability to the current situation, by further analysis and/or experiments.

Table 4.2 Cases Suppressing Formation of $GdPO_4 \cdot 10H_2O$

02_03 (base case)	Maximum volume of ingots that fit in a DOE can with a minimum ingot liner thickness (1 mm). 2 stage run: Degrade ingots and then expose glass. Low glass rate, mean drip rate, high ingot and SS rates.			
Reactant Fully Degraded	**Time (years)**	**pH**	**% Gd Remaining**	**% U Remaining**
Ingots	1,506	5.44	77.35%	96.69%
WP Liner	30,091	5.75	77.21%	96.42%
Glass	229,650	8.68	77.21%	0.00%
End	633,820	8.07	77.06%	0.00%
md02_03 Suppress $GdPO_4 \cdot 10H_2O$	Maximum volume of ingots that fit in a DOE can with a minimum ingot liner thickness (1 mm). 2 stage run: Degrade ingots and then expose glass. Low glass rate, mean drip rate, high ingot and SS rates.			
Reactant Fully Degraded	**Time (years)**	**pH**	**% Gd Remaining**	**% U Remaining**
Ingots	1,506	5.68	18.09%	96.71%
WP Liner	30,091	5.75	0.00%	96.44%
Glass	229,090	8.84	0.00%	0.07%
End	633,820	8.07	0.00%	0.00%
md02_06 (base case)	Maximum volume of ingots that fit in a DOE can with a minimum ingot liner thickness (1 mm). Ingots and glass degrade together, low glass rate, mean SS and drip rates, low ingot rate.			
Reactant Fully Degraded	**Time (years)**	**pH**	**% Gd Remaining**	**% U Remaining**
WP Liner	60,134	5.85	100.00%	99.97%
Glass	248,180	8.67	100.00%	29.17%
Ingots	519,930	8.07	99.62%	19.09%
End	633,800	8.07	99.37%	18.44%
md02_06 Suppress $GdPO_4 \cdot 10H_2O$	Maximum volume of ingots that fit in a DOE can with a minimum ingot liner thickness (1 mm). Ingots and glass degrade together, low glass rate, mean SS and drip rates, low ingot rate.			
Reactant Fully Degraded	**Time (years)**	**pH**	**% Gd Remaining**	**% U Remaining**
WP Liner	60,134	5.85	88.49%	99.98%
Glass	248,220	8.83	84.24%	29.22%
Ingots	519,930	8.07	83.37%	18.98%
End	633,820	8.07	83.12%	18.33%

In another case (md02_06), even with the $GdPO_4 \cdot 10H_2O$ formation suppressed, 83% of the Gd remains, as compared to the 99% that remained in the case where $GdPO_4 \cdot 10H_2O$ was allowed to form, since $GdOHCO_3$ is less likely to form than $GdPO_4 \cdot 10H_2O$. The suppression of $GdPO_4 \cdot 10H_2O$ formation does not affect the percentage of U remaining in either case. Such calculations further illustrate the effects of selective assumption and support the need for peer review of geochemistry calculations indicating complete loss of Gd.

4.3.3.2 Suppressing the Formation of Iron Minerals to Control Ionic Strength

Hematite and goethite are predicted to form in the waste package under normal running of EQ6. At early times in the EQ3/6 runs when the stainless steels are degrading, the pH is low and the ionic strength is high due to the presence of Ni^{++}, $Cr_2O_7^{--}$, and $HCrO_4^-$ ions in solution. If the most stable iron oxides (hematite and goethite) are suppressed in the EQ3/6 runs, then the more soluble $Fe(OH)_3$ forms. Allowing $Fe(OH)_3$ to form causes the pH to increase closer to neutral and the ionic strength to decrease to less than 1.0. For the purpose of investigating the sensitivity of such considerations, the formation of these minerals was mathematically suppressed to

determine if there is any effect on the results. Table 4.3 provides the results of suppressing the formation of various iron minerals.

Table 4.3 Cases Suppressing the Formation of Various Minerals

md02_03 (base case)	Maximum volume of ingots that fit in a DOE can with a minimum ingot liner thickness (1 mm). 2 stage run: Degrade ingots and then expose glass. Low glass rate, mean drip rate, high ingot and SS rates.					
Reactant Fully Degraded		**Time**	**pH**	**% Gd Remaining**	**% U Remaining**	**% Al Remaining**
	Ingots	1,506	5.44	77.35%	96.69%	99.75%
	WP Liner	30,091	5.75	77.21%	96.42%	99.74%
	Glass	229,650	8.68	77.21%	0.00%	99.74%
	End	633,820	8.07	77.06%	0.00%	99.74%
fe02_03	Maximum volume of ingots that fit in a DOE can with a minimum ingot liner thickness (1 mm). 2 stage run: Degrade ingots and then expose glass. Low glass rate, mean drip rate, high ingot and SS rates. Suppressed Fe minerals for 1st 1,000 years (andradite, goethite, and hematite).					
Reactant Fully Degraded		**Time**	**pH**	**% Gd Remaining**	**% U Remaining**	
	Ingots	1,506	5.03	60.79%	98.14%	
	WP Liner	30,091	5.75	60.23%	97.81%	
	Glass	229,220	8.84	60.23%	0.07%	
	End	633,820	8.07	60.09%	0.00%	
fs02_03	Maximum volume of ingots that fit in a DOE can with a minimum ingot liner thickness (1 mm). 2 stage run: Degrade ingots and then expose glass. Low glass rate, mean drip rate, high ingot and SS rates. Suppressed Fe minerals for 1st 150 years and suppressed $GdPO_4 \cdot 10H_2O$.					
Reactant Fully Degraded		**Time**	**pH**	**% Gd Remaining**	**% U Remaining**	
	Ingots	1,506	5.68	18.09	96.49	
	WP Liner	30,091	5.75	0.00	96.22	
	Glass	229,030	8.84	0.00	0.07	
	End	443,540	8.26	0.00	0.00	
he02_03	Maximum volume of ingots that fit in a DOE can with a minimum ingot liner thickness (1 mm). 2 stage run: Degrade ingots and then expose glass. Low glass rate, mean drip rate, high ingot and SS rates. Suppressed Hematite for the whole run.					
Reactant Fully Degraded		**Time**	**pH**	**% Gd Remaining**	**% U Remaining**	
	Ingots	1,506	5.21	78.12	96.76	
	WP Liner	30,090	5.27	75.07	95.87	
	Glass	276,660	8.27	74.92	0.00	
	End	633,820	8.12	74.54	0.00	
al02_03	Maximum volume of ingots that fit in a DOE can with a minimum ingot liner thickness (1 mm). 2 stage run: Degrade ingots and then expose glass. Low glass rate, mean drip rate, high ingot and SS rates. Suppressed Al minerals Diaspore and Gibbsite					
Reactant Fully Degraded		**Time**	**pH**	**% Gd Remaining**	**% U Remaining**	**% Al Remaining**
	Ingots	1,506	5.5857	76.84%	97.12%	99.67%
	WP Liner	30,092	5.7452	76.72%	96.89%	99.64%
	Glass	236,080	8.9339	76.69%	0.07%	99.62%
	End	633,820	8.0771	76.52%	0.00%	99.62%

The percentage of Gd remaining for these cases varies considerably. When the formation of the three iron minerals is suppressed in case fe02_03, the pH is lower from 1,000 to 3,000 years, and therefore more of the Gd is washed out of the waste package during that time. The case that also suppresses $GdPO_4 \cdot 10H_2O$ formation (case fs02_03) loses all the Gd, but it is unlikely that $GdPO_4 \cdot 10H_2O$ will not form. Case he02_03 retains more Gd because the pH is slightly higher from 1,000 to 1,200 years, as the ingots finish degrading, and that higher pH allows more $GdPO_4 \cdot 10H_2O$ to form.

Although the majority of these geochemistry calculations showed that more than 80% of the initial ingot Gd content will be retained as the waste package degrades, the sensitivity studies discussed above (albeit mathematically formulated and deemed unrealistic) identified a need for formulating waste package criticality models addressing depletion of Gd under such conditions and are discussed in the next section.

4.4 Criticality Analysis

4.4.1 *Items Important to Criticality Control and Acceptance*

As part of the criticality licensing strategy, items that are important to criticality control will be identified during evaluation of the representative fuel types designated by the National Spent Nuclear Fuel Program. As a result of the analyses performed for the evaluation of the codisposal viability of Al-based DOE-owned fuel, several items are identified as important to criticality control. The DOE SNF canister shell is naturally an item that is important to criticality control since it initially confines the fissile elements to a specific geometry and location within the waste package. The fissile mass limit in the canister, the linear density of the ^{235}U in the DOE SNF canister, and the fuel enrichment are also important to criticality control.

All calculations are based on a maximum of 38.3 kg ^{235}U per DOE SNF canister. The degraded configurations of the melt-dilute ingots bound the other types of Al-based DOE-owned spent nuclear fuel, as long as the limits on mass of uranium and its enrichment, and the linear density are not exceeded.

Hence, the total mass of fissile element (^{235}U) should not exceed the mass used in deriving the conclusions of this report, which is 38.3 kg of ^{235}U per DOE SNF canister. The maximum ^{235}U enrichment is 20 wt%. The linear density of the ^{235}U should not exceed 151 g/cm in the DOE SNF canister. This value is calculated by considering the maximum diameter and the maximum U content (18.2 wt%) for the MD ingots.

4.4.2 Criticality Computer Software

The Monte Carlo particle transport code, MCNP, Version 4B2LV, is used to estimate the effective neutron-multiplication factor (k_{eff}) of the codisposal waste package. The information regarding the code and its acceptance to use for the criticality analysis is documented in Reference 5.

The MCNP Version 4B2LV is used to estimate the k_{eff} values for various geometrical configurations of the MD-SNF in the 5-DHLW/DOE SNF-short waste package. The k_{eff} results represent the average combined collision, absorption, and track-length estimator from the MCNP calculations. The standard deviation (σ) represents the standard deviation of k_{eff} related to the average combined collision, absorption, and track-length estimate due to the Monte Carlo calculation statistics. The calculations are performed using ENDF/B-V continuous energy cross-section libraries that are part of the qualified MCNP code system.

The MCNP calculated results are presented in the following sections to demonstrate that all foreseeable intact and degraded configurations inside the codisposal waste package have been investigated and the values of k_{eff} are below the interim critical limit of 0.93. Although each of the degradation configurations discussed in Reference 1 is not specifically modeled, the criticality

configurations selected were designed to be bounding type analyses and representative of the waste package degradation configurations discussed previously.

4.4.3 Intact Geometry Criticality Analysis

The first criticality configuration selected was a breached, but intact-geometry representing a water intrusion situation. This criticality configuration (see Figure 4.6) represents a waste package, which has been breached, allowing inflow of water but internal components of the waste package have maintained their as-loaded geometry. This waste package criticality model assumed end boundaries which act as a reflective mirror (i.e., no neutron leakage). Variations of postulated water intrusion were examined to identify examine the range of calculated k_{eff} values for possible water intrusion conditions. The results are shown in Table 4.4.

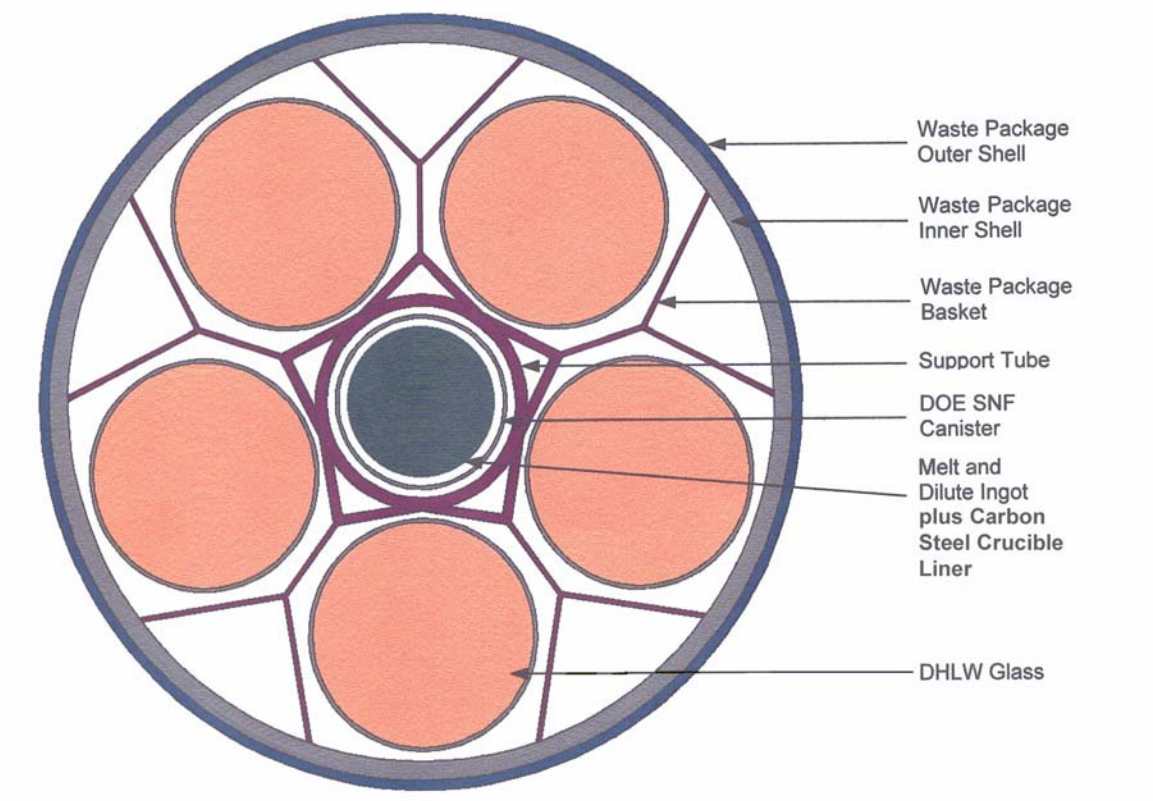

Figure 4.6 Cross-section View of the Codisposal Waste Package Used for Criticality Analyses Representing an As-Loaded Configuration

Intact cases were investigated first with a gadolinium loading of 0.5 wt% and the MD-SNF form completely filling the DOE SNF canister. For these cases, approximately 212 kg of U and 5.8 kg of Gd are used. Cases were run with the MD ingot composition filling the interior of the DOE SNF canister and the 10% void in the MD ingots dry, half-filled, and filled with water. Ingot/gap height combinations from 10 to 60 cm high were also run to investigate the effects of ingot height. An additional case was evaluated to determine the effect of 2 wt% Si in the MD ingot composition. This case simulates the composition of the MD-SNF form that is expected to result from the treatment of U-Al-Si base, Al-clad SNF.

The results show that the configuration with the wet ingot (10% void in the MD ingots filled with water) has higher $k_{eff}+2\sigma$ than the case with dry ingots. The addition of 2 wt% Si in the MD ingot has negligible effect to criticality (0.3561 versus 0.3571 for case without Si). The highest $k_{eff}+2\sigma$ occurs for the case with the wet ingot filling the entire DOE SNF canister. For this case $k_{eff}+2\sigma = 0.3571$. Variation of ingot height $k_{eff}+2\sigma$ results in a lower $k_{eff}+2\sigma$. Most important is the finding that a highly moderated case without Gd in the waste package resulted in a $k_{eff}+2\sigma$ below 0.90, thereby confirming, for the water-filled but intact waste package, no Gd is required in the MD ingots to maintain subcriticality. This finding is significant since it represents potential conditions prior to the onset of long-term degradation.

Table 4.4 Criticality Results for an Intact Geometry Waste Package

Ingot Height	Ingot Type	wt% Gd	$k_{eff}+2\sigma$
Full canister height	Dry ingot/Dry WP	0.5	0.1521
Full canister height	Wet ingot	0.5	0.3571
Full canister height	Dry ingot/Filled WP	0.5	0.2155
Full canister height	Half-wet ingot	0.5	0.2969
Full canister height	Wet ingot w/ 2 wt% Si	0.5	0.3561
19cm (1cm water gap)	Wet ingot	0.5	0.3475
29cm (1cm water gap)	Wet ingot	0.5	0.3464
59cm (1cm water gap)	Wet ingot	0.5	0.3450
9cm (1cm water gap)	Wet ingot	0.5	0.3482
8cm (2cm water gap)	Wet ingot	0.5	0.3014
8cm (2cm water gap)	Wet ingot	0.0	0.8949

The following sections discuss degraded conditions represented by the IP-1, IP-2, and IP-3 WP degradation scenarios described in Section 4.2.

4.4.4 Melt Dilute Ingots Degrade Prior to Other Internal Components of the Waste Package

Cases where the DOE/SNF waste form degrades before any other internal components of the waste package are investigated and corresponds to configurations IP-1-1A/B (see Section 4.2.2). This criticality configuration (see Figure 4.7) assumes a rapid degradation of the ingots in the canister while the rest of the codisposal package contents remain intact.

This configuration is different from the IP-1 illustration (see Figure 4.3) because the following conditions were added: a) the waste package internal components (but external to the DOE SNF canister) were considered intact and at the closest position relative to the MD-SNF, b) the waste package was completely filled with water (to maximize reflection and moderation), and c) the uranium is conservatively represented in the form of UO_2 that is distributed in the SNF canister. The incorporation of U degradation products as UO_2 maximizes the available water volume. This UO_2 is mixed with water, gibbsite [$Al(OH)_3$], and gadolinium and above this MD bearing mixture is a mixture of water and gibbsite. In all the cases considered, various amounts of the ingot Al material were assumed to remain in the canister and 90% of the original gadolinium was assumed

to be dissolved and removed. The amount of gibbsite that was removed from the canister was varied in order to observe the effects of different degrees of moderation.

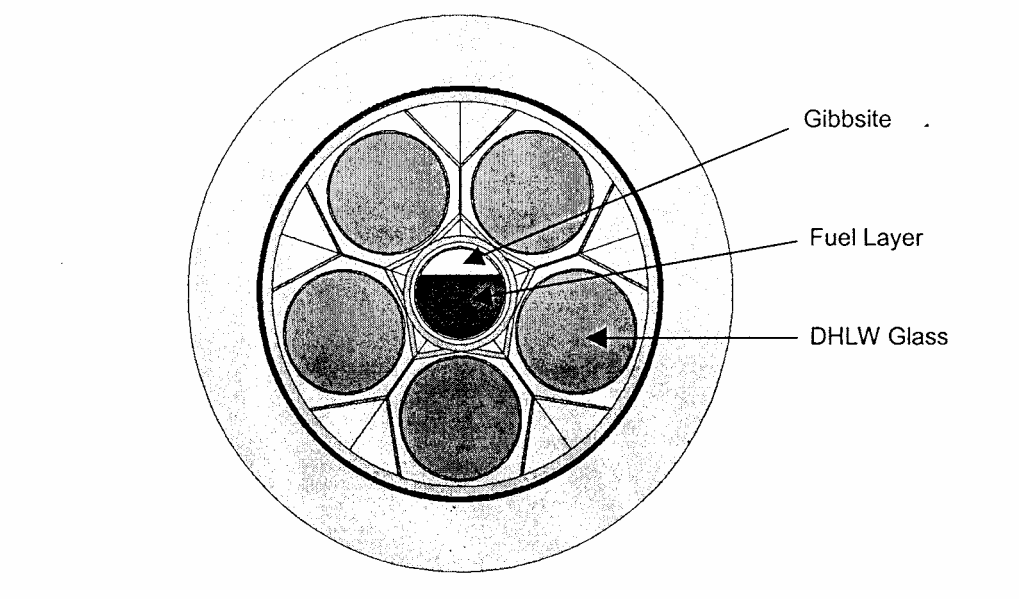

Figure 4.7 Cross-section View of Degraded Fuel in an Intact Waste Package

Cases were run with the height of the accumulation of degradation products in the canister varying the cord height from 10 to 40 cm. For each height investigated the gibbsite fraction was varied from 100% to 0% of the original mass (water replaces gibbsite). The results from geochemistry calculations indicate that less than 20% of the initial Gd content would be lost in this configuration and therefore these cases have a factor of 8 margin in Gd concentration. Degradation of most of the steel components would also be required to allow the loss of the Gd from the degraded MD ingots.

Table 4.5 shows results for criticality calculations where the void regions in the waste package are filled with water and the content of the gadolinium remaining in the waste package is chosen to be consistent with 90% of the original gadolinium leaving the system. Various mixtures of UO_2, gibbsite, and water are run to identify optimum compositions. Water replaces gibbsite as the water fraction goes up.

Table 4.6 shows results for calculations where the void regions of the waste package are left void. These cases have approximately 191.3 kg of U and 0.5 kg of Gd in the degraded fuel layer (constrained by the original dimensions of the ingots). The column titled water volume % in Tables 4.5 and 4.6 refers to the available volume after UO_2 is considered.

In all cases shown in Tables 4.5 and 4.6, all of the UO_2 was assumed to remain in the MD ingot canister and 90% of the original gadolinium was assumed to be "washed away." The amount of gibbsite that was "washed away" was varied in order to observe the effects of different degrees of moderation. Cases were run with the height of accumulated degraded products within the canister varying from 10 to 40 cm. For each height investigated the gibbsite fraction was varied from 100% to 0% of the original space not occupied by UO_2 (water replaces the gibbsite) in the layer. The water fraction in the gibbsite/water layer above the UO_2 - bearing layer matches the

UO_2 – bearing layer value. For all cases calculated, the $k_{eff} + 2\sigma$ was less than 0.80. The water filled cases (Table 4.5) had slightly lower values than those with empty void space (Table 4.6).

Table 4.5 Results for Degraded Fuel in Intact DOE SNF Canister and Waste Package with Void Space Filled with Water

Chord Height (cm)	Water Volume %	$k_{eff}+2\sigma$
10	0	0.6609
10	20	0.6791
10	40	0.6743
10	60	0.6736
10	80	0.6694
10	100	0.6699
20	0	0.7507
20	20	0.7671
20	40	0.7612
20	60	0.7610
20	80	0.7559
20	100	0.7488
30	0	0.7852
30	20	0.7822
30	40	0.7782
30	60	0.7804
30	80	0.7712
30	100	0.7682
40	0	0.7818
40	20	0.7816
40	40	0.7766
40	60	0.7800
40	80	0.7757
40	100	0.7740

4.4.5 Criticality Model Assumptions - All Components Internal to Waste Package Degraded

This condition represents the final stage of all degradation scenarios IP-2, IP-1-C, IP-2-A and IP-3A (see Section 4.2.2). Reference 4 gives the composition of the clay resulting from the degradation of the internal components of the waste package, which is referred as post-breach clay. If all of the U is eventually removed while $GdPO_4$ remains there is no potential for criticality. However, if the Gd is removed before the U is all gone criticality can occur. Homogenizing the Gd in the clay will only increase its effectiveness in absorbing neutrons.

Reference 4 also gives a post-breach degraded component composition for an alternative EQ3/6 case. In this case, the MD ingots degrade with the steel components of the waste package, but before the DHLW glass degrades and removes the U. $GdPO_4$ formation was suppressed in the EQ3/6 calculations which lead to led to the removal of Gd before the U is removed (see Section 4.3). MCNP cases were run where the amount of water in this mix is varied to determine the

optimum moderation. Figure 4.8 illustrates a criticality geometry representation of the degraded waste package in this final stage of degradation.

Table 4.6 Results for Degraded Fuel in Intact DOE SNF Canister and Waste Package with Void Space Empty

Chord Height (cm)	Water Volume %	$k_{eff}+2\sigma$
10	0	0.6922
10	20	0.6933
10	40	0.6874
10	60	0.6913
10	80	0.6886
10	100	0.6832
20	0	0.7831
20	20	0.7824
20	40	0.7765
20	60	0.7735
20	80	0.7759
20	100	0.7704
30	0	0.7994
30	20	0.7949
30	40	0.7949
30	60	0.7903
30	80	0.7854
30	100	0.7858
40	0	0.7947
40	20	0.7938
40	40	0.7981
40	60	0.7957
40	80	0.7902
40	100	0.7929

The maximum water fraction in the fuel-bearing layer is very conservatively assumed to be 50%. Cases were run with a layer of UO_2 mixed with water and for various mixtures of UO_2, water, and degraded components. Determination of the minimum mass of Gd or Hf is made to cause the $k_{eff}+2\sigma$ to fall below 0.93. The geochemistry calculation demonstrates that Hf remains in the DOE SNF canister or waste package in each of the limited number of conditions considered.

The effect of limited tilting of the waste package to the $k_{eff}+2\sigma$ was also investigated for a tilt angle of 13.72° as shown in Figure 4.9. The slope is chosen arbitrarily and the case was included for completeness.

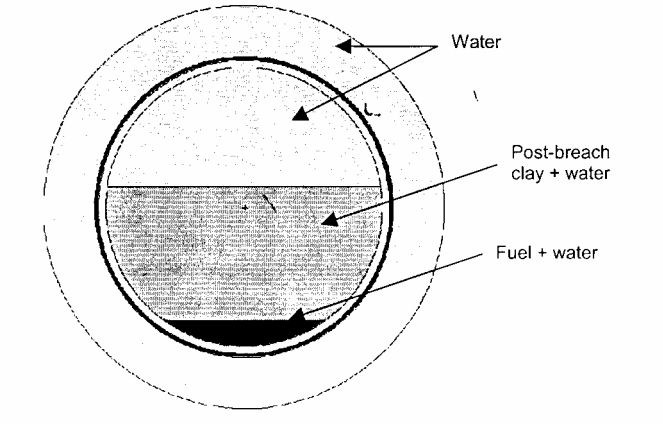

Figure 4.8 Criticality Model Cross-section View of WP with All Components Degraded

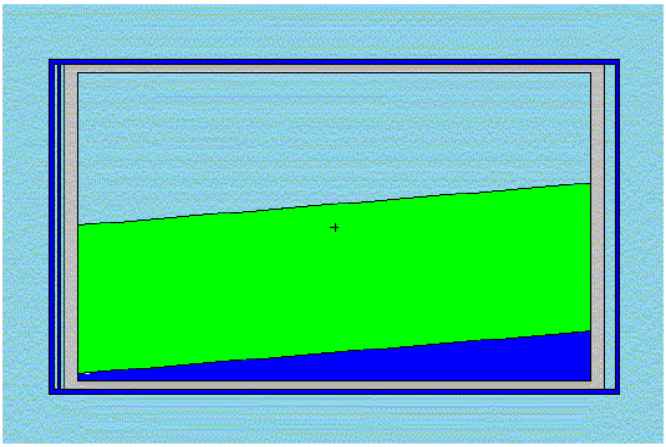

Figure 4.9 Side Sectioned View of Simulated Tilt of Waste Package

4.4.5.1 Stratified Layers of UO_2 and Post-breach Clay Without Neutron Absorber

Table 4.7 shows results for cases comprised of a fuel layer (UO_2 and water) on bottom and clay layer on top. The cases are for 50% water content and 75% water content in the fuel layer, respectively, and there is no neutron absorber in the fuel layer and are represented by Figure 4.8. These cases have 191.3 kg of U in the fuel layer.

Table 4.7 Results for Stratified UO_2 and Clay Inside Waste Package

Water Content (%)	$k_{eff}+2\sigma$
50	0.6949
75	0.9270

The result shows that there is no criticality concern for this particular configuration when the water content in the fuel layer is 50%. The case with 75% water content in the fuel layer shows

$k_{eff}+2\sigma$ of 0.9270, which is just below the critical limit. However, this configuration is not realistic due to lack of physical mechanism that could promote homogenization of 25% UO_2 with 75% water in stratified layers.

4.4.5.2 Layers of Fuel Mixed with Clay

Table 4.8 summarizes criticality analysis results for a layer of UO_2 mixed with the alternate post-breach clay composition corresponding to the extreme case where Gd is lost (see Section 4.3) sitting on the bottom of the waste package as illustrated by Figure 4.8. This post-breach clay composition, without U, is on top. All these cases have 191.3 kg of U in the fuel layer. Following are cases to demonstrate the minimum mass of Hf or Gd required to prevent criticality.

The results show that approximately 2.5% of the original Gd loading (131.4 g) must remain with this mixture to prevent criticality or approximately 25% of the Hf (approximately 5 kg) in the alternate MD ingot composition must remain. The geochemistry calculations[4] have demonstrated that Hf remains in the DOE SNF canister or waste package in each of the limited number of conditions considered. If confidence in the thermodynamic data for $GdPO_4$ formation is not sufficient to make the loss of Gd incredible, then the MD ingot composition with Gd and Hf will prevent a critical condition.

Table 4.8 Layers of Fuel Mixed with Clay

Case #	Case Description	Clay Content (vol%)	Water Content (vol%)	UO_2 Content (vol%)	Neutron Absorber		$k_{eff}+2\sigma$
					Type	Content (g)	
1	Configuration shown in Figure 4.8	25	50	25	-	-	0.8074
2		30	50	20	-	-	0.8490
3		40	50	10	-	-	0.9654
4		45	50	5	-	-	1.0182
5		47.50	50	2.50	-	-	0.9510
6		45	50	5	Gd	525.59	0.6642
7		45	50	5	Gd	262.8	0.7862
8		45	50	5	Gd	131.4	0.8825
9		45	50	5	Hf	525.59	1.0124
10		45	50	5	Hf	5255.9	0.9347
11	Similar to case 6, but the WP is tilted 13.72°	45	50	5	Gd	525.59	0.7285
12	Similar to case 8, but 30-cm thick water is used as a reflector	45	50	5	Gd	131.4	0.8096
13	Similar to case 8, but 30-cm thick tuff is used as a reflector	45	50	5	Gd	131.4	0.8307

The effect of tilting the waste package is investigated in case 11 (see Table 4.8), for the maximum tilt angle possible. The $k_{eff}+2\sigma$ increased to 0.7285, which is significantly less than the critical limit.

Replacing the reflective boundary condition with a 30-cm thick water or tuff reflector decreases $k_{eff}+2\sigma$. This shows that use of the reflective boundary condition for this case is very conservative.

4.4.6 Internal Components of the Waste Package Degraded (outside intact DOE SNF canister) and Intact Ingots

This section describes criticality configurations and calculations representative of degradation scenario IP-3 (see Figure 4.5). Criticality calculations presented in this section used the configurations shown in Figures 4.8 & 4.9.

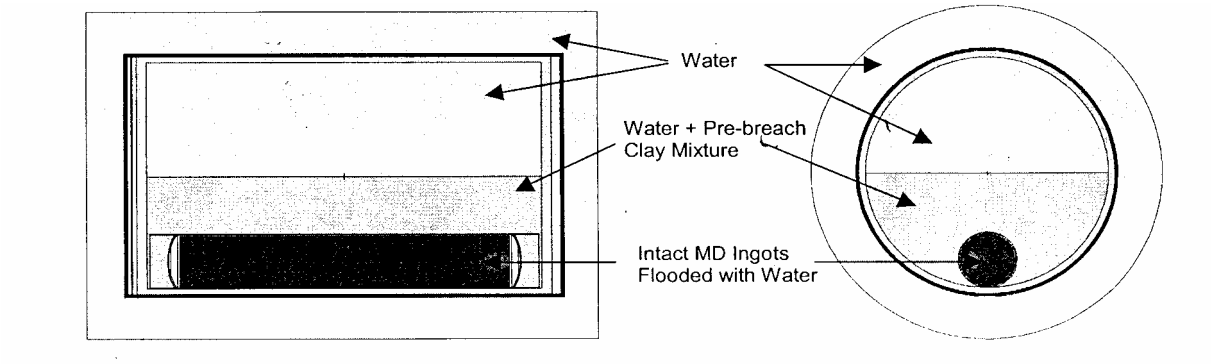

Figure 4.10 Cross-section Views of Criticality Model Used for an Intact DOE SNF Canister with Degraded Internal Waste Package Components

This configuration is different from that represented by IP-3 in the sense that the features considered most conservative were added, i.e. the waste package internal components (external to the DOE SNF canister, which was considered intact) were considered completely degraded into a homogeneous slurry in which the DOE SNF canister is completely immersed (for best reflection). The amount of water mixed in this clay varies. There is ^{238}U present in the slurry from the degraded glass, but it is neglected in these calculations. The MD ingot-bearing canister is assumed to have dropped down to the bottom of the waste package and is surrounded by a mixture of water and clay. Although the DOE SNF canister and MD ingots are assumed intact, they are also assumed fully flooded with water, which was determined to be the most reactive composition. Since the MD ingot is flooded, it is assumed contain 10% water by volume. This conservatively bounds the dry ingot case, since filling the porosity with water will increase (to the maximum limit) the moderation of the already under-moderated intact ingots. Both the gadolinium content of the ingots and the water volume fraction in the clay were varied. The density of dry pre-breach clay is 3.682 g/cm^3.

The next stage of degradation involves the configuration described above with the degraded MD ingots within the DOE SNF canister. The most conservative conditions identified in the previous calculations were used to characterize this combination. The minimum mass of Gd required to remain in the canister was identified and the effect of thinning the canister wall was also demonstrated. A case was run to simulate the effect of tilting of the DOE SNF canister inside the waste package as shown in Figure 4.11. The volume of the fuel region was conserved while the tilt angle was chosen as the maximum tilt that is conceivable for the DOE SNF canister inside the waste package, which is 13.72°.[5]

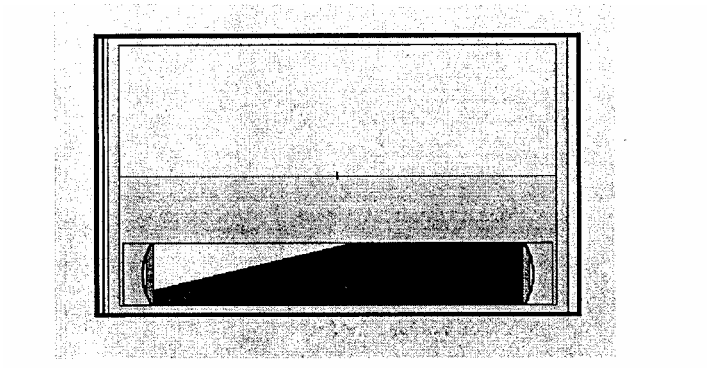

Figure 4.11 Cross-section View of Simulated Tilt of Intact DOE SNF Canister with Degraded Fuel and Degraded Internal Waste Package Components

An additional bounding criticality configuration was considered where ingots form an array inside the waste package and are surrounded by water as shown in Figure 4.12. The gadolinium linear density was chosen to be consistent with 90% of the original gadolinium leaving the system. Calculation was performed for short ingots (25.4 cm) forming an array with 9 units and for long ingots (76.2 cm) forming a array with 3 units inside the waste package.

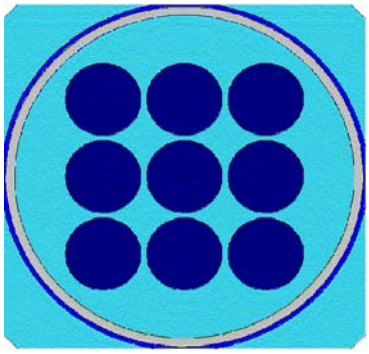

Figure 4.12 Array of 9 Ingots Inside the Waste Package Surrounded with Water

4.4.6.1 Wet Intact Ingots with Full or Partial Gd

Table 4.9 presents the results of the calculations for wet ingots with full Gd content of 0.5 wt% (5.8 kg/waste package) and a U content of 212 kg, corresponding to the MD fuel form completely filling the canister. The composition of the wet intact ingots is as described in Section 4.4.3 and corresponds to the highest k_{eff} values in Section 4.4.4. The basic case is illustrated in Figure 4.10, which shows the DHLW glass canisters and all the basket structure as degraded and forming a layer of pre-breach clay surrounding the DOE SNF canister. $k_{eff}+2\sigma$ is highest for the case when there is no water present in the pre-breach clay.

Table 4.10 presents the results of the calculations for wet ingots with partial Gd content of 0.05 wt% (0.58 kg/WP) and the MD fuel form completely filling the canister.

Table 4.9 Wet Ingots with Full Gd Content

Water Content in Clay (volume % [vol%])	keff+2σ
0	0.4264
20	0.3934
40	0.3736
60	0.3589
80	0.3521
100	0.3428

Table 4.10 Wet Ingots with Partial Gd Content

Water Content in Clay (vol%)	keff+2σ
0	0.6075
20	0.5601
40	0.5335
60	0.5146
80	0.5005
100	0.4949

Again, $k_{eff}+2\sigma$ is highest for the case when there is no water in the pre-breach clay.

Table 4.11 presents the results of the calculations for wet ingots with partial Gd content of 0 wt% to 0.025 wt% (0.263 kg/WP). The MD fuel form is filling the canister completely.

Table 4.11 Wet Ingots with Low Gd Content

Water Content in Clay (vol%)	Gd Content (g/WP)	keff+2σ
0	263	0.6586
20	263	0.6083
40	263	0.5840
60	263	0.5653
80	263	0.5530
100	263	0.5476
0	26.3	0.7503
0	0	0.7634

4.4.6.2 Intact Melt-Dilute Ingots within the Waste Package

Table 4.12 shows results for cases of ingots forming an array inside the waste package. The maximum value of $k_{eff}+2\sigma$ is 0.8157 for case with 3 ingots. The first case is an array of 9 short

ingots as shown in Figure 4.12 and the second case is for 3 long ingots. The ingots are sized such that they all fit within the DOE SNF canister. These cases have 0.05 wt% Gd.

Table 4.12 Results for Array of Ingots Inside Waste Package

Ingot Length (cm)	$k_{eff}+2\sigma$
25.4	0.7257
76.2	0.8157

4.4.6.3 Degraded Melt-Dilute Ingots

This configuration has degraded ingots within the intact DOE SNF canister as described in Section 4.4.4, but with degraded waste package internals. This configuration would be similar to the one shown in Figure 4.9, but with degraded MD ingots. The composition with which the highest $k_{eff}+2\sigma$ values are associated from Section 4.4.4 is used (the case in Table 4.6 with a chord height of 30 cm and a water volume of 0%). The pre-breach clay with 0% water, with which the highest k_{eff} values are associated in Section 4.4.4 is used. Table 4.13 presents the results for this configuration. These cases have approximately 191.3 kg of U. The initial case has 10% of the original Gd loading.

Table 4.13 Degraded Ingots in Intact DOE SNF Canister with Degraded Waste Package Internals

Case #	Case Description	Gd Content in WP		$k_{eff}+2\sigma$
		% of Initial Gd	(g)	
1	Degraded Ingots in the DOE SNF Canister and Intact Waste Package (chord height is 30 cm and water volume 0%)	10.0	525.59	0.8161
2		7.5	394.19	0.8914
3		5.0	262.80	1.0031
4		2.5	131.40	1.1425
5		1.0	52.56	1.2678
6	Similar to case 2, but the DOE SNF canister wall thinned to 0.3175 cm	7.5	394.19	0.8940
7	Similar to case 1, but the DOE SNF canister is tilted 13.72°	10.0	525.59	0.8443
8	Similar to case 2, but 30-cm thick water is used as a reflector	7.5	394.19	0.8810
9	Similar to case 2, but 30-cm thick tuff is used as a reflector	7.5	394.19	0.8810

4.5 Summary

The results of three-dimensional Monte Carlo criticality calculations for all anticipated intact- and degraded-mode configurations developed through the degradation analysis show that the requirement of $k_{eff}+2\sigma$ values less than or equal to the interim critical limit of 0.93 is satisfied for the MD codisposal package if at least 7.5% of the original Gd loading (394.2 g) remains mixed with the fissile material. In the alternate MD ingot composition, Hf remains in the DOE SNF canister or waste package under all conditions, therefore preventing a critical condition even if all Gd is removed from the system.

4.6 References

[1] ***"Disposal Criticality Analysis Methodology Topical Report,"*** YMP/TR-004Q, Rev. 01. Las Vegas, Nevada: Yucca Mountain Site Characterization Office. ACC: MOL.20001214.0001 (2000).

[2] ***"Evaluation of Codisposal Viability for Melt and Dilute DOE-Owned Fuel,"*** Bechtel SAIC Report TDR-EDC-NU-000006, Rev. 0 (July 2001).

[3] Vinson, D. W. and Serkiz, A. W., ***"Melt-Dilute Spent Nuclear Fuel Form Criticality Summary Report,"*** WSRC-TR-2001-00421 (September 2001).

[4] ***"EQ6 Calculation for Chemical Degradation of Melt and Dilute Waste Packages,"*** CAL-EDC-MD-000012 REV 00, Las Vegas, Nevada: Bechtel SAIC Company. MOL.20010719.0064 (2001).

[5] ***"Intact and Degraded Mode Criticality Calculations for the Codisposal of Melt and Dilute Ingots in a Waste Package,"*** CAL-EDC-NU-00006-REV. 00. Las Vegas, Nevada: Bechtel SAIC Company (2001).

5.0 DEGRADATION CHARACTERISTICS OF MD-SNF FORM

5.1 Introduction

The corrosion/dissolution/reconfiguration of Al-SNF under repository environments will differ from other DOE SNF, commercial SNF, and DHLW materials. The corrosion/dissolution and materials transport characteristics of Al-SNF is needed as part of the TSPA. Reconfiguration of the degraded Al-SNF is needed to evaluate near-field and far-field criticality.

In general, corrosion/dissolution/reconfiguration information is obtained through testing of SNF and SNF surrogates. Models are also developed to facilitate input to the TSPA. For example, the abstracted DOE SNF form models provide forward-reaction-rates (unmitigated by back-reaction) as input into TSPA analyses. Using these models, the forward reaction rate for the mobilization of radionuclides, as solutes or colloids, away from the waste form/water interface by contact with repository groundwater can be calculated. By using models for degradation that bound the actual rates for the DOE SNF and conservative estimates of the exposed surface area, assurance is provided that the repository performance is bounded.

The OCRWM has issued an Analysis/Model Report (AMR) to select and/or abstract conservative degradation models for DOE- (U.S. Department of Energy) owned spent nuclear fuel (DOE SNF) for application in the proposed monitored geologic repository post closure Total System Performance Assessment.[1] These models were derived by combining the empirical material degradation models, which predict degradation in units of mass of DOE SNF dissolved per unit of exposed surface area per unit time, with conservative estimates of the exposed surface area of the SNF available for water contact.

The information summarized in this section support the application of TSPA degradation models for Al-SNF. In addition, the information can be used as a database for accurate and representative corrosion/dissolution/reconfiguration information.

A recent ASTM standard guide (C1431-99) identified the considerations and test methods appropriate to evaluate corrosion/dissolution/reconfiguration of Al-SNF. The information in this section provides a description of testing performed in accordance with the standard guide.

5.2 Investigative Approach

A test program to understand the environmental degradation of Al-SNF was conducted as a part of the waste qualification program. Tests were performed on four irradiated fuel types[2]: UAl, UAl_x, U_3O_8, and U_3Si_2 and also on unirradiated UAl alloys ranging from 10 to 25 wt % U.[3]

The test samples for this study were both irradiated Al-SNF and unirradiated U-Al alloys. The irradiated fuel samples were prepared at Argonne National Laboratory. The unirradiated U-Al alloys were prepared at SRS.

Single-pass flow tests were utilized to measure dissolution rates of radionuclides from the Al-SNF. Unirradiated UAl alloys ranging from 10 to 25 wt% U were also tested.[3] Test variables were the solution chemistry, temperature (25 or 90 °C), alloy composition of the fuel, and alloy fabrication technique. The nominal J-13 composition was based on water chemistry from a well near the Yucca Mountain repository excavation site. The irradiated fuels were tested in nominal

J-13 well water (J-13), a low pH nitric solution and a bicarbonate solution at 25 °C.[2] Unirradiated testing was performed using solutions, which were nominal J-13, low pH, high pH and high Cl^- variants of J-13 at both 25 and 90 °C.

Static coupon tests were also performed on the unirradiated alloys to discern the effects of material degradation mechanism on the U dissolution rate. The tests were operated with the same solutions and at the same temperatures as the unirradiated flow through tests. In addition, the effect of galvanic coupling to stainless steel was also explored. The degradation was observed to follow a two-stage process. The results of these studies and their impact on understanding the environmental degradation rate are discussed herein. Data developed in these corrosion experiments provide preliminary input to perform an assessment of the materials redistribution and reconfiguration related to criticality concerns.

5.3 Experimental Procedure

5.3.1 Single-Pass Flow Tests

Single-pass flow tests were configured to measure the dissolution rates of radionuclides. These single pass flow tests maintained the uranium concentration below the solubility limits thereby allowing the forward rate of reaction of the fuel with the water to be measured. Such flow tests have been used previously to study the dissolution of commercial nuclear fuels.[4-5] The primary flow test parameters were fuel composition, water chemistry, and temperature. For the Al-SNF, two different flow test apparatuses were used, but each maintained the conditions of single pass and low flow rates.

Flow tests have been performed at Pacific Northwest National Laboratory (PNNL) in stainless steel systems where the water was mechanically pumped.[2] The PNNL test apparatus is shown schematically in Figure 5.1. Reciprocating plunger, positive displacement pumps pulsed the water at an average flow rate of 12 ml/h.

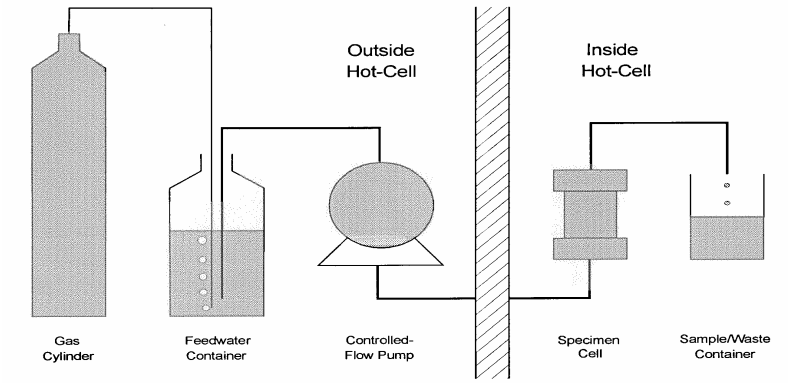

Figure 5.1 PNNL Flow Test Set-Up

Two different systems were used at SRS to control the flow rate, although both were similar to the PNNL design. All flow apparatuses were single pass and low flow. One system was a gravity feed. The flow initiated from a feed reservoir that fed four cells simultaneously through individual metered stopcocks. The stopcocks were adjusted to control the flow in a range of 10-15 ml/hr. The second drive system was similar to the PNNL design and used mechanical

pumps. The pumps maintained the flow rate at a more constant level. The water dripped from the stopcock into a feed line for each cell. Tygon tubing was used from the pump to the feed line.

As shown in Figure 5.2, the water flowed into the feed line and through the bottom of the flow cell, discharging from the top of the cell. The test cell was made from borosilicate glass and did not have filters since the samples were monoliths. Four coupons were in each cell and separated by a glass support tree. The cell was 12.7-mm ID and 63.5 mm long. Samples were taken each week for chemical analysis of uranium, aluminum, and the other primary constituents of the solution. Tests were conducted at room temperature and 90 °C.

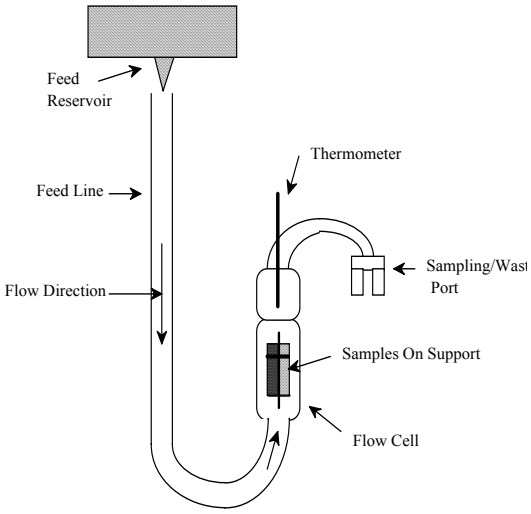

Figure 5.2 SRS Flow Test Cell

Samples that had the dimensions of 0.25 in. × 0.25 in. × 0.5 in. were exposed for 2-3 months. Surfaces were initially prepared with a 1000 grit finish. After testing, representative samples were examined using light and electron microscopy to characterize the corrosion morphology. Samples were also weighed to monitor weight changes resulting from corrosion or oxidation.

5.3.2 Static Testing

For the static tests, the procedures and apparatus were developed from ASTM G31.[6] The test apparatus consisted of a 2.5-liter glass vessel, heating mantle, and temperature controller. The static tests were conducted so that the U-Al samples were coupled to either a stainless steel or aluminum plate for investigating galvanic and crevice corrosion. Figure 5.3 shows a schematic of the test apparatus. Temperatures of 25 and 90 °C were used.

The samples were bolted to the plates with nylon hardware, which passed through a central hole drilled through the sample. The samples were 0.5-inch cubes with surfaces ground to a 1000 grit finish. Pre- and post-test characterization, including optical metallography and SEM, were performed for each sample to detect changes in structure. Samples were also weighed to monitor weight changes resulting from corrosion or oxidation.

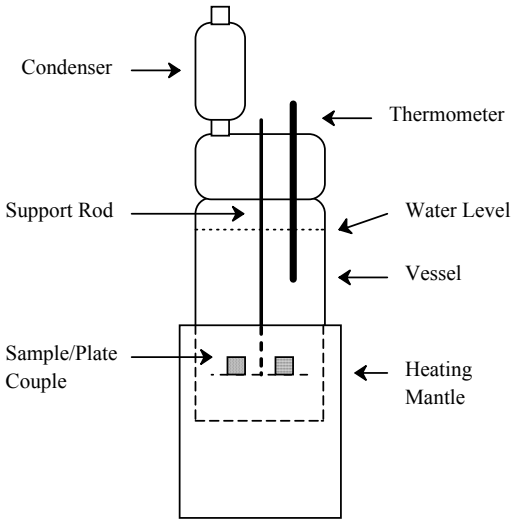

Figure 5.3 Schematic of Static Test Apparatus

The tests were performed for one month. Samples were removed from the vessel at intervals of 7, 14, and 28 days which provided data for the time dependence of the degradation rate. Solution samples were also taken to determine species dissolution. Chemical analyses included inductively coupled plasma electron spectroscopy (ICPES) for aluminum and Chemcheck™ for uranium. After the test, the solution was filtered to remove any particulate that was subsequently analyzed using scanning-electron microscopy (SEM) and EDS.

The samples were 0.5 inch cubes which were mounted in a cold cure epoxy. The surface was polished to an 800 grit surface finish and cleaned prior to immersion. After the test, a sample was visually evaluated for corrosion morphology. Solution samples were taken after testing for chemical analysis.

5.3.3 Irradiated Al-SNF Samples

The irradiated samples for the PNNL flow test were sectioned from four irradiated Al-SNF each with a different fuel material. The fuel materials were U-Al, UAl_x-Al (x = 3 or 4), U_3O_8-Al, and U_3Si_2-Al. These plate-type fuels ranged in thickness from 1.3-4.1 mm. The aluminum cladding was removed to expose the actual fuel material on one side. All the coupons, 12 mm by 25 mm, were polished to 1-μm surface finish. The geometric surface areas of the polished faces were ~2.8 cm^2 and of the unpolished edges of exposed fuel meat were 0.2 to ~1.4 cm^2. Photomicrographs of the four fuels are shown in Figure 5.4. The results with the samples with removed cladding can be used to project the potential for release of radionuclides from a repository after the cladding has corroded away or in the event that the fuel is somehow physically damaged after emplacement.

The radionuclides and quantities of U and Al in the irradiated test specimens were measured from three 0.1 gram pieces cut from a coupon of each fuel type. The pieces were completely dissolved through the following steps: 6 M HCl to dissolve the aluminum and concentrated nitric to dissolve the fuel material. The U_3Si_2 fuel did not fully dissolve, so the residue was treated by fusing with KOH, and then dissolving in a mixture of HNO_3 and HCl. The solution analyses included U, Al, $^{239+240}Pu$, ^{238}Pu, ^{137}Cs, ^{99}Tc, and ^{90}Sr and the results are shown in Table 5.1. The listed analyses are for fuel core and aluminum matrix materials.

The table lists the averages of the triplicate analyses except for the UAl_x fuel where one of the three analyses differed somewhat from the other two and was not included in the average. Residue from the initial U_3Si_2 dissolution was found to be predominantly Si and, in particular, contained completely negligible amounts of the elements and radionuclides. The totals, obtained by adding the Al and original U quantities, were 95-100% of the weights of the analyses specimens. This high percentage was considered a good mass balance agreement.

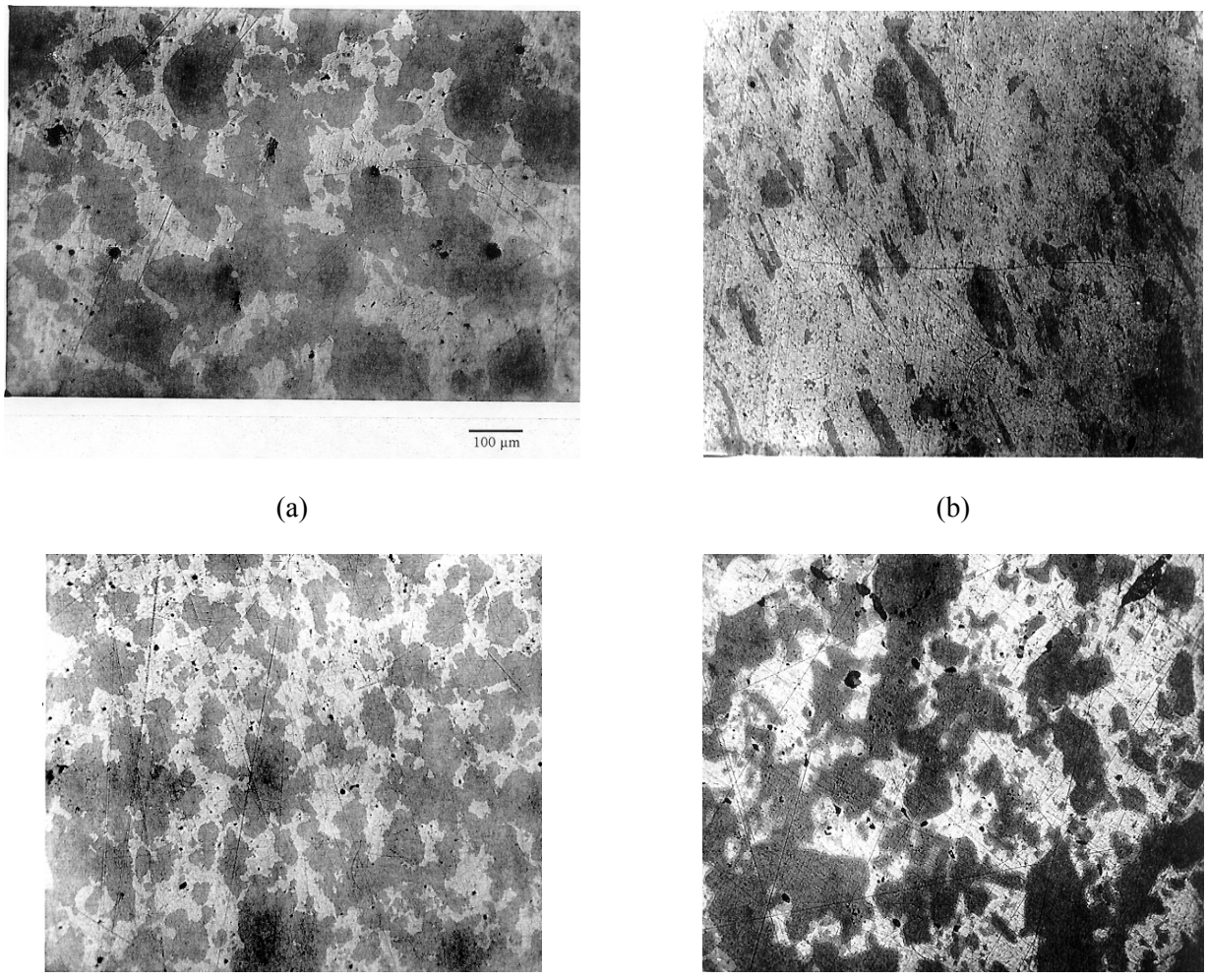

Figure 5.4 Photomicrographs of Al-SNF: a) UAl_x, b) UAl, c) U_3O_8, d) U_3Si_2

Table 5.1 Radionuclides Content of Irradiated Al-SNF*

Fuel	Enrich. (%^{235}U)	Burnup (%)	Al (g/g)	U (g/g)	$^{239+240}$Pu (mCi/gU)	^{238}Pu (mCi/gU)	^{137}Cs (mCi/gU)	^{99}Tc (mCi/gU)	^{90}Sr (mCi/gU)
UAl_x	45	73	0.750	0.138	1.83	21.7	1240	0.113	1010
UAl	80	40	0.763	0.144	0.61	28.8	1210	0.108	1050
U_3O_8	45	72	0.763	0.134	1.69	16.5	1140	0.106	960
U_3Si_2	20	93	0.387	0.449	1.26	15.5	500	0.040	410

* Activities of radionuclides are based on U content. The quantities for Al and U are based on total sample weight.

5.3.4 Unirradiated U-Al Alloy Samples

In addition to the irradiated fuels, a range of U-Al alloys were also tested. The compositions were 10, 13.2 (eutectic), 19, and 25 wt % U with the balance aluminum (10 UAl, 13 UAl, 19 UAl, and 25 UAl). The 19 UAl sample was unirradiated version of the UAl fuel. This alloy was tested at both PNNL and SRS, while the remaining U-Al alloys were tested at SRS only.

The U-Al alloys were produced from a supply of bulk aluminum ingots (1100 Al) and depleted uranium. The materials were melted in an induction furnace between 800 and 1400 °C, depending on the alloy composition. The alloys were cast into molds and cooled in air. Metallographic analyses indicated that the microstructures were fairly uniform throughout the cross-section of the ingots. Several ingots of the 13.2 and 25 UAl alloys were extruded and rolled to produce a wrought structure. The wrought and cast structures were representative of either unprocessed or melt and diluted Al-SNF, respectively. Samples were cut from the ingots with either an electric discharge machine or a mill.

The surfaces of the coupons were examined using SEM prior to initiating the tests. Figure 5.5(a) shows a micrograph of the 10 UAl cast material. The dark area was the primary aluminum phase, while the light, skeletal areas are the eutectic phase. The eutectic consists of the lamellae of aluminum and the UAl_4 phase. The cast microstructure consists mostly of aluminum dendrites with eutectic filling the interdendritic regions. Figure 5.5(b) shows a micrograph of the 13.2 UAl cast material, the eutectic composition. A greater fraction of the surface is covered with eutectic than was observed for the 10 UAl cast.

Additionally, a few light, blocky structures are present in the midst of the aluminum matrix. These blocky structures are the UAl_3 phase. Figure 5.5(c) shows a micrograph of the 25 UAl cast material. The UAl_3 phase was much more apparent at this composition. Small regions of the eutectic phase were also seen. The diamond shape particles with the dark center (i.e., aluminum phase) are also the UAl_4 phase. Figure 5.5(d) shows a micrograph of 13.2 UAl wrought material. Due to the rolling of the material the particles were crushed and are aligned in the rolling direction.

5.3.5 Test Solutions

The solutions for all the tests were based on the composition of water taken near a proposed repository site. The nominal composition of water sampled from well J-13 is shown in Table 5.2. Variations of the J-13 water were used to simulate various scenarios due to interactions with soils and other waste forms. The J-13 water with a pH of ~8 had a nominal composition similar to that used in Reference 7. For the PNNL flow tests two other water chemistries were used, 2×10^{-2} M $NaHCO_3$ at pH of 8, and nitric acid at pH of 3.

Three other variants of J-13 were used for the remaining tests: low pH (~3), high pH (~11), The low and high pH J-13 waters were made by additions of either nitric acid or sodium hydroxide, respectively. Additional sodium chloride was added to make the high Cl J-13. The conductivities of these J-13 waters ranged as follows: nominal J-13, 250-350 μS; low pH, 450-600 μS; high pH, 1200-7500 μS; high Cl, 400-450 μS.

Solution analyses were performed on small samples taken during the tests at various intervals to determine the dissolution and corrosion rates. For the irradiated coupons, 10 mL samples were collected initially twice a week and then approximately once each week. Samples were analyzed for the following elements and radionuclides: U, Al, $^{239+240}$Pu, ^{238}Pu, ^{137}Cs, ^{99}Tc, and ^{90}Sr. For the unirradiated coupons, sampling was similar, but analyses included only U and Al.

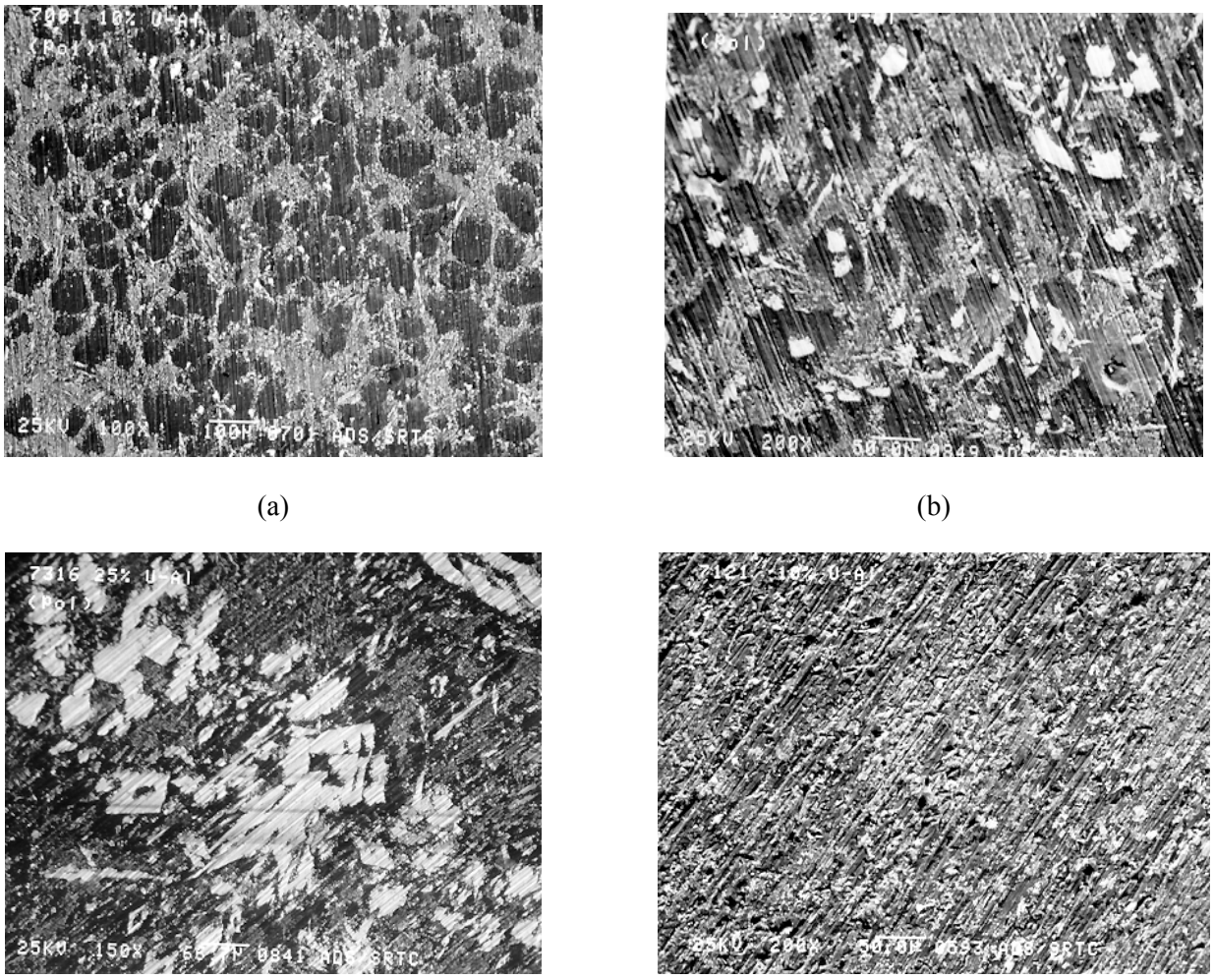

(a) (b)

(c) (d)

Figure 5.5 Microstructures of U-Al Test Samples: a) 10 UAl cast, b) 13.2 UAl cast, c) 25 UAl cast, d) 13.2 UAl wrought and high chloride (60 ppm Cl⁻).

Table 5.2 Solution Composition of Nominal J-13 Well Water

Constituent	(ppm)	Constituent	(ppm)
Calcium	13	Chloride	7.1
Potassium	5.3	Fluoride	2.3
Magnesium	1.9	Nitrate	8.1
Sodium	44	Sulfate	18
Silicon	33	Carbonate	120

5.4 Experimental Results

The preliminary dissolution rates of radionuclides from the enriched Al-SNF were based on the results of flow tests from both irradiated and unirradiated samples. In conjunction with this test, corrosion testing was conducted using static, electrochemical, and galvanic tests to determine the effect of the degradation mechanism of Al-SNF on the dissolution rates of the radionuclides. The results from the different tests are presented in the following section.

5.4.1 Irradiated Al-SNF Samples

Dissolution rates for the irradiated samples were measured for not only the primary constituent uranium, but also for aluminum, cesium, plutonium, strontium, and technetium. The average dissolution rates for uranium from the different fuels are presented in Table 5.3 for the three test solutions, that is the J-13 well water simulant, nitric acid, and bicarbonate. The dissolution rate (R) was calculated by the following equation:

$$R = (C_i \times F) / A ,$$

where C_i is the elemental concentration of either U or Al (ppm), F is the flow rate, 0.2 ml/min, and A is the geometric surface area (m^2) of the sample exposed to the solution. The dissolution data, in general, were variable, so a standard averaging protocol was not used.

Table 5.3 Uranium Dissolution Rates at 25 °C for Al-SNF ($mgU/m^2/d$)[2]

Fuel		J-13 Well Water	Nitric Acid	Bicarbonate
Unirradiated UAl*		0.20	230	25
Irradiated	UAl	0.17	99	33
	UAl_x	0.19	28	22
	U_3O_8	0.14	31	33
	U_3Si_2	0.22	36	36

* Al-19 wt% U sample was prepared in a manner similar to fuel (cast and rolled)

During the initial stages of the test in the J-13 well water, the water samples were found to be contaminated from uranium in the hot cell. The average dissolution rates for the radionuclides were based on the rates calculated between 50 and 209 days. As shown in Table 5.3, the U dissolution rates from the four fuels varied between 0.14 to 0.22 $mgU/m^2/d$. Figure 5.6 shows the dissolution rate of uranium (and other radionuclides) for J-13 at 25 °C over the course of the test. These dissolution rates, however, are normalized to a calculated surface area of the fuel meat exposed to the test solution, which for UAl was 31% of the geometric area. The Al concentration in the analysis sample was generally below the detection limit of 60 μg/L except for the first

sample drawn at 12 days. The Al concentrations in the J-13 corresponded to a dissolution rate of 30-50 mg Al/m^2/d. Tc was not analyzed for the J-13 water because the low U concentrations indicated the Tc concentration would be below the detection limit. The other radionuclides varied for each of the fuels, but in general were similar or lower than that of uranium. The Cs and Sr dissolution rates for UAl and U_3Si_2 were the only exceptions and were higher than that of uranium.

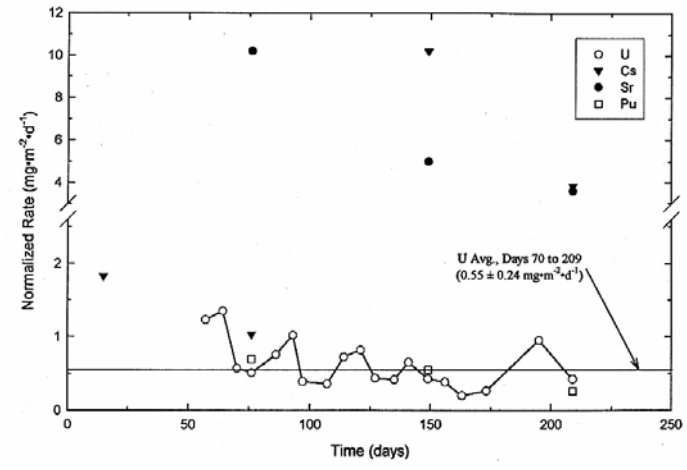

Figure 5.6 Dissolution Rate(s) in Nominal J-13 at 25 °C for Irradiated UAl

The U dissolution rate in the nitric acid ranged between 28-99 mgU/m^2/d for the four fuels as shown in Table 5.3. The initial 8-day transients were not included in calculating the average. The data for the U_3O_8 sample were not stable for the first 44 days, so these were excluded from the average. The UAl coupon had the most variable data over the course of the 236-day test period as shown in Figure 5.7 and also had the highest average dissolution rate. The dissolution rates in the figure are normalized to a calculated surface area of the fuel meat exposed to the test solution, which for UAl was 31% of the geometric area. Aluminum, in the range of 1000 mg Al/m^2/d, dissolved faster than the uranium for all the fuels except for the UAl coupon. For UAl, the U and Al dissolution rates were similar. Cs and Sr dissolution rates from the fuels were also similar to that of uranium, except for U_3Si_2 where the rates were higher. The Pu dissolution rates were similar to that of uranium for all the fuels. The Tc concentrations were low and irregular, but sufficiently above the detection limit to negate analytical uncertainty. The Tc concentration also depended on the fuel. For example, with UAl_x the Tc data were congruent with the U data, whereas for the UAl fuel several points were abnormally high.

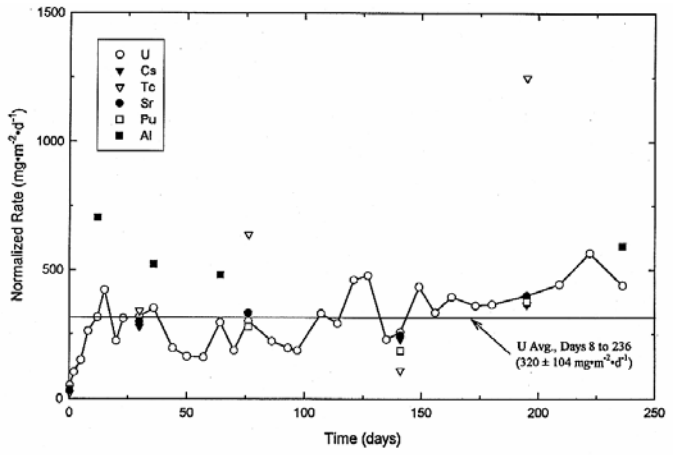

Figure 5.7 Dissolution Rate(s) in the Nitric Acid Solution at 25 °C for Irradiated UAl

The measured U concentrations in the bicarbonate solution over the 222-day test period were more variable than in the other two solutions as shown in Figure 5.8 for the UAl fuel. The dissolution rates in the figure are normalized to a calculated surface area of the fuel meat exposed to the test solution, which for UAl was 31% of the geometric area. The stable data for the fuels also varied, although the U dissolution rates were fairly similar, ranging from 22 to 36 mgU/m^2/d as shown in Table 5.3. The U concentration dropped after 135 days for all but the U_3Si_2, which remained stable. Initially, the Al dissolution rate was higher than that of uranium, but then had similar rates for the remainder of the test. The Cs and Sr dissolution rates were similar to that of uranium, except for U_3Si_2 where the rates were higher. The Pu dissolution rates were lower than that of U for all the fuels and the Pu concentration was on the order of 10^{-9} mol/L. As for the nitric acid solution, the Tc dissolution rates were inconsistent and varied for all the fuels.

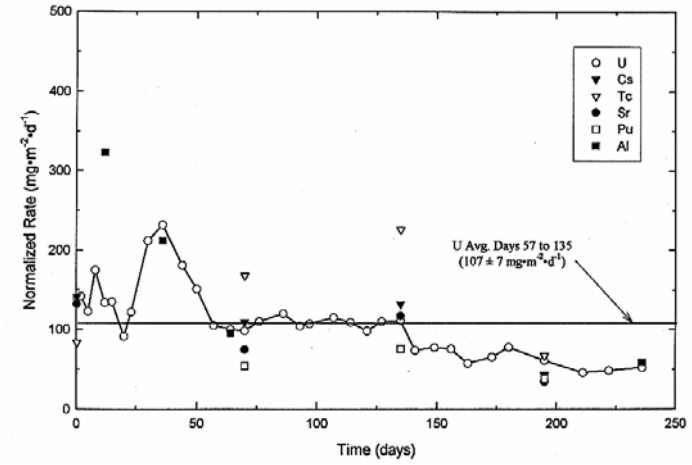

Figure 5.8 Dissolution Rate(s) in the Bicarbonate Solution at 25 °C for Irradiated UAl

5.4.2 Unirradiated U-Al Alloy Samples Tests

The unirradiated test samples were alloys with the following U concentrations: 10, 13.2, 19, and 25 wt %. The 19 UAl is discussed separately from the other alloys since its composition is

similar to the irradiated U-Al fuel. Additionally, the other alloys were tested in variants of J-13 and not the nitric acid and bicarbonate solutions.

5.4.2.1 19 U Al Alloy Tests Single-Pass Flow Tests

The dissolution rates of aluminum and uranium were measured in the same solutions as the irradiated coupons at PNNL. For the J-13 water, the U dissolution rate was 0.2 mgU/m^2/d for the 113-day test (see Table 5.3). From the limited aluminum measurements, the Al dissolution rate appeared to be greater than that of uranium. In the nitric acid solution, the Al dissolution rate was also greater than the U dissolution rate, which was 230 mgAl/m^2/d. In the bicarbonate solution, however, the U and Al dissolution occurred at the same rate of 25 mg/m^2/d.

The microstructural characteristics of the alloy varied depending on the solution chemistry as shown in Figure 5.9(a)-(d). In Figure 5.9(a), which shows the untested coupon, the microstructure consisted of U-Al particles embedded in an Al matrix. After 113 days, the J-13 water had a minimal effect as shown in Figure 5.9(b). In the nitric acid, both the matrix and U-Al particles were attacked as shown in Figure 5.9(c). Since the aluminum dissolution was greater than that of the uranium, the U-Al particles typically protruded from the surface. The 19 UAl in the bicarbonate solution had a mud-cracked appearance typical of aluminum oxide. In Figure 5.9(d), the coupon was washed to remove any dried salts.

A duplicate test was performed at SRS with another 19 UAl coupon to assess alloy variability. The U dissolution rate from this test was approximately 1.8 mgU/m^2/d, which was ten times greater than the first measurement. Some of the variability may have been associated with experimental error and differences in the test procedures, but the trends of each experiment are similar (i.e., both samples exhibiting dissolution rates close to the minimum observed).

5.4.2.2 10, 13.2, and 25 UAl Alloy Single-Pass Flow Tests

The flow test for these unirradiated alloys was performed to measure U dissolution rates and to characterize Al-SNF degradation mechanisms and the effects of the fuel microstructure. The flow test results consisted of the dissolved U and Al concentrations, the visual and microscopic observations of the coupons, and the weight changes of the alloys. The U dissolution rates were similar for the three alloys and were dependent primarily on the solution chemistry, temperature, and the subsequent corrosion mechanisms.

The U and Al dissolution rates are shown in Table 5.4 for the different alloys in each J-13 water chemistry at temperatures of 25 and 90 °C, although the data at 25 °C is limited. These average values were calculated from measured weekly concentrations and are not normalized to the initial elemental inventory. The U dissolution rate was always less than that for aluminum, generally by an order of magnitude. The elements reacted differently to the J-13 waters, thus leading to differences in the sensitivity of dissolution rates to solution chemistry. As can be seen in the table for the low and high pH J-13, U dissolution was less sensitive to pH changes than aluminum. The order of aggressiveness in increasing severity for each element were as follows: for U, high Cl <nominal<high pH<low pH; for Al, high Cl ≈nominal<low pH<high pH. From the available data, a temperature change of 25 to 90 °C increased the dissolution rates. The rates did not increase as much in the low pH J-13. Some long-term flow tests are continuing which may further define the effect of temperature.

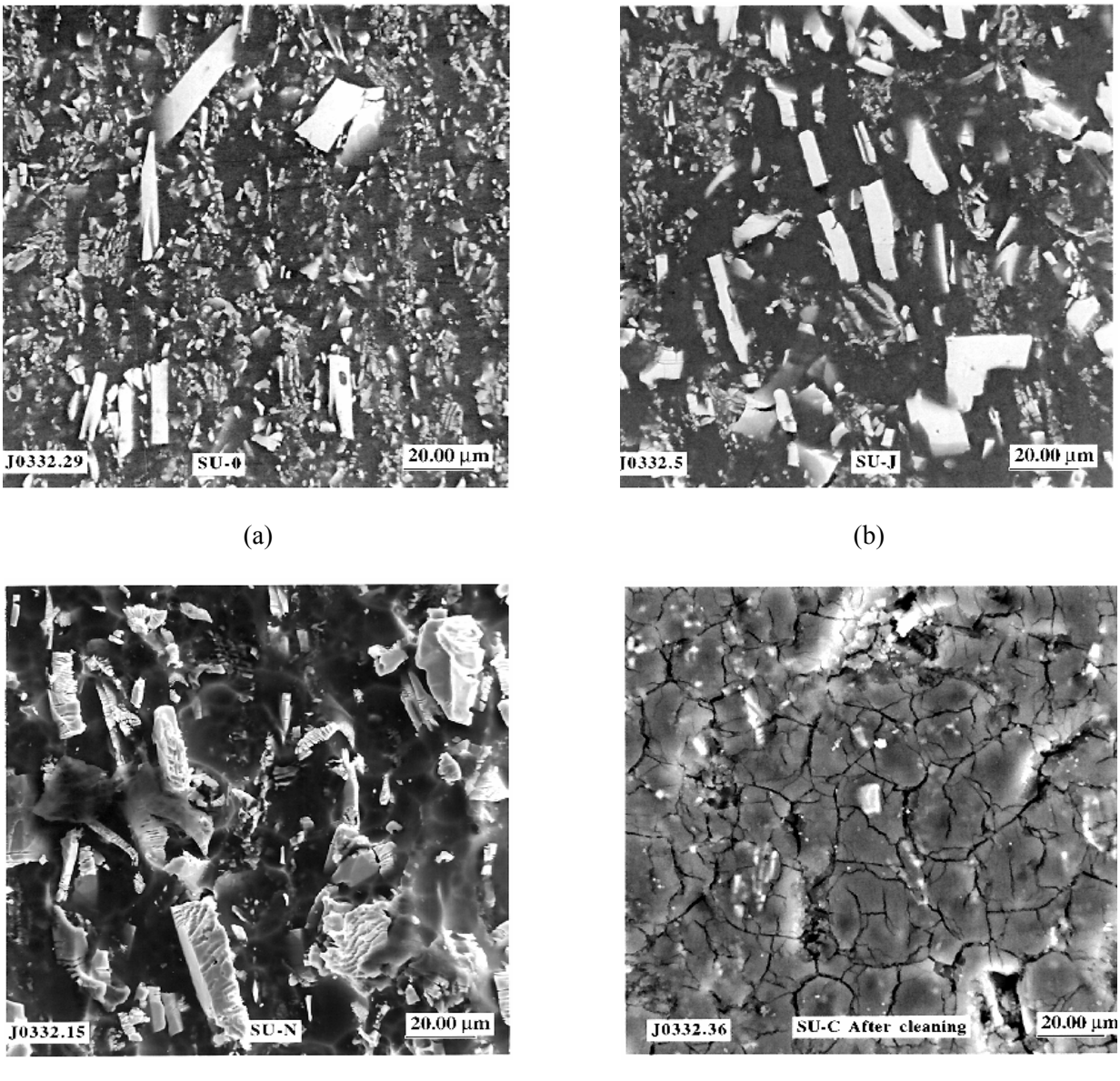

Figure 5.9 19 UAl Microstructure: a) Before Test, b) After Test in Nominal J-13, c) After Test in Nitric Acid Solution, d) After Test in Bicarbonate Solution

The trends of the U and Al dissolution rates, which are shown in Figure 5.13, were dependent on both solution chemistry and temperature. The dissolution rates shown in the figures were based on the geometric surface area of the sample. Figure 5.10 shows the U dissolution rates at 90 °C for the 13.2 UAl cast coupons in the different J-13 waters. The other alloys had similar trend curves. As can be seen in the figure, the uranium dissolution was initially high and then decreases. Especially for the more aggressive solutions of high and low pH, rate increases were observed near the end of the test. Even with these perturbations, the dissolution rates of uranium were found generally to have similar trends as reported for commercial nuclear fuel.[4-5] As shown

in Figure 5.11, aluminum also had high initial rates that dropped off. Increases in rates were not observed later in the test. The high pH data was not shown because the values were much larger than the other waters. At 25 °C the trends differ with rates increasing later in the test period or remaining constant for most of the test period. Figure 5.12 shows the U dissolution rates at 25 °C for the different solutions. The aluminum rates in the low pH J-13 were more variable for the 13.2 and 25 UAl alloys as shown in Figure 5.13.

Table 5.4 Average Uranium and Aluminum Dissolution Rates (mg/m^2/d) for Unirradiated UAl Alloys from Single-Pass Flow Tests*

		25 °C				90 °C			
Alloy/ Fabricat.	Water Chemistry	Uranium		Aluminum		Uranium		Aluminum	
		Mean	σ	Mean	σ	Mean	σ	Mean	σ
13.2/cast	J-13	1.7	0.9	BD	BD	24.2	53.8	225	228
13.2/wrt		ND	ND	ND	ND	8.2	5.6	102	120
25/cast		ND	ND	ND	ND	26.9	27.7	120	121
19/wrt		1.8	0.8	BD	BD	ND	ND	ND	ND
13.2/cast	Low pH	139	78	1110	544	215	120	1350	699
13.2/wrt		ND	ND	ND	ND	188	115	1110	501
25/cast		227	111	973	544	420	444	1333	712
13.2/cast	High pH	ND	ND	ND	ND	86	57	5250	3045
13.2/wrt		ND	ND	ND	ND	248	210	5440	2731
25/cast		ND	ND	ND	ND	96	105	4710	2034
13.2/cast	High Cl	1.4	0.6	BD	BD	18	9	198	143
13.2/wrt		ND	ND	ND	ND	8.4	3.9	157	163
25/wrt		2.6	3.0	BD	BD	14	7.0	134	97

* ND and shading indicates that data were not measured for this condition.
BD indicates that the measured value is below the detectable limit of the technique.

The concentration of aluminum ions in the water followed a similar trend to the uranium profiles, peaking initially then decreasing to a lower value. This trend was also observed for the high pH solution in contrast to the uranium concentration. The aluminum concentrations were lowest in the nominal and high Cl J-13 averaging at about 1 ppm, Peak values, however, differed; the peaks were approximately 2 and 12 ppm for nominal and high Cl J-13, respectively. For the low pH solutions, the average and peak concentrations were ~5 ppm and 13 ppm, respectively. For the high pH solutions, the average and peak concentrations were 20 ppm and 60 ppm, respectively. The higher rates in the high pH J-13 corresponds to the lack of significant oxide formation on the U-Al samples.

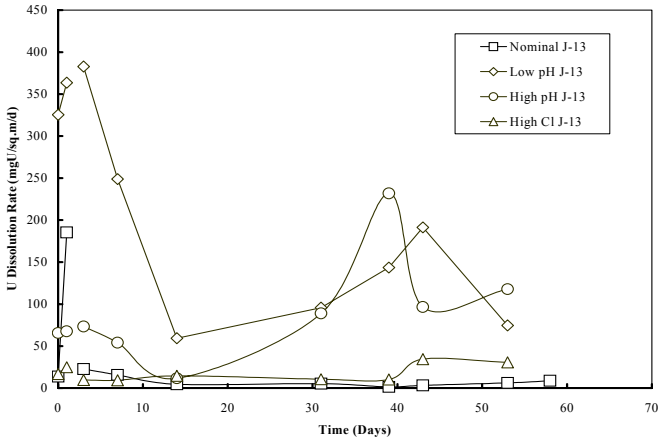

Figure 5.10 U Dissolution Rates for Unirradiated Cast 13.2 UAl Coupons in J-13 Waters at 90 °C

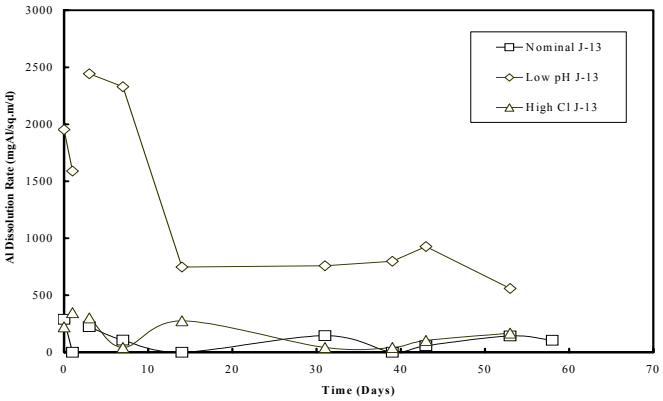

Figure 5.11 Al Dissolution Rates for Unirradiated Cast 13.2 UAl Coupons in J-13 Waters at 90 °C

At 90 °C the alloys exposed to nominal J-13, 13.2 UAl (cast and wrought) and 25 UAl (cast), had variable surface characteristics. The surfaces generally darkened although spotty regions of shiny metal remained after 13 weeks. Various amounts of white corrosion products and surface roughening were observed. The 25 UAl alloy had the most uniform surface. In low pH J-13, the surfaces were smooth, were covered with a thin brown/white oxide layer which was mottled, and had minimal voluminous corrosion products. In contrast to the nominal J-13 results, the 25 UAl alloy had the most variable surface morphology. The U-Al alloys exposed to the high pH J-13 had a heavy layer of corrosion products, which covered a darkened, smooth appearing surface. The 13.2 UAl alloy had the fewest corrosion products. In high Cl J-13, the surfaces had many localized spots of voluminous white corrosion products. The remainder of the surface had a dark and rough appearance. In this water, the 13.2 UAl alloy had the most corrosion products.

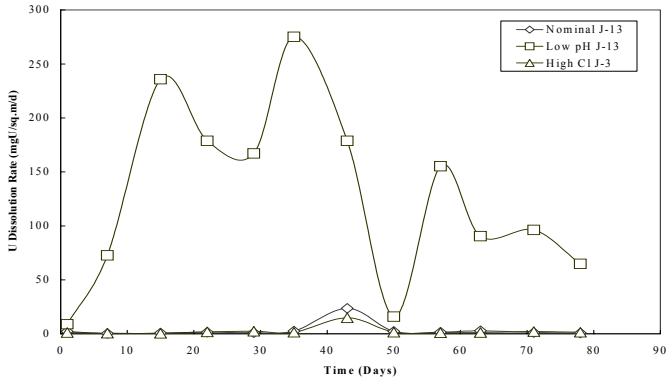

Figure 5.12 U Dissolution Rates for Unirradiated Cast 13.2 UAl Coupons in J-13 Waters at 25 °C

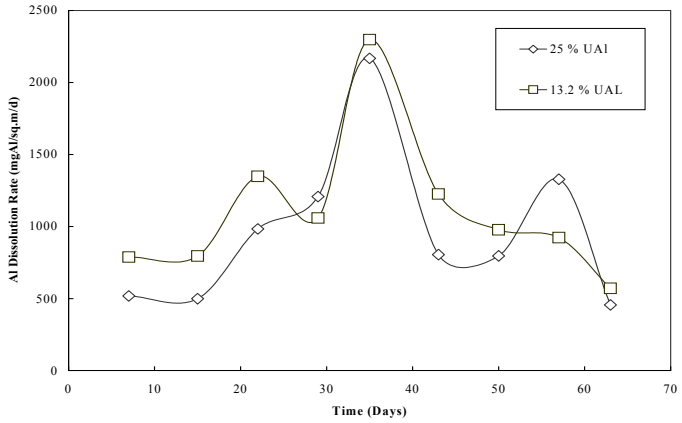

Figure 5.13 Al Dissolution Rates for Unirradiated Cast 13.2 and 25 UAl Coupons in Low pH J-13 at 25 °C

The 25 UAl samples from the nominal and low pH J-13 were also examined under high magnification using the SEM. The surfaces were observed both planar and in cross-section. The shiny regions observed visually were found to be areas not covered by oxide or corrosion product, but were active corrosion sites where aluminum corroded preferentially to the U-Al phases as shown in Figure 5.14. The oxides were primarily aluminum oxide, but also contained sulfur, uranium, and silicon. Calcium compounds, which are also seen in the photomicrograph, were also found to occur regularly on the surface. In the low pH J-13, the samples were found to form an aluminum oxide which uniformly covered the surface, as shown in Figure 5.15. The surface smoothness noted macroscopically was probably related to the formation of this oxide. The relief of the U-Al particles resulted from the preferential corrosion of the aluminum. Similar to the nominal J-13, the deposits that did form on the surface were calcium compounds.

The degradation at 25 °C was not as severe as at the higher temperature. In the nominal J-13, the surfaces varied from shiny metallic to a dulled, light etch appearance. Some areas were covered

with a powdery white corrosion product. In the low pH J-13, the surfaces had a dull, flat appearance with minimal white deposits. Drop-outs or regions where aluminides were dislodged were readily apparent in the 25 UAl, although none were seen for the 13.2 UAl. The appearances of the coupons from the high Cl J-13 were similar to those for nominal J-13. Some areas had a significant build up of white corrosion products.

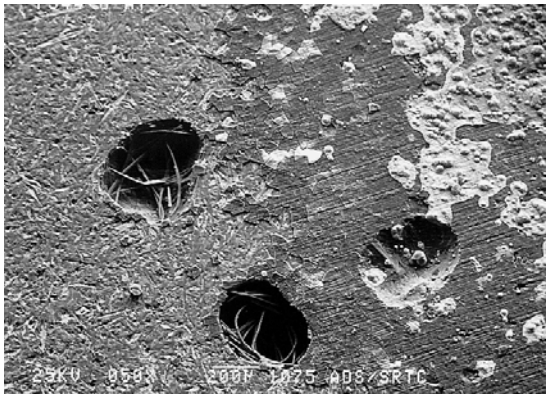

Figure 5.14 Planar View of Surface of 25 UAl Cast In Nominal J-13

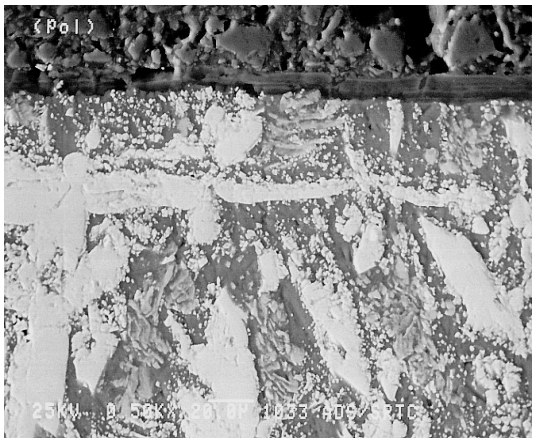

Figure 5.15 Cross-section of 25 UAl Cast in Low pH J-13

The weight changes for the samples were also measured for the 90 °C coupons as shown in Table 5.5. In general, the 13.2 UAl cast samples had the smallest weight change, which is an indication that the alloy was the least reactive. Weight changes were dependent on the solution chemistry. Weight losses were generally observed in both the low and high pH J-13 with larger weight losses in the high pH J-13 where solubility of aluminum is greater. The samples in the high Cl and nominal J-13 experienced weight gains, with larger gains in the high Cl J-13, attributed to the voluminous corrosion products.

Table 5.5 Weight Changes of Unirradiated U-Al Alloys in J-13 Well Water*

Type of J-13 Water	Alloy Composition (wt % U)		
	13.2 wrought	13.2 cast	25 cast
Nominal	-0.0039	-0.0007	-0.0024
Low pH	+0.0139	+0.006	+0.0117
High pH	+0.0255	+0.0128	+0.0342
High Cl	-0.0054	-0.0082	-0.007

* A negative number indicates a weight gain, while a positive number indicates a weight loss.

5.4.3 Static Test Results

The overall degradation that occurred during the static tests was minor with the majority of the corrosion occurring on the sides of the coupon rather than the bottom crevice area. However, there were changes in the appearance of the coupons that depended primarily upon the test environment. These changes were unaffected by the composition of the material or its fabrication method. Coupling the coupons to stainless steel increased the severity of attack for a given test solution, as did increasing the temperature of the environment. Concentrations of dissolved uranium and aluminum were in agreement with the observed degradation of the coupon. Although relatively small changes in the weights of the coupons were measured, general trends were in agreement with the observed degradation.

5.4.3.1 Corrosion Mechanism of U-Al Alloys

Coupons immersed in nominal J-13 visually showed only slight evidence of degradation with only a few white corrosion products indicative of pitting of the aluminum matrix. Figure 5.16 shows the degraded microstructure of a 13.2 UAl cast coupon that was exposed to nominal J-13. Original grinding marks are seen on the aluminum surface indicating that minimal general corrosion occurred. However, the aluminum matrix adjacent to the U-Al eutectic has been preferentially corroded leaving the particles in relief. The micrograph also shows evidence that eutectic particles became dislodged from the surface. Figure 5.17 shows loosened U-Al particulate that was collected from a filtered solution. Evidence of these particles was observed from all test solutions.

In low pH J-13, a whitish film was observed on the surface of the coupon with no associated white deposits. Figure 5.18 shows the surface of a 13.2 UAl cast coupon that was immersed in low pH J-13. A thick oxide film covered the surface indicating a more general form of attack. The oxide contained many cracks and fissures and many U-Al particles were embedded in the film. Figure 5.19 shows a cross-sectional view of the same coupon. As in the case of nominal J-13, the aluminum adjacent to the UAl_4 eutectic particles corroded preferentially. This preferential dissolution of the aluminum matrix led to the particles dislodging and either falling out or becoming embedded in the oxide film.

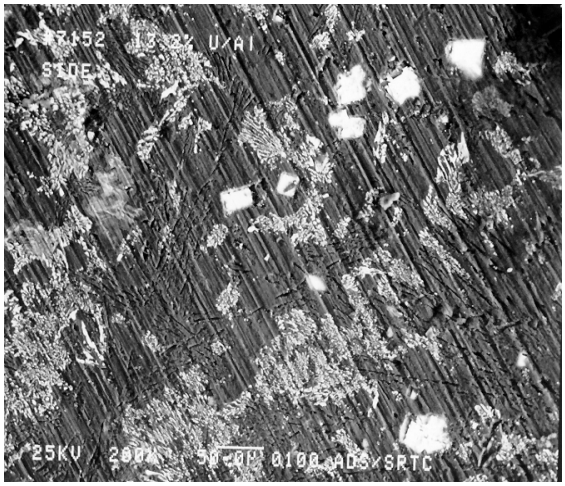

Figure 5.16 Post-test Microstructure of Unirradiated Cast 13.2 UAl from Nominal J-13 at 90 °C

Exposure of the coupons to high Cl J-13 resulted in the coupon becoming black with numerous white corrosion products indicative of pitting. Figure 5.20 shows the surface of a 13.2 UAl cast coupon that was immersed in high Cl J-13. As with the nominal J-13, minimal general attack of the aluminum surface was observed however preferential attack of the aluminum matrix occurred next to the U-Al particles. Pitting of the aluminum matrix was more severe than with the nominal J-13. Several large volcanic-like aluminum oxide formations were observed on the surface.

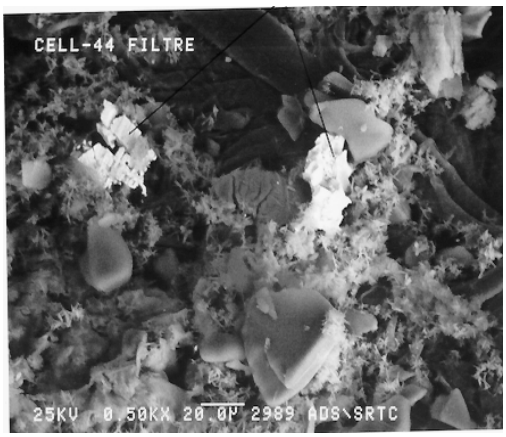

Figure 5.17 SEM Micrograph of Dislodged U-Al Particles from Unirradiated Wrought 25 UAl in High pH J-13 at 90 °C

The high pH J-13 resulted in the coupon becoming dark with no white deposits on the coupon. Figure 5.21 shows the degraded microstructure of the 13.2 UAl cast coupon that was exposed to the high pH J-13. Large, skeletal-like regions of the eutectic remained after the aluminum preferentially corroded. In contrast to the low pH J-13, there was no oxide film present on the surface. The general attack of the aluminum was the most severe of all the test solutions.

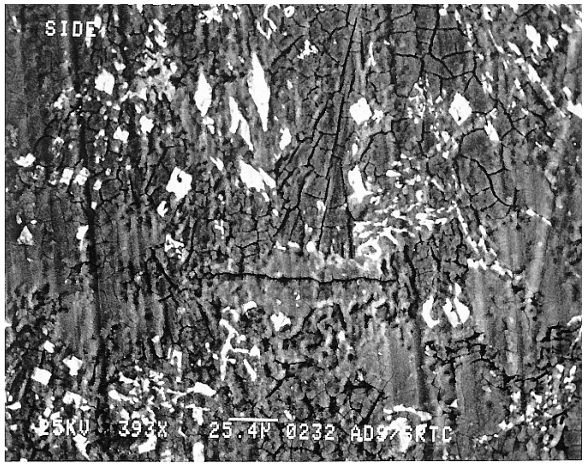

Figure 5.18 Post-test Microstructure of Unirradiated Cast 13.2 UAl from Low pH J-13 at 90 °C

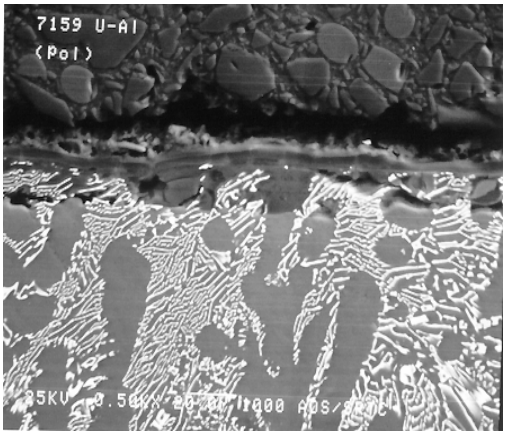

Figure 5.19 Cross-sectional View of Post-test Microstructure of Unirradiated Cast 13.2 UAl from Low pH J-13 at 90 °C

As mentioned previously, depending on the uranium concentration the U-Al particles consisted of two possible phases, UAl_3 and UAl_4, each with a distinct microstructure. The 10 UAl coupons consisted of primary aluminum and the eutectic UAl_4 phase. The degradation of the microstructure was the same as that observed for the 13.2 UAl. The 25 UAl coupons on the other hand consisted of both U-Al phases. Figure 5.22 shows a cross-sectional view of a 25 UAl cast coupon, which contained both phases, from the test in nominal J-13 at 90 °C. As with the UAl_4 phase, preferential corrosion of the aluminum matrix occurred around the blocky UAl_3 particles. The aluminum corroded beneath the particle followed by the formation of aluminum oxide that created pressure on the UAl_3 particle. As a result the particle cracked and began to spall from the surface. Thus, both UAl_3 and UAl_4 can be dislodged from the aluminum matrix without significant degradation of the particle. Thus, under these various test conditions the alloys within this composition range had similar corrosion mechanisms. The effect of alloy composition on the dissolution rate should be similar.

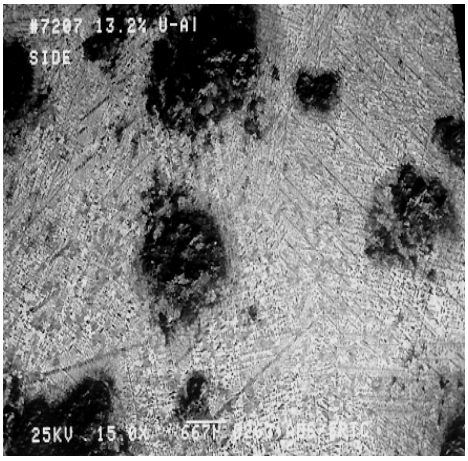

Figure 5.20 Post-test Microstructure of Unirradiated Cast 13.2 UAl from High Cl J-13 at 90 °C

Figure 5.21 Post-Test Microstructure of Unirradiated Cast 13.2 UAl from High pH J-13 at 90 °C

Although the fabrication process of the material affected the microstructural features, the corrosion mechanism was not affected. Figure 5.23 shows a cross-sectional view of a 13.2 UAl wrought coupon that had been immersed in low pH J-13 at 90 °C. As was observed with the 13.2 UAl cast coupons, the aluminum matrix has preferentially corroded and the U-Al particles have become embedded in the oxide. The only difference is that the sizes of the particles that are dislodged from the surface of the wrought material are smaller than those that are released from the cast material. The release of these small U-Al particles should only have a small impact on the dissolution rates of the radionuclides, since the rates in J-13, as discussed previously, were very low.

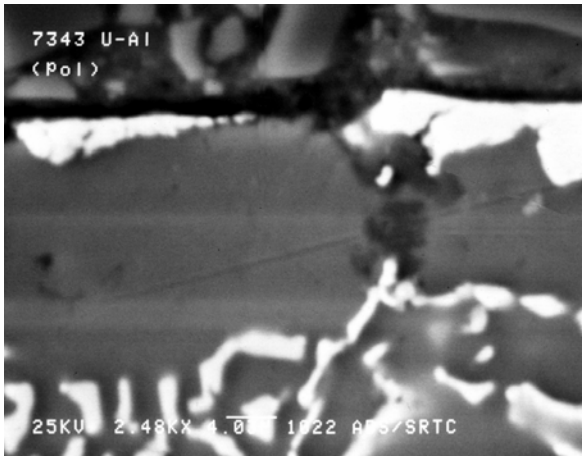

Figure 5.22 Cross-sectional View of Post-test Microstructure of Unirradiated Cast 25 UAl from Nominal J-13 at 90 °C

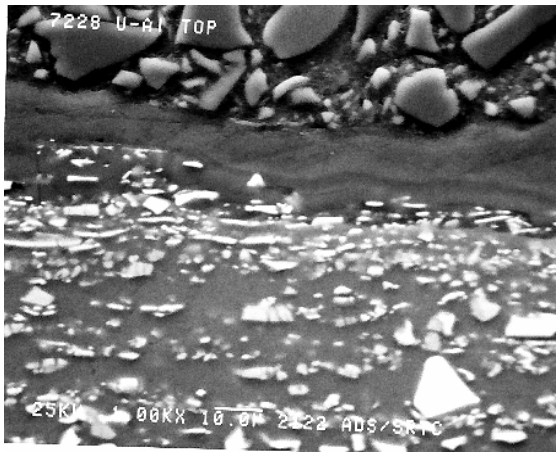

Figure 5.23 Cross-sectional View of Post-test Microstructure of Unirradiated Wrought 13.2 UAl from Low pH J-13 at 90 °C

Aluminum-aluminum and Aluminum-stainless steel coupled specimens were tested. The type of galvanic couple and the temperature of the environment affected the severity of attack. For example, in the high Cl J-13 the number of pits was much greater for coupons attached to the stainless steel disk than to the aluminum disk (see Figure 5.24). Increasing temperature also increased the severity of attack. At 25 °C in the high Cl and high pH J-13, the number of pits was significantly less than at 90 °C. The number of deposits on the surface was less at the lower temperature than at the higher, although the deposits were more voluminous than at the higher temperature. This result probably reflects the lower solubility of the aluminum oxide at the lower temperature.

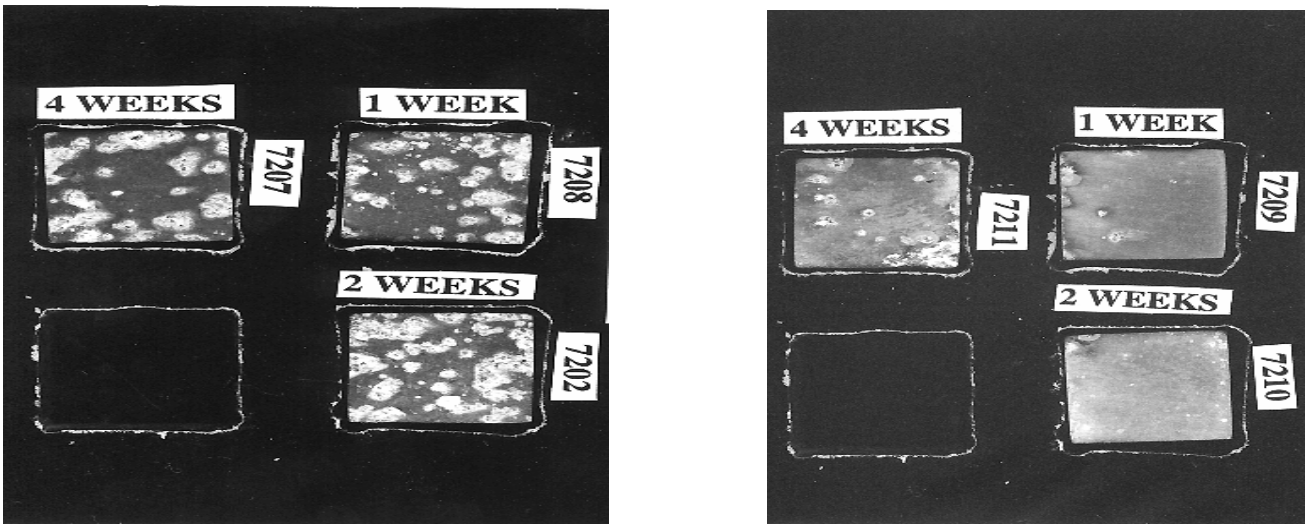

(a) (b)

Figure 5.24 Visual Appearance of Unirradiated Cast 13.2 UAl from High Cl J-13 at 90 °C and Coupled to a) Stainless Steel and b) Aluminum (2X)

The crevice area of the coupons demonstrated little evidence of attack. The primary site of degradation was near the edge of the coupon. Figure 5.25 shows a typical crevice surface with a relatively thick oxide that contained striations. These markings were similar to the grinding marks from the stainless steel and aluminum disks as shown in the figure. Areas where this oxide had cracked and spalled were observed intermittently. Preferential dissolution of the aluminum was also seen at these local areas.

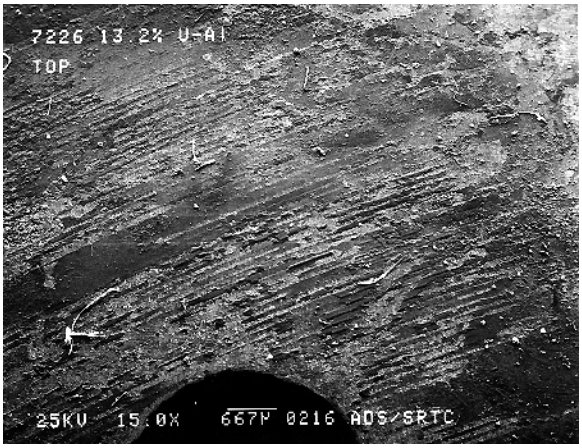

Figure 5.25 Post-test Surface of Crevice Area of 13.2 UAl Wrought from Nominal J-13 at 90 °C

5.4.3.2 Analysis of Test Solutions Dissolved Species

Table 5.6 shows the dissolved uranium concentration for static tests at 90°C as a function of test solution, galvanic couple, and alloy composition. The test solution had the most significant effect on the amount of uranium dissolved. For each galvanic couple the relative severity of the

solution was similar. For the stainless steel, the amount of dissolved uranium increased in the following order: high Cl < nominal < low pH < high pH J-13 with a ratio of 1:2:4:10. For the aluminum, the amount of dissolved uranium increased in the following order: high Cl, nominal < low pH < high pH J-13 with a ratio of 1:10:20. The amount of uranium dissolved in each of these solutions was in agreement with the severity of degradation that was observed on the coupons. The high pH and low pH J-13 were the most aggressive environments while the chloride and nominal were the least aggressive.

The galvanic couple affected the severity of attack. The amount of uranium dissolved was 2 to 10 times greater in solutions with coupons attached to the stainless steel than with coupons coupled to the aluminum. This result is in agreement with the observations that the coupons attached to the stainless steel showed more evidence of degradation.

No effects of alloy composition or fabrication on the uranium dissolution were apparent. In general, the amount of dissolved uranium was constant for the different alloys. This result was consistent with the result that the primary degradation mechanism was unaffected by alloy composition or fabrication technique.

Table 5.6 Concentration (ppm) of Dissolved Uranium in Coupled Static Tests at 90 °C:

a) Coupled to Stainless Steel

Solution	10 UAl cast	13.2 UAl cast	13.2 UAl wrought	25 UAl cast	25 UAl wrought
J-13	0.2-0.8	0.6-0.7	0.5-0.6	0.5-0.6	0.6-0.7
Low pH	0.5-0.6	2.5	2-2.5	1-2	2.5-3
High Cl^-	0.2	0.25-0.3	0.2-0.25	0.25-0.4	0.3
High pH	1-4	3.5-4.5	1-1.2	3-4	15-20

b) Couple to Aluminum

Solution	13.2 UAl cast	13.2 UAl wrought	25 UAl cast	25 UAl wrought
J-13	0.05	0.05	0.1	0.05-0.2
Low pH	1-1.5	0.5-0.8	0.25-0.75	0.9-1
High Cl^-	0.05	N/A	0.08-0.1	0.1
High pH	0.1	N/A	2	1.2-1.4

Table 5.7 shows the effect of temperature on the dissolved uranium concentration. The tests were performed on 13.2 UAl cast material coupled to stainless steel. For coupons tested in nominal, high Cl, and low pH J-13 the amount of dissolved uranium increased by a factor of 3 to 10 as the temperature increased from 25 to 90 °C. The coupons tested in the high pH J-13 showed an even stronger dependence on temperature as the dissolved uranium concentration increased by a factor of 100. These results agree with the observations that the severity of attack increased with temperature.

Table 5.7 Concentration (ppm) of Dissolved Uranium for 13.2 UAl Cast Material Couple to Stainless Steel in Static Tests as a Function of Temperature

Solution	25 °C	90 °C
J-13	0.05-0.09	0.6-0.7
Low pH	0.5-0.7	2.5
High Cl	0.08-0.13	0.25-0.3
High pH	0.03	3.5-4.5

The dissolved aluminum concentration was also analyzed for the static tests and the results for tests at 90 °C are shown in Table 8. The effect of solution composition on the dissolved aluminum concentration was slightly different than for the dissolved uranium concentration. The nominal, high Cl, and low pH J-13 dissolved relatively the same amount of aluminum. The high pH J-13, however, dissolved 5-10 times more than the other solutions. This result correlates with the higher solubility of aluminum in alkaline solutions.[8] The other observed effect was that for the low pH J-13 a maximum dissolved aluminum concentration was achieved after 1 week. The decrease was likely due to precipitation of an aluminum oxide film. This mechanism is in agreement with the thick oxide that formed on the coupons that were immersed in the low pH J-13.

The galvanic couple affected the dissolved aluminum concentration differently than the dissolved uranium. For three of the solutions, nominal, high Cl, and high pH J-13, the tests with the aluminum plate produced a greater dissolved aluminum concentration than those with the stainless steel. This result probably reflects the corrosion and dissolution of additional aluminum from the plate. On the other hand coupons exposed to the low pH J-13 and coupled to stainless steel resulted in the higher dissolved aluminum concentration. This result likely was due to the formation of the aluminum oxide on both the plate and the coupon.

As with the dissolved uranium concentration, no effects of alloy composition or fabrication on the dissolved aluminum concentration were apparent. With only a couple of exceptions the amount of dissolved aluminum was constant for a given galvanic couple and test solution.

5.5 Input to Total System Performance Assessment

The dissolution testing of SNF and SNF surrogates provides the information necessary to support the development of TSPA SNF degradation models.

Preliminary indications from the TSPA have shown that the overall performance of an MGR is relatively insensitive to degradation rates of the SNF forms. However, as part of the Analysis/Model Report process, the OCRWM has developed hierarchical structure to corrosion/degradation/release data usage and model development. This hierarchical structure consists of three levels of conservatism which all may be employed as part of the TSPA depending on the scenario being evaluated. A description of this modeling hierarchy is provided as follows.[1]

> **Level 1--Upper-limit Degradation Models-**The upper-limit degradation model provides the most conservative estimate of dissolution rate to be used in any postclosure waste package or EBS performance case. The upper-limit model generally gives unrealistically high estimates of the degradation rate of the waste forms. An upper-limit model may be

appropriate in cases where the results of the TSPA or other performance analyses are either very insensitive to the degradation rate of the waste form or where the use of such a model still results in acceptable performance of the MGR. An upper-limit model uses dissolution data, or models abstracted from experimental data, only in that such data clearly shows that the bounding model predicts release rates always well in excess of actual dissolution rates.

Level 2--Conservative Degradation Models-The conservative degradation models provide an estimate of dissolution rate that reflects the higher rate end of dissolution data available. A conservative model for waste-form degradation would be appropriate in cases where the dissolution database, from which the model was developed, showed wide data spreads or sensitive dependency on waste-form characteristics that could not be definitively controlled, described, or determined for the emplacement condition. A conservative model would be expected to encompass the dissolution kinetics of all SNF types within a DOE SNF TSPA group

Level 3--Best-estimate Degradation Models-Best-estimate models would be appropriate when the use of overly conservative formulations in the TSPA produce results that indicate marginal MGR performance. Best-estimate models might also be used in analyses not directly related to TSPA, such as parametric studies, waste package design support, or other such analyses where full validation of the model might not be required. Best-estimate models would generally require the most extensive experimental data to support validation. Moreover, in many cases the best estimate model itself is the result of a conservative analysis of the experimental data. A best-estimate model would be used when sufficient dissolution data exists to abstract one, and the characteristics of the waste form can be shown to correspond to the characteristics of the materials that provided the dissolution database.

Based on this modeling hierarchy with decreasing conservatism, the OCRWM has reviewed the open literature for the 11 TSPA fuel categories and selected the most appropriate dissolution/release rate data to develop models for each level. As part of this effort, dissolution/release data for Al-Based SNF—TSPA Group 9—was reviewed and data sets were selected for ***Level 2 and 3*** model development.

5.6 Analysis/Model

The data reviewed for the AMR is provided in Section 5.4. Based on this data the following values were recommended: 1) since bicarbonate is a potentially more aggressive water condition, the bicarbonate data is used as the basis for the conservative model, 2) the J-13 well-water data is selected for the best-estimate degradation model because the groundwater chemistry at the time of waste-package failure is expected to be approximately that of the J-13 well water. Use of this data would provide the following ranges of dissolution/release for Al-SNF from 25-90 °C:

***Level 2*—Conservative Model: 36-360 mgU/m^{2}day**

***Level 3*—Best Estimate Model: 0.22-2.20 mgU/m^{2}day**

An evaluation of the data selected in the AMR for model development by the authors of this report has lead to full concurrence/agreement with the selection.

5.7 Summary

Testing specified in ASTM 1431-99 was performed to characterize corrosion/dissolution behavior of aluminum-base SNF forms under repository relevant conditions. Single pass flow tests were utilized to measure dissolution rates of radionuclides from the Al-SNF. Tests were performed on four irradiated fuel types: UAl, UAl_x, U_3O_8, and U_3Si_2 in nominal J-13 well water (J-13), as discussed in Section 5.3. The irradiated fuels showed dissolution rates that ranged from approximately 0.2 mgU/m^2/d (for all the fuels in nominal J-13) to 30-100 mgU/m^2/d (in the nitric acid solution). Dissolution rates for radionuclides such as Cs, Sr, and Pu were approximately the same as the U dissolution rate over the duration of the test (see Section 5.4.1).

Unirradiated UAl alloys ranging from 10 to 25 wt% U were also tested. The variables were the solution chemistry, temperature (25 or 90 °C), alloy composition of the fuel, and alloy fabrication technique. Unirradiated testing was performed using solutions, which were nominal J-13, low pH, high pH and high Cl^- variants of J-13 at both 25 and 90 °C. These unirradiated alloys had dissolution rates ranging from 0.2 mgU/m^2/d in nominal J-13 at 25 °C to 200-400 mgU/m^2/d in low pH J-13 at 90 °C (see Section 5.4.2).

Static coupon tests were also performed on the unirradiated alloys to discern the effects of material degradation mechanism on the U dissolution rate. The tests were operated with the same solutions and at the same temperatures as the unirradiated flow through tests. In addition, the effect of galvanic coupling to stainless steel was also explored. The degradation was observed to follow a two-stage process as discussed in Section 5.4.3. The alloys were also susceptible to pitting in these environments. A galvanic couple with stainless steel also increased the U dissolution in the static test.

The results from all three tests showed that the test environment, which included aqueous phase chemistry and temperature, had the greatest effect. Alloy composition and fabrication technique had a minimal effect on corrosion behavior. The degradation rate of these fuels was derived from the dissolution rate of UAl fuel in J-13 water at 25 °C (i.e., 0.2 – 2.2 mgU/m^2/d). A more conservative degradation rate was derived from an experimental release rate, which bounds the uranium release rate for UAl fuels in all solutions at 25 and 90 °C (i.e., 36 - 360 mgU/m^2/d). The release of other radionuclides can be estimated to be similar to uranium.

In order to meet the license application requirements for approval by the NRC, models of radionuclide release and transport have been generated for use in the TSPA (as summarized in this section). The models rely on currently available data from independent corrosion studies of DOE SNF. However, detailed studies can only be performed in the long term to determine radionuclide release from these wastes in an interactive codisposal environment. Based on solution chemistries and corrosion products observed in corrosion studies of the individual components, it is expected that significant material interactions will occur in a codisposal repository environment. The chemical consequences of codisposal should be validated experimentally. The results may be included in TSPA models of waste package and waste form corrosion. Furthermore, more significant interactions (that control radionuclide release) involve the potential generation and immobilization of radionuclide-associated colloids, accelerated container corrosion, and/or mobilization of neutron absorbers. Dissolution testing on combined waste forms, waste package materials, and groundwater may be used to evaluate these effects. Results of the research will provide critical data inputs in support of the TSPA-LA and subsequent performance confirmation.

5.8 References

[1] Thornton, T. A., ***"DSNF and Other Waste Form Degradation Abstraction,"*** ANL-WIS-MD-000004 Rev 1 (October 2000).

[2] Gray, W. J., ***"Dissolution Rates of Aluminum-Based Spent Fuels Relevant to Geological Disposals,"*** PNNL-11979 (1998).

[3] Wiersma, B. J. and Mickalonis, J. I., ***"Preliminary Report on the Dissolution Rate and Degradation of Aluminum Spent Nuclear Fuels in Repository Environments,"*** WSRC-TR-98-00290, WSRC, Aiken, S. C. (August 1998).

[4] Gray, W. J. and Wilson, C. N., ***"Spent Fuel Dissolution Studies: FY 1991 to 1994,"*** PNL-10540. Pacific Northwest National Laboratory, Richland, Washington (1995).

[5] W. J. Gray, Leider, H. R., and Steward, S. A., ***"Parametric Study of LWR Spent Fuel Dissolution Kinetics,"*** **Journal of Nuclear Materials**, Vol. 190. Pp. 46-52 (1992).

[6] ASTM G31-72, ***"Standard Practice for Laboratory Immersion Corrosion Testing of Metals,"*** American Society for Testing And Materials, Philadelphia, PA (1996).

[7] Beavers, J. A., Thompson, N. G., and Durr, C. L., ***"Approaches To Life Prediction For High-Level Nuclear Waste Containers In the Tuff Repository,"*** **Application of Accelerated Corrosion Tests to Service Life Predicted of Materials**, ASTM 1194. G. Cragnolino and N. Sridhar (eds.), American Society for Testing and Materials, Philadelphia (1994).

[8] Pourbaix, M., **Atlas of Electrochemical Equilibria in Aqueous Solutions,** National Association of Corrosion Engineers. Houston, TX (1974).

This Page Intentionally Left Blank

6.0 DECAY HEAT CHARACTERIZATION

6.1 Introduction

This section summarizes an analysis performed to characterize the decay heat sources representative of research reactor spent nuclear fuel assemblies stored, or to be received, at SRS. The decay heat sources developed in this analysis have been used in thermal design calculations for studies assessing the direct codisposal and melt-dilute fuel disposition options. The decay heat analysis included a review of the physical and exposure characteristics of the SRS-bound research reactor fuels and is based upon two assembly designs that are considered to be representative of bounding and nominal fuels for purposes of the thermal design calculations. Section 2.0 describes the codisposal waste package and contents represented by Figure 6.1.

Research reactor fuel shipments to SRS are expected to continue during the next 10 – 20 years, so that the SRS fuel inventory will exceed 20,000 assemblies. The majority of these assemblies will be Materials Test Reactor (MTR) type, but other fuel types will be in the inventory because of variations in reactor core designs. This analysis considers just the aluminum clad, Al-based fuels that can be melted at the relatively low temperatures proposed for the melt-dilute disposition option.

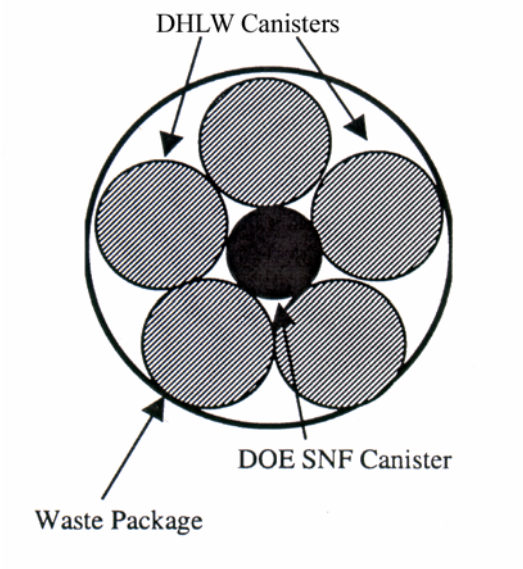

Figure 6.1 Waste Package Geometry

For the direct codisposal option, up to 16 standard-sized MTR type assemblies can be packed into each fuel basket, for a total of 64 MTR assemblies in a DOE SNF canister. This decay heat analysis does not address the question of how many assemblies will actually fit into the DOE SNF canisters; instead the decay heat results are presented as power per standard-sized MTR assembly. Assemblies that are larger than standard-sized MTR fuel may also have higher decay heat. Thus, heat load constraints may not allow these assemblies to be as densely packed when loaded into the DOE SNF canisters.

For the melt-dilute fuel disposition option, the decay heat results are also presented as power per standard-sized MTR assembly, leaving open the question of how many assemblies will be melted and diluted in a DOE SNF canister. The decay heat source for assemblies processed in the melt-dilute option is slightly lower than for assemblies in the direct codisposal option because melting may release all of the ^{85}Kr and ~80% of cesium isotopes, ^{134}Cs and ^{137}Cs, including the ^{137m}Ba daughter product.

This section also provides a decay heat source term for a DHLW glass canister as derived from the DWPF Waste Form Compliance Plan. This source term is also needed in the thermal design calculations for the waste package

6.2 Methodology

The decay heat calculations were made using the SAS2H control module within the SCALE 4.3 code package. The codes executed on a HP Vectra computer with the Windows NT operating system. To verify that the SAS2H sequence executed as intended, the four sample problems from the SCALE package were executed and outputs compared with those provided in the package.[1]

The SAS2H control module was used to generate the sequence of fuel depletion calculations as shown Figure 6.2. The sequence executes 2 cycles to obtain core isotopics at beginning and middle of the specified core life. Within each cycle there are 2 passes, each executing BONAMI, NITAWL and XSDRNPM. The BONAMI and NITAWL codes compute the Bondarenko and Nordheim cross-section resonance treatments, respectively. The XSDRNPM code does a one-dimensional transport calculation of the neutron spectrum for weighting the cross sections, using S8 angular quadrature, P3 order scattering, and 44 neutron energy groups. Axial leakage is accounted for using a buckling term based on a 60.96 cm (24") active fuel length.

As Figure 6.2 shows, the first pass with the BONAMI, NITAWL and XSDRNPM codes calculates the cell-weighted macroscopic fuel cross sections. In this pass the XSDRNPM calculation uses 14 spatial mesh points to model the 0.2 cm half-width of the fuel cell using symmetric slab geometry. In the second pass, the XSDRNPM calculation changes to a 200 mesh point model of the full core in cylindrical geometry. The equivalent core radius for these calculations was 14.89 cm for the 12 assembly bounding core and 17.20 cm for the 16 assembly nominal core. The cores had an additional 30 cm thick light water reflector.

Overall there are 2 cycles; each cycle having 2 passes through the BONAMI, NITAWL and XSDRNPM codes. The ORIGEN code executes at the end of each cycle to calculate the fuel depletion isotopics. The SAS2H input files for these calculations are presented in Reference 2 along with a sample output file.

A final ORIGEN code execution calculates the total isotopic decay heat and was made independent of the SAS2H sequence. Since the ORIGEN code structure limits decay heat outputs to just 10 time steps, ORIGEN was executed twice for a total of 20 decay heat points. The ORIGEN input for the first execution is presented in Reference 3, and the input for the second execution is identical except for the time steps of the decay heat outputs.

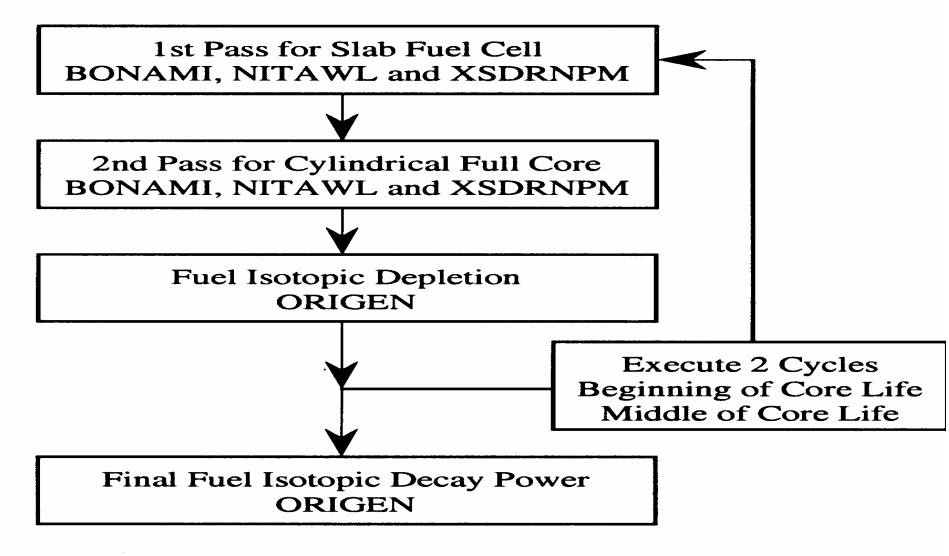

Figure 6.2 SAS2H Calculation Sequence Diagram

6.3 SRS Research Reactor Fuel Characteristics

For this decay heat analysis, bounding and nominal assembly designs were selected as representative of the Al-clad research reactor fuels stored or to be received at SRS. To demonstrate that the bounding and nominal assemblies are representative, comparisons have been made with two databases. The first database discussed in Section 6.3.1 was developed by Jim Matoes of Argonne National Lab to describe foreign reactor fuels to be received at SRS. The second database, discussed in Section 6.3.2, is the Spent Nuclear Fuel (SNF) database that is the central repository at SRS for reactor fuel information.

6.3.1 The Matoes Database

The Matoes database describes about 200 research reactor fuels that have been or will be shipped to SRS. These fuels are all from foreign countries and all Al clad.

Figure 6.3 presents depletion data from this database plotting the initial ^{235}U loading vs. the mass of ^{235}U burned. The plot identifies 3 categories of fuels: the undepleted fuels, the HEU & MEU fuels, and the LEU fuels. The depletion data points in the figure are averages for groups of similar assemblies all having the same initial ^{235}U mass, so individual assemblies would actually be more or less depleted than the average. Individual points in the plot may represent hundreds of assemblies or just a few assemblies.

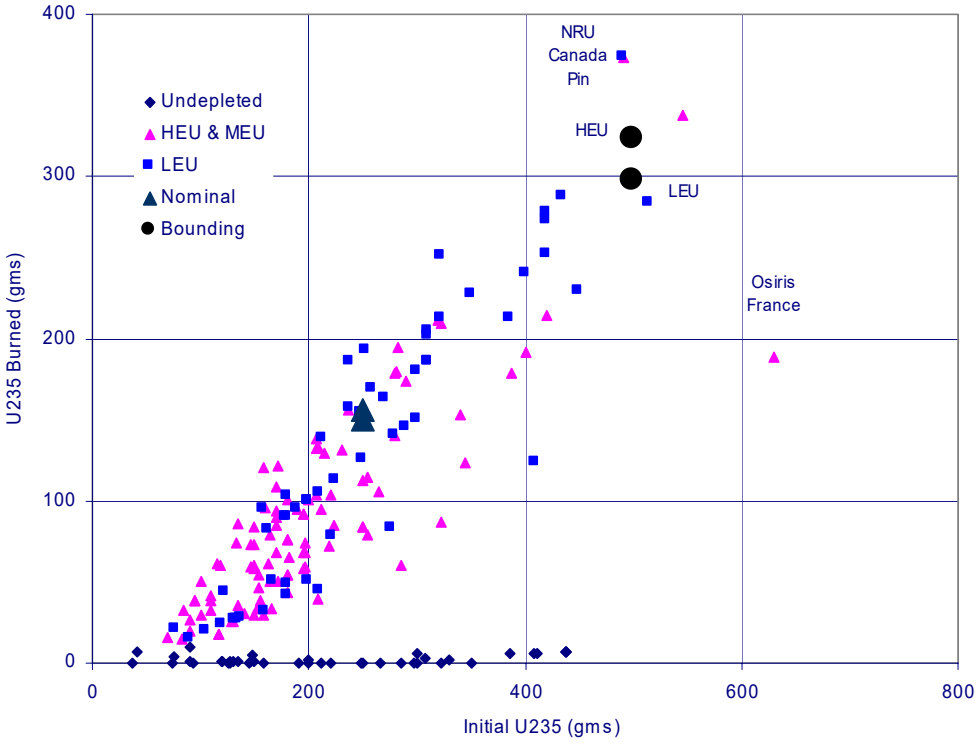

Figure 6.3 Matoes' Foreign Research Reactor Fuel Group Depletion

For comparison Figure 6.3 also plots the depletion characteristics of the proposed bounding and nominal assemblies having initial ^{235}U loadings of 500 and 250 grams, respectively. The bounding assembly is proposed with both HEU and LEU enrichment, so the figure shows 2 bounding assembly data points. Both the HEU and LEU bounding assemblies were depleted for 3,100 MegaWatt-days (MWd). During this depletion, less ^{235}U mass was burned in the LEU assembly because some ^{238}U was converted to Pu and then burned. Thus, Figure 6.3 shows a separation between the ^{235}U depletion of the HEU and LEU bounding assemblies. There is a similar separation for the HEU and LEU nominal assemblies, but the difference is not as large because less ^{238}U is converted to Pu.

Figure 6.3 shows a trend toward LEU fuels having higher initial ^{235}U loading and also higher ^{235}U depletion. On average the LEU fuels in the figure have 20% higher initial ^{235}U loading than the HEU & MEU fuels. In general, LEU fuels have higher initial loadings because extra ^{235}U is needed to overcome the reactivity loss caused by loading more ^{238}U into the fuel. The bounding HEU and LEU assembly designs proposed in this analysis have the same initial ^{235}U so that the effect of enrichment alone upon decay heat can be observed.

On average for the fuel data plotted in Figure 6.3, the LEU fuels have 53% ^{235}U depletion compared to 45% ^{235}U depletion for the HEU & MEU fuels. In general, LEU fuels have higher depletion because of the higher initial loading and also because some ^{238}U is converted to Pu and then burned.

The most important observation about Figure 6.3 is that the bounding assembly designs selected for this analysis bound, to a reasonable extent, the fuels described in the Matoes database. This figure shows that a few fuel types have initial loadings or depletions exceeding the proposed

bounding design. However, these outlying fuel types also have physical designs that vary significantly from the MTR standard. The assemblies with the highest ^{235}U depletion in Figure 6.3 are from the NRU reactor in Canada and have a pin, rather than, flat plate design. Other assemblies considered to have outlying fuel designs are from the Osiris and Reactor a Haut Flux (RHF) reactors in France, and also from the MURR reactor at the University of Missouri. These outlying fuel types will not be as densely packed in the DOE SNF canisters as the standard MTR assemblies will. Thus, the decay heat sources from these outlying fuel types are not specifically addressed for this bounding analysis. The outlying fuels may require individual analysis considering both their power and packing density in the DOE SNF canister.

As a final observation, Figure 6.3 shows that the proposed assemblies with an initial 250 gram ^{235}U loading are a reasonable nominal design. The 250 gram loading is near, but not exactly at, the average for the fuel data plotted. The proposed nominal assembly design has about 60% ^{235}U depletion which is slightly higher than the ~50% average depletion for the fuels in Figure 6.3.

6.3.2 The SNF Database

The SNF database has information about all fuels in the SRS inventory. As Table 6.1 shows, the data extracted from the SNF database for the decay heat analysis excluded some outlying, DOE and power reactor fuels. The outlying fuels, discussed earlier, come from various research reactors that do not use the standard MTR type fuel. Fuels from DOE reactors, such as the Experimental Breeder Reactor-II (EBR-II) and Heavy Water Components Test Reactor (HWCTR), were excluded because these fuels will not be dispositioned within the scope of the direct codisposal or melt-dilute projects. Fuels from power reactors, such as the SAXTON reactor in Missouri and Elk River Reactor (ERR), were similarly excluded.

Figure 6.4 shows the fuel depletion data extracted from the SNF database for about 3,000 assemblies. This plot differs from that described in the previous section for the Matoes database because each point represents an assembly depletion, rather than being an average for a group of assemblies. The plot identifies some of the large groups of fuel, such as from the High Flux Beam Reactor (HFBR) and MURR. Figure 6.4 provides support for the selection of bounding and nominal assembly characteristics in the current decay heat analysis.

6.3.3 Bounding and Nominal Fuel Designs

Table 6.2 presents the physical characteristics the bounding and nominal assembly designs. These assembly designs were partially based upon designs from earlier radionuclide inventory analysis[1,4] using the ORIGEN code. The designs are for a generic 18 plate MTR fuel, rather than, a specific reactor fuel. Figure 6.4 shows that the nominal assembly has an initial ^{235}U loading that is very similar to the R-2 assemblies from the Studsvik reactor.

Table 6.1 Fuels in SNF Database

Research Reactor Fuels		Outlying, DOE & Power Reactor Fuels
Included		Excluded
ANLJ	MURR	EBR-II
B&W	MNR	EBWR
DR-3	NEREIDE	ERR
ENEA	ORR	HFIR
FMRB	OSU	HWCTR
FRG-0	OWR	SAXTON
GRR	R-1	SRP
GTRR	RECH-1	RHF
HFBR	RINC	TRR
HOR	Saphir	
JEN-0	UM	
JMTR	UMRR	
MIT	UVA	

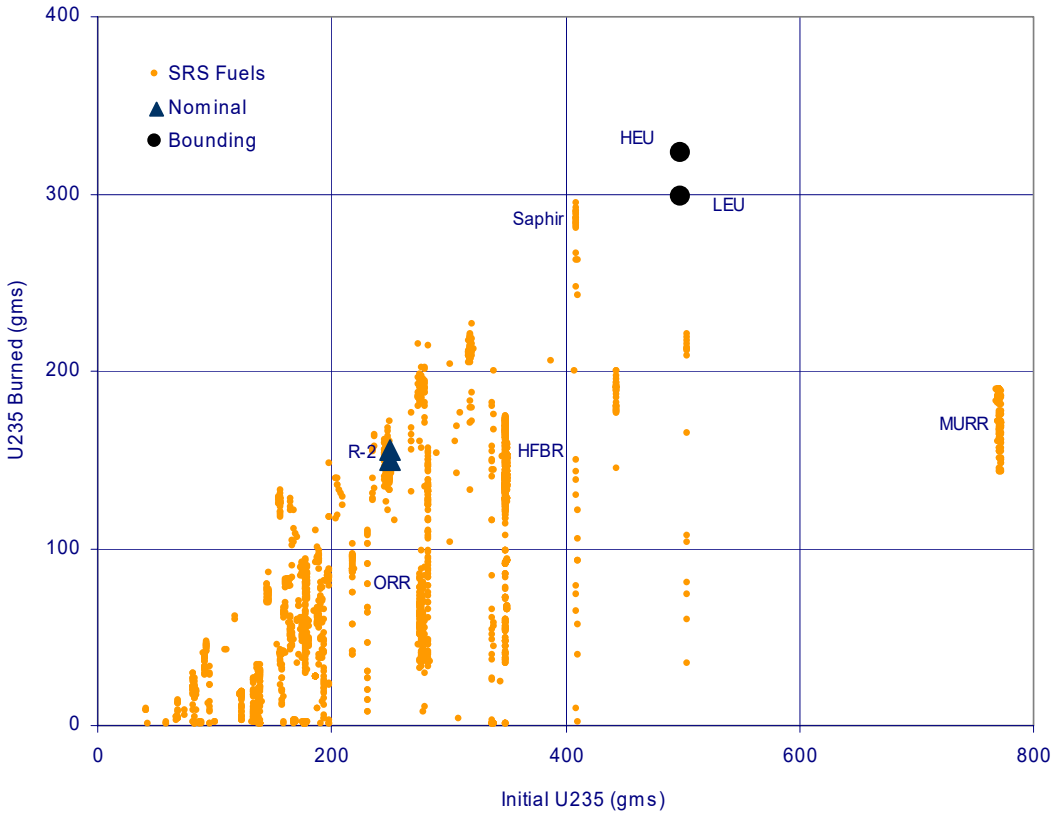

Figure 6.4 SNF Database Research Reactor Fuel Assembly Depletion

The decay heat analysis assumed a 24" active fuel length and 3" x 3" square assembly cross-section. The assembly designs were based upon fuel core, clad, and plate thickness of 20, 15 and 50 mils, respectively for the HEU fuels and similarly, thickness of 40, 15 and 70 mils for the LEU fuels. The decay heat analysis used a 2.7-gm/cm^3 Al density and assumed that the fuel meat was U-Al. Some Al-clad research reactor fuels at SRS have U-Si or U oxide cores. However, these variations in fuel type should have no significant impact on calculated decay heat, and are not explicitly considered in this analysis.

Calculations for the HEU fuels considered the trace isotopics of ^{234}U. The natural abundance of ^{234}U is 0.0055% compared to 0.72% for ^{235}U. If the ^{235}U enriched is 93.5%, the ^{234}U enrichment could be near 1%. However, ORIGEN calculations showed that the decay heat was slightly lower if 1 % ^{234}U enrichment was used, in comparison to assuming the 6.5% non-^{235}U fraction was entirely ^{238}U. For this reason, the ^{234}U was replaced with ^{238}U in the final calculations.

Table 6.2 Bounding and Nominal Assembly Designs

	Bounding		Nominal		
	HEU	LEU	HEU	LEU	units
ORIGEN Input					
Initial Assembly ^{235}U Mass	500	→	250	→	gms
Initial Core ^{235}U Mass	6,000	→	4,000	→	gms
Assemblies / Core	12	→	16	→	
^{235}U Enrichment	93.5	19.6	93.5	19.6	%
Fuel Meat Thickness	0.0508	0.1016	0.0508	0.1016	cm
Plate Thickness	0.1270	0.1778	0.1270	0.1778	cm
Plate Pitch	0.4011	→	→	→	cm
U mass fraction in U-Al$_x$ meat	45	45	23	23	%
Equivalent Core Radius	14.893	→	17.197	→	cm
Core Fuel Meat Volume	5,097	10,194	6,796	13,592	cm^3
Core Power	40	→	10	→	MW
Core Exposure	3,100	→	2,000	→	MWD
Meat Mass Fractions					
^{235}U	42.075	8.82	21.505	4.508	%
^{238}U	2.925	36.18	1.495	18.492	%
Al	55.	55.	77	77.	%
Total	100.	100.	100.	100.	%
ORIGEN Output					
^{235}U Depletion	322.5	297.5	155.6	150.0	gms
^{235}U Depletion	64.5	59.5	62.3	60.0	%
^{235}U Depletion Rate	1.25	1.15	1.25	1.20	gms/MWD

The last few lines in Table 6.2 present results from the ORIGEN decay heat calculations. The ^{235}U depletion rate was calculated by dividing the output ^{235}U core mass depletion by the input core exposure. As a rule of thumb, ^{235}U depletes at about 1.25 gms/MWD, so the calculated depletion rates presented at the bottom of Table 6.2 provide a verification of the SAS2H input setup.

Another way the SAS2H input setup was verified, was to review the initial core ^{235}U mass in the ORIGEN output. The SAS2H input requires fuel core density, total fuel core volume and also ^{235}U mass fraction within the fuel core. From this input, the codes calculate initial core ^{235}U

mass. Experience shows it is important to verify that the ORIGEN calculation for beginning of life outputs the correct ^{235}U mass inventory.

6.4 Decay Heat Results

This section presents the decay heat results calculated using the ORIGEN code. Section 6.4.1 discusses the decay heat results for the intact bounding and nominal fuels considered in the codisposal option. Section 6.4.2 discusses the modification of these same decay heat sources to account for fission product release in the melt-dilute option. Finally, Section 6.4.3 gives decay heat results for the design basis DHLW canister.

6.4.1 Direct Codisposal Fuel Assembly Decay Heat

Figure 6.5 and Table 6.3 show the decay heat sources calculated by the ORIGEN code for the bounding and nominal assemblies. These results show that the assembly decay heats are dependent, to first order, upon the ^{235}U depletion or assembly exposure. For example, in comparing the bounding to the nominal HEU assemblies, the ^{235}U depletion is 107% higher and as a consequence after a year of decay the decay heat is 133% higher, as Table 6.3 shows.

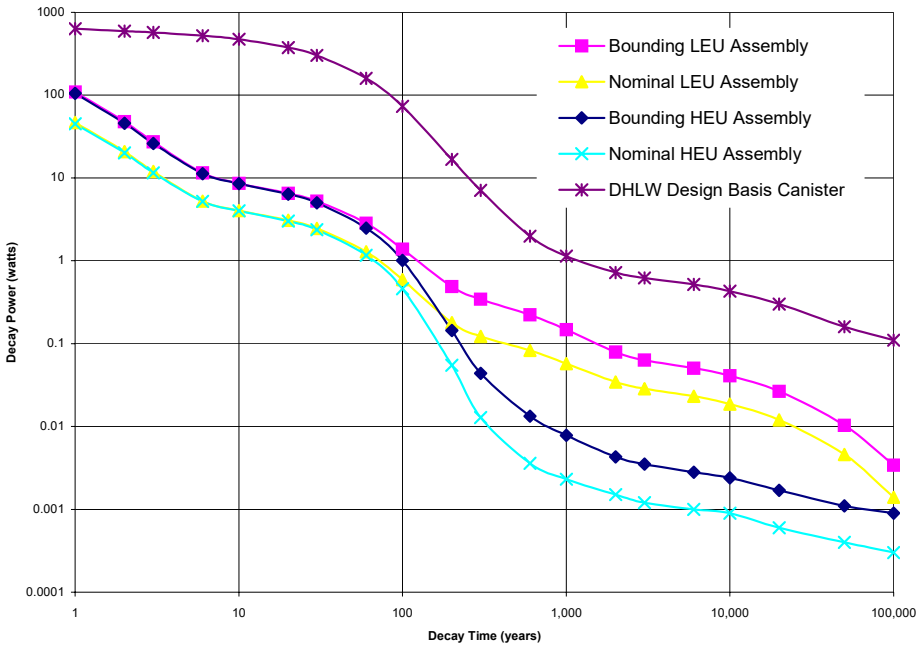

Figure 6.5 Decay Heat Sources for Bounding and Nominal Assemblies and DHLW Glass

The results also show fuel enrichment has a second order effect on the assembly decay heat. During the first 100 years of decay, when fission product decay dominates, there is little difference between the HEU and LEU assembly decay heat. For the longer decay times, when the actinide decay dominates, the LEU assemblies have significantly more decay heat than the HEU assemblies. This is a consequence of the LEU assemblies having more ^{238}U that transmutes to higher actinides that dominate the decay heat release after 100 years.

Table 6.3 Decay Heat Sources for Bounding and Nominal Assemblies and DHLW Glass

Decay Time (years)	Decay Heat (watts)								
	Direct Codisposal Assembly				Melt-Dilute Assembly				DHLW Canister Design Basis*
	Bounding		Nominal		Bounding		Nominal		
	HEU	LEU	HEU	LEU	HEU	LEU	HEU	LEU	
1	105.23	108.89	45.18	46.61	96.704	100.360	41.795	43.157	634.70
2	45.64	47.67	20.05	20.88	38.675	40.710	17.206	17.984	594.02
3	26.14	27.24	11.55	12.00	20.308	21.403	9.112	9.521	568.37
6	11.30	11.52	5.20	5.26	7.372	7.583	3.441	3.485	520.49
10	8.52	8.58	4.01	4.03	5.583	5.629	2.629	2.640	472.30
20	6.367	6.530	3.023	3.073	4.247	4.403	2.000	2.044	375.99
30	4.997	5.243	2.371	2.453	3.330	3.567	1.567	1.644	301.35
60	2.480	2.830	1.163	1.284	1.656	2.000	0.764	0.883	159.50
100	1.010	1.382	0.461	0.594	0.6838	1.0534	0.3027	0.4351	73.10
200	0.144	0.487	0.055	0.179	0.1119	0.4539	0.0393	0.1631	16.81
300	0.0438	0.3442	0.0128	0.1224	0.0406	0.3409	0.0112	0.1208	7.09
600	0.0133	0.2218	0.0036	0.0826					1.98
1,000	0.0078	0.1468	0.0023	0.0574					1.14
2,000	0.0043	0.0794	0.0015	0.0345					0.72
3,000	0.0035	0.0630	0.0012	0.0285	For Decay times greater than 300 years, use the same decay heat as for the direct codisposal assembly.				0.62
6,000	0.0028	0.0505	0.0010	0.0232					0.52
10,000	0.0024	0.0410	0.0009	0.0187					0.43
20,000	0.0017	0.0265	0.0006	0.0120					0.30
50,000	0.0011	0.0103	0.0004	0.0046					0.16
100,000	0.0009	0.0034	0.0003	0.0014					0.11

* The decay heat for the DHLW design basis canister is based upon the time of canister production, assuming 5 year old sludge and 15 year old precipitate.

6.4.2 Melt-Dilute Fuel Decay Heat

The right half of Table 6.3 presents a modified decay heat source for assemblies in the melt-dilute process. The decay heat has been removed for those isotopes that would volatilize or be released during the melting of the assemblies into the DOE SNF canister. The melting process is assumed to operate at temperatures somewhat above the 660°C Al melting point (~ 850 °C).

An ORIGEN calculation for the bounding LEU assembly was analyzed to help identify which isotopes contribute significantly to the decay heat and would volatilize. Table 6.4 presents these results by showing the maximum fractional contribution of various isotopes to the total decay heat. The calculation spanned decay times from 1 to 20,000 years using just 10 time steps. The maximum fractional contribution could be slightly higher at times intermediate between any of the 10 time steps.

Table 6.4 Peak Decay Heat Contribution by Isotope

Isotope	Peak Decay Heat (%)	Isotope	Peak Decay Heat (%)	Isotope	Peak Decay Heat (%)
^{239}Pu	83	^{144}Ce	4.5	^{244}Cm	0.20
^{241}Am	72	^{147}Pm	1.4	^{99}Tc	0.20
^{144}Pr	51	^{154}Eu	1.4	^{95}Zr	0.16
^{90}Y	42	**^{85}Kr**	**0.81**	^{126m}Sb	0.10
^{240}Pu	36	^{243}Am	0.51	^{242}Cm	0.08
^{137m}Ba	**30.6**	^{237}Np	0.45	^{106}Ru	0.08
^{106}Rh	12.4	^{236}U	0.35	^{241}Pu	0.07
^{134}Cs	**11.2**	^{95}Nb	0.34	^{214}Po	0.07
^{238}Pu	9.2	^{125}Sb	0.30	^{238}U	0.06
^{137}Cs	**9.1**	^{242}Pu	0.29	^{218}Po	0.05
^{90}Sr	8.7	^{234}U	0.28	^{222}Rn	0.05

The table lists the isotopes in decreasing order of importance starting with ^{239}Pu which contributes ~83% of the total decay heat at ~20,000 years of decay time. The ^{241}Am contributes ~72% of the total decay heat at ~7,200 years of decay time. The fractional decay heats in the table do not sum to 100% because each peak occurs at a different time in the decay calculation.

From Table 6.4, the ^{134}Cs and ^{137}Cs were identified as important isotopes that would volatilize. The volatilization fraction for Cs was conservatively estimated at 80% based upon fission product release studies of Al-base, plate type fuels.[5] Along with volatilizing 80% of the ^{137}Cs, 80% of the ^{137m}Ba daughter product would also be removed since $^{137}Ba_m$ has a 2.55 minute half-life. Additionally, 100% of the ^{85}Kr would be released during the melting. No additional isotopes from Table 6.4 were identified as being released. Since the half-lives of ^{134}Cs, ^{137}Cs and ^{85}Kr are 2.06, 30.07 and 10.77 years, respectively, Table 6.3 shows no difference between the codisposal and melt-dilute assemblies after 300 years.

6.4.3 DHLW Glass Canister Decay Heat

A heat load characterization for DHLW glass, produced at the Defense Waste Processing Facility (DWPF) at SRS, canisters is also needed in modeling the waste package. The potential heat loads from DHLW canisters span a wide range, but this analysis proposes that the heat load from the design basis DHLW canister is most appropriate for use in modeling the waste package. The maximum heat generation rate for any canister shipped to the MGDS is limited to 1,500 watts at the time of shipment.[6] This maximum heat load applies to canisters from all DOE sites, and projections are that some canisters from Hanford may approach the 1,500 watt limit. Canisters produced at SRS will have considerably lower power.

Of the more than 200 DHLW canisters already produced at DWPF, all have less than 10 watts of decay power. This relatively low power in the current DHLW production batch is a consequence of processing only waste sludge without any supernate precipitate. A total of 400 to 500 DHLW canisters will be produced in the next few years. It is expected that these DHLW glass canisters will not exceed 30 watts. For subsequent DHLW batches, the canister heat loads will increase. Forecasts show 4 batches of roughly 1,000 canisters each having peak canister heat loads of 286, 483, 375 and 255 watts at the time of production.[7]

The SRS design basis or maximum heat load canister has 710 watts of power at the time of production. Table 6.5 shows the isotopic inventory of this DHLW design basis canister for nominal canister fill conditions. Figure 6.5 and the right most column in Table 6.3 give the decay heat calculated by the ORIGEN code for this canister. The ORIGEN results in Table 6.3 are essentially the same as given in DWPF design documents[7], except that Table 6.3 presents more output time steps.

Table 6.5 Isotopic Inventory of the DHLW Design Basis Canister

Isotope	Inventory (Curies)	Isotope	Inventory (Curies)	Isotope	Inventory (Curies)
^{60}Co	170.	^{125}Sb	860.	^{234}U	0.0342
^{59}Ni	0.0239	^{134}Cs	336.	^{238}U	0.0105
^{63}Ni	2.97	^{135}Cs	0.0992	^{237}Np	0.00886
^{79}Se	0.17	^{137}Cs	43,300.	^{238}Pu	1,480.
^{90}Sr	48,200.	^{137m}Ba	41,400.	^{239}Pu	12.9
^{90}Y	47,700.	^{144}Ce	9,840.	^{240}Pu	8.67
^{93m}Nb	0.	^{144}Pr	9,850.	^{241}Pu	1,660.
^{99}Tc	3.07	^{147}Pm	24,100.	^{242}Pu	0.0122
^{106}Ru	2,240.	^{151}Sm	239.	^{241}Am	11.
^{106}Rh	2,250.	^{154}Eu	620.	^{243}Am	0.00579
^{107}Pd	0.0147	^{155}Eu	491.	^{244}Cm	107.
^{126}Sn	0.438	^{230}Th	0.	Sum	234,882.

Some DHLW glass canister analyses consider design basis canisters in an overfill condition having a 5.9% higher glass loading and 752 watt heat output at production. However, this overfilled condition is overly conservative for the purposes of this analysis. The nominally filled design basis canister provides a conservative estimate of the decay heat load because bounding inventories have been used for each of the heat producing isotopes.

The design basis inventory in Table 6.5 is for the time of the canister production. The sludge feed for the canister production was aged just 5 years while the supernate precipitate feed was aged 15 years. The relatively low age of these sludge and precipitate feeds introduces conservatism to the calculated maximum power for the design basis canister. The age of the waste sludge at SRS exceeds 20 years on average and there is practically no sludge that has not aged at least 5 years.

Analysis of the DHLW glass assumed the 5-year sludge age in the design basis canister by considering the potential for future production reactor operation. If a reactor were to operate in the future and the reactor's fuel where rapidly reprocessed through a canyon, then waste sludge might reach DWPF and be shipped offsite in a glass log within 5 years. However, this scenario seems very unlikely and it is reasonable to allow additional decay of the heat load in the design basis canister.

The precipitate was aged 15 years in the design basis calculations because of processing restrictions within the saltstone facility. Waste tank supernate is allowed to cool at least 15 years before processing to saltstone. This cooling time reduces the activity of some isotopes in the saltstone, such as ^{144}Ce and ^{106}Ru. This processing restriction in the saltstone facility means that all supernate precipitate reaching DWPF is at least 15 years old.

6.5 Verification

To verify the ORIGEN calculations in the decay heat analysis, Figures 6.6 and 6.7 shows a comparison of the decay heat data for the bounding fuel design with other SRS research reactor fuels. Decay heat data for SRS research reactor fuels are collected in "Appendix A" documents completed by personnel at the various research reactor facilities. At SRS, the data provided by these "Appendix A" documents are gathered in the SNF database that was previously described. The decay heat analysis extracts the decay heat data from the SNF database and plots a comparison with the ORIGEN results for the bounding fuel design.

The decay heat data from the SNF database has been not verified and the methods of calculation are undocumented. Some of the decay heat data are probably quite accurate, coming from calculations made using ORIGEN or other similar codes. In other cases, the data may only be a rough estimate of the actual assembly decay heat. It is unlikely that any of the decay heat data are from thermal measurements.

Figure 6.6 compares the decay heats calculated for the bounding assemblies with data for the HFBR, MURR and Saphir fuels. The data compared in this figure were normalized by calculating the assembly decay heat in watts produced per gram of ^{235}U depleted. Thus, for the decay heat comparison to be accurate, the assembly decay heat, the ^{235}U depletion and the cooling time data from the "Appendix A" document would all have to be correct. The figure shows normalized decay heat as a function of decay time after reactor shutdown. The ORIGEN results for the bounding LEU and HEU assemblies are plotted as solid curves in the figure and show only slight difference. The LEU decay heat is slightly higher because Pu build-up causes less ^{235}U to be depleted. The curves show that fuel enrichment does not a have strong influence in normalized decay heat comparisons. Variations in other parameters, such as fuel exposure and neutron spectrum, are not expected to have a strong influence in the decay heat comparisons. Thus, we should expect most of the decay heat results in the figure to be fairly close to the two curves calculated by ORIGEN.

Figure 6.6 shows good agreement between the ORIGEN calculation for the bounding assemblies and the MURR fuel data, although the MURR assemblies have less than 3 years of decay time. The ORIGEN results do not compare as well with the HFBR and Saphir fuel data. For these fuels, many decay heat data points are considerably higher than the ORIGEN results. Some of these higher points that form a straight vertical line may be discounted because the vertical line indicates that a single decay heat value was input for a group of assemblies all having the same decay time yet varying ^{235}U depletion.

Figure 6.7 presents further decay comparison between the ORIGEN bounding assembly results and other SRS research reactor fuels. These comparisons show less agreement than in Figure 6.7. Again, data on a vertical line, like that for the FMRB and R-2 fuels, show that inaccurate decay heat data were provided. The data that trend toward being parallel, but higher than the bounding assembly results, are of more concern. For example, the data for the FRG and GRR fuels, show roughly the same decrease in decay heat with time, but the decay heat is roughly twice that predicted for the ORIGEN bounding assemblies.

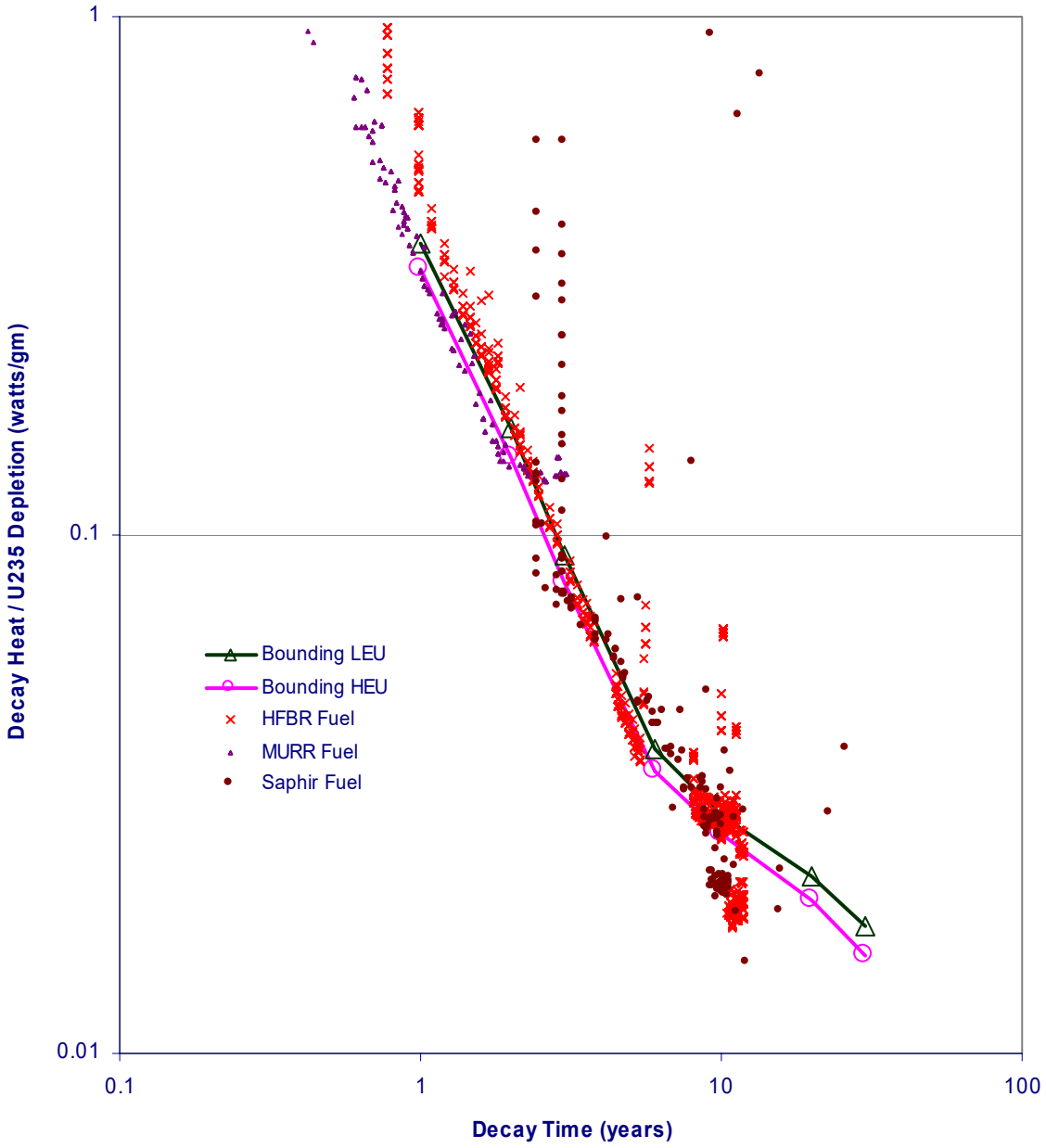

Figure 6.6 Decay Heat Comparison between Bounding Assemblies and HFBR, MURR, and Saphir Fuels

Overall, the comparisons in Figure 6.6 show reasonable, but not exceptional, agreement between the ORIGEN results and the data from the HFBR, MURR and Saphir research reactors. In Figure 6.7 the agreement is not as good; some of the data are clearly incorrect, but other data indicates that the reactor facilities predicted higher decay heat than the ORIGEN calculations.

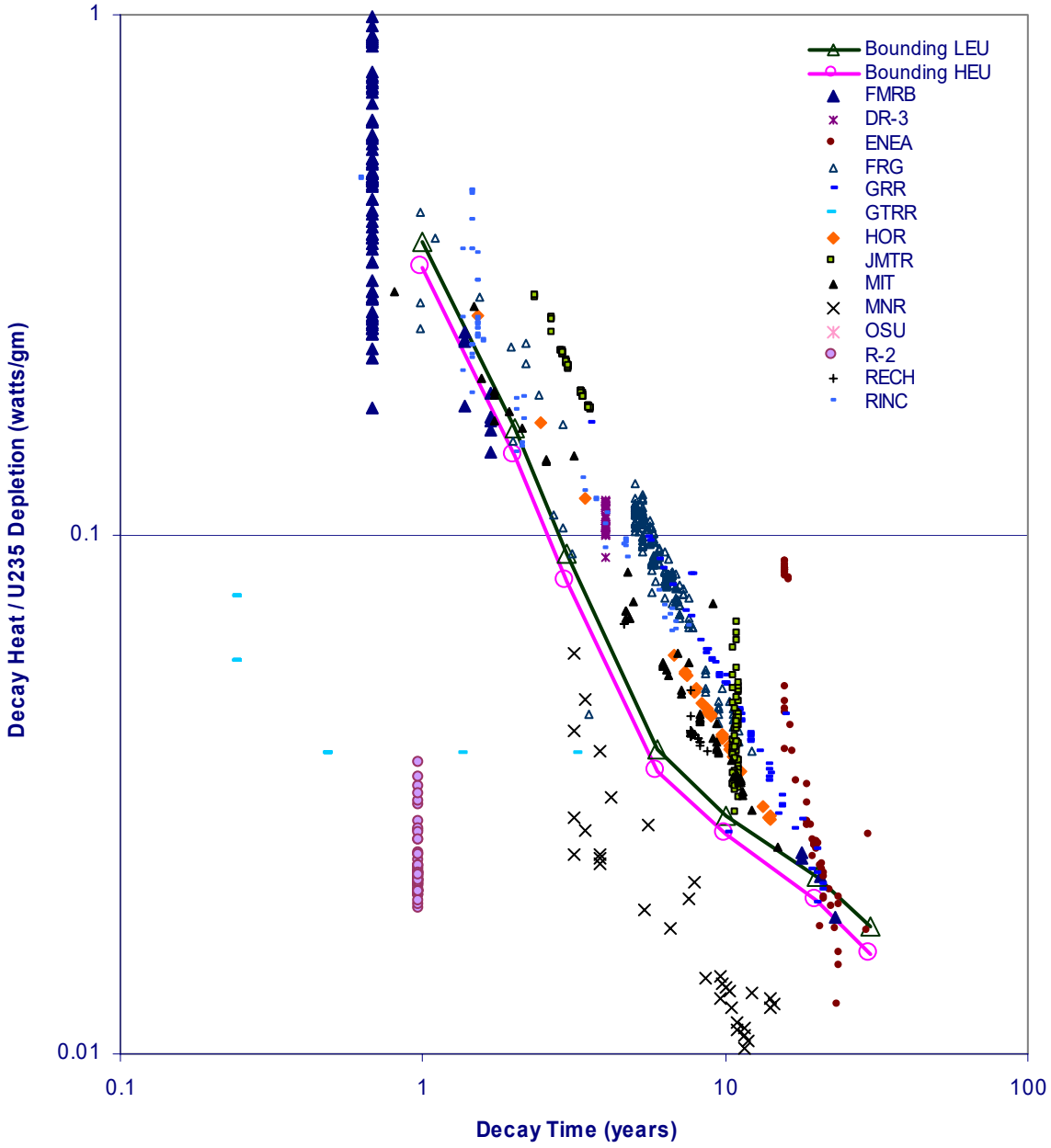

Figure 6.7 Decay Heat Comparison between Bounding Assemblies and Other Fuels

6.6 Summary/Conclusions

The decay heat analysis has provided bounding and nominal assembly designs for use in thermal design calculations of the waste packages to be emplaced at the MGR. Through comparisons with physical and depletion characteristics of the SRS research reactor fuels, this analysis shows the proposed assembly designs to be reasonably bounding or nominal.

The decay heat results for the bounding and nominal assemblies calculated with the ORIGEN code are presented in Figure 6.5 and Table 6.3. The analysis is based upon the decay heat output

from a standard-sized, generic MTR fuel assembly. The analysis does not specifically address the question of how many of these assemblies would be packed into the DOE SNF canisters inside the waste package.

The decay heat results do not include additional conservatism to account for uncertainty in this analysis. If such a conservative margin is to be included, it may be more appropriate to include the margin in the thermal design calculations, rather than in this decay heat source analysis. There are two types of uncertainties in this analysis; the calculational uncertainty within the computational methodology and the uncertainty due to difference between our design basis models and the actual waste package conditions in a repository.

Most of the computational uncertainty is within the decay heat computations of the ORIGEN code, rather than within the computations of the preceding codes in the SAS2H sequence. Assessment of the uncertainty in the ORIGEN decay heat computation is not readily available, perhaps because there is not a general need for highly accurate decay heat analyses. We might expect that the total uncertainty in the ORIGEN computations could be as high as 10% and due to uncertainties in parameters like isotopic half-lives, cross-sections, production rates and decay energy releases.

This analysis has additional uncertainty, generally conservative, because of the margin between the design basis models and the actual waste package conditions in a repository. Most research reactor assemblies loaded in waste packages will be considerably cooler than proposed bounding assemblies. There is additional margin because almost all DHLW canisters will be cooler than the design basis DHLW canister.

Finally, this analysis has uncertainty due to the cooling time delay before the fuels and the DHLW canisters are emplaced at the MGR. Cooling time information from the SNF database shows that, on average, fuel is stored about 5 years at the research reactor facilities before being shipped to SRS. The fuel will likely be stored at SRS for many years before processing and shipment to a repository. These delays due to fuel storage, processing and shipment cannot be definitively assessed, yet the delays reduce the decay heat considerably, especially in the early years. Similarly, the DHLW design basis canister decay heat is based upon the time of canister production, assuming 5 year old sludge and 15 year old precipitate. It may be appropriate to account for additional decay time because the waste will likely have considerably longer decay time before it finally reaches a repository.

6.7 References

[1] Losey, D. C., ***"SCALE 4.3 Testing on the HP Vectra Computer,"*** WSMS-CRT-98-0004 (January 1998).

[2] Losey, D. C., ***"ORIGEN Code Output for Proposed Bounding LEU Assembly in Decay Heat Analysis,"*** WSMS-CRT-98-0001 (January 1998).

[3] Losey, D. C., ***"Decay Heat Characterization of SRS Research Reactor Fuels,"*** WSRC-TR-98-00116, Rev. 0 (January 29, 1998).

[4] Hermann, O. W. and Westfall,R. M., ***"ORIGEN-S: SCALE System Module to Calculate Fuel Depletion, Actinide Transmutation, Fission Product Buildup and Decay, and Associated Radiation Source Terms,"*** NUREG/CR-0200, Rev. 5, Vol. 2, Sec. F7, ORNL/NUREG/CSD-2/V2/R5 (March 1997).

[5] Taleyarkhan, R. P., ***"Analysis and Modeling of Fission Product Release from Various Uranium-Aluminum Plate-Type Reactor Fuels,"*** Nuclear Safety 33, 6 (1992).

[6] ***"Waste Acceptance Systems Requirements Document,"*** Revision 04G (March 2001).

[7] Plodinec, M. J. and Marra, S. L., ***"Projected Radionuclide Inventories and Radiogenic Properties of the DWPF Product,"*** WSRC-IM-91-116-3, Rev 0 (October 1994).

7.0 CODISPOSAL WASTE PACKAGE THERMAL ANALYSIS

The engineering viability of disposal of spent nuclear fuel in a geologic repository requires a thermal analysis to provide the expected temperature history of the fuel waste forms within the disposal package. Calculated temperatures are used to demonstrate compliance with criteria for waste acceptance into the MGR and also to assess the chemical and physical behavior of the waste form within the codisposal WP. A thermal analysis methodology was developed and used to calculate peak temperatures and temperature profiles within the SRS Al-SNF and the surrounding DHLW glass logs. Figure 7.1 illustrates a horizontal emplacement of such waste in the codisposal WP.

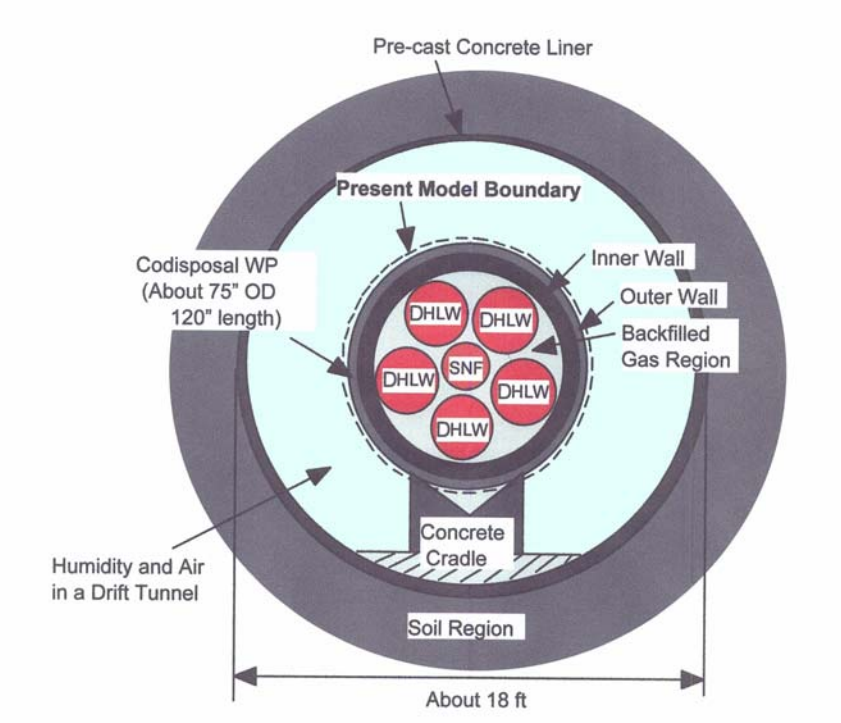

Figure 7.1 Horizontal Emplacement of Codisposal WP within a Repository Drift Tunnel

This section summarizes detailed analyses and findings reported in WSRC-TR-99-00366, "Thermal Performance Analysis of Melt-Dilute Aluminum SNF in Codisposal Waste Packages in the Geological Repository," December 1999,[1] which can be referred to for additional information as needed.

7.1 Acceptance Criteria

Sections 4.3.14 and 4.8.14 of the WASRD[2], state that "DOE SNF canisters shall have a thermal output at time of acceptance into the CRWMS less than 1,970 watts and that the total heat generation for canisters containing HLW or DHLW shall not exceed 2,540 watts per canister." The estimated decay heat for the SRS MD-SNF canister is less than 1200 watts and less than 500 watts per assembly for the DHLW glass canisters. These decay heat values were calculated using the decay heat generation data and methods discussed in Section 6.0. Table 7.1 illustrates

calculated decay heat values as a function of storage time representative of maximum MD-SNF canister loading and 100% Cs retention (a bounding design assumption).

Table 7.1 Decay heat source in SNF canister and DHLW regions for a codisposal WP filled to 100 % of MD-SNF volume and the MD-SNF ingot containing 100% Cs.

Storage Time (yrs)	Assembly Power (W/assembly)	Power per DHLW (W)	Total Power for SNF Can. (W)	Volumetric SNF Power (W/m^3)	Volumetric DHLW Power (W/m^3)
0	8.58	472.3	1158.30	2888.24	530.91
10	6.53	375.99	881.55	2198.16	422.65
20	5.243	301.35	707.81	1764.92	338.75
50	2.83	159.5	382.05	952.65	179.29
90	1.382	73.1	186.57	465.22	82.17
190	0.487	16.81	65.75	163.94	18.90
290	0.3442	7.09	46.47	115.87	7.97
590	0.2218	1.98	29.94	74.66	2.23
990	0.1468	1.14	19.82	49.42	1.28
1990	0.0794	0.72	10.72	26.73	0.81
2990	0.063	0.62	8.51	21.21	0.70
5990	0.0505	0.52	6.82	17.00	0.58
9990	0.041	0.43	5.54	13.80	0.48
19990	0.0265	0.3	3.58	8.92	0.34
49990	0.0103	0.16	1.39	3.47	0.18
99990	0.0034	0.11	0.46	1.14	0.12

Note: Storage time of zero years in the table corresponds to a time of ten years cool down following reactor operation with the assembly

WASRD Disposability Standard 2.4.21 – "Limits on Multi-Element Canister Thermal Design" – specifies that the SNF cladding surface temperatures, for assemblies placed into waste packages, shall not exceed 350 °C. In addition, Section 4.5.16 of the WASRD states that SNF cladding for DOE SNF of commercial origin placed in disposable multi-element canisters shall not exceed 350 °C for zircaloy-clad assemblies and 400 °C for stainless steel assemblies at the time of acceptance into the CRWMS.

A design goal of 350 °C was selected for the peak temperature of MD-SNF in the codisposal WP based on adopting present WASRD requirements for zircaloy-clad assemblies. Furthermore, the MD-SNF, an aluminum-based material, has the lowest melting temperature for all the waste forms envisioned for repository disposal. To avoid the potential impact to the disposal system, it is essential that the MD-SNF temperature remain below its melting temperature since molten aluminum can dissolve stainless steel materials and thus pose a threat to the waste package. In this regard, the temperature limit of 350°C for the MD-SNF is justified for evaluation of the thermal performance of the codisposal WP.

The thermal analyses discussed in this section are based on the estimated decay heat generation for the contents of the codisposal waste package representative of a 10000-year burial. Extensive design parameter sensitivity studies were performed to support achievement of the 350 °C melt-dilute SNF temperature goal. The following sections describe models developed and summarize key findings.

7.2 Analysis Approach

Two thermal analysis modeling regions were selected, one representing the codisposal WP and contents (called the "**WP Model**") emplaced in a repository drift tunnel, and the second region (called the "**Macro Model**") representing the surrounding repository geological media. These two modeling regions and the interfacing boundaries are illustrated in Figure 7.2. The WP Model and the Macro Model computational regions were coupled using expected natural convection and thermal radiation phenomena interfaces between the codisposal WP outer wall and the repository drift tunnel concrete liner inner wall.

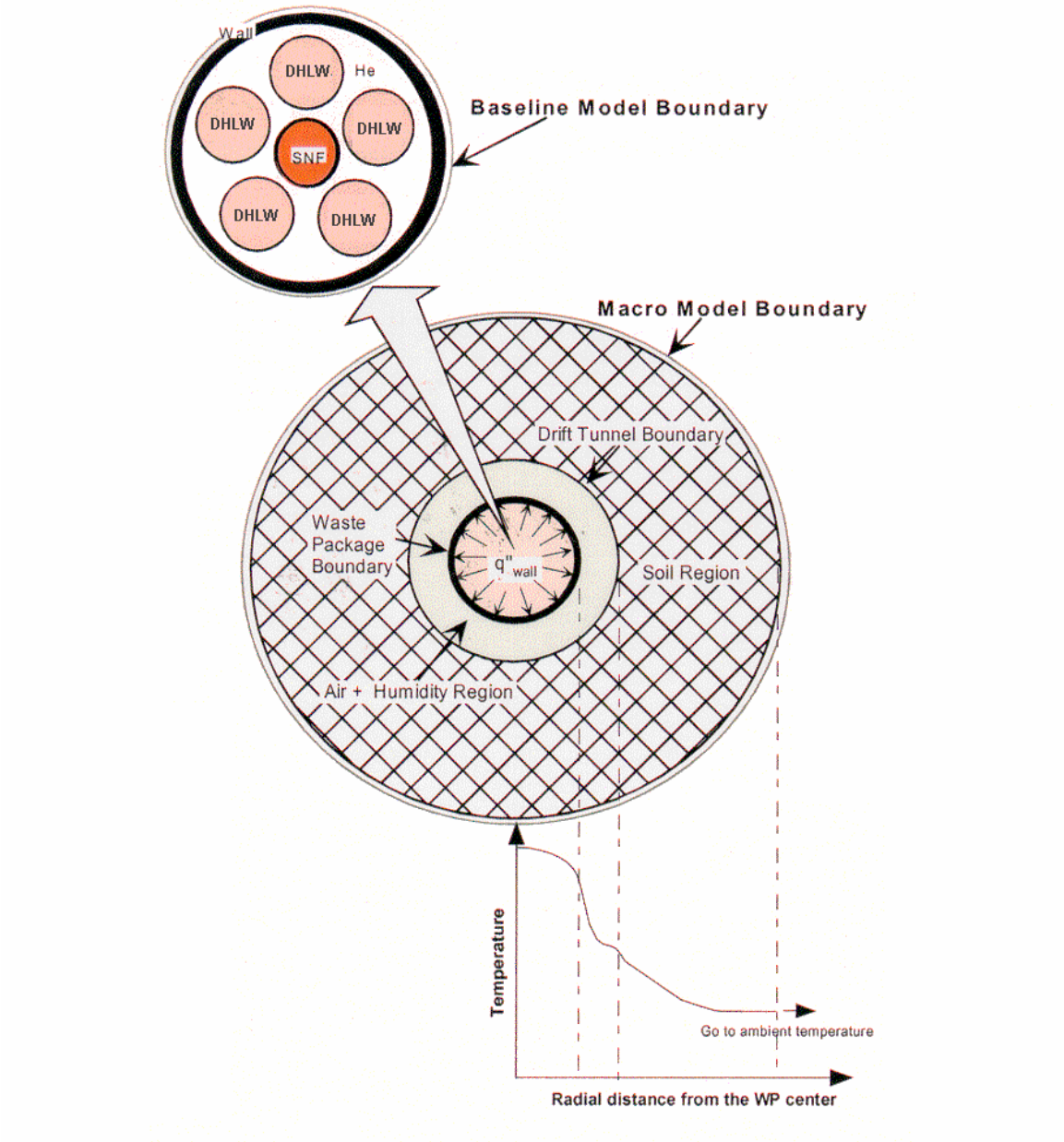

Figure 7.2 Baseline WP Model - Repository Geological Macro Model Interface Boundaries

Thermal models representative of intact codisposal WP design and contents, and surrounding geological repository conditions were created utilizing the CFX-4.2 code's body-fitted coordinate system capability, which allows for treatment of non-orthogonal geometries. These models, their computational purpose and modeling domain are summarized in Table 7.2. The computational coupling logic between the Macro and WP thermal modeling regions is shown in Figure 7.3.

Table 7.2 Thermal Modeling Regions and Models Employed

Models		Primary Purpose	Modeling Domain
Macro Model		- Provides boundary conditions to the WP model with and without engineered barrier system from geologic repository conditions and requirements.	- Includes the codisposal WP wall, drift tunnel region with / without engineered barrier system, and soil region around the WP (Figures 7.8 and 7.9).
WP Model	**Baseline Model**	- Assesses the thermal performance of the melt-dilute codisposal WP using the computationally efficient model in terms of the waste acceptance criteria.	- Includes the entire region of the codisposal WP containing the melt-dilute SNF canister (Figure 7.2).
	Detailed Model	- Assesses the conservatism of the baseline model imbedded in the baseline model. - Understands detailed cooling mechanism for the present codisposal WP configurations.	
	Conduction Model	- Investigates what is the most dominant mode of thermal energy transport among the three possible heat transfer processes, conduction, convection, and radiation, for the present codisposal WP configurations.	

The input requirements used to analyze the codisposal WP containing the melt-dilute SNF form is shown in Figure 7.4. This figure also illustrates why computationally efficient thermal models were necessary.

7.3 Waste Package (WP) Thermal Models

A 1/2 sector model of the codisposal WP was used as a computational domain for a better computational efficiency by imposing symmetrical boundary conditions on the diagonal centerline of the WP cross-sectional plane. Figure 7.5 illustrates the 1/2 sector model, including the symmetry plane and the different material zones.

A two-dimensional geometry file for the WP modeling was created using the multi-block preprocessor of the CFX code[3], using the body-fitted coordinate system, which allows the treatment of non-orthogonal geometry. An optimum grid of 8117 cells was established from the grid sensitivity analysis under SGI workstation environment. The WP canister model consists of 195 element blocks and 6 different material zones on the x-y computational plane. Non-uniform two-dimensional meshes of the computational domains used for the WP models are illustrated in

Figure 7.6. Numerical solution techniques to solve the governing equations are described in Reference 4.

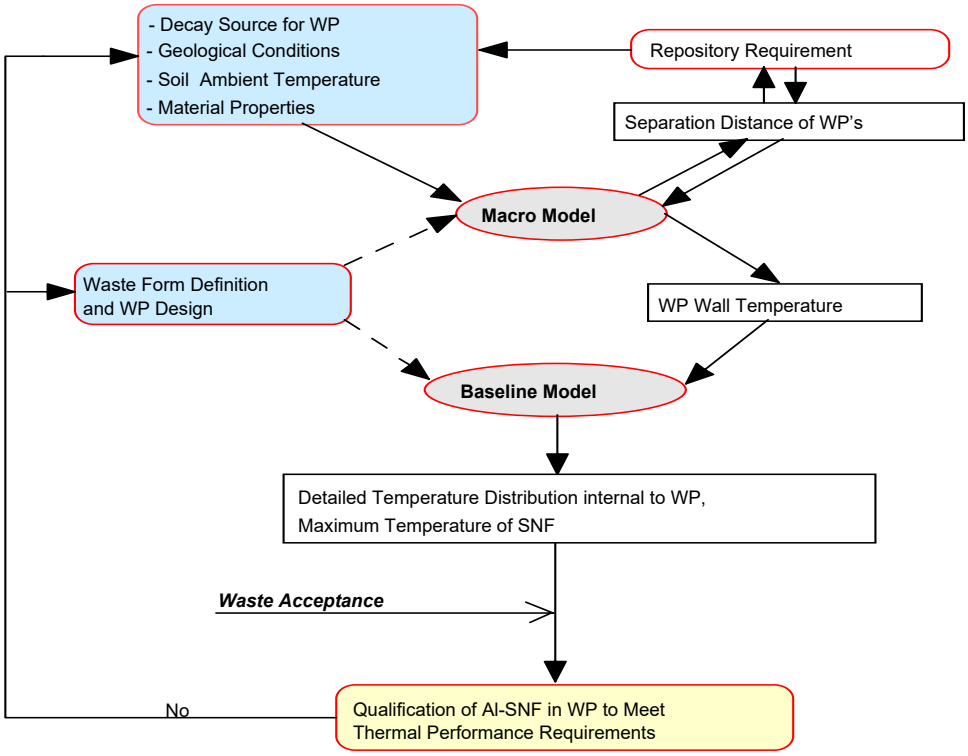

Figure 7.3 Computational Coupling Logic Used to Integrate Macro and WP Thermal Models

All WP thermal models (see Table 7.2) are represented by the geometric layout shown in Figure 7.5 and non-uniform geometric computational mesh represented by Figure 7.6.

7.3.1 WP Conduction Model

The conduction model was based on conduction heat transfer only and did not include any internal mechanical support structure such as the waste package support structure or the DOE SNF support tube (see Figure 2.1). The mathematical equations governing conductive cooling in this WP model were derived from the energy balance equation and neglected the contributions of thermal convection and radiation heat transfer. This model was used primarily to test the adequacy of the grid fineness for the solution accuracy, and residual error checking to demonstrate the adequacy of the grid fineness. These results were documented in Reference 4.

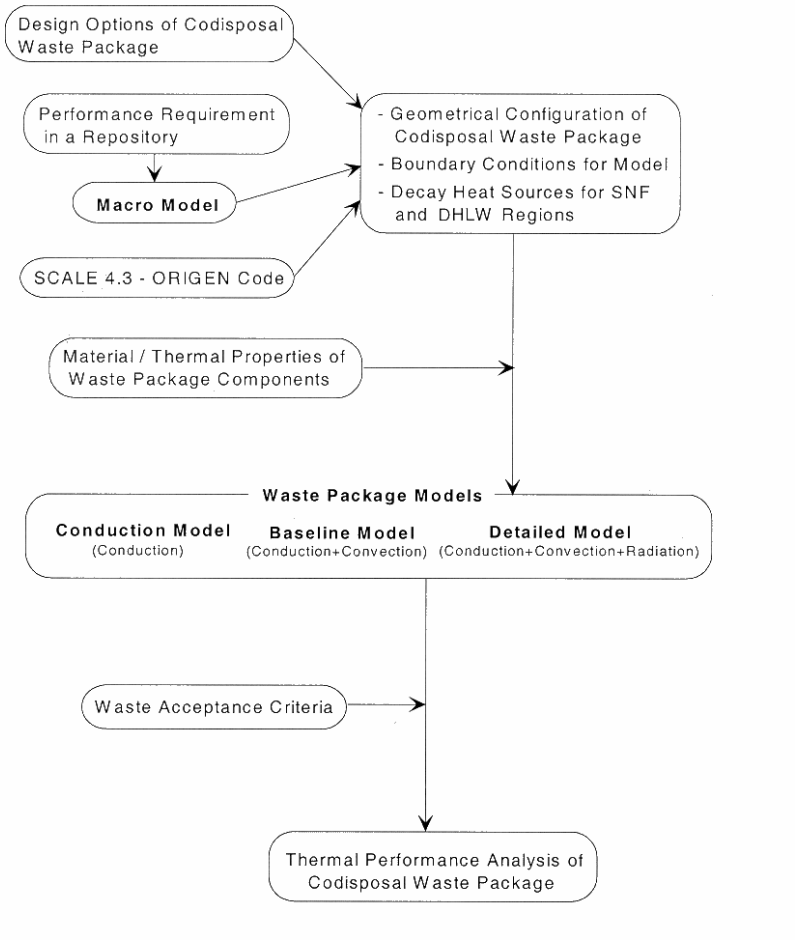

Figure 7.4 Thermal Analysis Logic Utilized for Waste Package Models

7.3.2 WP Baseline (Conduction – Radiation Coupled) Model

A computationally efficient baseline model, which neglects natural convection, was constructed to investigate combined radiative and conduction effects using the mesh distribution shown in Figure 7.6. Natural convection mass and momentum transport contributions were set to zero. The WP Baseline Model was used extensively for sensitivity studies directed at investigating design parameters and design conditions shown in Table 7.3. The thermal and radiation properties utilized for the codisposal SNF components shown in Figure 7.5 are shown in Table 7.4

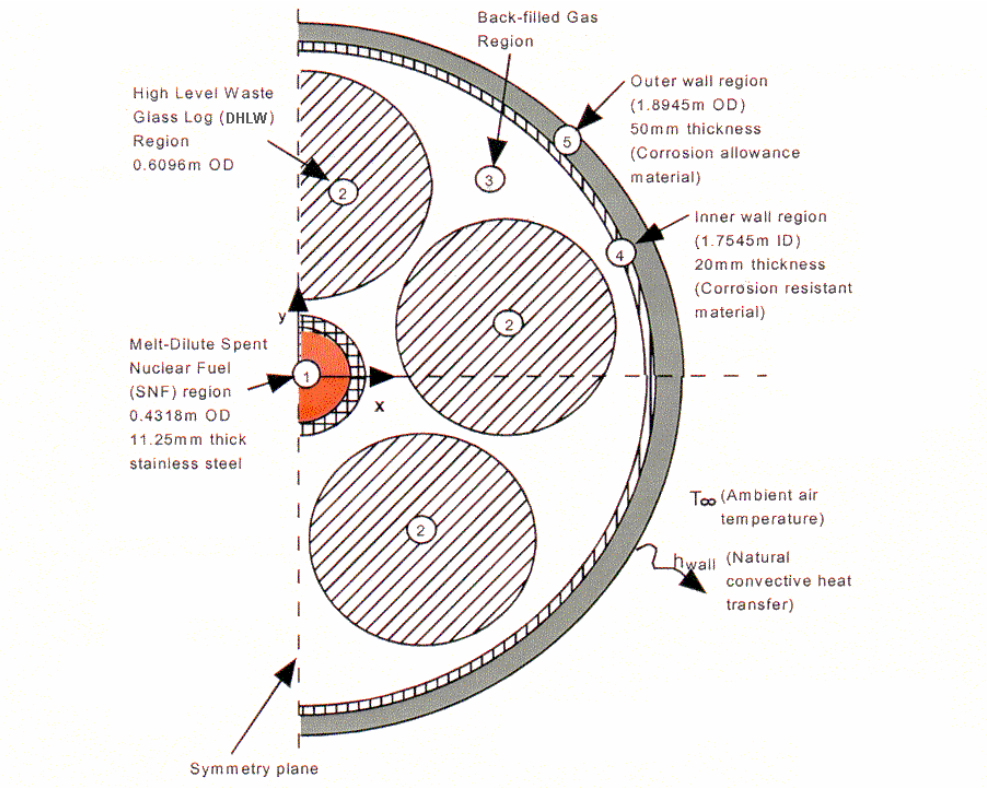

Figure 7.5 Thermal Modeling of a Codisposal SNF Waste Package

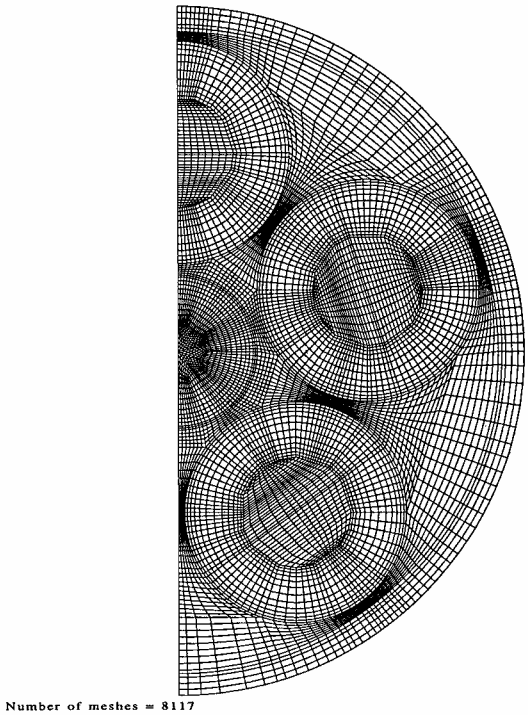

Figure 7.6 Non-Uniform Computational Mesh Used for Codisposal WP Thermal Analysis

.

Table 7.3 Reference Design Conditions Investigated for the Present Thermal Analysis of the Codisposal WP Models Containing MD-SNF Canister

Design Parameters	Design Conditions
• Back-filled gas inside / outside of MD-SNF canister in codisposal WP	• Helium gas inside and outside of SNF canister
• Transient decay heat loads for SNF and DHLW glass logs	• 100% Cs and 50-90 vol% melt-dilute loading within the canister and the DHLW design basis canister (bounding LEU in Reference 4)
• Initial reference time (storage time: "Year 0" in the present analysis)	• 10 years cooling time since discharge from reactor and production of HWGL
• Internal structure of the WP container	• Intact codisposal geometry w/o support structure
• WP boundary conditions	• Repository ambient temperature: 100 °C • Natural convection boundary condition at the WP wall
• Codisposal WP location in a repository tunnel	• Center of a drift tunnel

Table 7.4 Thermal and Radiation Properties of the Codisposal WP Components

Region Number in Figure 7.5	Materials		Thermal Conductivity	Emissivity
1	SNF canister	Melt-dilute region	175.2 W/mK	—
		Canister wall	17.30 W/mK	0.60
2	High-level Waste Glass Log (DHLW)		1.046 W/mK	0.60
3	Back-filled gas	Helium	0.205 W/mK	—
		Air	0.036 W/mK	—
4	Codisposal canister inner wall		10.977 W/mK	0.80
5	Codisposal canister outer wall		48.810 W/mK	—

7.3.3 Detailed WP Model

The "detailed" WP Model (see Table 7.2) incorporated conduction, convection, and radiation energy transport processes to investigate cooling mechanism of the sealed WP container containing one MD-SNF canister and five DHLW canisters for the purpose of evaluating the conservatism imbedded in the baseline model. The details of modeling these phenomena are described in detail in Reference 1.

The main design parameters investigated (see Figure 7.5) were:

- *Different combinations of back-filled gases* in the SNF canister and the WP container (e.g., air or helium in SNF canister, and air or helium in WP container).

- *Various sets of combinations of heat sources* (bounding or nominal SNF and DHLW decay heat sources) were investigated. Bounding decay heat sources for the SNF and DHLW were used for the present analysis since nominal Al-SNF source values were used for the sensitivity analysis in the previous work.[4]

- *Initial reference storage time* related to the spent fuel cooling time before the emplacement of aluminum-clad DOE SNF assemblies into the WP container: 10 years cooling time is used as the reference storage time "0" year for the present analysis.

- *Internal structure materials of codisposal canister*: The present analysis is assumed that SNF and DHLW canisters inside the WP remain intact.

- Various *different volume fractions* of Al-SNF inside the canister.

- *Repository temperature history* since emplacement of WP.

- *Waste package location in a repository drift tunnel* (center or corner of a drift tunnel): The present analysis is assumed that WP is located at the center of a drift tunnel repository.

The thermal performance analysis for the codisposal WP requires known values for the design parameters listed above and some of them are not available at this time. For the present work, the initial reference time is assumed to be 10 years cooling time since the discharge from reactor and production of DHLW. In addition, thermal conduction paths afforded by the support structure between the Al-SNF canister and the DHLW containers were ignored in this analysis pending final support structure design selection. Neglecting these mechanical support structures will likely result higher than component temperatures calculated in studies to-date.

7.3.4 Macro Model

The main purpose of the geological macro model was to provide the boundary conditions to the Waste Package (WP) models for a possible range of geologic conditions and repository requirements. The macro model includes WP wall, drift tunnel environment, and soil regions as the modeling boundary as shown in Figure 7.2. The soil region was modeled as a conductive cooling medium, and the drift tunnel region considered conduction, natural convection induced by buoyancy effect, and radiation with or without absorption effect inside humid medium. The intent was to establish principal modes of heat transfer.

The natural convective flow regime for the air-cooled design assumption was based on the non-dimensional Grashof number (Gr_L), which is the parameter describing the ratio of buoyancy to viscous forces. For a typical drift tunnel without forced air circulation, the estimated Gr was approximated as 2×10^9. This corresponds to turbulent convective flow based on applicable experimental correlations. For the present analysis, natural and forced mixed convection regimes within the enclosure are assumed to be turbulent.

Figure 7.7 illustrates the heat transfer characteristics employed between the horizontal curved surface of the WP into the ambient air region of a drift tunnel.

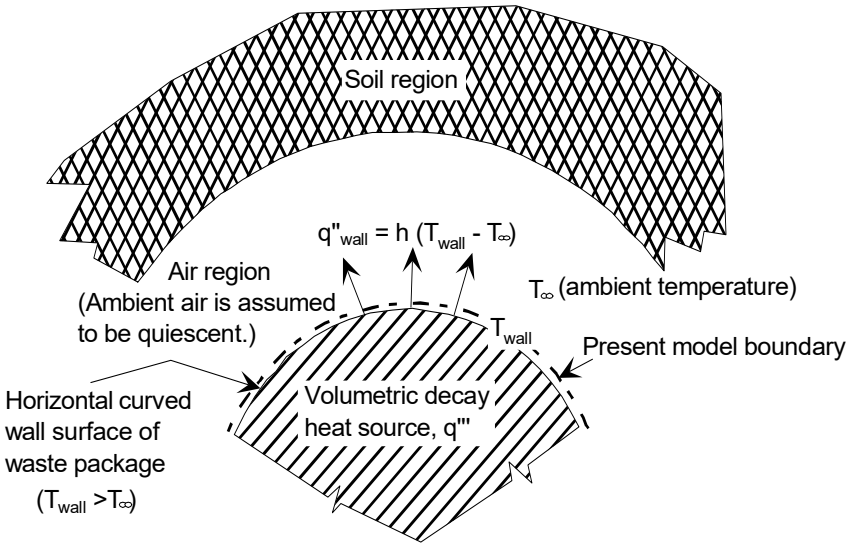

Figure 7.7 Convective Coupling between WP and Soil Region

At the outer macro boundary of the region (see Figure 7.2) surrounding the drift tunnel, a uniform soil temperature was used as external boundary condition for the macro model. The soil temperature was determined by the performance requirement of a geologic repository. Thermal performance analysis of the codisposal WP was conducted by using the reference geologic boundary conditions as defined in Table 7.2. Sensitivity analyses of the geologic parameters were performed with respect to the reference conditions in order to investigate parameter importance to WP cooling rate in a geologic repository.

Table 7.5 Geologic Reference Boundary Conditions for the Macro Model

Geologic Parameters	Reference Conditions
• Tunnel separation distance	160 ft between the two neighboring drift tunnels
• Equilibrium soil temperature	30 °C
• Effective thermal conductivity	1.59 W/mK
• Heat source loads	16 years cooling time for 100% Cs and 90 vol% melt-dilute Al-SNF and DHLW
• Tunnel humidity	100% relative humidity
• WP location in a drift tunnel	Center of a drift tunnel
• Drift tunnel structure	Drift tunnel with no engineered barrier system around the codisposal WP
• Drift tunnel surface emissivity	Emissivity = 0.94 (based on the rough concrete surface)
• Tunnel diameter	18 ft

7.3.5 Best Estimate Geological Boundary

The macro model that includes the geologic medium around the codisposal WP provides wall temperature boundary conditions for the WP models. In the model, thermal conductivity for the soil region was assumed to be constant since there is no experimentally confirmed value. The radiation absorption coefficient for water humidity was assumed to be independent of medium temperature for computational efficiency since the coefficient value is relatively insensitive to the temperature for the range of possible geologic conditions expected in the proposed mined

geologic repository. Natural convective flow regime within the drift tunnel region was examined under the present geometrical configurations and the geologic repository conditions.

Several key geologic parameters were investigated using the macro model in order to find out what parameters are the most important in terms of thermal performance of the codisposal package for the qualification studies of the WP containing the MD-SNF canister. The parameters are

- Humidity in the drift tunnel region
- Soil thermal conductivity
- Drift tunnel surface emissivity
- Engineered barrier system around the codisposal WP
- Separation distance between the two neighboring geologic WP's

The geological modeling domain for the repository without an engineered barrier system is shown in Figure 7.8, and computational domain for the geologic repository with an engineered barrier system is shown in Figure 7.9. For the numerical analysis, an optimum grid of 13120 cells was established from the grid sensitivity analysis for the computational domain of the macro model (see Figure 7.10).

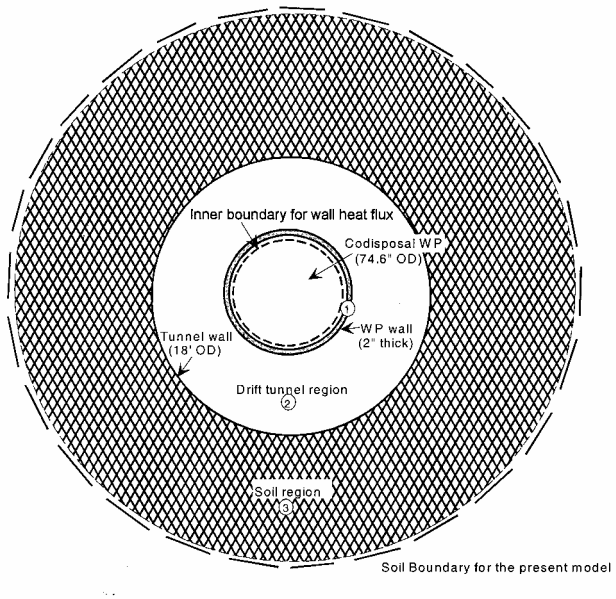

Figure 7.8 Macro Model Boundary of Codisposal WP to Include Geologic Media

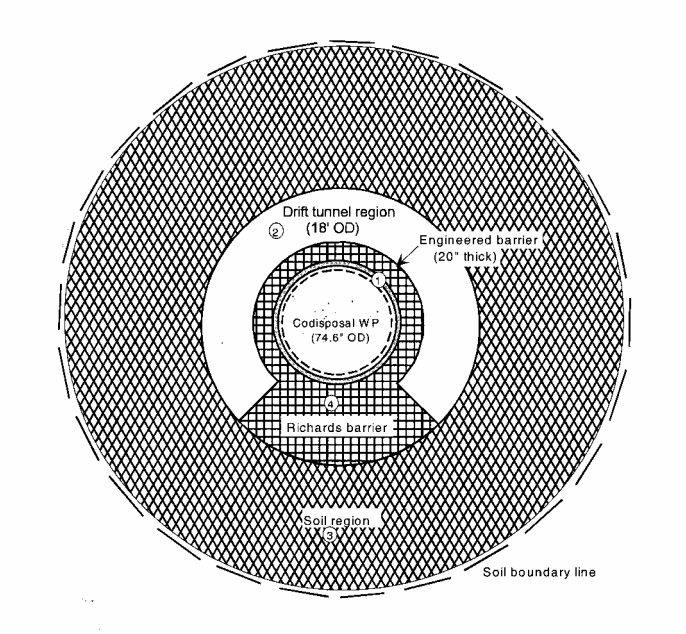

Figure 7.9 Macro Model with Engineered Barrier System Included

The WP canister model consists of 16 element blocks and 4 different material zones on the x-y computational plane. Non-uniform two-dimensional meshes of the computational domains for the macro model are presented in Figure 7.10.

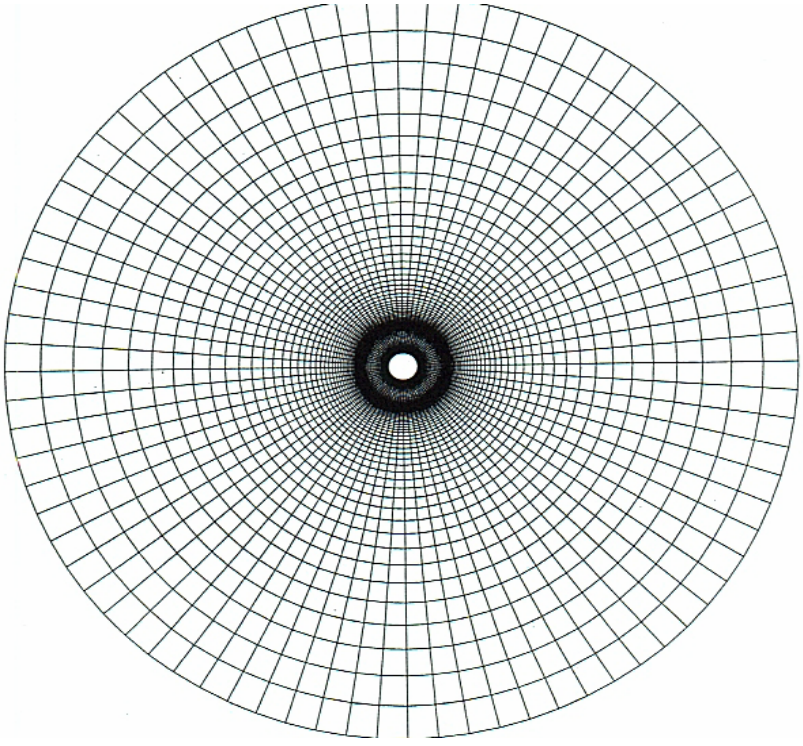

Figure 7.10 Two-dimensional Non-Uniform Computational Mesh used for the Geological Media Macro Model Surrounding the Codisposal WP

Natural convection due to internal gas movement inside the waste package is neglected in the "Baseline Model" (see Table 7.2). The effective thermal conductivity for the melt-dilute ingot of the SNF canister was based on a Al-13.2 wt% uranium metal alloy.[4,5] The heat load for each of the SNF and DHLW regions was represented as a volumetric heat input source by assuming that decay heat generation for each region is uniformly distributed. The bounding decay heat load was estimated by assuming that no cesium isotopes were removed during the melting process and that a volumetric heat load for the melt-dilute SNF ingot filled to 100% of the SNF canister volume. Table 7.1 illustrated the variability of decay heat as a function of storage time for one of the design assumptions analyzed. Parametric sensitivity analyses were performed using 50%, 75%, 90%, and 100% of SNF volume with the melt-dilute ingot retaining 100% Cs.

7.4 Waste Package Results & Discussion

Based on the approach methodology and the modeling assumptions discussed previously, two-dimensional conduction, conduction-radiation coupled and conduction + radiation + convective coupled models were utilized to investigate key design parameters and to find sensitivities to the changes to the design parameters and conditions shown in Table 7.3.

The "baseline" model was the principal analysis model used. Four cases were evaluated: a SNF canister filled with 100 vol% of melt-dilute ingot corresponding to 135 fuel assemblies, 90 vol% of the ingot corresponding to 121 fuel assemblies, 75 vol% corresponding to 101 assemblies, and 50 vol% corresponding to 67 assemblies. All ingots are 20% enriched alloy containing the composition of aluminum-13.2 wt% uranium. Both helium- and air- filled codisposal WP's (see Figure 7.5) having 100% cesium decay heat loads under various ambient temperatures of a repository region were evaluated

Figure 7.11 illustrates the qualitative temperature predictions for the three models used based on analysis results derived from the detailed model calculations

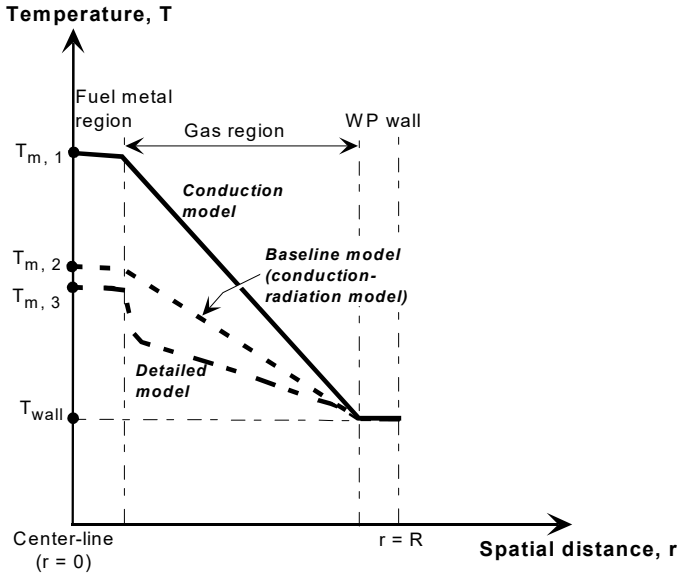

Figure 7.11 Qualitative Temperature Distributions Predicted by the Three Models Utilized

The level of cooling contribution for each of the three heat transfer mechanisms using notations employed in Figure 7.11 to the WP cooling may be approximately estimated in terms of the dimensionless ratio of temperature difference (θ_i) between the WP center and its wall boundary and its wall boundary (where i = *cond., conv., or rad*.) using Equations 1 – 3.

$$\theta_{rad} = 100\, x\, \frac{\left(T_{m,1} - T_{m,2}\right)}{\left(T_{m,1} - T_{wall}\right)} \quad (1)$$

$$\theta_{conv} = 100\, x\, \frac{\left(T_{m,2} - T_{m,3}\right)}{\left(T_{m,1} - T_{wall}\right)} \quad (2)$$

$$\theta_{cond} = 100 - \theta_{rad} - \theta_{conv} \quad (3)$$

The results for 100 and 50 SNF volume percentages loading of the canister are shown in Table 7.6. The results show that convection contribution to the cooling of the present codisposal WP is negligible in predicting the peak temperatures of the present codisposal WP. Such findings supported use of the "baseline" model for the majority of this thermal analysis effort.

Table 7.6 Typical Levels of Heat Transfer Cooling Contributions for a He-Cooled Codisposal WP Containing 100 vol% and 50 vol% MD-SNF Forms

SNF volume %	θ_{rad} (Radiation)	θ_{cond} (Conduction)	θ_{conv} (Convection)
100	~ 74%	~ 25%	~ 1%
50	~ 61%	~ 37%	~ 2%

Table 7.7 illustrates the peak WP temperature as a function of repository storage time and the radiative cooling contribution. This table also illustrates the WP design capability to meet the 350 °C temperature criteria.

Table 7.7 Thermal Performance of the He-Cooled Codisposal WP Containing 100 vol% MD-SNF Form as a Function of Storage Time

Storage Time (Years)	Peak Temperature of WP (°C)	θ_{rad} (defined by eq. (3)) (%)
0	297	74
10	266	69
50	177	62
90	142	52

Tables 7.8 and 7.9 illustrate WP peak temperatures calculated for the range of SNF canister loading and decay heat loads investigated as a function of storage time. The small temperature

difference between helium-filled versus air-filled conditions is attributable to the high thermal conductivity of the ingot materials versus the fill gas.

Table 7.10 illustrates the temperature variation as a function of SNF canister loading fraction and decay heat loads at a "zero" year storage time. When the metal ingot volume decreased to 90 vol%, the maximum temperature of the WP was 301 °C at 0 years of storage time. This result is 4 °C higher than that of the 100 vol% WP as a result of the offset effect of SNF heat source decrease and back-filled gas volume increase due to ingot volume reduction inside the SNF canister.

Table 7.8 Comparison of Peak Temperatures for the Codisposal WP with 100 vol% SNF Canister Containing 100% Cs in MD Alloy Ingot Based on the Baseline Model for Various Storage Times (Ambient Temperature = 100 °C)

Storage Times (Years)	Melt-Dilute WP (100 vol%)	Melt-Dilute WP (100 vol%)
	He-filled WP	Air-filled WP
0	297	301
10	266	269
20	235	239
50	177	181
90	142	148
190	110	113
590	100	102
1990	100	100

Table 7.9 Comparison of Peak Temperatures for the He-Cooled Codisposal WP with Various Volume Percentages of SNF Canister Containing 20% Cs and 100% Cs in MD Alloy Ingot Based on the Baseline Model for Various Storage Times (Ambient Temperature = 100 °C)

Storage Times (Years)	Melt-Dilute WP (75 vol% SNF)	Melt-Dilute WP (90 vol% SNF)	Melt-Dilute WP (100 vol% SNF)
	20% Cs decay load	20% Cs decay load	100% Cs decay load
0	284 (347*)	264 (286*)	297(301*)
10	247	238	266
50	168	168	177
90	135	133	142
190	115	107	110
590	104	101	100
1990	102	100	100

Note: * Peak temperature for the air-filled WP.

Table 7.10 Comparison of Peak and Wall Temperatures for the He-Cooled Codisposal WP with Various Volume Percentages of MD-SNF Canister Containing 100% Cs in MD Alloy Ingot Based on the Baseline Model at 0 Years of Storage Times

Max. and WP Wall Temperatures	50 vol%	75 vol%	90 vol%	100 vol%
SNF Decay Load (W)	482	530	557	577
Max. Temperature (°C)	293	298	301	297
WP Wall Temperature (°C)	206	216	226	226
ΔT *(°C)	87	82	75	71

Note: * Max. temperature difference of WP = (Max. temperature – WP wall temperature)

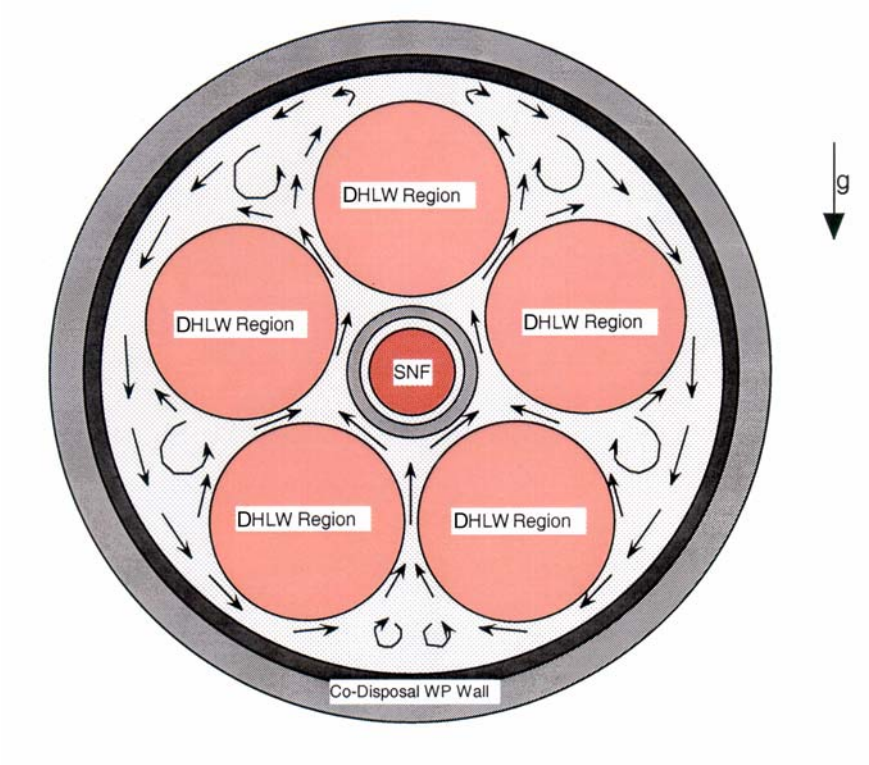

Figure 7.12 Illustrative WP Internal Convective Flow Patterns Due to Convective Cooling

Figure 7.12 illustrates the expected internal gas convective flow patterns within the codisposal WP. Figure 7.13 shows computed temperatures for a helium filled WP using the "baseline" model for the design conditions shown. The difference between a 100% and 90% volume melt-dilute loading is very small.

Figure 7.14 shows radial temperature distributions performed using the "baseline" model and the "detailed" model which included natural convective effects within the codisposal WP. These illustrative calculations show that the temperature gradient across the DHLW region for the "detailed" model is smaller than that of the "baseline" model due to the gas temperature mixing effect driven by the natural gas circulation inside the WP. However, as noted previously (see Table 7.6) the convective cooling contribution is very small.

Limiting thermal calculations have been performed using a 100% Cs decay heat load for the melt-dilute alloy ingot, which is located inside the SNF canister of the codisposal WP. The transient decay heat load was estimated in a conservative way by assuming that no cesium isotopes would be released during the melt-dilute fabrication process.

7.5 WP Model Results Combined with Macro Model

The two-dimensional multi-region model (see Figure 7.2) to include drift tunnel and soil regions, referred to as the macro model, were developed to investigate key parameters related to the characterization studies of the codisposal WP. The model was also used to find sensitivities to the changes of the geologic parameters on the thermal performance of the geologic WP. The reference boundary conditions for the macro model are defined in Table 7.3. The macro model also provided the best estimate boundary conditions to the WP baseline model for postulated geologic repository conditions. These analysis results were based on the reference boundary conditions and material properties provided in Tables 7.3 and 7.11.

A theoretical modeling approach for combined conduction and radiation in a non-absorbing medium was undertaken to verify the present computational model under the present geometrical and physical conditions are shown in Figure 7.15. This theoretical modeling approach is a coupling of the detailed WP model described in Section 7.3.3 and the macro model described in Section 7.3.4. Figure 7.16 illustrates the computed temperatures that support continued use of the baseline model for thermal analysis.

Effects of the radiation absorption due to the humidity present in the drift tunnel region on the thermal performance of the codisposal WP were also investigated by comparing with results of the non-absorbing approach. The thermal and material coefficients of the geological medium were assumed to be independent of the temperature for the present analysis. The details of this modeling approach are described in Section 5.2 of Reference 1.

Table 7.11 Thermal and Radiation Properties of the Geologic Repository with Engineered Barrier System used for the Present macro Model

Region Number in Figs. 7.8 and 7.9	Materials		Thermal Conductivity	Emissivity (Absorption coeff.)
1	Melt-dilute codisposal WP outer wall[4,6]		48.810 W/mK	0.64
2	Drift tunnel region[7]	Air	0.036 W/mK	–
		Humidity	0.036 W/mK	(10.0 m^{-1})
		Smooth wall	–	0.63
		Rough wall	–	0.94
3	Soil region around drift tunnel[8]		1.59 W/mK	–
4	Engineered barrier system[9]		1.59 W/mK	0.87

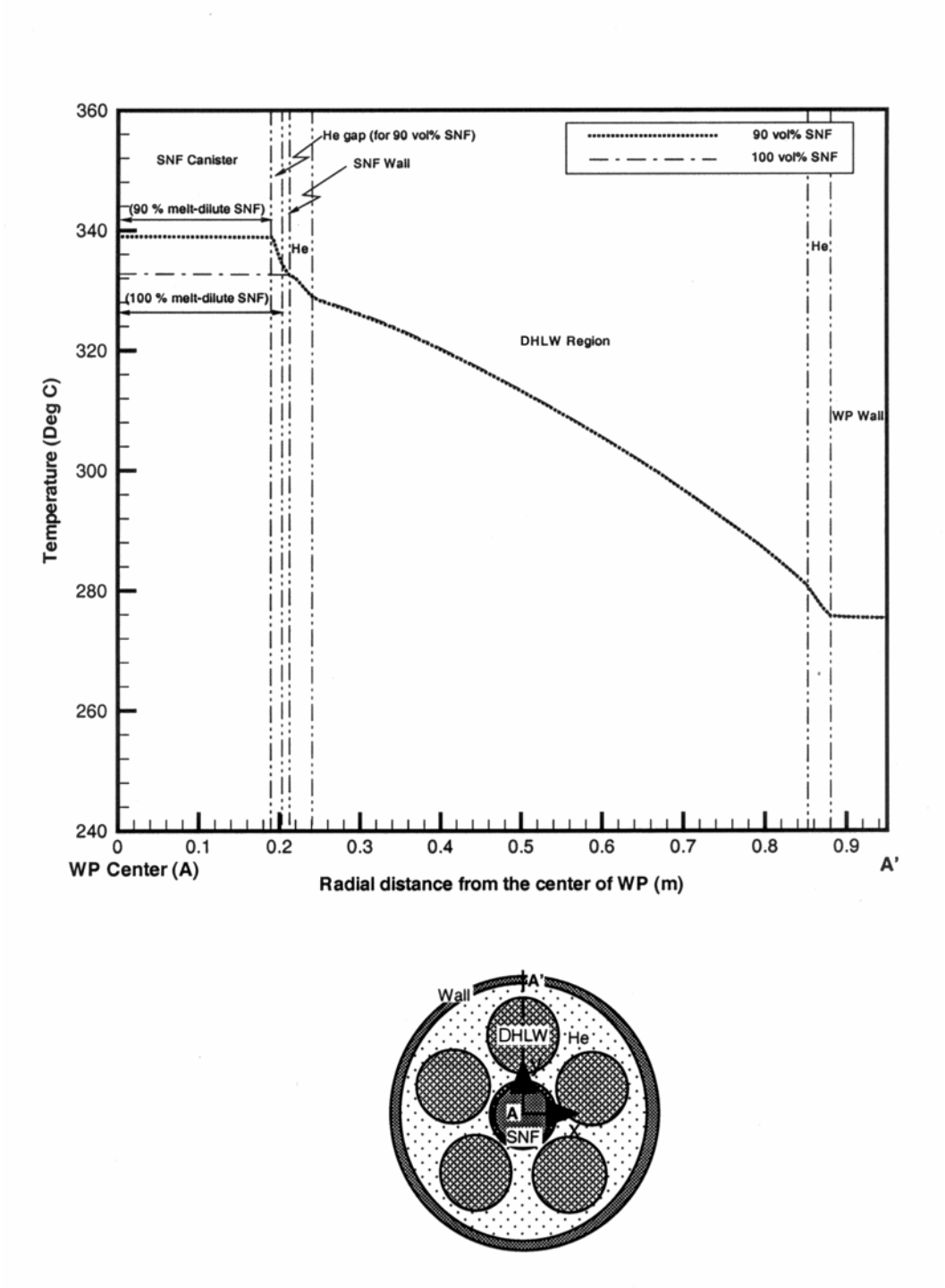

Figure 7.13 Comparison of Radial Temperatures for He-Cooled 100% and 90% Volume MD codisposal WP's for 0 year's Initial Reference Storage Time Based on "Baseline" Model (Ambient Temperature = 150 °C)

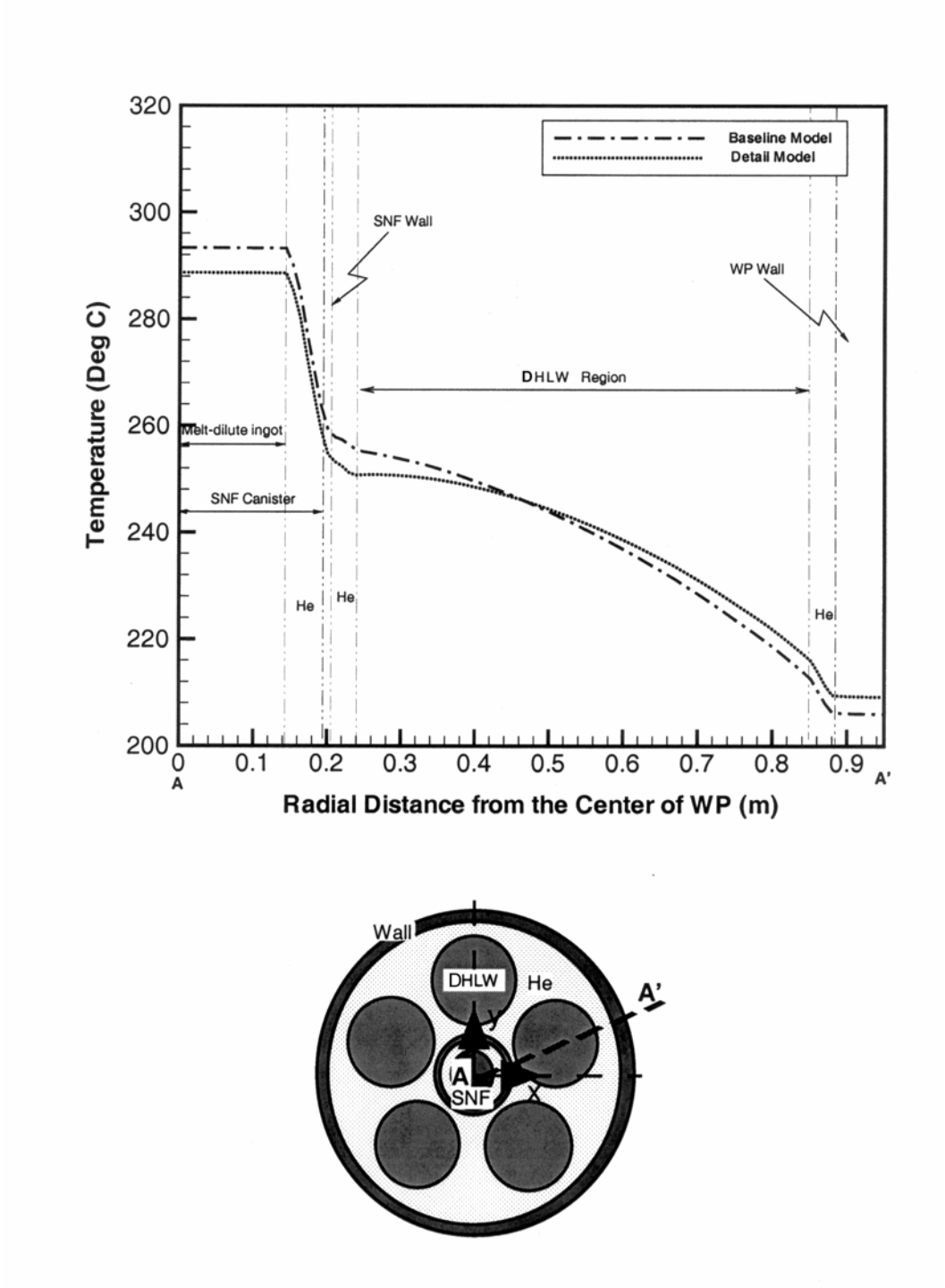

Figure 7.14 Comparison of Radial Temperature Distributions Along the Line A-A' Based on the Baseline Model and the Detailed Model for Helium-Cooled Direct Codisposal WP with 100% Cs Decay Heat Source at 0 years of Storage Time

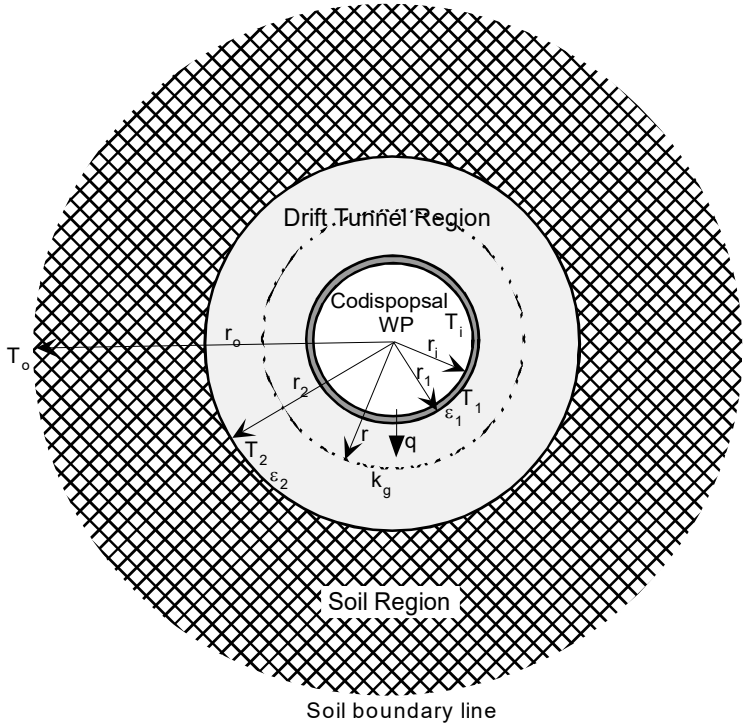

Figure 7.15 Theoretical Model to Compute Temperature Distribution for the Macro Model to Include the Conduction and Radiation without Radiative Absorption

From the present model, temperature differences between the inner and outer wall surfaces are 15 °C for 100% humidity and 8 °C for zero humidity in the drift tunnel region storing the codisposal WP containing 90 vol% melt-dilute 16 year-old SNF canister. The results for these two cases are presented in Figure 7.17.

Geologic temperature distributions including humid or dry tunnel region outside the codisposal WP containing 90 vol% melt-dilute SNF with 16 years cooling time at 0 years storage time using the conduction-radiation macro model are shown in Figure 7.17. It is noted that temperature at the center region of the tunnel is lower than the boundary layer temperatures adjacent to the wall regions due to the thermal radiation emission from the wall. In this case, natural convection effect was not considered primarily to determine the impact of radiation absorption into water humidity on the thermal performance of the WP.

Figure 7.18 shows the effect of natural convection on the gas medium for the drift tunnel region utilizing the conduction-convection model coupled with the radiation process in an absorbing radiation medium. These results show that temperature profile of the conduction-convection-radiation model for the humid tunnel region becomes more uniform due to the thermal mixing effect of natural convection flow except for thin boundary layer region compared with the results of the model without convection effect. Typically, the Grashof number for the drift tunnel region containing the codisposal WP is about 2×10^9. The Reynolds number for natural convective flow within the tunnel region was about 3×10^4, which corresponds to turbulent flow regime.

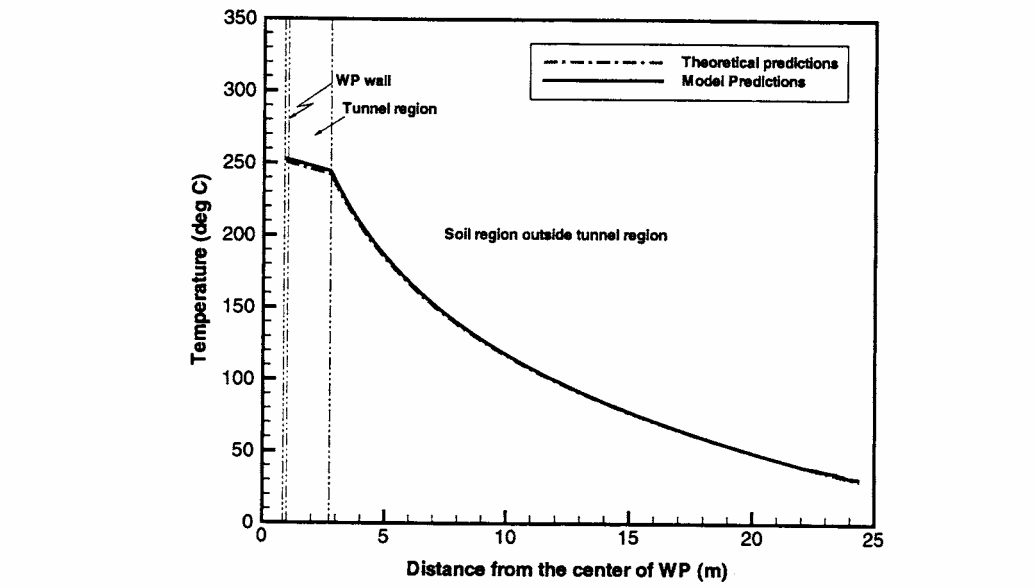

Figure 7.16 Comparison of the Present Macro Model Predictions with Theoretical Model Predictions for the 90 vol.% Melt-Dilute Codisposal WP Containing with 16 Years Cooling Time SNF at 0 Years Storage Time using the Conduction-Radiation Coupled Model without Radiation Absorption

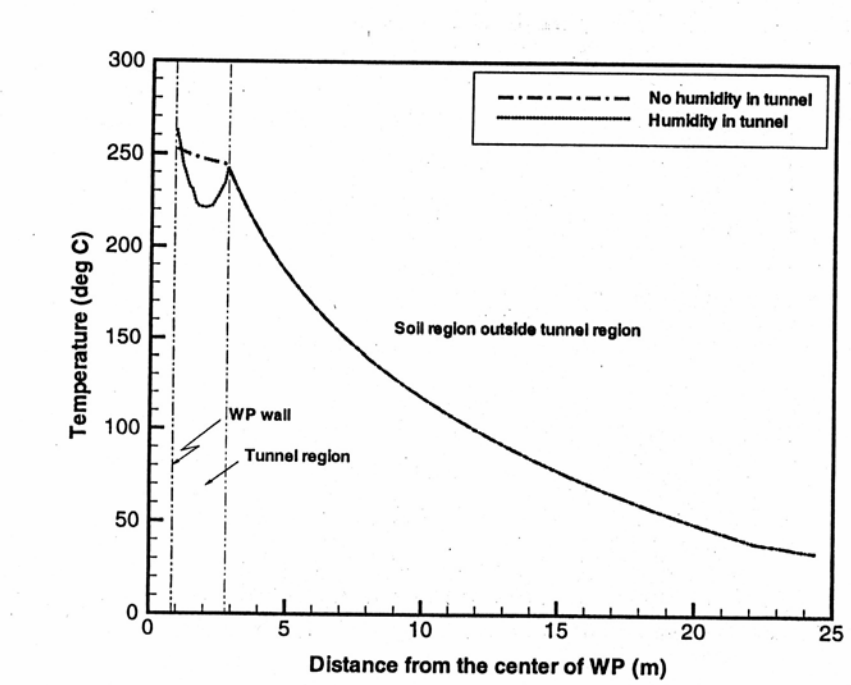

Figure 7.17 Geologic Temperature Distributions Including Humid or Dry Tunnel Region Outside the Codisposal WP Containing 90 vol% MD-SNF with 16 Years Cooling Time at 0 Years Storage Time using the Conduction-Radiation Macro Model

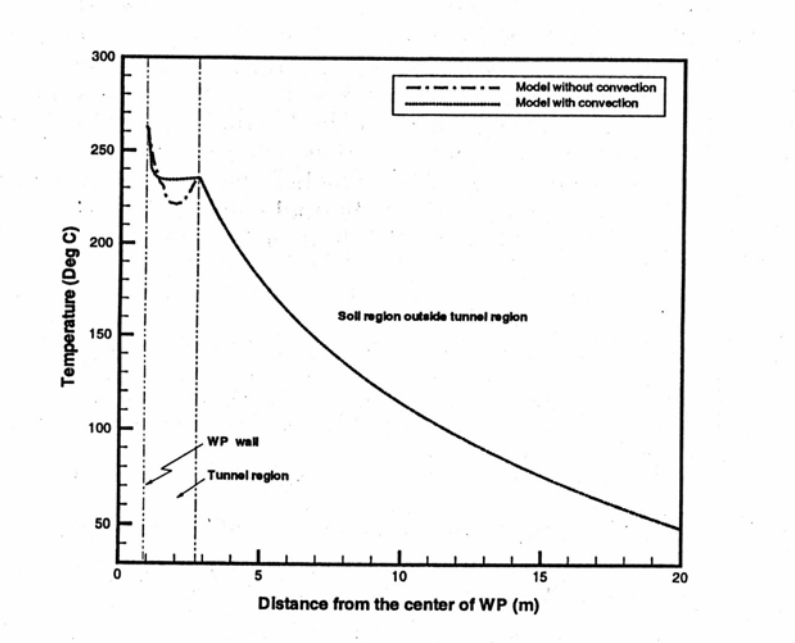

Figure 7.18 Natural Convection Effect on the Temperature Distributions Outside the Codisposal WP Containing 90 vol% MD-SNF with 16 Years Cooling Time at 0 Years Storage Time using the Macro Model Considering Radiation Absorption Effect

The WP baseline model was analyzed using the boundary conditions provided by the macro model under the geologic expected conditions. Table 7.12 presents minimum WP cooling times to satisfy the waste acceptance criterion from the thermal performance analysis of the geologic melt-dilute WP for several different soil temperatures at a distance of 80 ft from the WP center.

Table 7.12 Cooling Times for the He-Cooled Codisposal WP's with 90 and 100 Volume Percentages of SNF Canister Containing 100% Cs in MD Alloy Ingot of 16 Years Cooling Time at 80 ft Soil Region

Parameters	90 vol% melt-dilute SNF canister				100 vol% melt-dilute SNF canister	
Soil temperatures (°C)	30	50	70	100	30	50
Min. cooling time (years)	11	13	16	20	10	12

Using the codisposal WP model combined with the macro model, several key geologic parameters were investigated in relation to the thermal performance of the codisposal package with decay heat sources.

The parameters studied here were humidity inside drift tunnel, thermal conductivity of soil region, drift tunnel surface emissivity, the effect introduced by the presence of an engineered barrier system around the WP, and separation distance of the two adjacent drift tunnels. Results of these sensitivity calculations are shown in Tables 7.13 through 7.16 and will be used for the

qualification program and the thermal input to the material degradation model of the WP containing the melt-dilute Al-SNF canister.

Table 7.13 Comparison of Peak Temperatures for the He-Cooled Codisposal WP's with 90 Volume Percentage of SNF Canister Containing 100% Cs in MD Alloy Ingot of 16 Years Cooling Time at 0 years of Storage Time for Two Different Soil Temperatures

Soil Temperature at the 80ft from the center of the WP (°C)	Peak temperature of He-filled melt-dilute WP with 90 vol% melt-dilute SNF (°C)	
	100% Humidity (k_{soil}=1.59 W/mK)	0% Humidity (k_{soil}=1.59 W/mK)
30	314	307
50	333	325
100	377	365

Table 7.14 Comparison of Minimum Cooling Time of MD-SNF for the He-Cooled Codisposal WP's with 90 Volume Percentage of SNF Canister Containing 100% Cs in MD Alloy Ingot at 0 Years of Storage Time for Four Different Soil Distances

Distance from the center of the melt-dilute WP to the soil boundary of 30 °C (ft)	Minimum cooling time of melt-dilute SNF required to satisfy the acceptance criteria for He-filled WP with 90 vol% melt-dilute SNF (Years)	
	100% Humidity (k_{soil}=1.59 W/mK)	0% Humidity (k_{soil}=1.59 W/mK)
60	9	7
80	11	9
100	14	12
120	16	14

Table 7.15 Comparison of Peak Temperatures for the He-Cooled Codisposal WP's with 90 Volume Percentage of SNF Canister Containing 100% Cs in MD Alloy Ingot of 16 Years Cooling Time at 0 Years of Storage Time for Two Different Soil Temperatures (100% Tunnel Humidity)

Soil Temperature at the 80ft from the center of the melt-dilute WP (°C)	Peak temperature of He-filled melt-dilute WP with 90 vol% melt-dilute SNF (°C)		
	K_{soil}=1.59 W/mK	k_{soil}=1.10 W/mK	% Difference
30	314	340	~ 8%
50	333	355	~ 7%

Table 7.16 Comparison of Peak Temperatures for the He-Cooled Codisposal WP's with 90 Volume Percentage of SNF Canister Containing 100% Cs in MD Alloy Ingot of 16 Years Cooling Time at 0 Years of Storage Time for Various Soil Distances (100% Humidity Inside Drift Tunnel)

Parameters	30 °C Soil Temperature at various distances from the center of the melt-dilute codisposal WP				
	60 ft	80 ft	100 ft	120 ft	160 ft
Melt-dilute WP peak temperature (°C)	293	314	334	353	377

From the sensitivity change of the geologic parameters related to the thermal performance of the melt-dilute codisposal WP, it was found that thermal conductivity and separation space of the soil region around the drift tunnel region are key design parameters under geologic repository. It is also emphasized that engineered barrier system can decrease the thermal performance since radiation and convection energy transport processes are found to be dominant cooling mechanism from the analyses of the WP models. Table 7.17 illustrates the sensitivity to the parameters investigated.

Engineered barrier system around the codisposal WP:

Under the reference baseline conditions for the macro model, there was no engineered barrier system around the WP. When the geologic WP repository has the engineered barrier system as shown in Figure 7.9, peak temperature of the melt-dilute WP is increased by about 15 °C compared to the WP repository without engineered barrier system. Figure 7.19 shows the comparison of the temperature profiles from the center of the melt-dilute WP to the lower bottom of the soil region. In this case, a 30 °C soil temperature was used at 80-ft soil boundary from the WP center.

Temperature distributions of the drift tunnel region with and without engineered barrier system around the WP are shown in Figure 7.19. Calculations have shown that the natural convection cooling effect around the codisposal WP without engineered barrier system is much stronger than the WP with engineered barrier system. This is due to the enhanced buoyancy flow conditions illustrated in Figure 7.20 and is based on extensive CFD calculations which analyzed flow patterns and fluid temperatures (see Figure 7.21).

7.6 Conclusions – Thermal Analysis

Three thermal models and a geological "macro" model were developed and used to evaluate the thermal performance of a codisposal WP containing a melt-dilute Al-SNF canister plus five high level waste glass logs (DHLW). The three WP models were: the conduction model, the baseline model incorporating thermal conduction and radiation effects, and the detailed model which included all three possible modes (e.g. conduction, radiation and natural convection effects).

The "baseline" model was used for the majority of design parameter sensitivity studies. The "detailed" model was used to investigate the effect of internal convective heat transfer and also to benchmark conservatisms inherent in the "baseline" modeling. "Detailed" model calculations showed that temperature differences of about 10°C between top versus bottom WP surface could

exist when buoyancy-driven internal gas circulation was accounted for. This small temperature difference supported continued use of the "baseline model for design parameter sensitivity calculations performed.

Although the "detailed" model results also showed that temperature gradients across the DHLW regions were much smaller compared to the predictions of the baseline model, the predominant heat transfer mechanism within the codisposal WP was thermal radiation, followed by conduction through the internal mechanical support structure (see Table 7.6).

Incorporation of natural convective buoyancy effects into the thermal coupling the WP with the geological model resulted in the "detailed" model predicting peak internal temperatures of about 5 °C lower than "baseline" model temperatures. This difference was judged to be a small effect at this time, although the attendant effect of moving moisture away from the WP surface is an asset in reducing potential corrosion effects.

The results of the "baseline" model calculations showed that peak MD-SNF temperature for the 100 and 90 vol% filled configurations for the helium-filled and air-filled WP design options do not exceed 350 °C.

The results of the WP "baseline" model when coupled with the geologic "macro" model showed that proposed 90 vol% melt-dilute SNF disposition options for the helium-filled WP satisfied the present waste acceptance criteria under geologic reference conditions shown in Table 7.3.

Table 7.17 Summary of the Sensitivity Studies for the Geologic Parameters Related to the Thermal Performance of the Codisposal WP Containing MD-SNF Canister

Parameters	**Reference conditions**	**Parameter change, Δx**	**$T_{max,ref}$ change direction***	**Thermal performance change $100 \times (\Delta T/T_{max,ref})$**
Humidity (%)	100	From 100 to 0	−	~ 4 %
Soil thermal conductivity (W/mK)	1.59	From 1.59 to 1.10	+	~ 8 %
Surface roughness of drift tunnel	Rough (0.94)	From rough to smooth (0.94 to 0.63)	+	~ 4 %
Engineered barrier system	No	From No to Yes (about 20" thick around the WP)	+	~ 5 %
**Soil distance from the WP center (ft)	160	from 120 to 200	+	~ 6 %

Note: * + means to increase the peak temperature of the melt-dilute WP.

- means to decrease the peak temperature of the melt-dilute WP.

** Sensitivity analysis was performed using the fixed soil temperature at the various distances from the center of the melt-dilute WP

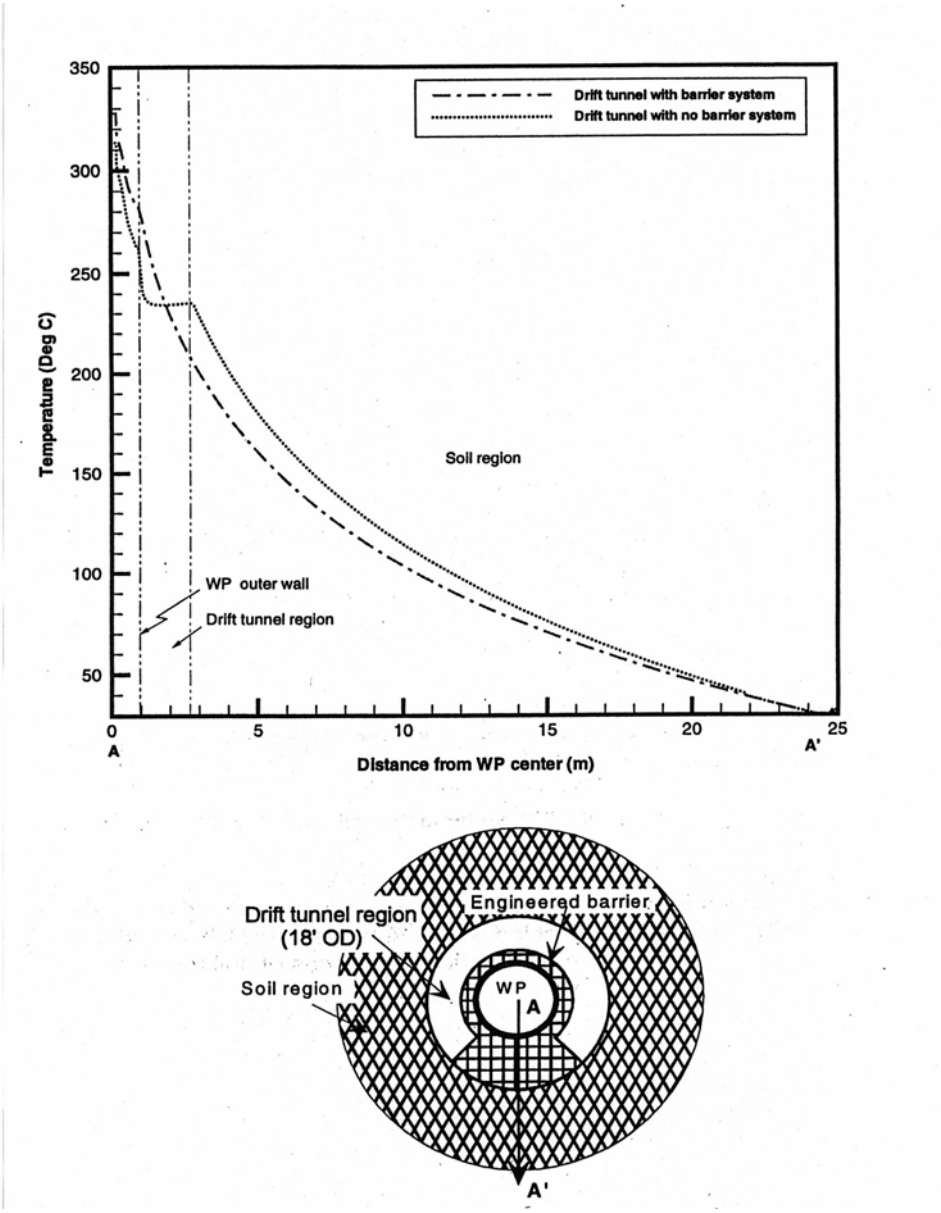

Figure 7.19 Comparison of Detailed Temperature Distributions of Drift Tunnel Region with and without Engineered Barrier System Inside the Drift Tunnel Region Around the Codisposal WP with He-Cooled 90 vol% MD-SNF Canister with 16 Years Cooling Time at 0 Years Storage Time

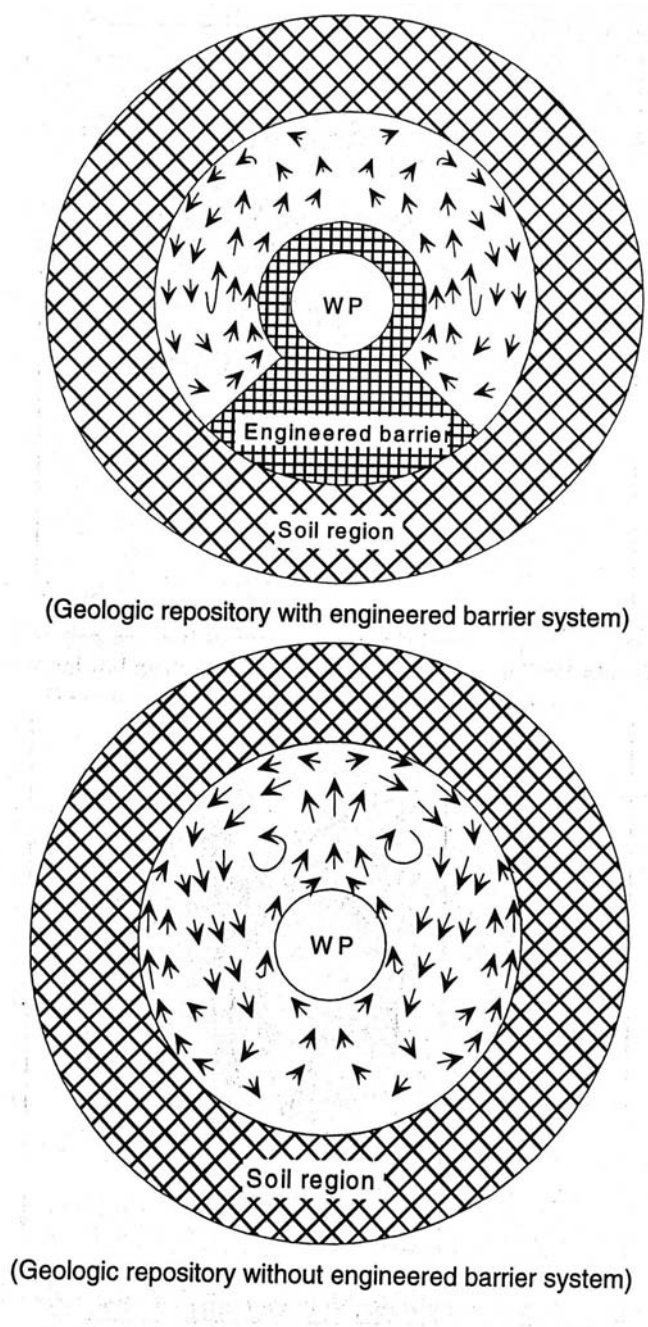

Figure 7.20 Natural Convection Flow Patterns Around the Codisposal WP - with and without the Engineered Barrier within the Drift Tunnel Region

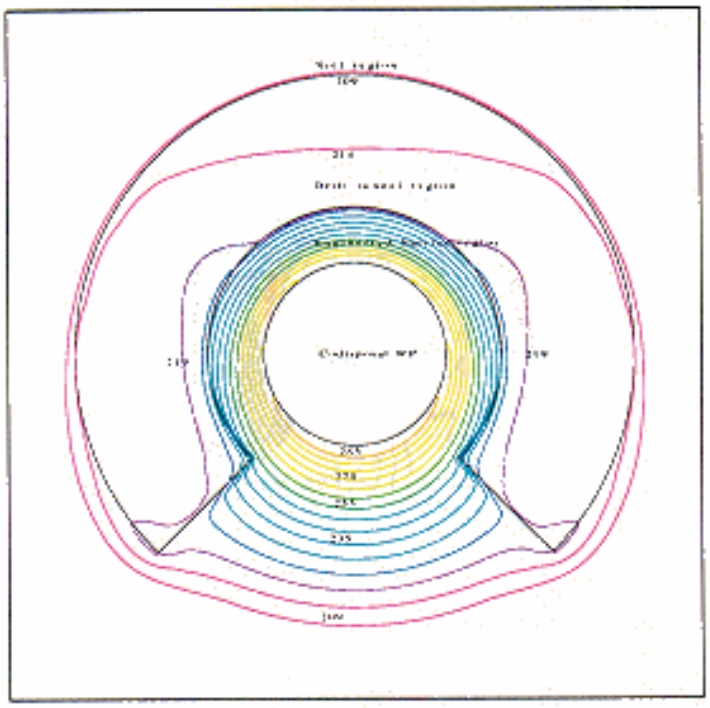

(Temperature distribution of the drift tunnel region with engineered barrier system)

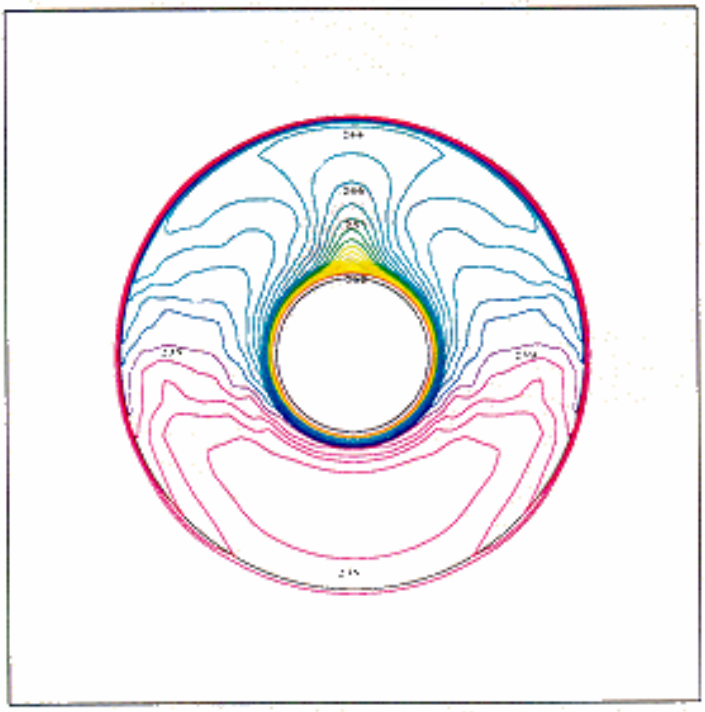

(Temperature distribution of the drift tunnel region without engineered barrier system)

Figure 7.21 Comparison of Temperature Distributions Between Dry and Humid Tunnel Regions

7.7 Recommendations for Additional Analyses

The following recommendations are made for the improvement of the codisposal WP thermal modeling prior to submittal to the NRC for additional reviews.

- The present thermal analysis is based on the geometric representation of codisposal WP shown in Figure 7.1, which does not include mechanical support structures which position the WP contents. Although these support structures will provide an additional thermal conduction path for decay heat removal, they will block thermal radiation heat transfer from the MD-SNF canister to the waste package outer wall (see Figure 2.1). The current analysis identifies thermal radiation as the predominant heat transfer mechanism for decay heat (see Table 7.6). Although intuitive judgement would conclude that this metal structure would reduce internal temperatures, the effect inter-positioned structures is unknown and warrants follow-up analysis. Similar support structures within licensed transport casks shipment of commercial LWR spent fuel shipment have had high emissivity coatings applied to these surfaces to ensure adequate heat transfer capability.

- The present analysis showed that thermal conductivity of the soil region was one of the key parameters in assessing the WP thermal performance within the geologic repository. NRC questioned the thermal conductivity values used for "crushed tuff"[10] citing measured conductivity values of 0.26 to 0.49 W/m-K versus 1.59 W/m-K used in this analysis. Additional calculations regarding all NRC comments received will be needed if this report will be used for a License Application.

- A more detailed hydro-geologic modeling of the soil medium, including the movement of water in the soil region due to the presence of the WP heat source, is also recommended.

- An assessment of the thermal loads that may be imposed on the MD codisposal package by adjacent or nearby BWR and PWR disposal packages placed within the same drift tunnel (see Figure ES.1). Although the thermal loads predicted for the SRS codisposal WP easily meet the emplacement criteria (3700 watts versus less than 11,790 watts), axial heat transfer within the repository tunnel has the potential has the potential to funnel heat back into the MD codisposal package and raise package temperatures since commercially generated LWR spent fuel waste will be packed to the highest allowable decay heat limit.

7.8 References

[1] Lee, S. Y. and Sindelar, R. L., ***"Thermal Performance Analysis of Melt-Dilute Aluminum SNF in Codisposal Waste Packages in the Geological Repository,"*** WSRC-TR-99-00366 (December 1999).

[2] ***"Waste Acceptance Systems Requirements Document,"*** Revision 04G (March 2001).

[3] **CFX-4.2: Environment**, AEA Technology (1997).

[4] Lee, S. Y. and Sindelar, R. L., ***"Thermal Analysis of Repository Codisposal Waste Packages Containing Aluminum Spent Nuclear Fuel (U),"*** WSRC-TR-09-00158 (April 1998).

[5] Adams, T., "Melt-Dilute Values," e-mail message (February 6, 1998). Also see WSRC-RP-89-489 report.

[6] Vinson, D., "Preliminary Material Property Data," e-mail message (September 5, 1997).

[7] Modest, M. F., **Radiative Heat Transfer**, McGraw-Hill, Inc., New York (1993).

[8] Wildenschild, D., Roberts, J. J., Hardin, E., and Lin, W., ***"Experimental Tests of Enhancement of Thermal Vapor Diffusion in Topopah Spring Tuff,"*** ANS Proceedings of the 8th International Conference on High-Level Radioactive Waste Management, Las Vegas, Nevada (May 11-14, 1998).

[9] Apted, M. J. and Pigford, T. H., ***"Reliable and Effective Design Strategies for Engineered Barriers at Yucca Mountain,"*** Proceedings of the 8th International Conference on High-Level Radioactive Waste Management, sponsored by ANS, pp. 477-480 (May 11-14, 1998).

[10] Reamer, C. W. (NRC/NMSS) letter dated November 14, 2000, to J. E. Anderson (DOE/SROO), "Review of the U.S. Department of Energy Evaluation of Aluminum-Based Research Reactor Spent Fuel Disposition Program," with a CNWRA enclosure titled: "Review of the U.S. Department of Energy Evaluation of Thermal Performance Analysis and Dissolution Rates of Melt and Dilute Aluminum-Based Spent Nuclear Fuel" (August 2000).

8.0 SHIELDING ANALYSIS

8.1 Introduction

Radiation produces radiolytic species (e.g., hydrogen peroxide and nitric acid) that may enhance the corrosion of the waste package components. A study that has evaluated the effect of radiation on the corrosion of the material used for the fabrication of waste packages in the environments expected at Yucca Mountain[1] showed that a dose rate of 10^4 rad/h is required before any influence of radiation is observed on copper/nickel alloys. Since the calculated dose rate at the external surface of the MD waste package is approximately 200 rad/h, it is expected that no observable effect on the corrosion of waste package materials will be present.

8.2 Use of Computer Software

The Monte Carlo particle transport code, MCNP, Version 4B2LV[2], is used to calculate average dose rates at the external surfaces of the waste package. The information regarding the code and its use for the shielding analysis is documented in Reference 3.

8.3 Design Analysis

The Monte Carlo method for solving the integral radiation transport equation, which is implemented in the MCNP computer program, is used to calculate radiation dose rates for the waste packages. MCNP uses continuous-energy cross sections processed from the evaluated nuclear data files ENDF/B-V.[4] These cross-section libraries are part of the qualified MCNP code. The flux averaged over a surface tally is specified in calculations and the neutron and gamma flux-to-dose rate conversion factors, which were extracted from ANSI 6.1.1-1977[5], are applied to obtain surface dose rates.

8.4 Shielding Source Term

The gamma and neutron source terms are presented in Table 8.1. The radiation source terms, which are provided per kilogram of MD ingot, have been derived for several fuel assemblies of various high-enriched U-Al-SNF types[6] and by selecting the values that generate the highest dose rate at the external surface of the DOE SNF canister. The calculations assumed a decay time of one year, which will conservatively bound all expected shipments of MD ingots to the monitored geologic repository.

The radiation source terms for the projected DHLW glass forms have been generated in Reference 7. The bounding radiation source term for all projected DHLW glass forms pertains to the Design-Basis glass from the DWPF at SRS[7]. The Design-Basis glass represents an upper bound in terms of the dose rate and the heat generation rate, expected from the DHLW forms. Table 8.2 presents the gamma and neutron source terms per 3-m-long SRS DHLW glass canister at year 2010.[7]

Table 8.1 Gamma and Neutron Source Terms per Kilogram of Melt-Dilute Ingots[3]

Photon Upper Energy Group Boundaries (MeV)	Gamma Intensity (photons/s)	Neutron Upper Energy Group Boundaries (MeV)	Neutron Intensity (neutrons/s)
0.05	2.1605E+13	0.10	0.0000E+00
0.10	7.0742E+12	0.40	1.7633E+04
0.20	7.3063E+12	0.90	9.0075E+04
0.30	1.6334E+12	1.40	8.2275E+04
0.40	1.2655E+12	1.85	6.0413E+04
0.60	7.0238E+12	3.00	1.0575E+05
0.80	1.8281E+13	6.43	9.6825E+04
1.00	2.7830E+12	20.00	8.6175E+03
1.33	4.1610E+11		
1.66	3.1092E+11		
2.00	2.3501E+10		
2.50	2.1331E+11		
3.00	8.7773E+08		
4.00	8.8118E+07		
5.00	1.4215E+04		
6.50	5.7054E+03		
8.00	1.1193E+03		
10.00	2.3766E+02		
Total	**6.7936E+13**	**Total**	**4.6159E+05**

Table 8.2 Gamma and Neutron Sources per 3-m-long SRS DHLW Glass Canister[7]

Gamma Source		Neutron Source	
Photon Upper Energy Boundary (MeV)	Intensity (photons/s)	Neutron Upper Energy Boundary (MeV)	Intensity (neutrons/s)
0.05	1.29E+15	0.10	1.54E+05
0.10	3.89E+14	0.40	1.60E+06
0.20	3.02E+14	0.90	5.58E+06
0.30	8.58E+13	1.40	5.98E+06
0.40	6.27E+13	1.85	5.21E+06
0.60	8.55E+13	3.00	2.12E+07
0.80	1.34E+15	6.43	2.74E+07
1.00	2.08E+13	20.00	2.99E+05
1.33	2.91E+13		
1.66	6.18E+12		
2.00	4.86E+11		
2.50	2.70E+12		
3.00	1.91E+10		
4.00	2.15E+09		
5.00	5.20E+05		
6.50	2.09E+05		
8.00	4.09E+04		
10.00	8.67E+03		
Total	**3.61E+15**	**Total**	**6.74E+07**

8.5 Calculations and Results

Reference 3 gives the details of the calculations and the results. The geometric representation of the waste package used in MCNP calculations is shown in Figure 8.1. The waste package contains two different radiation sources, which are volumetric sources uniformly distributed inside the cavity of the DOE SNF canister and the glass volume, respectively. A conservative approach is used, in which lower material densities for the SRS DHLW glass and the MD ingots are employed.

In the calculation, the external surfaces of the waste package are divided in segments and the dose rate is averaged over each segment to evaluate the spatial distribution of the dose rate. Figures 8.2 and 8.3 show the segments of the radial and axial segments used in the dose-rate calculations. The radial surface, between the bottom and top planes of DHLW glass, is equally divided into five segments, each of which is 47.886-cm high. The first radial segment (Segment 1), 64.57-cm high, corresponds to the empty portion of the DHLW canister, which is between the top of the waste package cavity and the top of the DHLW glass. The waste package top and bottom axial surfaces are divided into two radial segments of 0-30 cm (Segment 7) and 30-101.5 cm (Segment 8). For this waste package, the DOE canister is positioned in the center of the waste package and gamma source intensity of the MD ingots is twenty times the gamma source intensity of each individual SRS DHLW glass canister. Because the DHLW glass canisters are positioned near the disposal container, they attenuate the radiation emitted by the MD-SNF and mostly determine the dose rates on the angular segments adjacent to them (Segments B). However, due to their higher source intensity, the MD ingots contribute to the dose rates averaged over Segments A. Therefore, an angular dependence of the waste package radial dose is expected and the radial surface is divided into ten equal angular segments, as shown in Figure 8.3.

Tables 8.3 and 8.4 are lists of the radial and axial dose rates on the outer surface of the waste package containing the five SRS DHLW glass canisters and the DOE SNF canister. The neutron source has an insignificant contribution to the total dose and the gamma dose dominates the total dose.

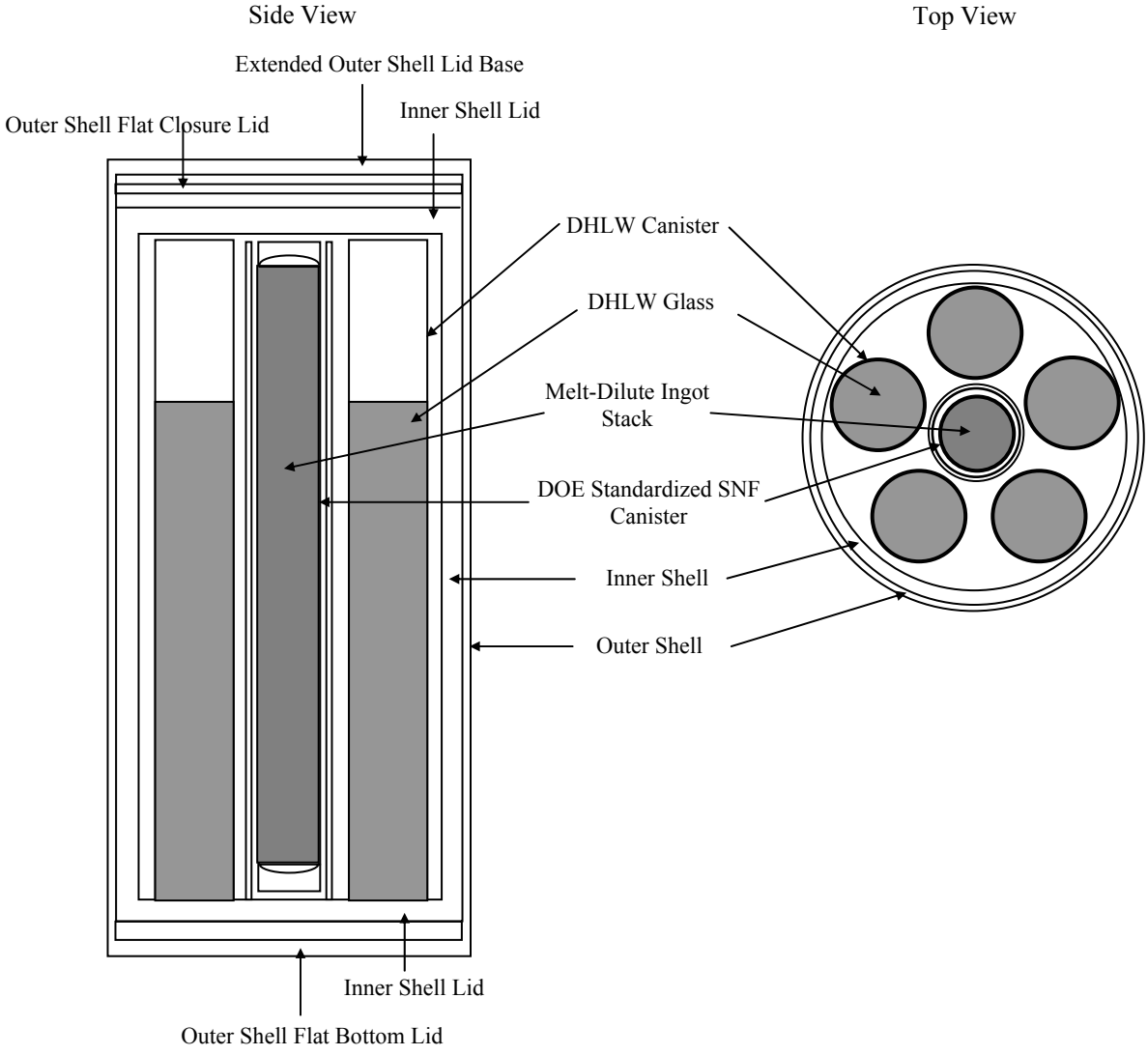

Figure 8.1 Vertical and Horizontal Cross Sections of MCNP Geometry Representation

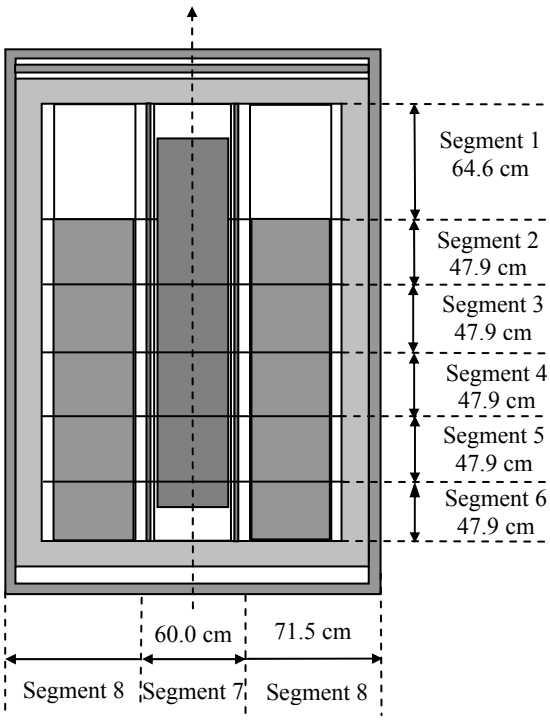

Figure 8.2 Surfaces and Segments (axial and radial) Used for Dose Rate Calculations

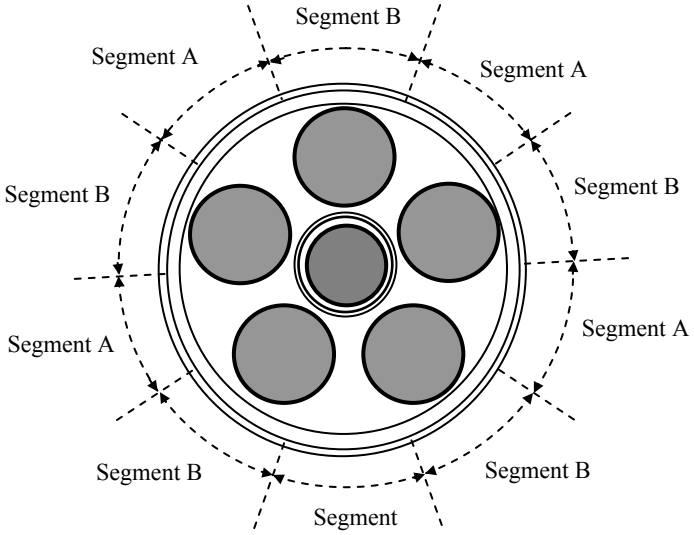

Figure 8.3 Angular Segments of the WP Outer Radial Surface Used in Dose Rate Calculations

Table 8.3 Dose Rates Averaged over Axial and Radial Segments of the WP Outer-Radial and Axial Surfaces[3]

Location	Gamma Dose Rate (rem/h)	Neutron Dose Rate (rem/h)	Total Dose Rate (rem/h)
Radial surface: Segment 1	85.47	0.14	85.61
Radial surface: Segment 2	133.53	0.14	133.67
Radial surface: Segment 3	144.49	0.15	144.64
Radial surface: Segment 4	143.34	0.15	143.49
Radial surface: Segment 5	136.42	0.14	136.57
Radial surface: Segment 6	105.20	0.11	105.31
Bottom surface: Segment 7	47.50	0.22	47.71
Bottom surface: Segment 8	13.76	0.08	13.84
Top surface: Segment 7	27.30	0.15	27.45
Top surface: Segment 8	4.82	0.08	4.89

NOTE: The dose rates listed in this table are the upper limits of the 95 percent confidence intervals of the Monte Carlo dose rate calculations.

The radial surface dose rates have an angular dependence, as shown in Table 8.4. The dose rate averaged over Segment A is approximately twice as much as the dose rate averaged over Segment B.

Table 8.4 Dose Rates Averaged Over Angular Segments of the WP Outer-Radial Surface[3]

Axial Location	Angular Segment A			Angular Segment B		
	Gamma Dose Rate (rem/h)	Neutron Dose Rate (rem/h)	Total Dose Rate (rem/h)	Gamma Dose Rate (rem/h)	Neutron Dose Rate (rem/h)	Total Dose Rate (rem/h)
Segment 1	104.33	0.16	104.49	74.42	0.14	74.56
Segment 2	182.66	0.19	182.85	98.68	0.11	98.79
Segment 3	199.69	0.20	199.89	103.21	0.11	103.32
Segment 4	199.13	0.20	199.33	101.38	0.10	101.48
Segment 5	185.52	0.20	185.72	100.46	0.11	100.57
Segment 6	132.09	0.14	132.23	92.80	0.08	92.88

NOTE: The dose rates listed in this table are the upper limits of the 95 percent confidence intervals of the Monte Carlo dose rate calculations.

8.6 Summary

The maximum dose rate at the external surfaces of the waste package occurs on the radial surface and is 199.89 rem/h. The radial dose rate shows an angular distribution, with dose rates on Segments A being approximately twice as much as those on Segments B. The dose rates on the bottom and top surfaces of the waste package are about one-third and about one-fifth, respectively, of the maximum dose rate on the outer radial surface. The design criterion specifies that the maximum dose rate at all external surfaces of the waste package is 1,450 rem/h.[8] The dose rates in rem/h and rad/h are practically the same due to the insignificant contribution of the neutron dose rate to the total dose rate.

8.7 References

[1] Shoesmith, D.W. and King, F., ***"The Effects of Gamma Radiation on the Corrosion of Candidate Materials for the Fabrication of Nuclear Waste Package,"*** AECL-11999. Pinawa, Manitoba, Canada: Atomic Energy of Canada Limited. ACC: MOL.19990311.0212.Shoesmith (1998).

[2] ***"Software Code: MCNP,"*** 4B2LV. HP. 30033 V4B2LV (1998).

[3] ***"Dose Rate Calculation for the Codisposal Waste Package of HLW Glass and the Melt and Dilute Al SNF,"*** CAL-DDC-NU-000004 REV 00. Las Vegas, Nevada: Bechtel SAIC Company. URN-xxx.BSC (2001).

[4] Briesmeister, J.F., ed., ***"MCNP-A General Monte Carlo N-Particle Transport Code,"*** LA-12625-M, Version 4B. Los Alamos, New Mexico: Los Alamos National Laboratory. ACC: MOL.19980624.0328 (1997).

[5] ANSI/ANS-6.1.1, ***"Neutron and Gamma-Ray Flux-to-Dose-Rate Factors,"*** La Grange Park, Illinois: American Nuclear Society. TIC: 239401 (1997).

[6] ***"Statement of Work for DOE - Office of Civilian Waste Management, Technical Assistance on Melt-Dilute Criticality and Shielding Analyses,"*** Revision 2. Las Vegas, Nevada: Bechtel SAIC Company, LLC. ACC: MOL.20010619.0626 (2001).

[7] ***"Source Terms for HLW Glass Canisters,"*** CAL-MGR-NU-000002 REV 01. Las Vegas, Nevada: CRWMS M&O. ACC: MOL.20000823.0004 (2000).

[8] ***"Waste Acceptance Systems Requirements Document,"*** Revision 04G (March 2001).

This Page Intentionally Left Blank

APPENDIX A

A.0 SCOPE OF FUEL AT SRS TO BE DISPOSITIONED

The SRS is presently consolidating the DOE Al-SNF from foreign and domestic research reactors. A description of these fuels using the best available information is provided in this appendix. The treatment of Al-SNF for ultimate disposition must deal with these fuels. Additional information on these fuels will be obtained through characterizations as discussed in the report. The inventory of Al-SNF in this appendix is that identified in the SRS EIS (**Savannah River Site Spent Nuclear Fuel Management Final Environmental Impact Statement.** USDOE-Savannah River Operations Office, DOE/EIS-0279 (2000)) and Record of Decision (**Record of Decision for the Savannah River Site Spent Nuclear Fuel Management Final Environmental Impact Statement.** USDOE-Savannah River Operations Office, 61 FR 69085 (August 7, 2000)).

A.1 Aluminum-Based Spent Nuclear Fuel

Aluminum-based spent nuclear fuel from research reactors will account for less than 1% of the total volume of SNF and high level waste that will require disposal in a geologic repository. However, much of the Al-SNF contains HEU with up to 93% enrichment. The Materials Test Reactor design assembly which is comprised of fuel elements or plates of aluminum-clad, aluminum-uranium alloy fuel is the dominant design (approximately 80% of total) and fuel material for research reactors. In addition, some reactor fuel assemblies were fabricated from aluminum-uranium silicide alloys or aluminum-uranium oxides. The fuel elements are clad with one of the aluminum alloys 1100, 5052, or 6061 or their foreign equivalents.

A.2 DOE SNF Repository Performance Categories

The DOE has categorized all of its spent fuel into fifteen categories. These categories were developed based upon fuel composition and characteristics.[1] The primary concern with grouping the spent fuels was assigning every fuel to a category and making certain that all of the spent fuel fit into a category. The total amount of DOE SNF, excepting Sodium bonded spent fuel (Category 14) and Navy spent fuel (Category 15), is approximately 2436 MTHM. This fuel (Categories 1-13) will be distributed among INEEL, Savannah River, and Hanford. Savannah River has responsibility for a total of 24.03 MTHM that includes fuel from Categories 5-7. Savannah River has 3.67 of the 87.93 MTHM comprising Category 5 and all of the fuels in Categories 6 and 7, 8.96 MTHM and 11.40 MTHM, respectively. The categorization of DOE SNF listed in Reference 1 is being re-categorized. The preliminary re-categorization lists Al-SNF as a single category. That is, Categories 5, 6, and 7 have been collapsed to one category based on their similar expected performance in the repository.

A.3 SRS Receipts—Al-SNF

A.3.1 Research Reactor Spent Nuclear Fuel Designs (Al-clad SNF Only)

Research reactors use a number of different fuel designs. These designs can be organized into three broad types: (1) materials and test reactor (MTR)-type design, which includes plate-type

designs and concentric tube-type designs, (2) pin-type design, and (3) involute-type design. The following summarizes specific characteristics of the different types of fuel named above.

A.3.1.1 Plate-Type Design

This type of fuel design is used in the majority of research reactors. The thermal power of these reactors ranges from 1 MW to 50 MW. Figures A.1and A.2 show typical fuel elements with this type of fuel design. The number of fuel plates in an element varies between 6 and 23, and the initial ^{235}U content varies between 37 g and 420 g per element. Similarly, the average burnup of a discharged spent nuclear fuel varies between 15 and 76 percent (^{235}U atom percent). The uranium enrichment used this type of fuel varies from just below 20 to 93 percent.

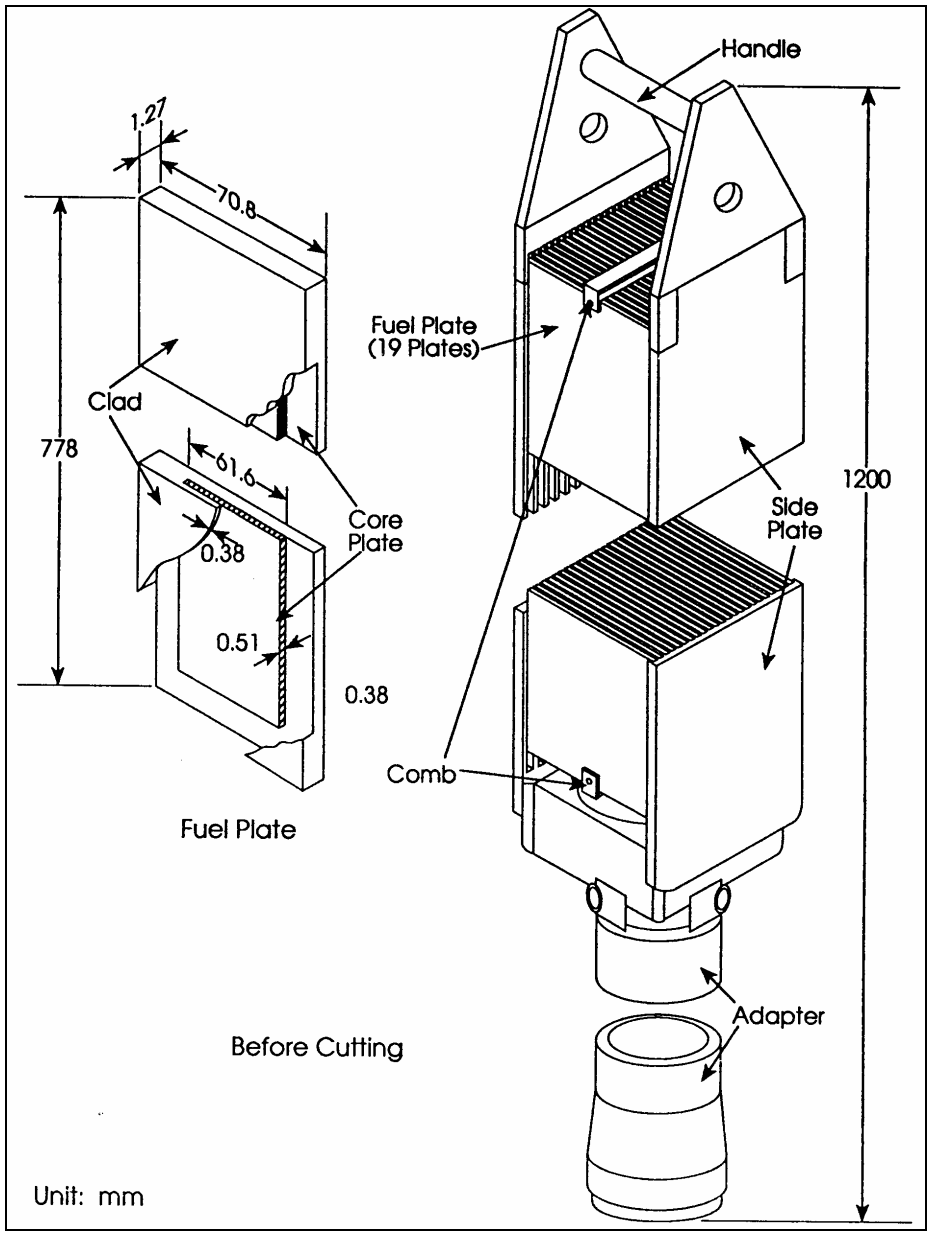

Figure A.1 Typical (Boxed-Type/Flat-Plate) Aluminum-Based Fuel Element Schematic

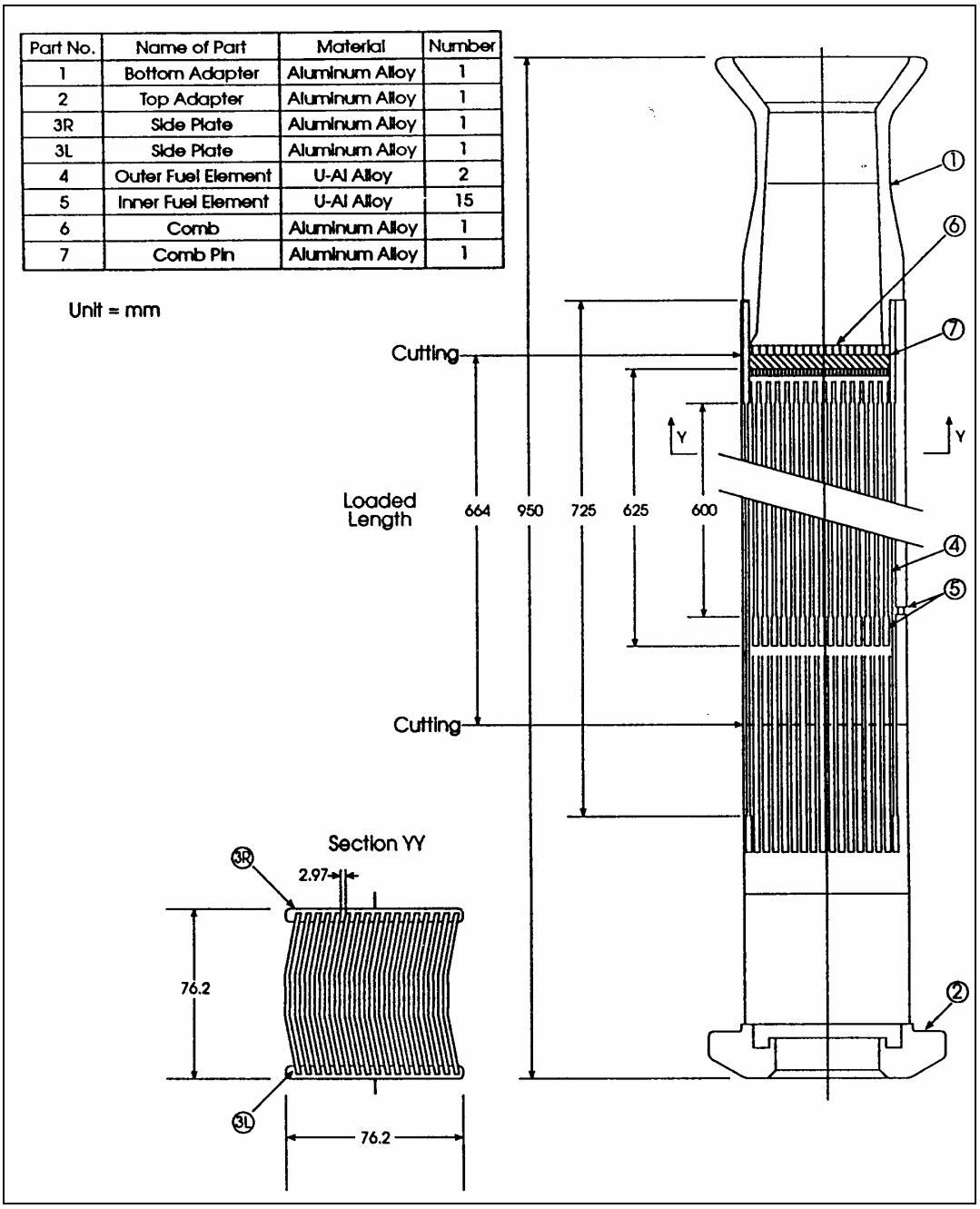

Figure A.2 Typical (Boxed-Type/Curved-Plate) Aluminum-Based Fuel Element Schematic

The following provides additional information on a typical plate-type spent nuclear fuel element that was used in a 50 MW research reactor, as shown in Figure A.1 and in Figure A.2.

The fuel element is made of an alloy of 23 percent by weight of 93 percent-enriched uranium in aluminum with a thin (0.38 mm) aluminum cladding. Each fuel element contains 19 fuel plates.

A.3.1.2 Concentric Tube Design

This type of fuel design is used in four foreign research reactors: Australian (HIFAR), Belgian (BR-2), Japanese (JRR-2) and Danish (DR-3).

The Belgian reactor is a 125 MW reactor, and the other three are each 10 MW. Figure A.3 shows a typical fuel element with concentric tube (tubular) fuel design type. The number of fuel tubes in an element varies between four (4) and six (6), and the initial ^{235}U content varies between 150 g and 400 g per element. The average burnup of discharged spent nuclear fuels from these reactors ranges between 47 and 55 percent (^{235}U atom percent). The uranium enrichment used in this fuel varies from just below 20 to 93 percent.

The following provides additional information on a typical tubular type spent nuclear fuel element (shown in Figure A.3 that was used in a 10 MW reactor).

This fuel element initially contains 220 g ^{235}U, and consists of five (5) concentric fuel tubes. Each tube is made of three curved fuel plates. The fuel is an alloy of uranium in aluminum with a thin (0.38 mm) aluminum cladding. Five (5) different curved fuel plate width sizes with 1.27 mm thickness and 625 mm height are used. The overall outside diameter of the outermost tube is 103 mm.

A.3.1.3 Pin-Type Design

Three types of foreign research reactors use pin-type design fuel. They are: the Canadian Safe LOW Power critical [K] Experiment (SLOWPOKE) (20 kW power); the Canadian NRU (125 MW power), NRX (24 MW power) and South Korean KMRR (30 MW) reactors. Among these reactors, the SLOWPOKE fuel pins are the smallest in size and uranium content.

The SLOWPOKE reactor fuel pins have an outside diameter of 4.73 mm, a length of 220 mm, and contain 93 percent enriched uranium fuels. The ^{235}U content of each pin is 2.8 g. The maximum fuel burnup of discharged spent nuclear fuels is about 2 percent (^{235}U atom percent) in 10 to 20 years of reactor operation.

The SLOWPOKE spent nuclear fuel pins are usually bundled together in 10 to 15 pins per bundle. In the past, this fuel was shipped to the Savannah River Site in 50.8-mm outside diameter; 2.9-m long canisters containing between 150 to 160 pins per canister.

The fuel type in the Canadian research reactors consists of clusters of about 3 m long uranium aluminum alloy fuel pins clad in aluminum. The initial ^{235}U content of each fuel cluster varies between 491 g and 545 g. The current operating reactor (NRU) uses a fuel element that consists of a cluster of 12 long pins containing 491 g of ^{235}U per cluster. Each fuel pin has an overall length of 296 cm, and the fuel portion is 274.3 cm long. The fuel cluster, including the flow tube, is cut to a length of 292.6 cm before shipment. The average burnup of discharged spent nuclear fuels from a NRU reactor is about 76 percent (^{235}U atom percent). Figure A.4 shows a 12-pin cluster NRU fuel element. The fuel in the South Korean research reactor consists of two types of fuel clusters. The first is 18 pins per cluster with an initial ^{235}U content of 248 g (8.7 oz). The second is 36 pins per cluster with an initial ^{235}U content of 435 g (1 lb). The expected burnup of a discharged spent nuclear fuel from this reactor is approximately 65 percent (^{235}U atom percent).

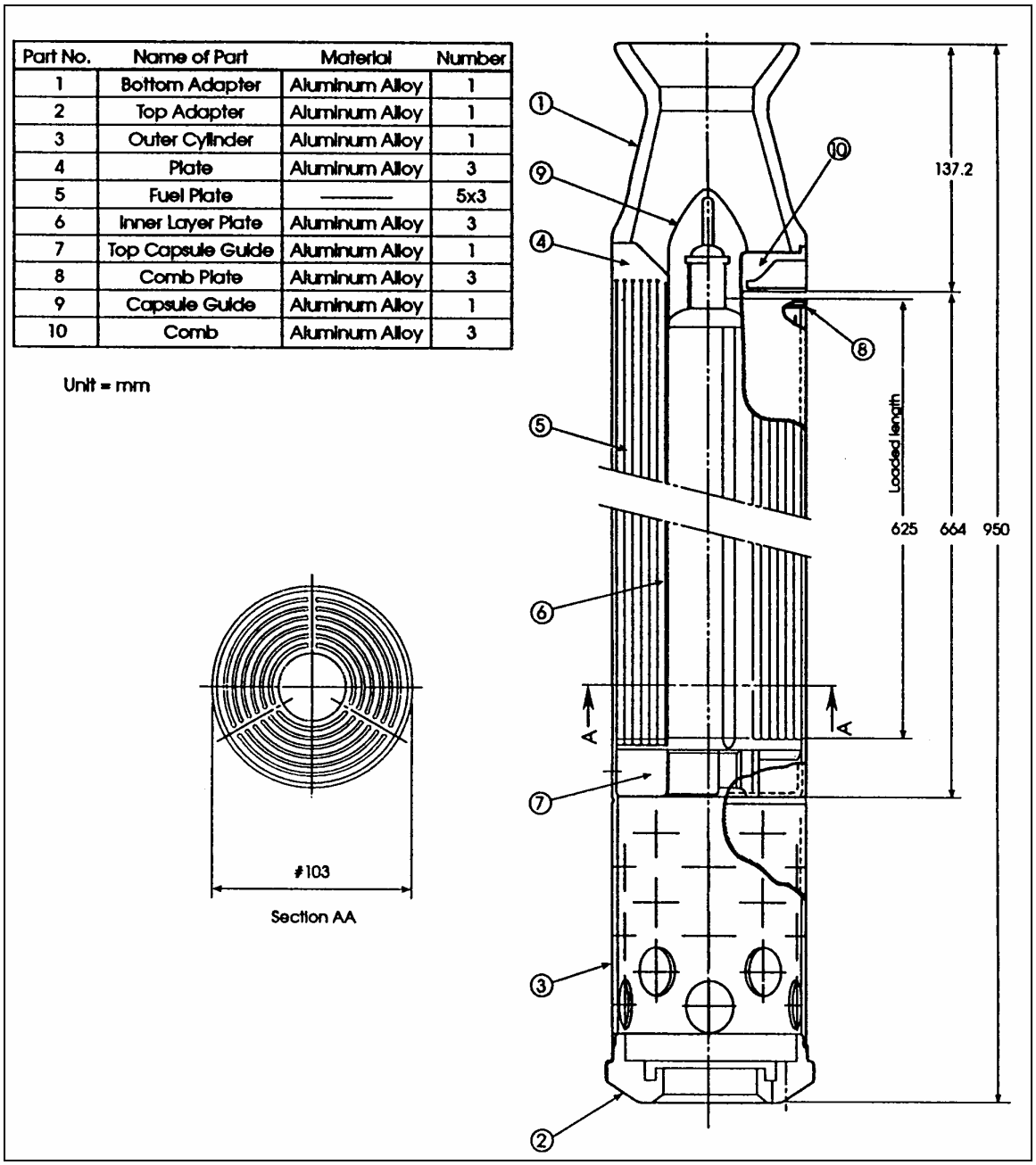

Part No.	Name of Part	Material	Number
1	Bottom Adapter	Aluminum Alloy	1
2	Top Adapter	Aluminum Alloy	1
3	Outer Cylinder	Aluminum Alloy	1
4	Plate	Aluminum Alloy	3
5	Fuel Plate	———	5x3
6	Inner Layer Plate	Aluminum Alloy	3
7	Top Capsule Guide	Aluminum Alloy	1
8	Comb Plate	Aluminum Alloy	3
9	Capsule Guide	Aluminum Alloy	1
10	Comb	Aluminum Alloy	3

Figure A.3 Typical MTR (Tube-Type) Aluminum-Based Fuel Element Schematic

A.3.1.4 Involute Type Design

The fuel used in the high flux reactors is an involute-type fuel element. These research reactors consist of a single fuel element. There are currently two reactors of this design anticipated to ship SNF to the SRS. They are the Oak Ridge National Laboratory (ORNL) High Flux Isotope Reactor (100 MW) and the French Reactor à Haut Flux (57 MW).

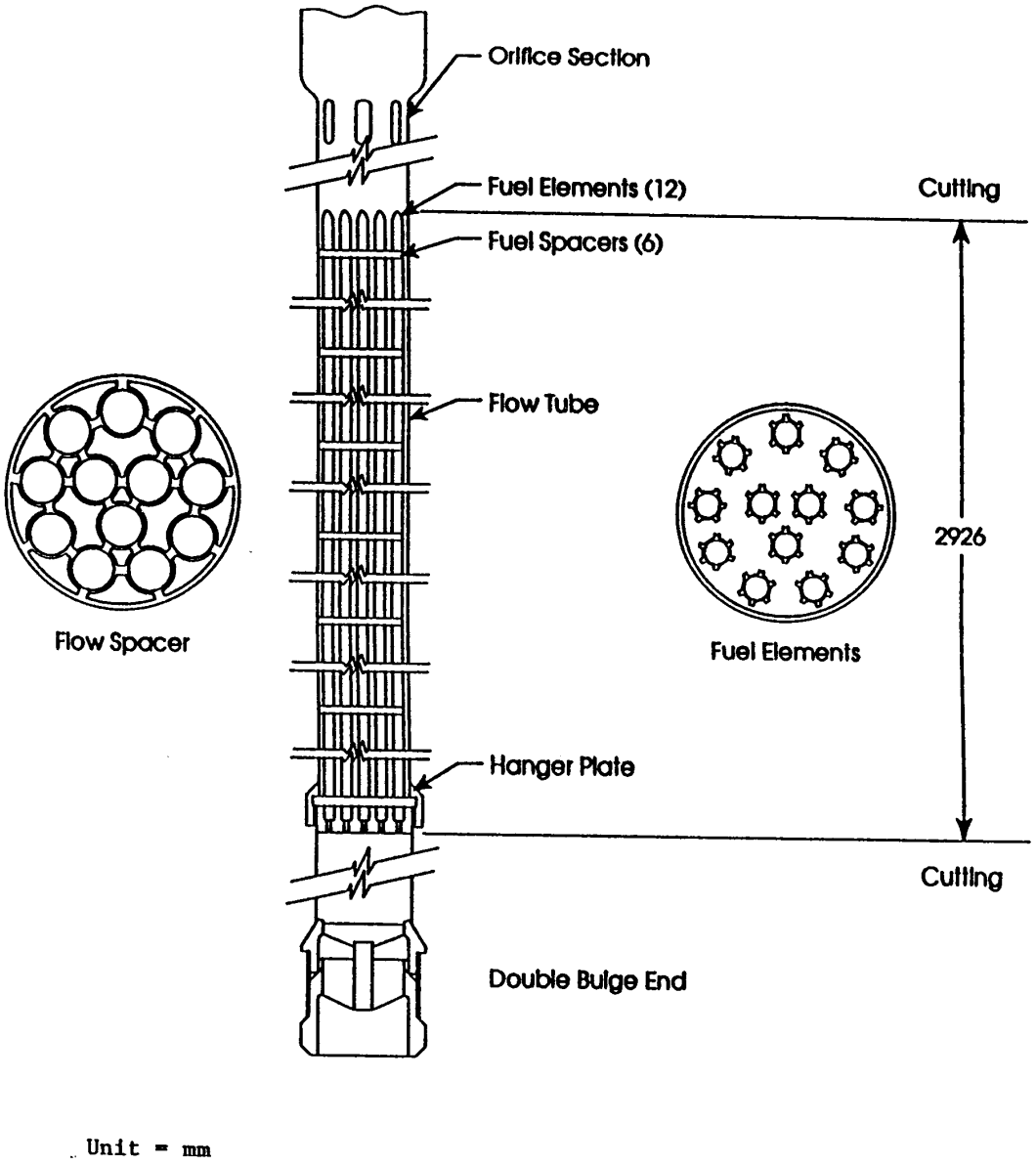

Figure A.4 Typical Pin-Type (Aluminum-Based) Fuel Element Schematic

The RHF fuel element contains 9.2 kg of uranium, enriched to 93 percent of ^{235}U in 280 involute fuel plates made of uranium aluminum alloy (UAl_3-Al), clad in aluminum. The weight of an element is about 100 kg. The fuel is in the annulus of two aluminum tubes: the inner tube has an outside diameter of 274 mm, and the outer tube has an outside diameter of 414 mm. The expected average burnup of a discharged spent nuclear fuel is 36 percent (^{235}U atom percent). Figure A.5 shows a schematic drawing of a configuration of annular fuel element similar to that of RHF fuels.

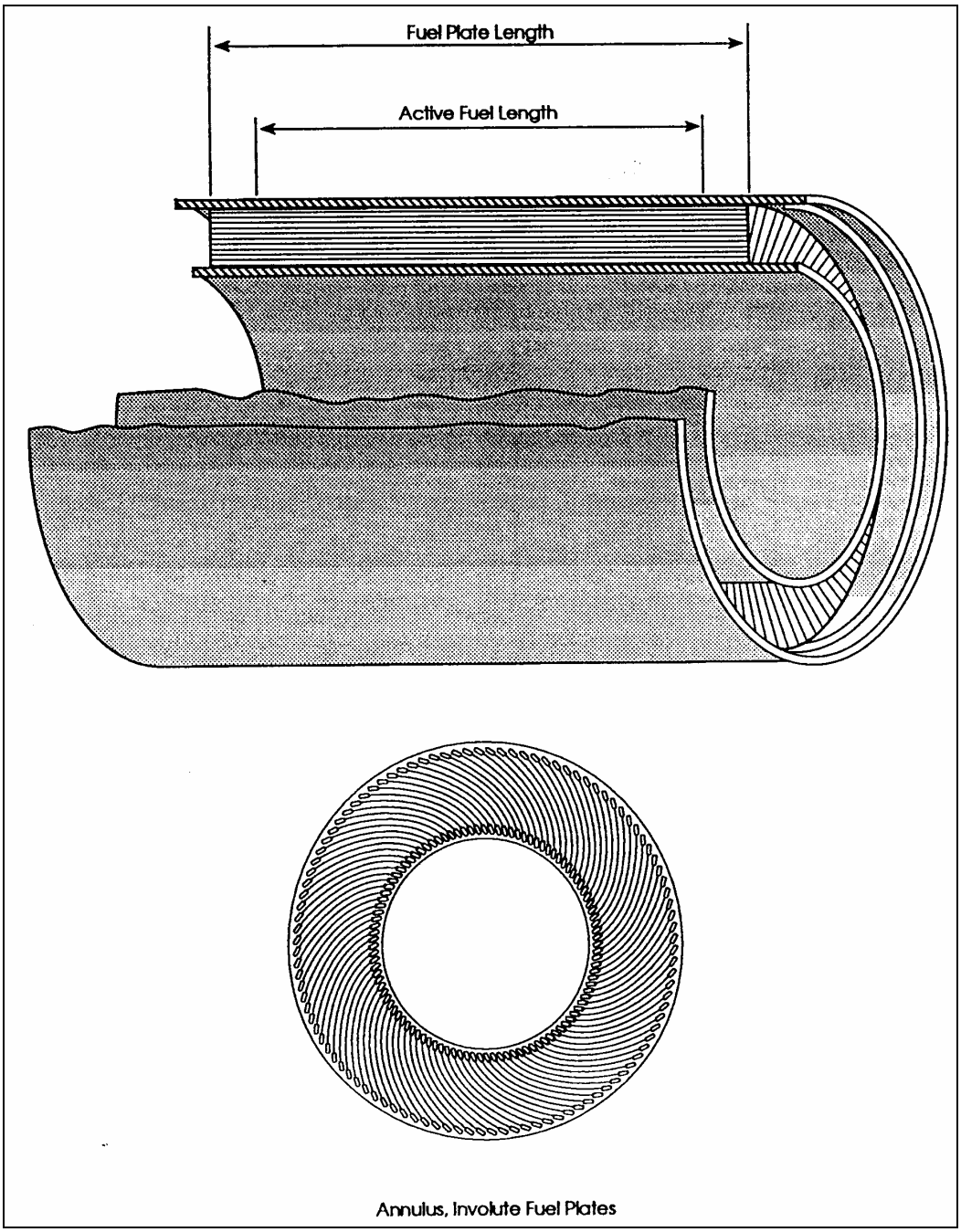

Figure A.5 Typical Involute(1)-Type (Aluminum-Based) Fuel Element Schematic

The HFIR fuel elements contain 10 kg of Uranium, enriched to 93% of ^{235}U. The element consists of an inner annulus (171 involute fuel plates) and an outer annulus (369 involute fuel plates). The material is uranium oxide - aluminum matrix, clad with aluminum. The total weight of the element is 136 kg. The tube is 80 cm long with an outer diameter of 43 cm. Figure A.6 shows a schematic drawing of a configuration of a typical HFIR fuel element.

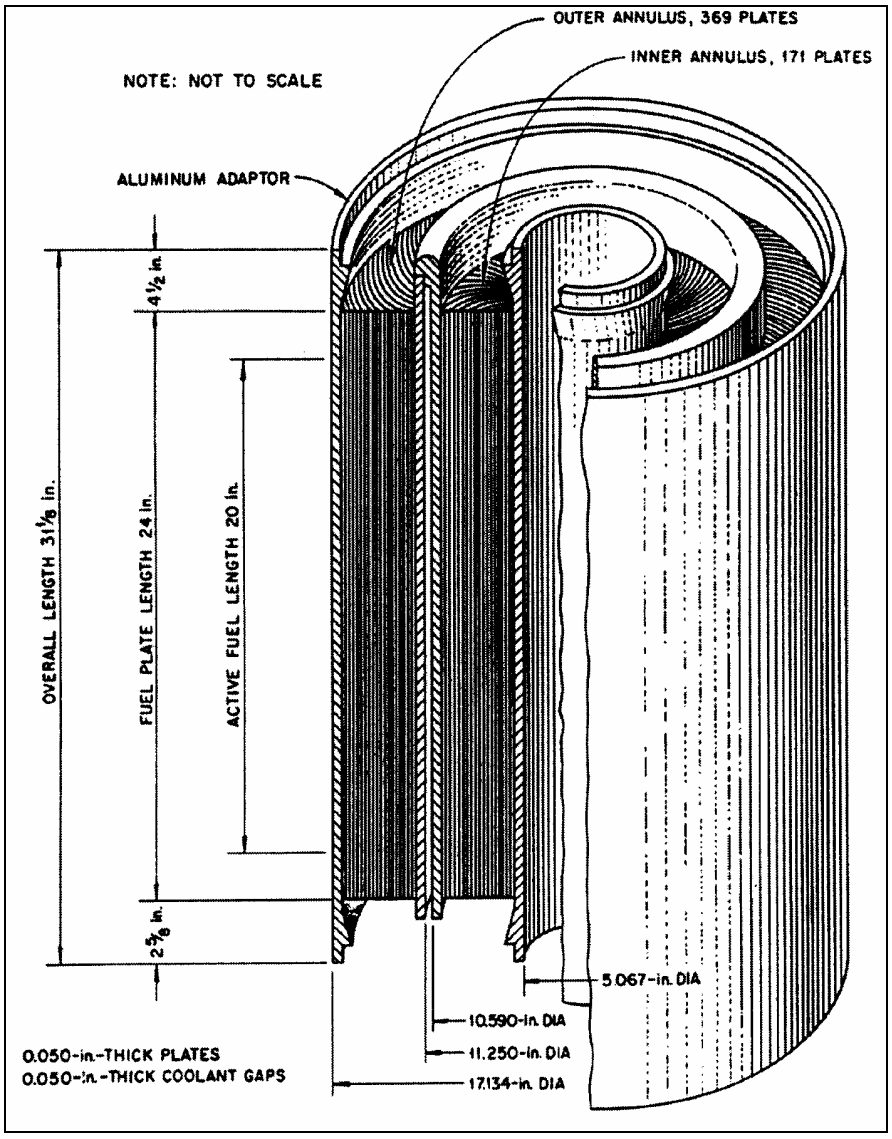

Figure A.6 Typical Involute(2)-Type (Aluminum-Based) Fuel Element Schematic

A.3.1.5 General Purpose Tubes

SNF elements may be received in SRS General Purpose Tubes, Square Cans, L-Basin Cans, or other aluminum bundling or canisterizing container. Onsite storage basins have utilized General Purpose Tubes to maximize storage space inventory, within radiological limits. The number of SNF elements within each General Purpose Tube may range from one to six, depending on the type and size of element(s). The SNF elements within a General Purpose Tube may be cropped and stacked with appropriate spacer material provided for radiological purposes. WSRC Drawings C-CS-L-0962, S4-2-609 and S5-2-6835 represent typical general-purpose tube design(s).

A.3.2 U Oxide/Failed Clad & Al

Tables A.1 and A.2 provide a detailed listing of the current projection of types and quantities of uranium oxide and mixed oxide fuel materials to be handled by TSF, respectively. The definition of the acronyms in the Reactor/Assembly Description column for these tables may be found in the International Atomic Energy Agency (IAEA) Directory of Nuclear Reactors and the IAEA Nuclear Research Reactors in the World. The tables may include some assemblies that are scheduled for reprocessing. The contents of the tables may change as processing is completed.

Table A.1 Uranium Oxide Inventory

Reactor/Assembly Description	Units	Configuration	Assembly Dimensions				Enrichment		U^{235} Mass (kg)		% Burnup	
			Hgt (cm)	Width (cm)	Lgth (cm)	Mass (kg)	% BOL ^{235}U	% EOL ^{235}U	BOL	EOL	U^{235}	Heavy Metal
U_3O_8												
ASTRA (AUSTRIA)	14	MTR PLATE TYPE	8.05	7.61	83.00	6.00		19.95		0.35	0.0	0.0
BSR	41	19 PLATE MTR ASS'Y	8.05	7.61	85.41	4.48		85.71		0.15		
FRG-1 (GERMANY)	7	MTR TYPE		7.62	95.00	3.50	19.73	9.11	0.27	0.11	58.8	10.7
HFBR	220	18 CURVED PLATES	8.17	7.31	62.23	4.38	93.17	79.95	0.35	0.21	39.8	29.9
HFBR	20	18 CURVED PLATES	8.17	7.31	62.23	4.38	93.17	79.95	0.35	0.21	39.8	29.9
HFBR	350	18 CURVED PLATES	8.17	7.31	62.30	4.38	93.12	80.67	0.35	0.22	38.1	28.6
HFBR	2450	18 CURVED PLATES	8.17	7.31	62.30	4.38	93.09	93.09	0.35	0.35	0.0	0.0
HFBR	700	18 CURVED PLATES	8.17	7.31	62.30	4.38	93.12	80.67	0.35	0.22	38.1	28.6
HFIR	14	2 CONCENTRIC TUBES		43.50	80.00	139.90	93.10	86.55	9.40	6.84	27.2	21.7
HFIR	161	2 CONCENTRIC TUBES		43.50	80.00	139.90	92.95	92.95	9.39	6.58	30.0	30.0
NIST	126	17 CURVED PLATES	8.55	7.60	68.80	6.00	93.16	67.41	0.15	0.05	65.0	51.7
NIST	880	17 CURVED PLATES	8.55	7.60	68.80	6.00	93.33	61.96	0.35	0.10	71.1	56.5
OMEGA WEST (204)	16	18 OR 19 FLAT PLATES	8.39	7.66	108.00	4.90	93.14	86.38	0.19	0.14	28.6	22.7
OMEGA WEST (236)	44	18 OR 19 FLAT PLATES	8.39	7.66	108.00	4.90	93.22	82.85	0.22	0.14	37.8	30.0
OMEGA WEST (250)	27	18 OR 19 FLAT PLATES	8.39	7.66	108.00	4.90	93.14	87.38	0.23	0.17	27.7	23.0
ORR	17	19 CURVED PLATES	8.03	7.60	65.09	5.00	93.14	79.04	0.28	0.15	45.9	36.2
ORR	101	19 CURVED PLATES	8.03	7.60	65.09	5.00	90.70	81.19	0.28	0.17	38.5	31.3
ORR	100	19 CURVED PLATES	8.03	7.60	65.09	5.00		14.56		0.23		
ORR - MISC	10	SCRAP IN CANISTER				26.50		6.74		0.23		
RP-10 (PERU)	6	MTR-C		7.62	88.00	6.00	20.00	11.11	0.21	0.10	50.0	10.0
RP-10 (PERU)	23	MTR-S		7.62	88.00	6.00	20.00	11.11	0.23	0.14	39.1	10.0
RSG-GAS-30 (INDONESIA)	165	MTR-S		7.62	88.00	7.50	20.00	11.11	0.25	0.13	50.0	10.0
STERLING FOREST OXIDE	677	PARTICULATE	7.62	6.35	40.64	2.00		93.32		0.14		
UMRR	28	24 CURVED PLATES	7.57	8.74	87.00	6.20		88.38		0.15		
UO_2												
FRR TARGET ARGENTINA	48	PARTICULATE				0.10	48.35	48.35	0.04	0.04	0.0	0.0
FRR TARGET CANADA	5952	PARTICULATE				0.10	48.35	48.35	0.04	0.04	0.0	0.0
FRR TARGET INDONESIA	48	PARTICULATE				0.10	48.35	48.35	0.04	0.04	0.0	0.0
HWCTR	45	TUBE		5.25	47.63	7.00		0.52		0.02		
WAPD (Na/K BONDED)	22	ROD		12.70	94.68	5.00		17.73		0.05		
TOTALS	12312					52970.24				2819.92		

Table A.2 Mixed Oxide Inventory

Reactor/Assembly Description	Units	Configuration	Fuel Material	Assembly Dimensions			Enrichment	U^{235} Mass (kg)	% Burnup	
				Width (cm)	Lgth (cm)	Mass (kg)	% EOL ^{235}U	EOL	U^{235}	Heavy Metal
EBR-II (MOX)	71	ROD	PUO2-UO2	0.59	154.94	2.00	78.74	0.03	4.7	2.9
SRE (U/TH)	37	CYLINDRICAL SLUGS	U-TH	8.89	280.04	103.00	74.27	4.00		
K/L/P NON-U TARGETS (PROCESSED)	104	ASSEMBLY	VARIOUS			23.83				
MARK 42 TARGETS (PU)	18	TUBE	PUO2	10.16	65.09	11.35				
TOTALS	230					6635.70		149.98		

A.3.3 UAl_x/Al

Table A.3 provides a detailed listing of the current projection of types and quantities of uranium aluminum fuel materials to be handled by TSF. The definition of the acronyms in the Reactor/Assembly Description column for this table may be found in the IAEA Directory of Nuclear Reactors and the IAEA Nuclear Research Reactors in the World. The table may include some assemblies that are scheduled for reprocessing. The contents of the table may change as processing is completed.

Table A.3 Uranium-Aluminum Inventory

Reactor/Assembly Description	Units	Configuration	Assembly Dimensions				Enrichment		U^{235} Mass (kg)		% Burnup	
			Hgt (cm)	Width (cm)	Lgth (cm)	Mass (kg)	% BOL ^{235}U	% EOL ^{235}U	BOL	EOL	U^{235}	Heavy Metal
ANLJ	19	ELEMENT		7.62	128.65	7.50	93.17	92.67	0.14	0.14	0.5	0.0
ARGONAUT REACTOR (BRAZIL)	28	MTR TYPE		7.62	95.00	5.50	20.00	19.98	0.20	0.20	0.1	0.0
ARMF	15	FLAT PLATES IN CAN	0.17	7.87	64.77	0.24	91.89	91.89	0.01	0.01	0.0	0.0
ARMF/CFRMF MARK I	56	15 FLAT PLATES	8.28	8.28	98.74	5.62	93.00	93.11		0.19		0.0
ARMF/CFRMF MARK I LL	2	15 FLAT PLATES	8.28	8.28	98.74	4.51	94.00	93.22		0.11		0.0
ARMF/CFRMF MARK II	8	15 FLAT PLATES	3.12	3.12	64.77	0.66	93.00	81.10		0.12		0.0
ARMF/CFRMF MARK III	4	15 FLAT PLATES	8.28	8.28	98.74	4.65	93.00	91.67		0.02		0.0
ASTRA (AUSTRIA)	14	MTR TYPE		7.62	95.00	4.40		90.00		0.31	67.0	62.3
ASTRA (AUSTRIA)	2	MTR TYPE		7.62	95.00	3.50		83.33		0.05	71.0	66.0
ASTRA (AUSTRIA)	22	MTR TYPE		7.62	95.00	4.90	93.00	82.71	0.28	0.10	64.0	59.5
ASTRA (AUSTRIA)	9	MTR TYPE		7.62	95.00	4.40		80.26		0.07	67.0	62.3
ASTRA (AUSTRIA)	5	MTR TYPE		7.62	95.00	5.30	45.00	22.26	0.32	0.11	65.0	29.2
ASTRA-(AUSTRIA)	26	19 FLAT PLATES	8.05	7.61	68.65	2.20	86.09	68.55	0.26	0.10	63.2	51.7
ATR	1096	19 CURVED PLATES	6.53	10.75	123.19	9.10	93.15	82.89	1.08	0.69	35.6	27.6
ATR	2780	19 CURVED PLATES	6.53	10.75	168.28	10.00	93.15	81.01	1.08	0.72	32.8	22.8
ATR	128	19 CURVED PLATES	6.53	10.75	123.19	9.10	93.15	79.96	1.08	0.62	42.4	32.9
ATR PLATES	30	MTR PLATE TYPE	0.25	10.75	121.90	2.00		92.00		0.01	0.0	0.0
ATSR	20	19 FLAT PLATES	8.20	7.61	64.50	2.45		93.18		0.15	0.2	0.0
BER-2 (GERMANY)	25	MTR-C TYPE		7.62	95.00	5.60	93.00	85.39	0.13	0.06	56.0	52.1
BER-2 (GERMANY)	71	MTR-S TYPE		7.62	95.00	5.50	93.00	85.39	0.18	0.08	56.0	52.1
BER-II (GERMANY)	66	MTR PLATE TYPE	8.10	7.62	90.00	5.40	93.12	75.90	0.17	0.08	51.3	40.2
BNL MEDICAL RX	68	18/19 CURVED PLATES	7.63	7.63	62.50	4.47		83.84		0.12		

Reactor/Assembly Description	Units	Configuration	Assembly Dimensions				Enrichment		U^{235} Mass (kg)		% Burnup	
			Hgt (cm)	Width (cm)	Lgth (cm)	Mass (kg)	% BOL ^{235}U	% EOL ^{235}U	BOL	EOL	U^{235}	Heavy Metal
(BMRR)												
BR-2 (BELGIUM)	16	ASSEMBLY		10.30	62.50	2.80	92.00	90.20	0.15	0.12	20.0	18.4
BR-2 (BELGIUM)	6	ASSEMBLY		10.30	62.50	4.10	90.00	90.00	0.14	0.14	0.0	0.0
BR-2 (BELGIUM)	5	ASSEMBLY		10.30	62.50	3.00	93.00	88.12	0.25	0.14	44.9	41.9
BR-2 (BELGIUM)	79	ASSEMBLY		10.30	62.50	3.60	93.00	88.04	0.34	0.22	36.0	33.1
BR-2 (BELGIUM)	1451	ASSEMBLY		10.30	62.50	3.80	93.00	87.36	0.40	0.21	48.0	44.6
BR-2 (BELGIUM)	40	ASSEMBLY		10.30	62.50	3.13	90.00	86.13	0.25	0.18	31.0	27.9
BR-2 (BELGIUM)	105	ASSEMBLY		10.30	62.50	5.80	93.00	84.52	0.39	0.21	46.0	41.9
BR-2 (BELGIUM)	64	ASSEMBLY		10.30	62.50	3.00	80.00	70.59	0.22	0.15	33.0	30.4
BSR	41	19 PLATE MTR ASS'Y	8.05	7.61	85.41	4.48		85.71		0.15		
DR-3 (DENMARK)	10	ASSEMBLY		10.30	62.50	2.70	90.00	86.92	0.15	0.07	50.0	46.5
DR-3 (DENMARK)	5	ASSEMBLY		10.30	62.50	2.50	90.00	86.68	0.12	0.06	51.0	47.4
DR-3 (DENMARK)	88	ASSEMBLY		9.34	62.50	2.80	89.10	69.38	0.15	0.07	53.0	39.8
DR-3 (DENMARK)	3	ASSEMBLY		9.34	62.50	2.80	19.88	10.28	0.18	0.08	54.6	12.1
ENEA (RANA-ITALY)	115	MTR TYPE	7.60	8.00	65.50	4.60		83.12		0.13	22.5	19.5
ENEA (RANA-ITALY)	33	MTR TYPE	7.61	8.04	65.50	4.90		19.42		0.13		
FMRB (GERMANY)	92	MTR TYPE		7.62	95.00	3.50	91.26	87.77	0.13	0.11	14.6	11.2
FRG-1 (GERMANY)	132	MTR TYPE		7.62	95.00	3.50	92.97	81.97	0.15	0.09	38.5	30.2
FRG-2 (GERMANY)	1	MTR-S TYPE		7.62	95.00	5.50	93.00	91.20	0.16	0.11	31.0	28.8
FRG-2 (GERMANY)	33	MTR-C TYPE		7.62	95.00	5.30	93.00	88.69	0.09	0.06	41.0	38.1
FRG-2 (GERMANY)	2	MTR-S TYPE		7.62	95.00	5.50	93.00	85.21	0.18	0.12	36.0	32.4
FRJ-2 (GERMANY)	200	ASSEMBLY		10.30	62.50	2.80	85.00	70.59	0.15	0.09	40.0	32.0
FRJ-2 (GERMANY)	200	ASSEMBLY		10.30	62.50	2.80	80.00	70.59	0.17	0.10	40.0	32.0
FRM (GERMANY)	10	MTR-S TYPE		7.62	95.00	5.50	93.00	91.20	0.16	0.11	31.0	28.8
FRM (GERMANY)	16	MTR-C TYPE		7.62	95.00	5.30	93.00	88.69	0.09	0.06	41.0	38.1
FRM (GERMANY)	13	MTR-S TYPE		7.62	95.00	5.60	93.00	85.10	0.23	0.10	57.0	53.0
FRM (GERMANY)	28	MTR-C TYPE		7.62	95.00	6.00	45.00	22.75	0.21	0.07	64.0	28.8
FRM (GERMANY)	74	MTR-S TYPE		7.62	95.00	5.80	45.00	22.75	0.28	0.10	64.0	28.8
FRR MTR ITALY	12	MTR TYPE		7.62	95.00	5.50		92.21		0.38		
FRR MTR ITALY	1	MTR TYPE		7.62	95.00	5.50		19.84		0.04		
FRR MTR SPAIN	1	MTR TYPE		7.62	95.00	5.50		49.63		0.13		
GENTR	16	STACKED DISKS		6.99	41.28	2.50	93.00	92.24	0.23	0.22	5.1	3.4
GRR-1 (GREECE)	107	MTR PLATE TYPE	7.62	7.62	77.80	4.90	91.96	84.60	0.16	0.11	28.3	22.0
GTRR	25	ASSEMBLY	7.04	7.52	69.85	10.74	93.07	90.27	0.19	0.16	14.1	11.4
HIFAR (AUSTRALIA)	187	ASSEMBLY		10.30	62.50	2.20	80.00	70.90	0.15	0.09	39.0	31.2
HIFAR (AUSTRALIA)	266	ASSEMBLY		10.30	62.50	2.20	90.00	65.83	0.12	0.05	53.0	42.4
HIFAR (AUSTRALIA)	52	ASSEMBLY		10.30	62.50	2.30	60.00	43.30	0.15	0.08	49.0	29.4
HIFAR (AUSTRALIA)	169	ASSEMBLY		10.30	62.50	2.30	60.00	41.35	0.17	0.08	53.0	31.8
HIFAR (AUSTRALIA)	289	ASSEMBLY		10.30	62.50	2.30	20.00	11.11	0.20	0.10	50.0	10.0
HFR-PETTEN (NETHERLANDS)	715	MTR-S TYPE		7.62	95.00	4.60	93.00	83.21	0.42	0.21	51.0	46.4
HFR-PETTEN (NETHERLANDS)	161	MTR-C TYPE		7.62	95.00	4.50	93.00	80.18	0.29	0.12	60.0	54.6
HOR (NETHERLANDS)	61	MTR-S TYPE		7.62	95.00	4.30	93.00	86.92	0.19	0.09	50.0	46.5
HOR (NETHERLANDS)	19	MTR-S TYPE		7.62	95.00	4.50	90.00	86.92	0.10	0.05	50.0	46.5
HOR (NETHERLANDS)	33	ASSEMBLY	7.62	7.62	88.00	5.50	93.13	77.50	0.18	0.09	49.0	38.8
IAE-R1 (BRAZIL)	4	MTR-O TYPE	7.62	7.62	95.00	6.50	93.00	91.42	0.13	0.10	20.0	18.6

Reactor/Assembly Description	Units	Configuration	Assembly Dimensions				Enrichment		U^{235} Mass (kg)		% Burnup	
			Hgt (cm)	Width (cm)	Lgth (cm)	Mass (kg)	% BOL ^{235}U	% EOL ^{235}U	BOL	EOL	U^{235}	Heavy Metal
IAE-R1 (BRAZIL)	6	MTR-C TYPE	7.62	7.62	95.00	6.50	93.00	90.33	0.09	0.06	30.0	27.9
IAE-R1 (BRAZIL)	33	MTR-S TYPE		7.62	95.00	5.60	93.00	90.29	0.18	0.13	30.0	27.9
IAE-R1 (BRAZIL)	6	MTR-C TYPE		7.62	95.00	6.50	20.00	19.99	0.08	0.08	0.0	0.0
IAE-R1 (BRAZIL)	33	MTR-S1 TYPE		7.62	95.00	5.60	20.00	16.67	0.16	0.13	20.0	4.0
IAE-R1 (BRAZIL)	34	MTR-S1 TYPE		7.62	95.00	5.60	20.00	16.32	0.16	0.12	22.0	4.4
IAE-R1 (BRAZIL)	5	MTR-S2 TYPE		7.62	95.00	5.60	20.00	15.43	0.18	0.13	27.0	5.4
IAE-R1 (BRAZIL)	6	MTR-C TYPE		7.62	95.00	6.50	20.00	13.23	0.08	0.05	39.0	7.8
IAN-R1 (COLUMBIA)	21	MTR TYPE		7.62	95.00	3.40		90.55		0.13	0.7	0.6
IRR-1 (ISRAEL)	31	MTR-C TYPE		7.62	95.00	4.80	93.00	84.16	0.16	0.06	60.0	55.8
IRR-1 (ISRAEL)	122	MTR-S TYPE		7.62	88.00	4.80	93.00	84.16	0.22	0.09	60.0	55.8
ISU - ARGONAUT	22	FLAT PLATES IN CAN		8.26	65.30	8.00	93.34	93.34	0.15	0.15	0.0	0.0
ISU - ARGONAUT	22	CAN		8.26	66.28	5.00	93.00	93.32		0.28	0.0	0.0
JEN-1 (SPAIN)	32	MTR TYPE	7.73	7.73	103.00	6.00	42.72	40.00	0.14	0.13	6.4	2.3
JEN-1 (SPAIN)	8	MTR TYPE	7.73	7.73	103.00	6.00	17.93	14.81	0.13	0.11	17.4	2.9
JMTR (JAPAN)	9	MTR-S TYPE		7.62	95.00	5.50	93.00	91.30	0.28	0.23	21.0	19.5
JMTR (JAPAN)	131	10 FLAT PLATES	7.62	7.62	120.00	6.00	93.21	88.51	0.27	0.21	21.2	17.0
JMTR (JAPAN)	165	MTR-C TYPE		7.62	95.00	4.50	45.00	39.86	0.21	0.17	19.0	8.6
JMTR (JAPAN)	675	MTR-S TYPE		7.62	95.00	6.00	45.00	37.39	0.32	0.24	27.0	12.1
JMTRC (JAPAN)	30	MTR TYPE		7.62	95.00	6.00	45.00	44.98	0.32	0.32	0.1	0.0
JRR-2 (JAPAN)	28	MTR TYPE		7.62	95.00	5.00	93.00	87.56	0.19	0.10	47.0	43.7
JRR-2 (JAPAN)	7	CONCENTRIC TUBES			66.40	5.00	93.00	87.56	0.19	0.10	47.0	43.7
JRR-2 (JAPAN)	138	CONCENTRIC TUBES			66.40	6.00	45.00	30.25	0.22	0.12	47.0	21.1
JRR-3(M) (JAPAN)	99	MTR-C TYPE		7.62	95.00	5.00	20.00	11.11	0.19	0.09	50.0	10.0
JRR-3(M) (JAPAN)	506	MTR-S TYPE		7.62	95.00	8.00	20.00	11.11	0.30	0.15	50.0	10.0
JRR-4 (JAPAN)	54	MTR TYPE		7.62	95.00	5.00	93.00	91.40	0.17	0.13	20.0	18.6
KUR (JAPAN)	54	MTR-C TYPE		7.62	95.00	4.30	93.00	91.24	0.09	0.07	22.0	20.5
KUR (JAPAN)	218	MTR-S TYPE		7.62	95.00	4.60	93.00	90.98	0.18	0.14	24.0	22.3
LFR (NETHERLANDS)	14	MTR TYPE		7.62	95.00	5.00	93.00	92.99	0.21	0.21	0.1	0.1
MINERVE (FRANCE)	32	MTR TYPE		7.62	95.00	5.00	93.00	92.99	0.25	0.25	0.0	0.0
MIT	277	15 FLAT PLATES	6.42	6.11	66.68	4.00	93.00	86.69	0.51	0.40	22.1	16.5
MIT	72	15 FLAT PLATES	6.11	6.11	66.68	4.00	93.39	83.73	0.47	0.29	39.2	32.2
MNR (CANADA)	23	MTR-C TYPE		7.62	95.00	3.67	90.00	89.17	0.11	0.07	38.0	35.3
MNR (CANADA)	53	MTR-S TYPE		7.62	95.00	3.92	93.00	89.17	0.20	0.12	38.0	35.3
MNR (CANADA)	21	MTR-S TYPE		7.62	95.00	3.92	93.00	89.17	0.20	0.12	38.0	35.3
MNR (CANADA)	41	MTR TYPE		7.62	95.00	3.92	93.07	81.35	0.18	0.11	39.7	31.0
MOATA ARGONAUT (AUSTRALIA)	12	ASSEMBLY		7.62	88.00	4.30	90.00	89.99	0.25	0.25	0.1	0.1
MRU/WMA (CANADA)	741	MULTI-PIN CLUSTER				4.70	93.00	71.62	0.50	0.09	81.0	75.3
MURR	32	24 CURVED PLATES	7.75	9.14	82.55	6.38	93.50	87.47	0.73	0.60	18.3	12.9
MURR	24	24 CURVED PLATES	7.75	9.14	82.55	6.38	93.50	87.16	0.73	0.59	20.1	14.3
MURR	184	24 CURVED PLATES	7.47	8.74	87.00	6.20	93.14	83.50	0.77	0.60	22.6	17.7
MURR (MTR-SI)	792	24 CURVED PLATES	7.04	14.63	82.55	6.20	93.00	90.15	0.77	0.58	25.1	22.8
NRCRR (IRAN)	7	MTR-C TYPE		7.62	95.00	4.10	94.50	90.29	0.11	0.08	30.0	27.9
NRCRR (IRAN)	22	MTR-S TYPE		7.62	95.00	4.10	93.00	87.00	0.20	0.14	30.0	27.9
NRX (CANADA)	131	MULTI-PIN CLUSTER				4.50	93.00	83.78	0.55	0.21	62.0	57.8
OHIO STATE	24	18 FLAT PLATES		7.62	88.90	50.00	93.25	93.24	0.13	0.13	0.1	0.0
ORPHEE (FRANCE)	148	MTR-C TYPE		7.62	95.00	8.00	93.00	90.39	0.63	0.44	30.0	27.9

Reactor/Assembly Description	Units	Configuration	Assembly Dimensions				Enrichment		U^{235} Mass (kg)		% Burnup	
			Hgt (cm)	Width (cm)	Lgth (cm)	Mass (kg)	% BOL ^{235}U	% EOL ^{235}U	BOL	EOL	U^{235}	Heavy Metal
ORPHEE (FRANCE)	148	MTR-S TYPE		7.62	95.00	9.00	93.00	90.39	0.84	0.59	30.0	27.9
PARR (PAKISTAN)	17	MTR-C TYPE		7.62	95.00	4.10	92.00	88.20	0.11	0.07	35.0	32.2
PARR (PAKISTAN)	65	MTR-S TYPE		7.62	95.00	4.10	92.00	88.20	0.20	0.13	35.0	32.2
PRR-1 (PHILIPPIINES)	20	MTR TYPE		7.62	95.00	4.10	93.00	90.10	0.16	0.12	25.0	23.2
PRR-1 (PHILIPPIINES)	30	MTR TYPE		7.62	95.00	4.50	20.00	16.68	0.14	0.11	20.0	4.0
PTR (CANADA)	14	MULTI-PIN CLUSTER				3.80	93.00	93.00	0.15	0.15	0.5	0.5
PTR (CANADA)	225	MULTI-PIN CLUSTER				4.70	93.00	76.54	0.49	0.12	76.0	70.8
PURDUE UNIVERSITY	124	10 FLAT PLATES	0.15	7.01	68.80	0.03	93.00	93.22	0.17	0.02	90.0	90.0
R-2 (SWEDEN)	6	MTR-C TYPE		7.62	95.00	4.30	90.00	88.44	0.12	0.10	15.0	13.5
R-2 (SWEDEN)	21	MTR-S TYPE		7.62	95.00	4.30	90.00	88.44	0.12	0.10	15.0	13.5
R-2 (SWEDEN)	48	MTR-C TYPE		7.62	95.00	4.60	93.00	76.12	0.16	0.04	76.0	70.7
R-2 (SWEDEN)	304	MTR TYPE	7.62	7.62	92.40	6.00	93.06	74.77	0.24	0.10	58.8	48.8
RA-3 (ARGENTINA)	36	MTR-C TYPE		7.62	95.00	4.30	90.00	85.40	0.15	0.10	35.0	31.5
RA-3 (ARGENTINA)	144	MTR-S TYPE		7.62	95.00	4.30	90.00	85.40	0.19	0.13	35.0	31.5
RA-6 (ARGENTINA)	14	MTR-C TYPE		7.62	95.00	4.30	90.00	86.31	0.15	0.11	30.0	27.0
RA-6 (ARGENTINA)	59	MTR-S TYPE		7.62	95.00	4.30	90.00	86.31	0.19	0.14	30.0	27.0
RA-O CORDOBA UNIV (ARGENTINA)	30	MTR TYPE		7.62	95.00	4.30	20.00	19.84	0.13	0.12	1.0	0.2
RECH-1 (CHILE)	28	MTR TYPE	7.61	7.61	99.30	5.00	80.00	61.00	0.16	0.08	48.6	32.6
RHF (FRANCE)	86	ASSEMBLY		41.40		110.00	90.00	88.85	8.50	5.10	40.0	37.2
RHF (FRANCE)	4	2 CONCENTRIC TUBES		40.64	97.00	102.00	92.97	81.44	8.58	5.19	39.4	30.9
RINSC	66	18 FLAT PLATES		7.62	62.50	2.00	93.14	90.55	0.12	0.11	11.6	9.1
RP-1 (PORTUGAL)	3	MTR-O TYPE		7.62	95.00	4.60	20.00	17.78	0.09	0.08	11.1	0.0
RP-1 (PORTUGAL)	9	MTR-C TYPE		7.62	95.00	5.30	20.00	17.18	0.09	0.07	17.0	3.4
RP-1 (PORTUGAL)	45	MTR-S TYPE		7.62	95.00	4.90	20.00	16.14	0.18	0.14	23.0	4.6
RPI (PORTUGAL)	9	MTR-C TYPE		7.62	95.00	4.90	93.00	88.85	0.15	0.09	40.0	37.2
RPI (PORTUGAL)	22	MTR-S TYPE		7.62	95.00	4.50	93.00	88.85	0.26	0.16	40.0	37.2
RU-1 (URAGUAY)	19	MTR TYPE		7.62	95.00	5.00	20.00	20.00	0.19	0.19	0.0	0.0
RV-1 (VENEZUELA)	120	MTR TYPE		7.62	95.00	6.00	20.00	16.66	0.14	0.11	20.0	4.0
SAFARI-1 (SO. AFRICA)	4	MTR-O TYPE	7.62	7.62	95.00	5.10	90.00	89.10	0.09	0.05	38.5	35.8
SAFARI-1 (SO. AFRICA)	40	MTR-S TYPE		7.62	95.00	4.20	90.00	86.78	0.20	0.10	50.6	47.1
SAFARI-1 (SO. AFRICA)	6	MTR-C TYPE		7.62	95.00	4.50	90.00	82.71	0.14	0.05	64.0	59.5
SAPHIR (SWITZERLAND)	128	MTR PLATE TYPE	8.05	7.62	87.50	4.11	62.08	35.13	0.28	0.11	61.9	32.6
SAPHIR (SWITZERLAND)	7	MTR-C1 TYPE		7.62	95.00	4.00	93.00	82.82	0.17	0.06	64.0	59.5
SAPHIR (SWITZERLAND)	11	MTR-C2 TYPE		7.62	95.00	4.20	93.00	82.71	0.21	0.07	64.0	59.5
SAPHIR (SWITZERLAND)	55	MTR-S TYPE		7.62	95.00	3.90	93.00	80.46	0.28	0.09	69.0	64.2
SCARABEE (FRANCE)	31	MTR TYPE		7.62	95.00	5.50	93.00	92.93	0.31	0.30	1.0	0.9
SILOE/MELUSINE (FRANCE)	97	MTR-C TYPE		7.62	95.00	5.40	93.00	87.96	0.25	0.14	45.0	41.9
SILOETTE (FRANCE)	30	MTR TYPE		7.62	95.00	5.90	93.00	92.97	0.33	0.33	0.5	0.5
SLOWPOKE-ALBERTA (CANADA)	2	ASSEMBLY				2.30	93.00	93.00	0.41	0.41	1.5	1.4
SLOWPOKE-HALIFAX (MONTREAL)	2	ASSEMBLY				2.40	93.00	93.00	0.44	0.43	1.5	1.4
SLOWPOKE-JAMAICA (JAMAICA)	2	ASSEMBLY				2.30	93.00	93.00	0.41	0.40	1.5	1.4
SLOWPOKE-KANATA AT AECL (CANADA)	2	ASSEMBLY				2.40	93.00	93.00	0.44	0.43	1.5	1.4
SLOWPOKE-MONTREAL (CANADA)	2	ASSEMBLY				2.40	93.00	93.00	0.44	0.43	1.5	1.4

Reactor/Assembly Description	Units	Configuration	Assembly Dimensions				Enrichment		U^{235} Mass (kg)		% Burnup	
			Hgt (cm)	Width (cm)	Lgth (cm)	Mass (kg)	% BOL ^{235}U	% EOL ^{235}U	BOL	EOL	U^{235}	Heavy Metal
SLOWPOKE-SASKATCHWAN (CANADA)	2	ASSEMBLY				2.40	93.00	93.00	0.44	0.43	1.5	1.4
SLOWPOKE-TORONTO (CANADA)	2	ASSEMBLY				2.10	93.00	93.00	0.39	0.38	1.5	1.4
SRS (PROCESSED)	5	TUBE				10.00	32.00	31.70		0.39		6.2
SRS DRIVER FUEL	449	ASSEMBLY				23.83		66.22		2.05		
SRS DRIVER FUEL	516	SCRAP				33.43		59.62		3.00		
SRS DRIVER FUEL	4	ASSEMBLY				1.32		31.05		0.06		
SRS DRIVER FUEL (PROCESSED)	902	ASSEMBLY				22.62		65.29		2.34		
SRS DRIVER FUEL (PROCESSED)	13	ASSEMBLY				33.08		61.18		3.18		
STERLING FOREST	200	ASSEMBLY				2.88		84.01		0.12		
STRASBOURG-CRONENBOURG (FRANCE)	48	MTR TYPE		7.62	95.00	5.00	90.00	89.98	0.12	0.12	0.5	0.5
THAR-ARGONAUT (TAIWAN)	23	MTR TYPE		7.62	95.00	3.00	20.00	19.83	0.30	0.30	0.0	0.0
THOR (TAIWAN)	34	MTR TYPE		7.62	95.00	5.10	93.00	90.77	0.14	0.10	26.0	24.2
TR-2 (TURKEY)	8	MTR-C TYPE		7.62	95.00	4.80	93.00	86.92	0.21	0.10	50.0	46.5
TR-2 (TURKEY)	2	MTR-O TYPE		7.62	95.00	4.80	93.00	86.92	0.17	0.09	50.0	46.5
TR-2 (TURKEY)	18	MTR-S TYPE		7.62	95.00	4.80	93.00	86.92	0.28	0.14	50.0	46.5
TRR-1/M-1 (THAILAND)	31	MTR TYPE		7.62	95.00	4.20	90.00	87.53	0.15	0.12	22.0	19.8
TSR FUEL	1	SPHERICAL		73.66		182.00		93.48		8.60		
TTR-1 (JAPAN)	27	MTR TYPE		7.62	95.00	6.50	20.00	19.94	0.13	0.13	0.4	0.1
ULYSSE-ARGONAUT (FRANCE)	48	MTR TYPE		7.62	95.00	5.00	90.00	89.98	0.12	0.12	0.5	0.5
UNIV OF FLORIDA (ARGONAUT)	256	11 FLAT PLATES	5.44	7.23	65.09	1.22	93.00	93.10	0.02	0.01	9.9	10.0
UNIV OF MASS-LOWELL	26	18 FLAT PLATES	7.62	7.62	101.60	8.85		92.71		0.15		
UNIV OF MICHIGAN	156	18 CURVED PLATES	7.47	8.26	87.38	4.56	19.75	15.26	0.17	0.11	33.6	14.1
UNIV OF MICHIGAN	48	18 CURVED PLATES	7.47	8.26	87.38	6.00	19.85	14.67	0.15	0.10	30.0	5.3
UNIV OF VIRGINIA	44	22 FLAT PLATES	8.26	7.93	95.38	6.50	92.94	86.92	0.17	0.14	17.6	13.5
UNIV OF WASHINGTON	26	11 FLAT PLATES	5.98	7.24	68.90	2.74		93.07		0.14		
UTR 300 (UNIV. OF GLASGOW -UK)	12	MTR TYPE		7.62	95.00	6.50	90.00	89.82	0.30	0.29	2.0	1.8
UTR-10 KINKI (JAPAN)	12	MTR TYPE	12.30	7.62	64.80	4.20	93.00	93.00	0.27	0.27	0.0	0.0
WORCESTER POLY INSTITUTE	26	18 CURVED PLATES	7.75	7.75	101.60	5.80	19.90	19.79		0.17		2.2
ZPRL (TAIWAN)	35	MTR TYPE		7.62	95.00	5.15	93.20	93.19	0.13	0.13	0.1	0.1
ZPRL (TAIWAN)	35	MTR TYPE		7.62	95.00	5.15	20.00	19.95	0.13	0.12	0.3	0.1
TOTALS	19763					162796.28		72.42		10505.90		

A.3.4 U-Si

Table A.4 provides a detailed listing of the current projection of types and quantities of uranium silicon fuel materials to be handled by TSF, respectively. The definition of the acronyms in the Reactor/Assembly Description column for this table may be found in the IAEA Directory of Nuclear Reactors and the IAEA Nuclear Research Reactors in the World. The table may include

some assemblies that are scheduled for reprocessing. The contents of the table may change as processing is completed.

Table A.4 Uranium/Silicon Inventory

Reactor/Assembly Description	Units	Configuration	Assembly Dimensions				Enrichment		U^{235} Mass (kg)		% Burnup	
			Hgt (cm)	Width (cm)	Lgth (cm)	Mass (kg)	% BOL ^{235}U	% EOL ^{235}U	BOL	EOL	U^{235}	Heavy Metal
ASTRA (AUSTRIA)	5	MTR TYPE	8.02	7.61	87.30	6.00		8.00		0.07	60.0	12.0
ASTRA (AUSTRIA)	15	MTR TYPE	8.05	7.61	87.30	6.40		8.00		0.09	60.0	12.0
ASTRA (AUSTRIA)	71	MTR TYPE	8.05	7.61	87.30	6.40		8.00		0.12	60.0	12.0
DR-3 (DENMARK)	556	TUBES		10.30	62.50	3.30	20.00	9.71	0.18	0.08	57.0	11.4
DR-3 (DENMARK)	135	TUBES		10.30	62.50	4.00	20.00	11.11	0.18	0.09	50.0	10.0
FRG-1 (GERMANY)	96	MTR-S TYPE	7.62	7.62	88.00	6.70	20.00	7.83	0.32	0.11	66.0	13.2
FRG-1 (GERMANY)	18	MTR TYPE		7.62	95.00	3.50	19.83	9.54	0.28	0.12	56.9	10.4
FRJ-2 (GERMANY)	18	TUBES		10.30	62.50	4.00	20.00	11.11	0.20	0.10	50.0	10.0
FRJ-2 (GERMANY)	135	TUBES		10.30	62.50	4.00	20.00	11.11	0.22	0.11	50.0	10.0
GRR-1 (GREECE)	18	MTR-C TYPE	7.62	7.62	88.00	5.70	20.00	9.09	0.12	0.08	35.0	7.0
GRR-1 (GREECE)	62	MTR-S TYPE	7.62	7.62	88.00	5.70	20.00	9.09	0.22	0.14	35.0	7.0
HFR-PETTEN (NETHERLANDS)	72	MTR-C TYPE		7.62	88.00	4.50	20.00	9.09	0.31	0.12	60.0	12.0
HFR-PETTEN (NETHERLANDS)	363	MTR-S2 TYPE	7.62	7.62	88.00	4.60	20.00	9.09	0.45	0.22	51.0	10.2
HOR (NETHERLANDS)	7	MTR-C TYPE		7.62	88.00	5.10	20.00	9.09	0.16	0.06	60.0	12.0
HOR (NETHERLANDS)	43	MTR-S TYPE		7.62	88.00	5.50	20.00	9.09	0.30	0.12	60.0	12.0
IR-1 (ISRAEL)	8	MTR-C TYPE	7.62	7.62	88.00	4.80	20.00	9.09	0.31	0.11	65.0	13.0
ISU - ARGONAUT	13	17 FLAT PLATES	14.06	7.62	66.04	2.33		19.77		0.31	2.5	2.4
JMTR (JAPAN)	149	10 FLAT PLATES		7.62	88.00	5.40	20.00	14.89	0.28	0.19	30.0	6.0
JMTR (JAPAN)	574	ASSEMBLY		7.62	88.00	7.30	20.00	14.89	0.41	0.29	30.0	6.0
JRR-4 (JAPAN)	47	MTR TYPE		7.62	88.00	6.00	20.00	15.79	0.20	0.15	25.0	5.0
KUR (JAPAN)	17	MTR-C TYPE	7.62	7.62	88.00	4.60	20.00	16.83	0.10	0.09	19.0	3.8
KUR (JAPAN)	70	MTR-S TYPE		7.62	88.00	5.40	20.00	16.49	0.21	0.17	21.0	4.2
MNR (CANADA)	8	MTR-C TYPE		7.62	88.00	4.90	20.00	9.09	0.16	0.08	50.0	10.0
MNR (CANADA)	35	MTR-S TYPE		7.62	88.00	5.40	20.00	9.09	0.29	0.14	50.0	10.0
NEREIDE (FRANCE)	46	12 CURVED PLATES	7.98	7.57	87.30	62.50	19.85	19.80	0.15	0.15	0.3	0.1
NRU (CANADA)	1527	MULTI-PIN CLUSTER				6.60	20.00	7.83	0.49	0.12	76.0	15.0
OHIO STATE	414	18 FLAT PLATES		7.62	88.90	0.48	19.75	19.73	0.20	0.01	93.8	93.8
ORR	32	19 CURVED PLATES	8.03	7.60	65.09	5.00	19.85	19.82	0.32	0.32	0.0	0.0
ORR - MISC	10	SCRAP IN CANISTER				26.50		6.74		0.23		
OSIRIS (FRANCE)	177	MTR-C TYPE	7.62	7.62	88.00	7.00	20.00	9.09	0.39	0.17	55.0	11.0
OSIRIS (FRANCE)	724	MTR-S TYPE	7.62	7.62	88.00	7.50	20.00	9.09	0.51	0.23	55.0	11.0
PURDUE UNIVERSITY	22	10 FLAT PLATES	0.15	7.01	68.80	1.70	19.00	19.00	0.22	0.22	0.0	0.0
R-2 (SWEDEN)	580	MTR-C TYPE	7.62	7.62	88.00	6.20	20.00	9.09	0.40	0.16	60.0	12.0
R-2 (SWEDEN)	82	MTR-C TYPE	7.62	7.62	88.00	6.20	20.00	9.09	0.25	0.06	76.0	15.2
RINSC	122	18 FLAT PLATES		7.62	100.33	5.50	19.90	18.79	0.28	0.26	6.0	1.2
SAPHIR (SWITZERLAND)	39	MTR PLATE TYPE	8.05	7.62	87.50	4.00	19.84	11.58	0.41	0.21	48.3	11.3
SEOUL 1&2 (SO. KOREA)	48	MULTI-PIN CLUSTER				4.30	20.00	8.68	0.25	0.09	62.0	12.4
SEOUL 1&2 (SO. KOREA)	120	MULTI-PIN CLUSTER				6.60	20.00	7.83	0.44	0.15	66.0	13.2
TR-2 (TURKEY)	9	MTR-C2 TYPE	7.62	7.62	88.00	5.60	20.00	9.09	0.31	0.12	60.0	12.0
TR-2 (TURKEY)	32	MTR-S TYPE	7.62	7.62	88.00	6.60	20.00	9.09	0.42	0.17	60.0	12.0

Reactor/Assembly Description	Units	Configuration	Assembly Dimensions				Enrichment		U^{235} Mass (kg)		% Burnup	
			Hgt (cm)	Width (cm)	Lgth (cm)	Mass (kg)	% BOL ^{235}U	% EOL ^{235}U	BOL	EOL	U^{235}	Heavy Metal
UMRR	28	24 CURVED PLATES	7.57	8.74	87.00	6.20	19.75	19.83	0.22	0.19	16.7	17.0
UNIV OF FLORIDA	25	11 FLAT PLATES	5.44	7.23	65.09	5.50	19.72	19.72	0.22	0.22	0.0	0.0
UNIV OF MASS-LOWELL	41	18 FLAT PLATES	7.62	7.62	101.60	8.86		19.73		0.26	0.0	0.0
UNIV OF MICHIGAN	330	18 CURVED PLATES	7.47	8.26	87.38	5.49	19.81	19.81	0.21	0.21	0.0	0.0
UNIV OF VIRGINIA	33	22 FLAT PLATES	8.26	7.61	93.88	5.80	19.75	19.03	0.28	0.23	14.6	11.4
TOTALS	6976					42149.33				1098.40		

A.4 Description of Al-SNF Materials

There are three basic fuel types that have been fabricated for research and test reactors. Originally fuel was made from cast aluminum-uranium alloys; later it was made using powder metallurgy techniques. These fuels include UAl_x, U_3O_8 and U_3Si_2 powders that are mixed with aluminum powder and hot/cold rolled to produce flat plates. Fuel elements are irradiated from 30 to 60% burnup.

A.4.1 U Oxide/Al

A photomicrograph of the U_3O_8 fuel at high burnup is shown in Figure A.7. During irradiation, centerline temperatures up to about 200 °C can occur which enhances diffusion of uranium and aluminum in the fuel meat. These effects produce chemical reactions between various fuel particles and matrix materials. For example, in U_3O_8 fuels a UAl_x type phase is formed. This phase can be seen in Figure A.7.

The kinetics of oxide dissolution in molten aluminum are slow because of the stability of the oxide phase, but the diffusion reactions in oxide fuels during irradiation will enhance the solubility of the fuel phase. During the MD treatment, the U_3O_8 fuel is expected to dissolve adequately when melted. For irradiated oxide fuels, the melting behavior is expected to be governed by the uranium-aluminum phase diagram shown in Figure A.8 of this report.

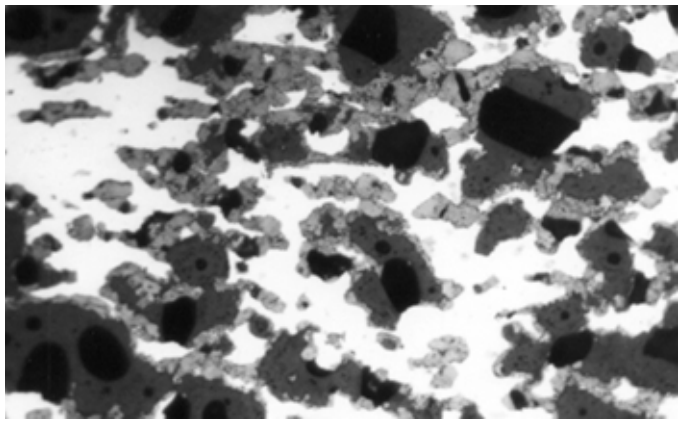

Figure A.7 High Burnup U_3O_8-Al Fuel Irradiated in Research and Test Reactors

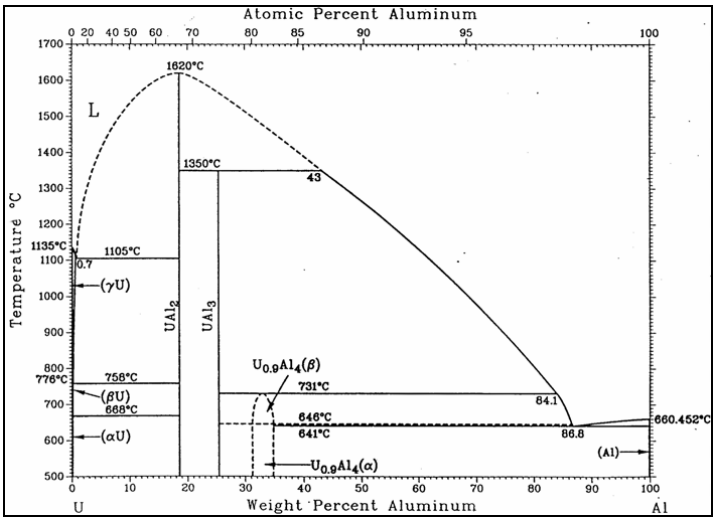

Figure A.8 Binary Phase Diagram of the Uranium-Aluminum System

A.4.2 UAl_x/Al

A photomicrograph of the UAl_x fuel at high burnup is shown in Figure A.9. During irradiation, centerline temperatures up to about 200 °C can occur which enhances diffusion of uranium and aluminum in the fuel meat. For aluminide fuels, no reaction occurs at the particle-matrix boundary because of the thermodynamic stability of the aluminide phase present in the fuel as shown in Figure A.9.

During the MD treatment, the UAl_x fuel is expected to dissolve adequately when melted. For aluminide fuels, the melting behavior is expected to be governed by the uranium-aluminum phase diagram shown in Figure A.8 of this report.

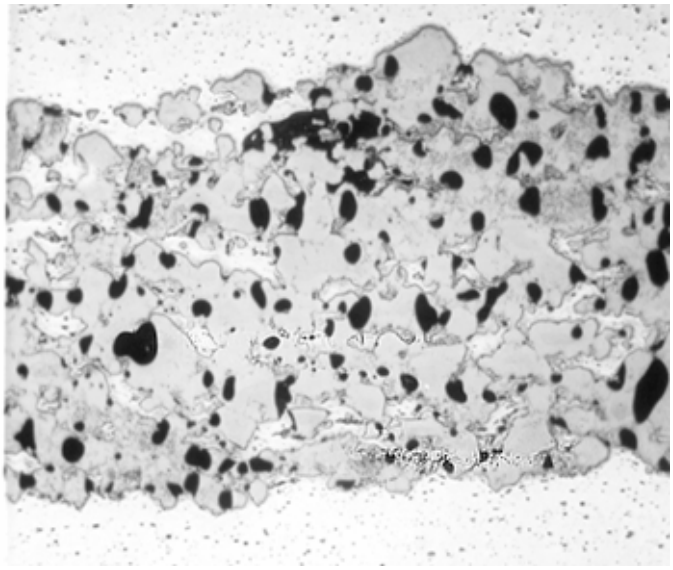

Figure A.9 High Burnup UAl_x-Al Fuel Irradiated in Research and Test Reactors

A.4.3 U-Si

A photomicrograph of the U_3Si_2 fuel at high burnup is shown in Figure A.10. During irradiation, centerline temperatures up to about 200 °C can occur which enhances diffusion of uranium and aluminum in the fuel meat. These effects produce chemical reactions between various fuel particles and matrix materials. In silicide fuels, aluminum-silicon phases form at the aluminum - U_3Si_2 particle interface. These phases can be seen in Figure A.10.

During the MD treatment, the U_3Si_2 fuel is expected to dissolve adequately when melted. For silicide fuels, the uranium-aluminum-silicon ternary phase diagram is necessary to predict process conditions. The ternary diagram at 950 °C was constructed from binary phase diagrams and is shown in Figure A.11.

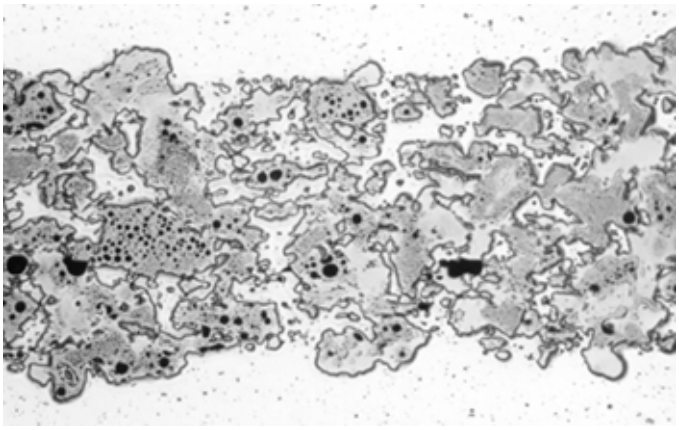

Figure A.10 High Burnup U_3Si_2-Al Fuel Irradiated in Research and Test Reactors

At 950 °C the aluminum-uranium-silicon system has a relatively large liquidus region near the aluminum-rich end of the phase diagram. Calculations, based on aluminide fuels, for the silicide loading indicate that the melt composition will be in the range of about 1 to10 wt% uranium, 0.1-0.8 wt% silicon, and 98.9-89.2 wt% aluminum for various MTR assemblies. According to these calculations, the alloy is expected to melt between 660 and 960 °C. Melting of silicide fuels can be accomplished using the same melt-dilute process; however, dilution may not be a concern for these low enriched elements. Melting and casting would, however, consolidate the fuel and produce a waste form consistent with other fuel types.

A.4.4 Sterling Forest Oxide-Type Material

This material consists of small particles of uranium-oxide fuel meat that has characteristics similar to that of Sterling Forest spent nuclear fuel.

A.4.5 Physical Condition of Fuel Assemblies

The SNF is typically stored under water where corrosion may be severe unless strict control of the water purity is maintained.[2] Several dry storage facilities are in use at foreign reactor sites. Prolonged underwater storage is not desirable because of the cost of operating and maintaining a properly controlled water system and the limited space and handling capabilities available at most reactor facilities.

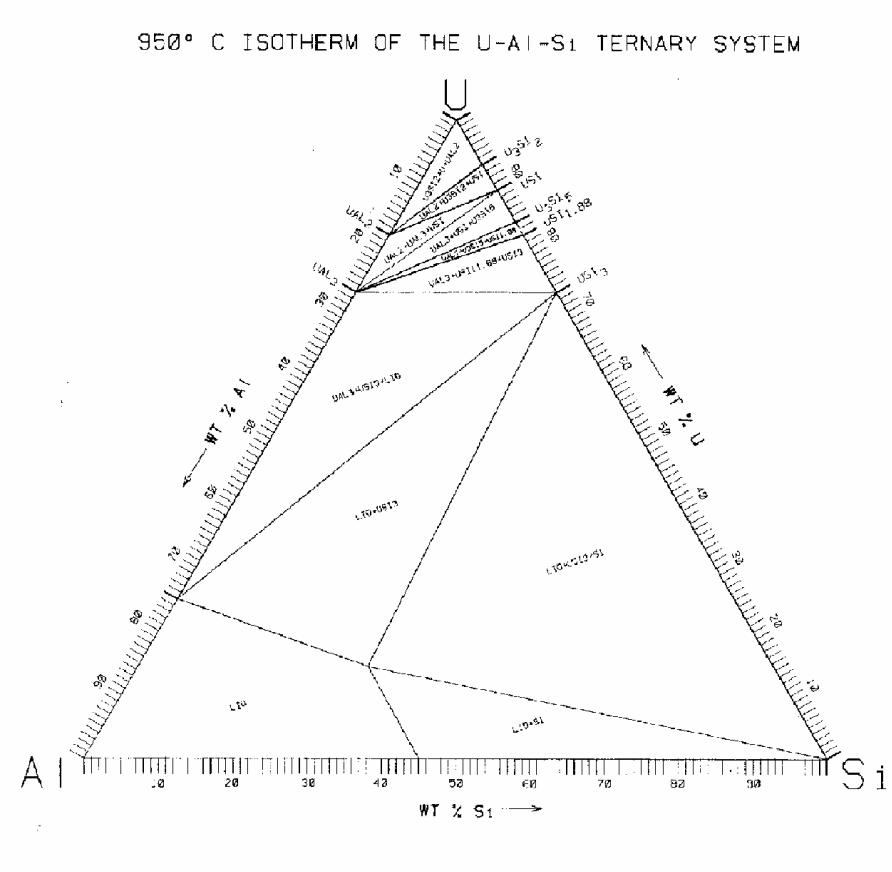

Figure A.11 Ternary Isothermal Section from the U-Al-Si System at 950°C

An evaluation of the physical condition of a large portion of the fuel assemblies in wet and dry storage at foreign and domestic research reactor sites was recently performed.[3] Only minor corrosion and mechanical damage indicating cladding penetration was observed in approximately 7% of the 1700 fuel assemblies examined.

New criteria for acceptance of Al-SNF for SRS basin storage without special canning are provided in Reference 4. These criteria should be used for pre-treatment or pre-drying basin storage for the TSF if using the melt-dilute or direct disposal technologies, respectively.

A.4.6 Constituents of DOE SNF

In order to ensure the proper operation of the melt-dilute process and offgas system it is fundamentally necessary to compile a complete list of all the possible chemical species available for reaction. These various chemical species are present as radionuclides from the fission process, cladding alloy additions, fuel meat alloy additions/impurities, and also from any melt-dilute process additions such as the depleted uranium used for dilution of the ^{235}U content. Table A.5 contains a listing of the chemical species expected for the various cladding materials that will be processed in the melt-dilute process. Table A.6 lists the composition of aluminum powder

used in UAl_x-fuel manufacturing. A chemical analysis of the depleted uranium used for dilution is provided in Table A.7.

Table A.5 Compositions of Typical MTR Cladding Alloys Manufactured by CERCA, NUKEM, and B&W

Elements	AG1	AG2	AG3	AlFeNi	AlMg1	AlMg2	6061
Mg	1.1-1.4	1.8-2.3	2.5-3.0	0.8-1.2	0.7-1.1	1.7-2.4	0.8-1.2
B	-	0.001	-	0.001	0.001	0.001	0.001
Cd	-	0.001	-	0.001	0.001	0.001	0.001
Cu	-	0.008	-	0.008	0.008	0.008	0.2-0.40
Fe	-	0.2-0.4	-	0.8-1.2	0.45	0.40	0.70
Si	-	0.3	-	0.30	0.30	0.30	0.40-0.80
Cr	-	0.3	-	0.2-0.5	0.10	0.30	0.04-0.35
Mn	-	0.7	-	0.2-0.6	0.15	0.30	0.15
Li	-	0.001	-	0.001	0.001	0.001	0.008
Zn	-	-	-	0.06-0.14	0.05	0.03	0.25
Ti	-	-	-	0.02-0.08	-	0.10	0.25
Al	-	Bal.	-	Bal.	Bal.	Bal.	Bal.
Others	-	0.03	-	0.03.	0.15	0.15	0.15

Table A.6 Composition of Al Powder Used for UAl_x Fuel Manufacturing

Element	Wt%
Al	99.00 min
Si+Fe	1.0 max
Cu	0.05-0.20
Mn	0.05 max
Zn	0.05 max
Other (each)	0.05 max
Others (total)	0.15 max

Table A.8 provides an assessment of the fission product, actinide, and light element inventories expected in the melt-dilute SNF form. The table contains results from ten cases that were developed to provide information on the bounding values for radioactive species that may be present in the melt-dilute SNF form. The values provided have units of grams of the given isotope/element per kilogram of melt-dilute product, and the ten cases were developed as follows. Each of the first four cases involved the modeling of a single uranium-aluminum alloy, aluminum clad, fuel assembly. For each of these cases, the ^{235}U content is maintained at a constant of 600 grams per assembly, while the enrichment is varied from 93.5 wt% (Case 1) to 5 wt% (Case 4). Cases 2 and 3 have enrichments of 40 and 20 wt%, respectively. Cases 5 through 7 involved the modeling of a single uranium-aluminum alloy, aluminum clad, fuel assembly with constant total uranium content fixed at 642 grams per assembly. The values of enrichment considered include 40 wt% (Case 5), 20 wt% (Case 6), and 5 wt% (Case 7). The final three cases involved the modeling of a single uranium-aluminum alloy, aluminum clad, fuel assembly with constant ^{238}U content fixed at 900 grams per assembly. The values of enrichment considered include 93.5 wt%

(Case 8), 20 wt% (Case 9), and 5 wt% (Case 10). In each of the cases, the burnup is chosen as 550 GWd/MTIHM. This burnup is expected to exceed all actual spent fuel burnups for aluminum based spent nuclear fuel. The final column in Table A.8 (Max) provides the maximum value of the other ten columns. These results from computer simulations are provided as bounding estimates of radionuclide content. It is therefore expected that the actual radionuclide content of any given melt-dilute SNF ingot may be significantly lower than the values shown in the table.

Table A.7 Chemical Analysis of the Depleted Uranium for Dilution

Element	Concentration, ppm
C	400
N_2	50
H_2	1
O_2	10
Al	< 6
B	< 0.15
Cd	< 20
Cr	10
Cu	3
Fe	125-225
Mg	< 4
Mn	5
Mo	< 6
Si	125-225
Sn	5
Zr	< 5

Table A.8 Bounding Estimates of Fission Product, Actinide, and Light Element Masses per Kilogram Melt-Dilute SNF Form (grams)

Radionuclide/ **Element**	**Case 1**	**Case 2**	**Case 3**	**Case 4**	**Case 5**	**Case 6**	**Case 7**	**Case 8**	**Case 9**	**Case 10**	**Max**
Am241	2.97E-02	2.32E-01	2.60E+00	2.88E-04	1.45E-01	1.41E-01	8.52E-02	5.75E-03	2.07E-01	8.43E-02	2.60E+00
Am242	0.00E+00	0.00E+00	4.53E-08	0.00E+00	0.00E+00	1.40E-06	0.00E+00	0.00E+00	0.00E+00	0.00E+00	1.40E-06
Am242m	4.49E-06	2.97E-05	3.53E-03	2.37E-08	3.09E-06	0.00E+00	4.65E-07	1.51E-05	6.50E-06	7.43E-07	3.53E-03
Am243	1.29E-02	2.13E-01	7.22E-01	2.11E-04	2.57E-01	5.12E-01	4.05E-01	1.66E-04	3.59E-01	2.94E-01	7.22E-01
Americium	**4.27E-02**	**4.45E-01**	**3.33E+00**	**4.99E-04**	**4.02E-01**	**6.53E-01**	**4.90E-01**	**5.93E-03**	**5.66E-01**	**3.78E-01**	**3.33E+00**
Sb121	8.80E-04	1.96E-03	5.72E-03	1.09E-03	2.48E-03	5.33E-03	5.08E-03	2.96E-04	4.24E-03	4.29E-03	5.72E-03
Sb123	1.17E-03	2.77E-03	7.70E-03	1.50E-04	3.20E-03	6.77E-03	6.83E-03	4.96E-04	5.95E-03	6.26E-03	7.70E-03
Sb125	2.00E-04	7.39E-04	1.90E-03	2.41E-04	7.17E-04	1.64E-03	1.89E-03	1.11E-04	1.65E-03	2.02E-03	2.02E-03
Antimony	**2.25E-03**	**5.47E-03**	**1.53E-02**	**1.48E-03**	**6.39E-03**	**1.37E-02**	**1.38E-02**	**9.02E-04**	**1.18E-02**	**1.26E-02**	**1.53E-02**
As 75	5.37E-05	7.88E-05	1.61E-04	2.79E-08	8.70E-05	1.26E-04	9.13E-05	3.22E-05	1.17E-04	8.85E-05	1.61E-04
Arsenic	**5.37E-05**	**7.88E-05**	**1.61E-04**	**2.79E-08**	**8.70E-05**	**1.26E-04**	**9.13E-05**	**3.22E-05**	**1.17E-04**	**8.85E-05**	**1.61E-04**

Radionuclide/ **Element**	**Case 1**	**Case 2**	**Case 3**	**Case 4**	**Case 5**	**Case 6**	**Case 7**	**Case 8**	**Case 9**	**Case 10**	**Max**
Ba132	6.64E-08	3.51E-07	1.15E-06	2.52E-07	1.96E-07	2.80E-07	2.57E-07	5.44E-07	7.23E-07	3.58E-07	1.15E-06
Ba134	1.49E-01	3.84E-01	6.20E-01	2.10E-02	3.37E-01	2.65E-01	1.76E-01	6.22E-02	7.57E-01	1.55E-01	7.57E-01
Ba135	5.98E-05	2.07E-03	4.66E-03	5.71E-04	4.54E-04	8.00E-04	8.60E-04	2.35E-03	3.71E-03	1.88E-03	4.66E-03
Ba136	7.22E-03	1.27E-01	6.42E-01	4.15E+00	5.47E-02	2.12E-01	4.13E-01	2.77E-01	3.70E-01	5.74E-01	4.15E+00
Ba137	1.21E-01	2.86E-01	5.90E-01	2.62E+00	2.79E-01	5.25E-01	5.31E-01	1.44E-01	5.21E-01	5.74E-01	2.62E+00
Ba137m	7.04E-08	1.63E-07	3.26E-07	5.54E-07	1.61E-07	3.04E-07	3.06E-07	6.61E-08	2.98E-07	3.29E-07	5.54E-07
Ba138	6.25E-01	1.36E+00	2.60E+00	5.78E+00	1.35E+00	2.43E+00	2.34E+00	6.16E-01	2.39E+00	2.51E+00	5.78E+00
Barium	**9.02E-01**	**2.15E+00**	**4.45E+00**	**1.26E+01**	**2.02E+00**	**3.43E+00**	**3.47E+00**	**1.10E+00**	**4.04E+00**	**3.81E+00**	**1.26E+01**
Be 9	0.00E+00	0.00E+00	4.03E-08	0.00E+00	0.00E+00	0.00E+00	0.00E+00	8.93E-09	0.00E+00	0.00E+00	4.03E-08
Be 10	6.07E-08	1.36E-07	2.69E-07	3.32E-08	1.22E-07	1.83E-07	0.00E+00	5.97E-08	0.00E+00	0.00E+00	2.69E-07
Beryllium	**6.07E-08**	**1.36E-07**	**3.10E-07**	**3.32E-08**	**1.22E-07**	**1.83E-07**	**0.00E+00**	**6.87E-08**	**0.00E+00**	**0.00E+00**	**3.10E-07**
Bk249	0.00E+00	4.71E-07	5.19E-08	5.70E-09	1.36E-07	2.30E-07	2.49E-07	0.00E+00	1.07E-06	6.35E-07	1.07E-06
Berkelium	**0.00E+00**	**4.71E-07**	**5.19E-08**	**5.70E-09**	**1.36E-07**	**2.30E-07**	**2.49E-07**	**0.00E+00**	**1.07E-06**	**6.35E-07**	**1.07E-06**
Br 79	5.02E-08	1.02E-07	2.07E-07	2.28E-07	9.86E-08	0.00E+00	0.00E+00	5.38E-08	1.67E-07	1.48E-07	2.28E-07
Br 81	9.55E-03	1.42E-02	2.83E-02	6.96E-04	1.63E-02	2.59E-02	2.12E-02	6.22E-03	2.42E-02	2.10E-02	2.83E-02
Bromine	**9.55E-03**	**1.42E-02**	**2.83E-02**	**6.97E-04**	**1.63E-02**	**2.59E-02**	**2.12E-02**	**6.22E-03**	**2.42E-02**	**2.10E-02**	**2.83E-02**
Cd108	0.00E+00	4.40E-07	1.33E-06	9.67E-06	2.61E-07	6.79E-07	9.19E-07	3.28E-08	1.06E-06	1.35E-06	9.67E-06
Cd109	0.00E+00	0.00E+00	0.00E+00	5.26E-09	0.00E+00	0.00E+00	0.00E+00	0.00E+00	0.00E+00	0.00E+00	5.26E-09
Cd110	5.90E-03	2.43E-01	6.42E-01	9.60E-01	1.81E-01	5.68E-01	8.66E-01	9.97E-03	6.93E-01	9.98E-01	9.98E-01
Cd111	2.43E-03	6.38E-02	1.70E-01	8.33E-01	4.56E-02	1.69E-01	3.21E-01	3.69E-03	2.05E-01	3.89E-01	8.33E-01
Cd112	1.78E-03	2.85E-02	7.13E-02	3.92E+00	2.27E-02	9.48E-02	2.53E-01	2.47E-03	9.86E-02	3.19E-01	3.92E+00
Cd113	2.64E-05	1.03E-04	3.15E-03	2.15E-02	7.22E-05	1.12E-04	1.16E-04	9.05E-05	9.03E-05	9.34E-05	2.15E-02
Cd113m	2.21E-05	4.19E-04	1.04E-03	3.17E+00	2.55E-04	1.17E-03	4.03E-03	7.12E-05	1.31E-03	5.80E-03	3.17E+00
Cd114	2.53E-03	1.52E-02	3.54E-02	2.23E+00	1.42E-02	3.78E-02	5.53E-02	2.03E-03	3.59E-02	6.17E-02	2.23E+00
Cd116	1.39E-03	5.02E-03	1.30E-02	6.63E-01	4.69E-03	1.06E-02	1.22E-02	1.30E-03	1.06E-02	1.34E-02	6.63E-01
Cadmium	**1.41E-02**	**3.56E-01**	**9.37E-01**	**1.18E+01**	**2.69E-01**	**8.81E-01**	**1.51E+00**	**1.96E-02**	**1.05E+00**	**1.79E+00**	**1.18E+01**
Cf249	1.46E-07	1.27E-03	1.41E-04	1.53E-05	3.64E-04	6.19E-04	6.71E-04	4.18E-09	2.89E-03	1.70E-03	2.89E-03
Cf250	0.00E+00	1.14E-04	9.50E-06	6.66E-04	5.49E-05	1.32E-04	1.67E-04	0.00E+00	4.15E-04	4.18E-04	6.66E-04
Cf251	0.00E+00	2.15E-04	2.42E-05	1.11E-06	6.18E-05	9.28E-05	8.62E-05	0.00E+00	4.88E-04	2.51E-04	4.88E-04
Cf252	0.00E+00	6.38E-05	4.84E-06	8.35E-07	1.89E-05	8.47E-05	1.47E-04	0.00E+00	3.38E-04	4.36E-04	4.36E-04
Californium	**1.46E-07**	**1.66E-03**	**1.79E-04**	**6.83E-04**	**5.00E-04**	**9.29E-04**	**1.07E-03**	**4.18E-09**	**4.13E-03**	**2.80E-03**	**4.13E-03**
C 14	0.00E+00	0.00E+00	5.46E-08	0.00E+00	0.00E+00	0.00E+00	0.00E+00	1.21E-08	0.00E+00	0.00E+00	5.46E-08
Carbon	**0.00E+00**	**0.00E+00**	**5.46E-08**	**0.00E+00**	**0.00E+00**	**0.00E+00**	**0.00E+00**	**1.21E-08**	**0.00E+00**	**0.00E+00**	**5.46E-08**
Ce140	6.25E-01	1.40E+00	2.64E+00	6.59E+00	1.41E+00	2.72E+00	2.86E+00	6.44E-01	2.66E+00	3.08E+00	6.59E+00
Ce142	5.76E-01	1.24E+00	2.27E+00	3.33E+00	1.32E+00	2.61E+00	2.80E+00	5.55E-01	2.31E+00	2.84E+00	3.33E+00
Ce144	6.69E-05	1.14E-04	1.72E-04	1.93E-05	1.32E-04	2.20E-04	1.95E-04	1.73E-05	1.99E-04	1.96E-04	2.20E-04
Cerium	**1.20E+00**	**2.64E+00**	**4.91E+00**	**9.92E+00**	**2.73E+00**	**5.33E+00**	**5.66E+00**	**1.20E+00**	**4.98E+00**	**5.92E+00**	**9.92E+00**
Cs133	3.67E-01	3.13E-01	1.50E+00	3.45E-02	3.78E-01	4.69E-01	3.68E-01	4.55E-01	6.27E-01	2.61E-01	1.50E+00
Cs134	5.24E-03	1.29E-02	1.97E-02	6.83E-04	1.18E-02	9.13E-03	6.01E-03	1.50E-03	2.56E-02	4.99E-03	2.56E-02
Cs135	8.36E-02	5.15E-01	2.19E+00	8.14E-02	3.99E-01	8.99E-01	1.08E+00	4.06E-01	1.58E+00	1.20E+00	2.19E+00
Cs137	4.62E-01	1.07E+00	2.14E+00	3.63E+00	1.06E+00	1.99E+00	2.00E+00	4.32E-01	1.96E+00	2.16E+00	3.63E+00
Cesium	**9.17E-01**	**1.91E+00**	**5.84E+00**	**3.75E+00**	**1.85E+00**	**3.36E+00**	**3.46E+00**	**1.29E+00**	**4.20E+00**	**3.63E+00**	**5.84E+00**

Radionuclide/ **Element**	**Case 1**	**Case 2**	**Case 3**	**Case 4**	**Case 5**	**Case 6**	**Case 7**	**Case 8**	**Case 9**	**Case 10**	**Max**
Cm242	0.00E+00	7.79E-08	9.24E-06	0.00E+00	0.00E+00	0.00E+00	0.00E+00	3.96E-08	0.00E+00	0.00E+00	9.24E-06
Cm243	6.64E-06	2.19E-04	3.56E-03	7.56E-08	4.04E-05	2.14E-05	6.03E-06	3.39E-06	1.34E-04	1.09E-05	3.56E-03
Cm244	8.54E-03	3.90E-01	4.58E-01	4.51E-04	4.30E-01	7.84E-01	6.40E-01	2.47E-05	9.73E-01	6.13E-01	9.73E-01
Cm245	2.02E-03	1.41E-01	6.78E-02	7.61E-05	8.09E-02	5.43E-02	2.41E-02	1.13E-06	1.40E-01	3.11E-02	1.41E-01
Cm246	2.81E-04	1.03E-01	2.07E-02	4.71E-04	1.04E-01	2.55E-01	3.17E-01	3.43E-07	3.81E-01	3.72E-01	3.81E-01
Cm247	1.13E-05	7.96E-03	1.36E-03	6.08E-06	6.34E-03	1.38E-02	1.54E-02	2.67E-08	2.76E-02	2.13E-02	2.76E-02
Cm248	3.00E-06	1.10E-02	1.39E-03	2.82E-05	5.46E-03	1.93E-02	3.33E-02	3.22E-08	4.61E-02	6.01E-02	6.01E-02
Cm250	0.00E+00	0.00E+00	0.00E+00	0.00E+00	0.00E+00	5.66E-07	2.74E-06	0.00E+00	6.27E-07	4.90E-06	4.90E-06
Curium	**1.09E-02**	**6.52E-01**	**5.52E-01**	**1.03E-03**	**6.27E-01**	**1.13E+00**	**1.03E+00**	**2.96E-05**	**1.57E+00**	**1.10E+00**	**1.57E+00**
Dy160	1.98E-04	1.88E-02	2.41E-02	2.49E-02	6.63E-03	1.30E-02	1.83E-02	1.74E-02	3.16E-02	2.65E-02	3.16E-02
Dy161	1.27E-04	2.54E-02	2.44E-02	1.21E-01	1.11E-02	4.30E-02	9.15E-02	1.93E-02	6.08E-02	1.11E-01	1.21E-01
Dy162	2.24E-05	6.60E-03	9.42E-03	1.21E-02	1.60E-03	9.17E-03	2.00E-02	9.65E-03	1.61E-02	2.90E-02	2.90E-02
Dy163	2.14E-05	8.67E-03	1.42E-02	2.18E-02	1.74E-03	1.28E-02	2.57E-02	1.74E-02	2.24E-02	4.31E-02	4.31E-02
Dy164	1.20E-05	7.35E-03	2.25E-02	5.62E-02	6.34E-04	1.98E-03	2.76E-03	3.02E-02	7.51E-03	5.95E-03	5.62E-02
Dysprosium	**3.81E-04**	**6.69E-02**	**9.46E-02**	**2.36E-01**	**2.17E-02**	**8.00E-02**	**1.58E-01**	**9.40E-02**	**1.38E-01**	**2.16E-01**	**2.36E-01**
Es254	0.00E+00	0.00E+00	0.00E+00	1.11E-07	0.00E+00	0.00E+00	0.00E+00	0.00E+00	0.00E+00	0.00E+00	1.11E-07
Einsteinium	**0.00E+00**	**0.00E+00**	**0.00E+00**	**1.11E-07**	**0.00E+00**	**0.00E+00**	**0.00E+00**	**0.00E+00**	**0.00E+00**	**0.00E+00**	**1.11E-07**
Er166	3.27E-06	5.94E-03	8.76E-03	2.01E-01	1.34E-03	2.26E-02	9.71E-02	2.65E-02	3.25E-02	2.15E-01	2.15E-01
Er167	6.64E-08	1.68E-04	2.72E-04	5.82E-03	3.02E-05	5.14E-04	2.24E-03	8.38E-04	8.86E-04	5.68E-03	5.82E-03
Er168	1.69E-07	1.03E-03	1.81E-03	1.50E+01	1.68E-04	4.88E-03	5.33E-02	9.73E-03	8.13E-03	1.60E-01	1.50E+01
Erbium	**3.51E-06**	**7.14E-03**	**1.08E-02**	**1.52E+01**	**1.53E-03**	**2.80E-02**	**1.53E-01**	**3.71E-02**	**4.15E-02**	**3.80E-01**	**1.52E+01**
Eu151	8.62E-04	1.11E-03	4.93E-03	5.48E-04	6.80E-04	6.11E-04	3.97E-04	4.61E-04	8.92E-04	4.08E-04	4.93E-03
Eu152	4.75E-07	3.85E-07	6.03E-06	5.09E-08	1.10E-07	0.00E+00	0.00E+00	9.77E-07	2.09E-07	0.00E+00	6.03E-06
Eu153	3.98E-02	4.75E-02	1.69E-01	1.29E-02	6.56E-02	8.62E-02	5.12E-02	1.45E-02	9.42E-02	5.49E-02	1.69E-01
Eu154	8.80E-03	1.21E-02	7.83E-02	2.32E-03	5.81E-03	3.70E-03	1.30E-03	6.57E-03	8.92E-03	2.08E-03	7.83E-02
Eu155	3.82E-04	5.72E-04	2.26E-03	2.56E-04	6.31E-04	8.47E-04	5.90E-04	1.80E-04	1.09E-03	6.56E-04	2.26E-03
Europium	**4.98E-02**	**6.13E-02**	**2.54E-01**	**1.60E-02**	**7.27E-02**	**9.13E-02**	**5.35E-02**	**2.17E-02**	**1.05E-01**	**5.80E-02**	**2.54E-01**
Gd152	2.09E-06	3.37E-06	2.86E-05	3.44E-07	1.40E-06	1.15E-06	6.64E-07	6.81E-06	2.62E-06	6.03E-07	2.86E-05
Gd153	0.00E+00	0.00E+00	0.00E+00	0.00E+00	0.00E+00	0.00E+00	0.00E+00	5.04E-10	0.00E+00	0.00E+00	5.04E-10
Gd154	1.10E-02	1.55E-02	1.01E-01	2.89E-03	7.29E-03	4.63E-03	1.63E-03	9.40E-03	1.13E-02	2.61E-03	1.01E-01
Gd155	1.30E-03	1.95E-03	8.27E-03	8.71E-04	2.15E-03	2.88E-03	2.01E-03	8.54E-04	3.68E-03	2.23E-03	8.27E-03
Gd156	3.27E-02	1.90E-01	6.51E-01	3.49E-02	1.10E-01	1.54E-01	1.52E-01	1.56E-01	3.37E-01	1.85E-01	6.51E-01
Gd157	1.80E-03	5.72E-03	8.62E-02	9.33E-03	9.61E-03	1.47E-02	1.40E-02	2.45E-02	1.09E-02	1.19E-02	8.62E-02
Gd158	2.71E-02	5.28E-01	7.39E-01	4.00E-01	3.90E-01	9.69E-01	1.75E+00	3.51E-01	1.29E+00	1.56E+00	1.75E+00
Gd160	7.44E-05	1.47E-03	3.95E-03	1.03E-03	1.35E-03	3.83E-03	5.02E-03	4.16E-05	3.63E-03	5.23E-03	5.23E-03
Gadolinium	**7.41E-02**	**7.42E-01**	**1.59E+00**	**4.49E-01**	**5.20E-01**	**1.15E+00**	**1.92E+00**	**5.42E-01**	**1.66E+00**	**1.77E+00**	**1.92E+00**
Ga 71	0.00E+00	7.83E-08	2.40E-07	0.00E+00	0.00E+00	0.00E+00	0.00E+00	1.22E-08	0.00E+00	0.00E+00	2.40E-07
Gallium	**0.00E+00**	**7.83E-08**	**2.40E-07**	**0.00E+00**	**0.00E+00**	**0.00E+00**	**0.00E+00**	**1.22E-08**	**0.00E+00**	**0.00E+00**	**2.40E-07**
Ge 72	1.45E-06	5.28E-06	1.34E-05	1.16E-07	3.64E-06	4.11E-06	1.56E-06	1.32E-06	3.46E-06	1.60E-06	1.34E-05
Ge 73	5.24E-06	9.99E-06	2.48E-05	0.00E+00	7.69E-06	4.65E-06	3.37E-07	2.90E-06	4.87E-06	2.55E-07	2.48E-05
Ge 74	5.81E-06	1.74E-05	3.64E-05	6.31E-07	1.27E-05	1.24E-05	3.37E-07	7.95E-06	1.30E-05	2.80E-07	3.64E-05
Ge 76	1.95E-04	3.42E-04	5.81E-04	4.05E-04	3.48E-04	5.29E-04	3.99E-04	1.91E-04	5.06E-04	4.14E-04	5.81E-04
Germanium	**2.07E-04**	**3.75E-04**	**6.55E-04**	**4.06E-04**	**3.72E-04**	**5.50E-04**	**4.01E-04**	**2.03E-04**	**5.27E-04**	**4.16E-04**	**6.55E-04**

Radionuclide/ **Element**	**Case 1**	**Case 2**	**Case 3**	**Case 4**	**Case 5**	**Case 6**	**Case 7**	**Case 8**	**Case 9**	**Case 10**	**Max**
He 3	0.00E+00	0.00E+00	4.84E-08	5.72E-07	0.00E+00	0.00E+00	0.00E+00	1.07E-08	0.00E+00	0.00E+00	5.72E-07
He 4	8.58E-05	4.58E-04	9.15E-04	1.10E-02	3.64E-04	8.21E-04	9.44E-04	2.10E-04	9.07E-04	1.13E-03	1.10E-02
He 4	5.76E-04	5.32E-03	7.66E-03	1.32E-02	4.02E-03	6.27E-03	5.06E-03	3.83E-04	8.24E-03	5.00E-03	1.32E-02
Helium	**6.62E-04**	**5.78E-03**	**8.57E-03**	**2.42E-02**	**4.39E-03**	**7.09E-03**	**6.00E-03**	**5.93E-04**	**9.14E-03**	**6.14E-03**	**2.42E-02**
Ho165	6.64E-06	5.54E-03	8.10E-03	3.73E-02	1.25E-03	1.25E-02	2.67E-02	1.38E-02	2.33E-02	5.87E-02	5.87E-02
Ho166m	4.66E-08	9.46E-05	1.57E-04	1.98E-01	1.52E-05	2.34E-04	1.15E-03	5.47E-04	4.93E-04	3.72E-03	1.98E-01
Holmium	**6.69E-06**	**5.64E-03**	**8.25E-03**	**2.35E-01**	**1.27E-03**	**1.28E-02**	**2.79E-02**	**1.43E-02**	**2.38E-02**	**6.24E-02**	**2.35E-01**
H 1	1.28E-04	6.64E-04	1.32E-03	1.61E-02	5.26E-04	1.12E-03	1.30E-03	3.45E-04	1.26E-03	1.57E-03	1.61E-02
H 2	1.02E-06	6.56E-06	1.24E-05	9.02E-04	5.96E-06	2.24E-05	4.57E-05	3.10E-06	1.85E-05	5.27E-05	9.02E-04
H 3	0.00E+00	3.15E-08	6.38E-08	7.59E-07	0.00E+00	0.00E+00	0.00E+00	1.41E-08	0.00E+00	0.00E+00	7.59E-07
H 3	1.25E-05	3.16E-05	6.73E-05	9.60E-05	3.11E-05	6.07E-05	6.31E-05	1.10E-05	5.98E-05	6.79E-05	9.60E-05
Hydrogen	**1.42E-04**	**7.03E-04**	**1.40E-03**	**1.71E-02**	**5.63E-04**	**1.21E-03**	**1.41E-03**	**3.59E-04**	**1.33E-03**	**1.69E-03**	**1.71E-02**
In113	1.41E-05	2.68E-04	6.78E-04	2.01E+00	1.63E-04	7.47E-04	2.55E-03	4.79E-05	8.41E-04	3.69E-03	2.01E+00
In115	1.70E-04	5.28E-04	1.09E-03	1.02E-01	7.31E-04	1.45E-03	1.46E-03	3.51E-05	1.19E-03	1.56E-03	1.02E-01
Indium	**1.84E-04**	**7.96E-04**	**1.76E-03**	**2.12E+00**	**8.94E-04**	**2.20E-03**	**4.01E-03**	**8.30E-05**	**2.03E-03**	**5.25E-03**	**2.12E+00**
I127	9.72E-03	2.75E-02	7.35E-02	2.93E-03	3.25E-02	7.18E-02	7.71E-02	3.12E-03	8.60E-02	7.13E-02	8.60E-02
I129	6.29E-02	1.52E-01	3.78E-01	1.66E-02	1.47E-01	2.41E-01	1.81E-01	4.57E-02	2.66E-01	1.91E-01	3.78E-01
Iodine	**7.26E-02**	**1.79E-01**	**4.51E-01**	**1.95E-02**	**1.80E-01**	**3.12E-01**	**2.58E-01**	**4.88E-02**	**3.52E-01**	**2.62E-01**	**4.51E-01**
Kr 80	0.00E+00	4.07E-08	1.39E-07	0.00E+00	0.00E+00	0.00E+00	0.00E+00	6.34E-09	0.00E+00	0.00E+00	1.39E-07
Kr 81	0.00E+00	3.63E-08	8.89E-08	3.99E-07	0.00E+00	0.00E+00	0.00E+00	3.22E-08	0.00E+00	0.00E+00	3.99E-07
Kr 82	7.70E-04	3.28E-03	5.54E-03	2.48E-04	2.69E-03	4.22E-03	3.35E-03	1.70E-03	5.00E-03	3.96E-03	5.54E-03
Kr 83	2.12E-02	1.63E-02	4.08E-02	2.90E-04	1.25E-02	6.87E-03	3.21E-03	8.61E-03	1.17E-02	3.78E-03	4.08E-02
Kr 84	6.82E-02	1.36E-01	2.12E-01	1.40E-01	1.44E-01	2.30E-01	1.90E-01	8.14E-02	2.22E-01	2.01E-01	2.30E-01
Kr 85	7.88E-03	1.32E-02	2.03E-02	4.88E-02	1.35E-02	1.95E-02	1.39E-02	7.34E-03	1.95E-02	1.50E-02	4.88E-02
Kr 86	1.12E-01	1.80E-01	2.76E-01	3.38E-01	1.87E-01	2.69E-01	1.91E-01	1.12E-01	2.64E-01	2.05E-01	3.38E-01
Krypton	**2.10E-01**	**3.49E-01**	**5.55E-01**	**5.27E-01**	**3.60E-01**	**5.30E-01**	**4.02E-01**	**2.11E-01**	**5.22E-01**	**4.28E-01**	**5.55E-01**
La138	3.63E-06	1.25E-05	2.64E-05	2.04E-04	9.12E-06	1.65E-05	1.05E-05	9.14E-06	1.30E-05	6.76E-06	2.04E-04
La139	5.81E-01	1.17E+00	2.30E+00	3.41E-01	1.17E+00	1.89E+00	1.55E+00	5.24E-01	1.96E+00	1.66E+00	2.30E+00
Lanthanum	**5.81E-01**	**1.17E+00**	**2.30E+00**	**3.41E-01**	**1.17E+00**	**1.89E+00**	**1.55E+00**	**5.24E-01**	**1.96E+00**	**1.66E+00**	**2.30E+00**
Pb208	0.00E+00	3.03E-07	5.76E-07	0.00E+00	0.00E+00	0.00E+00	0.00E+00	2.08E-07	0.00E+00	0.00E+00	5.76E-07
Lead	**0.00E+00**	**3.03E-07**	**5.76E-07**	**0.00E+00**	**0.00E+00**	**0.00E+00**	**0.00E+00**	**2.08E-07**	**0.00E+00**	**0.00E+00**	**5.76E-07**
Li 6	7.74E-08	4.03E-08	2.07E-07	0.00E+00	0.00E+00	0.00E+00	0.00E+00	1.61E-08	1.15E-07	0.00E+00	2.07E-07
Li 7	0.00E+00	0.00E+00	0.00E+00	0.00E+00	0.00E+00	0.00E+00	0.00E+00	4.67E-09	0.00E+00	0.00E+00	4.67E-09
Lithium	**7.74E-08**	**4.03E-08**	**2.07E-07**	**0.00E+00**	**0.00E+00**	**0.00E+00**	**0.00E+00**	**2.08E-08**	**1.15E-07**	**0.00E+00**	**2.07E-07**
Mg 24	5.15E-04	2.73E-03	5.50E-03	6.37E-02	2.18E-03	4.92E-03	5.62E-03	1.26E-03	5.42E-03	6.74E-03	6.37E-02
Mg 25	3.03E-07	4.18E-06	5.81E-06	2.08E-03	4.20E-06	2.28E-05	5.82E-05	1.91E-06	1.69E-05	6.88E-05	2.08E-03
Mg 26	1.21E-05	6.51E-05	1.32E-04	1.74E-03	5.19E-05	1.20E-04	1.37E-04	2.90E-05	1.31E-04	1.64E-04	1.74E-03
Magnesium	**5.27E-04**	**2.80E-03**	**5.64E-03**	**6.75E-02**	**2.24E-03**	**5.06E-03**	**5.81E-03**	**1.29E-03**	**5.57E-03**	**6.98E-03**	**6.75E-02**
Mo 95	4.02E-01	6.60E-01	1.15E+00	6.56E-02	7.59E-01	1.25E+00	1.09E+00	1.94E-01	1.16E+00	1.09E+00	1.25E+00
Mo 96	7.48E-03	1.21E-01	2.86E-01	7.28E-02	3.72E-02	7.61E-02	8.43E-02	2.26E-01	1.56E-01	1.64E-01	2.86E-01
Mo 97	3.61E-01	7.44E-01	1.45E+00	4.65E-01	7.57E-01	1.33E+00	1.20E+00	3.57E-01	1.28E+00	1.24E+00	1.45E+00
Mo 98	3.89E-01	8.93E-01	1.75E+00	2.55E+00	8.71E-01	1.61E+00	1.60E+00	4.14E-01	1.60E+00	1.73E+00	2.55E+00
Mo100	4.21E-01	9.46E-01	1.93E+00	1.17E+00	9.47E-01	1.76E+00	1.74E+00	3.98E-01	1.72E+00	1.87E+00	1.93E+00
Molybdenum	**1.58E+00**	**3.36E+00**	**6.57E+00**	**4.32E+00**	**3.37E+00**	**6.02E+00**	**5.72E+00**	**1.59E+00**	**5.91E+00**	**6.09E+00**	**6.57E+00**

Radionuclide/ **Element**	**Case 1**	**Case 2**	**Case 3**	**Case 4**	**Case 5**	**Case 6**	**Case 7**	**Case 8**	**Case 9**	**Case 10**	**Max**
Nd142	7.79E-03	9.24E-02	1.64E-01	7.34E-01	5.28E-02	1.46E-01	1.64E-01	9.12E-02	1.84E-01	2.40E-01	7.34E-01
Nd143	4.12E-01	3.81E-01	1.08E+00	7.46E-02	3.20E-01	3.02E-01	1.84E-01	1.73E-01	3.20E-01	1.70E-01	1.08E+00
Nd144	6.86E-01	1.80E+00	2.85E+00	3.38E+00	1.91E+00	3.56E+00	3.56E+00	8.85E-01	3.52E+00	3.69E+00	3.69E+00
Nd145	2.75E-01	2.63E-01	6.20E-01	1.01E-01	3.54E-01	4.92E-01	3.68E-01	9.05E-02	4.48E-01	3.47E-01	6.20E-01
Nd146	3.99E-01	1.16E+00	2.05E+00	5.74E+00	1.08E+00	2.10E+00	2.24E+00	6.00E-01	2.07E+00	2.41E+00	5.74E+00
Nd148	2.09E-01	4.84E-01	8.84E-01	8.15E-01	5.30E-01	1.03E+00	1.12E+00	1.50E-01	9.73E-01	1.14E+00	1.14E+00
Nd150	6.51E-02	1.75E-01	3.97E-01	1.34E-02	1.75E-01	3.58E-01	3.83E-01	5.51E-02	3.45E-01	3.97E-01	3.97E-01
Neodymium	**2.05E+00**	**4.35E+00**	**8.04E+00**	**1.09E+01**	**4.42E+00**	**7.98E+00**	**8.02E+00**	**2.04E+00**	**7.86E+00**	**8.40E+00**	**1.09E+01**
Ne 21	0.00E+00	5.81E-08	1.56E-07	3.53E-05	0.00E+00	0.00E+00	0.00E+00	7.57E-08	9.06E-08	1.26E-07	3.53E-05
Ne 22	0.00E+00	0.00E+00	0.00E+00	8.91E-06	0.00E+00	0.00E+00	0.00E+00	0.00E+00	0.00E+00	0.00E+00	8.91E-06
Neon	**0.00E+00**	**5.81E-08**	**1.56E-07**	**4.42E-05**	**0.00E+00**	**0.00E+00**	**0.00E+00**	**7.57E-08**	**9.06E-08**	**1.26E-07**	**4.42E-05**
Np236	6.60E-07	5.98E-06	1.10E-05	4.22E-08	2.04E-06	1.84E-06	3.87E-07	4.45E-06	3.88E-06	5.96E-07	1.10E-05
Np237	9.33E-01	1.02E+00	1.40E+00	6.95E-06	1.34E+00	6.64E-01	6.95E-02	6.28E-01	4.73E-01	2.61E-02	1.40E+00
Np239	0.00E+00	1.83E-07	6.20E-07	0.00E+00	2.21E-07	4.40E-07	3.50E-07	0.00E+00	3.10E-07	2.54E-07	6.20E-07
Neptunium	**9.33E-01**	**1.02E+00**	**1.40E+00**	**6.99E-06**	**1.34E+00**	**6.64E-01**	**6.95E-02**	**6.28E-01**	**4.73E-01**	**2.61E-02**	**1.40E+00**
Nb 93	2.18E-07	3.63E-07	6.86E-07	1.61E-07	3.85E-07	6.05E-07	4.75E-07	2.55E-07	5.66E-07	4.72E-07	6.86E-07
Nb 93m	9.28E-07	1.49E-06	2.71E-06	3.99E-07	1.61E-06	2.51E-06	1.98E-06	8.61E-07	2.37E-06	2.01E-06	2.71E-06
Nb 94	9.81E-08	2.81E-07	8.71E-07	0.00E+00	2.51E-07	3.95E-07	0.00E+00	4.32E-08	1.38E-07	0.00E+00	8.71E-07
Niobium	**1.24E-06**	**2.13E-06**	**4.26E-06**	**5.60E-07**	**2.25E-06**	**3.51E-06**	**2.45E-06**	**1.16E-06**	**3.07E-06**	**2.48E-06**	**4.26E-06**
O 18	0.00E+00	0.00E+00	0.00E+00	1.25E-07	0.00E+00	0.00E+00	0.00E+00	0.00E+00	0.00E+00	0.00E+00	1.25E-07
Oxygen	**0.00E+00**	**0.00E+00**	**0.00E+00**	**1.25E-07**	**0.00E+00**	**0.00E+00**	**0.00E+00**	**0.00E+00**	**0.00E+00**	**0.00E+00**	**1.25E-07**
Pd104	5.37E-02	3.51E-01	1.06E+00	5.83E-01	2.03E-01	4.69E-01	6.01E-01	1.91E-01	6.88E-01	8.19E-01	1.06E+00
Pd105	3.10E-02	1.29E-01	5.81E-01	1.63E-01	6.55E-02	7.63E-02	5.72E-02	5.26E-02	1.61E-01	9.34E-02	5.81E-01
Pd106	8.98E-02	8.27E-01	2.01E+00	4.13E+00	7.88E-01	2.18E+00	2.84E+00	9.36E-02	2.07E+00	3.02E+00	4.13E+00
Pd107	1.77E-02	2.48E-01	6.95E-01	5.50E-01	2.42E-01	6.25E-01	6.83E-01	1.14E-02	5.96E-01	6.87E-01	6.95E-01
Pd108	9.94E-03	1.52E-01	4.24E-01	2.00E-01	1.59E-01	4.44E-01	5.43E-01	4.69E-03	3.84E-01	5.00E-01	5.43E-01
Pd110	3.93E-03	6.38E-02	1.69E-01	6.28E-02	5.86E-02	1.67E-01	2.22E-01	2.51E-03	1.60E-01	2.33E-01	2.33E-01
Palladium	**2.06E-01**	**1.77E+00**	**4.94E+00**	**5.68E+00**	**1.52E+00**	**3.96E+00**	**4.94E+00**	**3.56E-01**	**4.05E+00**	**5.36E+00**	**5.68E+00**
P 31	0.00E+00	0.00E+00	0.00E+00	1.02E-06	0.00E+00	4.77E+02	4.67E-07	0.00E+00	0.00E+00	3.18E-07	4.77E+02
Phosphorus	**0.00E+00**	**0.00E+00**	**0.00E+00**	**1.02E-06**	**0.00E+00**	**4.77E+02**	**4.67E-07**	**0.00E+00**	**0.00E+00**	**3.18E-07**	**4.77E+02**
Pu236	8.84E-08	7.96E-07	1.46E-06	0.00E+00	1.97E-07	0.00E+00	0.00E+00	5.02E-07	2.25E-07	0.00E+00	1.46E-06
Pu238	3.62E-01	1.53E+00	1.76E+00	4.79E-06	4.73E-01	9.42E-02	4.65E-03	2.49E-01	2.91E-01	3.12E-03	1.76E+00
Pu239	1.86E-01	1.41E+00	2.27E+01	1.25E-03	1.47E+00	2.45E+00	2.12E+00	2.32E-01	2.02E+00	1.62E+00	2.27E+01
Pu240	2.69E-02	4.24E-01	7.30E+00	7.30E-04	4.19E-01	7.84E-01	6.71E-01	6.30E-02	8.31E-01	5.80E-01	7.30E+00
Pu241	4.84E-02	3.76E-01	4.14E+00	4.68E-04	2.36E-01	2.28E-01	1.38E-01	8.65E-03	3.34E-01	1.37E-01	4.14E+00
Pu242	2.43E-02	2.99E-01	2.16E+00	3.86E-04	3.47E-01	7.90E-01	6.52E-01	1.59E-03	5.09E-01	4.77E-01	2.16E+00
Pu244	0.00E+00	2.00E-07	0.00E+00	0.00E+00	9.94E-08	3.50E-07	6.07E-07	0.00E+00	8.31E-07	1.09E-06	1.09E-06
Plutonium	**6.47E-01**	**4.03E+00**	**3.80E+01**	**2.84E-03**	**2.94E+00**	**4.34E+00**	**3.58E+00**	**5.55E-01**	**3.98E+00**	**2.81E+00**	**3.80E+01**
Pr141	5.32E-01	1.03E+00	2.06E+00	2.05E-01	1.02E+00	1.45E+00	1.02E+00	4.45E-01	1.67E+00	1.15E+00	2.06E+00
Pr144	0.00E+00	0.00E+00	7.26E-09	0.00E+00	0.00E+00	0.00E+00	0.00E+00	7.28E-10	0.00E+00	0.00E+00	7.26E-09
Praseodymium	**5.32E-01**	**1.03E+00**	**2.06E+00**	**2.05E-01**	**1.02E+00**	**1.45E+00**	**1.02E+00**	**4.45E-01**	**1.67E+00**	**1.15E+00**	**2.06E+00**
Pm145	0.00E+00	0.00E+00	0.00E+00	0.00E+00	0.00E+00	0.00E+00	0.00E+00	6.32E-09	0.00E+00	0.00E+00	6.32E-09
Pm146	5.32E-07	1.37E-06	3.31E-06	5.03E-06	9.50E-07	1.14E-06	7.57E-07	1.16E-06	2.08E-06	1.25E-06	5.03E-06
Pm147	4.07E-03	2.38E-03	6.42E-03	2.53E-03	3.99E-03	7.32E-03	6.05E-03	4.49E-04	4.78E-03	4.99E-03	7.32E-03
Promethium	**4.07E-03**	**2.38E-03**	**6.43E-03**	**2.54E-03**	**3.99E-03**	**7.32E-03**	**6.05E-03**	**4.50E-04**	**4.78E-03**	**4.99E-03**	**7.32E-03**

Radionuclide/ **Element**	**Case 1**	**Case 2**	**Case 3**	**Case 4**	**Case 5**	**Case 6**	**Case 7**	**Case 8**	**Case 9**	**Case 10**	**Max**
Pa231	5.28E-08	0.00E+00	0.00E+00	0.00E+00	0.00E+00	0.00E+00	0.00E+00	5.71E-08	0.00E+00	0.00E+00	5.71E-08
Pa233	3.17E-08	3.45E-08	4.75E-08	0.00E+00	0.00E+00	0.00E+00	0.00E+00	2.14E-08	0.00E+00	0.00E+00	4.75E-08
Protactinium	**8.45E-08**	**3.45E-08**	**4.75E-08**	**0.00E+00**	**0.00E+00**	**0.00E+00**	**0.00E+00**	**7.85E-08**	**0.00E+00**	**0.00E+00**	**8.45E-08**
Rh102	0.00E+00	8.14E-08	2.70E-07	2.61E-07	0.00E+00	0.00E+00	0.00E+00	5.67E-08	1.14E-07	8.04E-08	2.70E-07
Rh103	1.51E-01	2.66E-01	5.28E-01	3.16E-01	3.98E-01	7.96E-01	7.43E-01	1.61E-02	5.93E-01	6.14E-01	7.96E-01
Rhodium	**1.51E-01**	**2.66E-01**	**5.28E-01**	**3.16E-01**	**3.98E-01**	**7.96E-01**	**7.43E-01**	**1.61E-02**	**5.93E-01**	**6.14E-01**	**7.96E-01**
Rb 85	6.16E-02	9.90E-02	1.55E-01	1.25E-01	1.03E-01	1.50E-01	1.07E-01	6.08E-02	1.47E-01	1.14E-01	1.55E-01
Rb 87	1.46E-01	2.30E-01	3.53E-01	2.26E-01	2.41E-01	3.41E-01	2.34E-01	1.42E-01	3.36E-01	2.51E-01	3.53E-01
Rubidium	**2.08E-01**	**3.29E-01**	**5.08E-01**	**3.51E-01**	**3.44E-01**	**4.91E-01**	**3.42E-01**	**2.03E-01**	**4.82E-01**	**3.65E-01**	**5.08E-01**
Ru 99	2.11E-05	2.59E-05	5.98E-05	9.44E-06	3.61E-05	6.17E-05	6.05E-05	7.63E-06	3.04E-05	5.87E-05	6.17E-05
Ru100	1.25E-01	6.86E-01	1.20E+00	2.46E+00	5.20E-01	1.04E+00	1.25E+00	3.45E-01	1.19E+00	1.78E+00	2.46E+00
Ru101	3.03E-01	5.28E-01	1.17E+00	3.08E-01	6.18E-01	1.19E+00	1.24E+00	1.69E-01	1.04E+00	1.24E+00	1.24E+00
Ru102	3.43E-01	1.13E+00	2.33E+00	7.07E+00	9.90E-01	1.98E+00	2.16E+00	4.87E-01	2.11E+00	2.51E+00	7.07E+00
Ru104	1.53E-01	7.08E-01	1.68E+00	2.73E+00	6.67E-01	1.64E+00	2.08E+00	1.31E-01	1.58E+00	2.23E+00	2.73E+00
Ru106	4.00E-05	4.00E-04	9.55E-04	2.06E-04	3.87E-04	1.05E-03	1.35E-03	1.14E-05	9.81E-04	1.38E-03	1.38E-03
Ruthenium	**9.24E-01**	**3.05E+00**	**6.38E+00**	**1.26E+01**	**2.80E+00**	**5.85E+00**	**6.73E+00**	**1.13E+00**	**5.92E+00**	**7.76E+00**	**1.26E+01**
Sm146	5.19E-07	1.43E-06	3.76E-06	5.37E-06	9.18E-07	1.07E-06	6.89E-07	2.59E-06	2.04E-06	1.16E-06	5.37E-06
Sm147	5.37E-02	3.12E-02	8.54E-02	3.30E-02	5.22E-02	9.57E-02	7.90E-02	6.12E-03	6.25E-02	6.52E-02	9.57E-02
Sm148	6.86E-03	1.28E-02	4.39E-02	1.07E-03	8.24E-03	9.83E-03	5.82E-03	3.02E-02	1.77E-02	8.30E-03	4.39E-02
Sm149	1.22E-02	1.06E-02	5.32E-02	1.65E-02	1.21E-02	1.40E-02	9.77E-03	4.98E-03	1.56E-02	1.03E-02	5.32E-02
Sm150	1.58E-01	1.72E-01	4.93E-01	7.91E-02	1.94E-01	2.10E-01	1.27E-01	5.34E-02	2.65E-01	1.37E-01	4.93E-01
Sm151	1.08E-02	1.38E-02	6.16E-02	6.84E-03	8.50E-03	7.63E-03	4.96E-03	5.75E-03	1.11E-02	5.10E-03	6.16E-02
Sm152	2.99E-02	3.59E-02	9.86E-02	1.16E-02	5.04E-02	7.73E-02	5.66E-02	9.40E-03	6.91E-02	5.23E-02	9.86E-02
Sm154	3.52E-02	2.64E-01	3.54E-01	4.73E-01	3.27E-01	8.00E-01	1.05E+00	2.81E-02	7.49E-01	9.68E-01	1.05E+00
Samarium	**3.07E-01**	**5.40E-01**	**1.19E+00**	**6.21E-01**	**6.53E-01**	**1.21E+00**	**1.34E+00**	**1.38E-01**	**1.19E+00**	**1.25E+00**	**1.34E+00**
Se 76	5.54E-06	3.10E-05	5.32E-05	6.19E-08	1.90E-05	2.10E-05	1.19E-05	2.04E-05	3.33E-05	1.50E-05	5.32E-05
Se 77	4.00E-04	6.16E-04	1.22E-03	1.86E-05	5.96E-04	6.34E-04	3.06E-04	3.04E-04	7.49E-04	3.26E-04	1.22E-03
Se 78	1.17E-03	2.67E-03	5.37E-03	2.60E-03	2.68E-03	5.16E-03	5.02E-03	1.21E-03	4.95E-03	5.32E-03	5.37E-03
Se 79	2.35E-03	4.71E-03	9.42E-03	1.08E-02	4.63E-03	7.53E-03	6.27E-03	2.35E-03	7.85E-03	6.94E-03	1.08E-02
Se 80	7.00E-03	1.30E-02	2.40E-02	2.60E-02	1.32E-02	2.14E-02	1.81E-02	6.91E-03	2.14E-02	1.98E-02	2.60E-02
Se 82	1.79E-02	3.17E-02	5.50E-02	6.57E-02	3.24E-02	5.06E-02	4.07E-02	1.77E-02	5.01E-02	4.39E-02	6.57E-02
Selenium	**2.88E-02**	**5.27E-02**	**9.51E-02**	**1.05E-01**	**5.35E-02**	**8.53E-02**	**7.05E-02**	**2.85E-02**	**8.50E-02**	**7.63E-02**	**1.05E-01**
Si 28	5.76E-02	2.78E-01	2.43E-01	5.92E+00	6.04E-01	3.35E+00	7.41E+00	4.08E-02	1.54E+00	5.71E+00	7.41E+00
Si 29	1.25E-05	2.04E-04	1.60E-04	1.07E-01	5.41E-04	8.43E-03	4.18E-02	3.98E-05	2.43E-03	3.11E-02	1.07E-01
Si 30	0.00E+00	4.09E-08	0.00E+00	8.56E-05	3.58E-07	2.04E-05	2.43E-04	0.00E+00	2.93E-06	1.66E-04	2.43E-04
Silicon	**5.77E-02**	**2.78E-01**	**2.43E-01**	**6.03E+00**	**6.04E-01**	**3.36E+00**	**7.45E+00**	**4.08E-02**	**1.54E+00**	**5.74E+00**	**7.45E+00**
Ag107	0.00E+00	2.68E-07	7.66E-07	5.91E-07	2.59E-07	6.71E-07	7.32E-07	1.34E-08	6.42E-07	7.40E-07	7.66E-07
Ag108m	0.00E+00	4.25E-07	1.28E-06	1.93E-05	2.53E-07	6.71E-07	9.24E-07	3.16E-08	1.04E-06	1.37E-06	1.93E-05
Ag109	4.03E-03	4.71E-02	1.37E-01	5.65E-02	5.61E-02	1.32E-01	1.37E-01	1.15E-03	1.11E-01	1.27E-01	1.37E-01
Ag110m	7.74E-09	2.47E-07	5.85E-07	4.50E-07	1.94E-07	4.20E-07	3.89E-07	5.26E-09	5.66E-07	4.44E-07	5.85E-07
Silver	**4.03E-03**	**4.71E-02**	**1.37E-01**	**5.66E-02**	**5.61E-02**	**1.32E-01**	**1.37E-01**	**1.15E-03**	**1.11E-01**	**1.27E-01**	**1.37E-01**
Na 23	0.00E+00	0.00E+00	0.00E+00	1.78E-06	0.00E+00	0.00E+00	0.00E+00	3.51E-09	0.00E+00	0.00E+00	1.78E-06
Sodium	**0.00E+00**	**0.00E+00**	**0.00E+00**	**1.78E-06**	**0.00E+00**	**0.00E+00**	**0.00E+00**	**3.51E-09**	**0.00E+00**	**0.00E+00**	**1.78E-06**

Radionuclide/ **Element**	**Case 1**	**Case 2**	**Case 3**	**Case 4**	**Case 5**	**Case 6**	**Case 7**	**Case 8**	**Case 9**	**Case 10**	**Max**
Sr 86	6.51E-04	4.29E-03	5.85E-03	8.94E-02	2.74E-03	4.83E-03	4.16E-03	4.04E-03	6.05E-03	5.68E-03	8.94E-02
Sr 87	1.80E-06	5.37E-05	8.76E-05	5.16E-03	1.87E-05	7.26E-05	1.10E-04	9.89E-05	9.74E-05	1.85E-04	5.16E-03
Sr 88	2.13E-01	3.40E-01	5.10E-01	8.83E-01	3.54E-01	5.04E-01	3.54E-01	2.16E-01	4.92E-01	3.75E-01	8.83E-01
Sr 90	2.73E-01	4.24E-01	6.25E-01	5.43E-01	4.44E-01	6.15E-01	4.09E-01	2.59E-01	6.04E-01	4.38E-01	6.25E-01
Strontium	**4.86E-01**	**7.68E-01**	**1.14E+00**	**1.52E+00**	**8.01E-01**	**1.12E+00**	**7.67E-01**	**4.79E-01**	**1.10E+00**	**8.18E-01**	**1.52E+00**
S 32	0.00E+00	0.00E+00	0.00E+00	1.24E-08	0.00E+00	0.00E+00	0.00E+00	0.00E+00	0.00E+00	0.00E+00	1.24E-08
Sulfur	**0.00E+00**	**0.00E+00**	**0.00E+00**	**1.24E-08**	**0.00E+00**	**0.00E+00**	**0.00E+00**	**0.00E+00**	**0.00E+00**	**0.00E+00**	**1.24E-08**
Tc 98	2.61E-06	1.42E-05	2.80E-05	1.07E-04	9.01E-06	1.47E-05	1.48E-05	1.18E-05	2.08E-05	2.59E-05	1.07E-04
Tc 99	2.93E-01	2.87E-01	7.13E-01	1.08E-01	4.45E-01	7.18E-01	6.34E-01	7.22E-02	5.28E-01	5.64E-01	7.18E-01
Technetium	**2.93E-01**	**2.87E-01**	**7.13E-01**	**1.08E-01**	**4.45E-01**	**7.18E-01**	**6.34E-01**	**7.22E-02**	**5.28E-01**	**5.64E-01**	**7.18E-01**
Te122	2.16E-04	1.72E-03	4.04E-03	2.23E-03	1.30E-03	3.15E-03	4.20E-03	4.69E-04	3.58E-03	4.72E-03	4.72E-03
Te123	5.94E-06	1.61E-04	2.95E-04	1.78E-03	6.37E-05	1.82E-04	3.23E-04	3.67E-05	3.14E-04	5.18E-04	1.78E-03
Te124	2.11E-04	2.21E-03	5.32E-03	9.99E-03	1.32E-03	3.15E-03	4.24E-03	1.04E-03	4.33E-03	5.85E-03	9.99E-03
Te125	2.39E-03	9.06E-03	2.47E-02	1.27E-02	8.54E-03	1.96E-02	2.28E-02	2.16E-03	2.03E-02	2.48E-02	2.48E-02
Te125m	2.85E-06	1.05E-05	2.69E-05	3.43E-06	1.02E-05	2.32E-05	2.69E-05	1.58E-06	2.36E-05	2.87E-05	2.87E-05
Te126	1.06E-04	1.27E-03	3.32E-03	2.65E-02	7.64E-04	2.02E-03	2.96E-03	5.16E-04	2.75E-03	4.19E-03	2.65E-02
Te128	3.13E-02	9.15E-02	2.20E-01	1.77E-01	8.70E-02	1.82E-01	1.99E-01	3.00E-02	1.88E-01	2.17E-01	2.20E-01
Te130	1.55E-01	3.71E-01	7.88E-01	1.09E+00	3.63E-01	6.87E-01	6.89E-01	1.52E-01	6.86E-01	7.47E-01	1.09E+00
Tellurium	**1.90E-01**	**4.77E-01**	**1.04E+00**	**1.32E+00**	**4.62E-01**	**8.97E-01**	**9.23E-01**	**1.86E-01**	**9.05E-01**	**1.00E+00**	**1.32E+00**
Tb159	1.16E-03	5.76E-02	7.08E-02	6.60E-02	3.31E-02	9.19E-02	1.69E-01	4.38E-02	1.35E-01	1.84E-01	1.84E-01
Terbium	**1.16E-03**	**5.76E-02**	**7.08E-02**	**6.60E-02**	**3.31E-02**	**9.19E-02**	**1.69E-01**	**4.38E-02**	**1.35E-01**	**1.84E-01**	**1.84E-01**
Th228	0.00E+00	1.73E-07	3.24E-07	0.00E+00	0.00E+00	0.00E+00	0.00E+00	1.15E-07	0.00E+00	0.00E+00	3.24E-07
Th230	4.22E-07	1.75E-06	2.09E-06	0.00E+00	5.39E-07	0.00E+00	0.00E+00	4.16E-07	3.32E-07	0.00E+00	2.09E-06
Th232	1.25E-06	6.47E-07	1.21E-06	0.00E+00	5.56E-07	2.16E-07	0.00E+00	1.42E-06	1.94E-07	0.00E+00	1.42E-06
Thorium	**1.67E-06**	**2.57E-06**	**3.62E-06**	**0.00E+00**	**1.10E-06**	**2.16E-07**	**0.00E+00**	**1.95E-06**	**5.26E-07**	**0.00E+00**	**3.62E-06**
Sn114	0.00E+00	1.32E-06	8.01E-06	1.50E-01	2.64E-07	1.22E-06	5.08E-06	3.92E-06	2.95E-06	1.30E-05	1.50E-01
Sn115	4.62E-05	2.45E-04	6.16E-04	1.12E-01	1.95E-04	3.09E-04	2.55E-04	5.06E-05	3.31E-04	2.27E-04	1.12E-01
Sn116	8.01E-04	5.24E-03	1.25E-02	3.39E+00	4.44E-03	1.11E-02	1.83E-02	1.13E-03	1.50E-02	1.60E-02	3.39E+00
Sn117	9.42E-04	4.71E-03	1.34E-02	2.64E+00	4.20E-03	9.89E-03	1.14E-02	9.20E-04	1.05E-02	1.23E-02	2.64E+00
Sn118	9.46E-04	4.04E-03	1.09E-02	2.79E+00	3.63E-03	8.68E-03	1.09E-02	9.97E-04	8.82E-03	1.20E-02	2.79E+00
Sn119	1.05E-03	4.16E-03	1.11E-02	1.53E+00	3.72E-03	8.23E-03	9.09E-03	1.09E-03	8.61E-03	1.01E-02	1.53E+00
Sn119m	0.00E+00	5.06E-08	1.05E-07	2.11E-04	2.81E-08	6.42E-08	8.82E-08	1.23E-08	9.47E-08	1.41E-07	2.11E-04
Sn120	1.04E-03	3.94E-03	1.03E-02	9.64E-02	3.67E-03	8.56E-03	1.04E-02	1.02E-03	8.53E-03	1.13E-02	9.64E-02
Sn121	0.00E+00	0.00E+00	0.00E+00	8.56E-09	0.00E+00	0.00E+00	0.00E+00	0.00E+00	0.00E+00	0.00E+00	8.56E-09
Sn121m	6.95E-06	3.86E-05	1.14E-04	1.97E-04	3.18E-05	7.26E-05	7.84E-05	6.30E-06	6.99E-05	8.05E-05	1.97E-04
Sn122	1.34E-03	4.97E-03	1.33E-02	1.68E-02	4.61E-03	1.04E-02	1.19E-02	1.28E-03	1.06E-02	1.31E-02	1.68E-02
Sn124	2.26E-03	7.96E-03	2.13E-02	5.31E-03	7.50E-03	1.68E-02	1.90E-02	2.04E-03	1.70E-02	2.06E-02	2.13E-02
Sn126	4.11E-03	1.96E-02	5.59E-02	8.10E-02	1.77E-02	4.28E-02	5.08E-02	3.81E-03	4.46E-02	5.62E-02	8.10E-02
Tin	**7.71E-03**	**3.26E-02**	**9.06E-02**	**1.03E-01**	**2.98E-02**	**6.99E-02**	**8.18E-02**	**7.13E-03**	**7.22E-02**	**8.98E-02**	**1.03E-01**

Radionuclide/ **Element**	**Case 1**	**Case 2**	**Case 3**	**Case 4**	**Case 5**	**Case 6**	**Case 7**	**Case 8**	**Case 9**	**Case 10**	**Max**
U232	8.10E-07	7.35E-06	1.37E-05	2.79E-08	1.81E-06	5.64E-07	0.00E+00	4.83E-06	2.07E-06	0.00E+00	1.37E-05
U233	3.31E-06	3.45E-06	4.88E-06	0.00E+00	4.49E-06	2.22E-06	2.32E-07	2.39E-06	1.60E-06	0.00E+00	4.88E-06
U234	2.97E-02	1.24E-01	1.45E-01	3.84E-07	3.83E-02	7.63E-03	3.74E-04	2.49E-02	2.36E-02	2.52E-04	1.45E-01
U235	5.37E+00	1.04E-01	1.21E+00	3.54E-07	2.13E-02	7.03E-04	6.01E-04	5.53E+00	7.32E-04	4.57E-04	5.53E+00
U236	4.24E+00	2.13E+00	3.89E+00	6.82E-07	1.87E+00	7.20E-01	5.82E-02	4.28E+00	6.22E-01	1.99E-02	4.28E+00
U237	0.00E+00	0.00E+00	1.25E-07	0.00E+00	0.00E+00	0.00E+00	0.00E+00	0.00E+00	0.00E+00	0.00E+00	1.25E-07
U238	1.06E+00	2.14E+01	4.08E+02	2.44E-02	2.31E+01	5.84E+01	5.84E+01	1.37E+00	5.60E+01	5.10E+01	4.08E+02
Uranium	**1.07E+01**	**2.38E+01**	**4.13E+02**	**2.44E-02**	**2.51E+01**	**5.91E+01**	**5.85E+01**	**1.12E+01**	**5.66E+01**	**5.10E+01**	**4.13E+02**
Xe128	1.71E-03	2.02E-02	4.80E-02	3.29E-02	1.12E-02	2.86E-02	4.20E-02	6.53E-03	6.09E-02	6.13E-02	6.13E-02
Xe129	2.08E-05	7.08E-04	1.41E-03	3.26E-03	3.57E-04	1.70E-03	4.26E-03	2.81E-04	2.90E-03	6.02E-03	6.02E-03
Xe130	4.14E-03	3.84E-02	7.26E-02	3.99E-01	3.42E-02	1.25E-01	1.92E-01	2.01E-02	1.08E-01	2.16E-01	3.99E-01
Xe131	1.18E-01	8.58E-02	2.10E-01	2.22E-02	1.70E-01	3.02E-01	2.51E-01	1.07E-02	1.85E-01	1.83E-01	3.02E-01
Xe132	5.28E-01	1.49E+00	3.21E+00	3.50E+00	1.38E+00	2.67E+00	3.00E+00	6.12E-01	4.29E+00	3.54E+00	4.29E+00
Xe134	7.61E-01	1.75E+00	3.30E+00	7.90E+00	1.89E+00	3.97E+00	5.49E+00	7.24E-01	3.81E+00	4.77E+00	7.90E+00
Xe136	1.13E+00	2.67E+00	3.36E+00	9.78E+00	2.72E+00	5.12E+00	5.14E+00	5.69E-01	5.02E+00	5.50E+00	9.78E+00
Xenon	**2.54E+00**	**6.05E+00**	**1.02E+01**	**2.16E+01**	**6.20E+00**	**1.22E+01**	**1.41E+01**	**1.94E+00**	**1.35E+01**	**1.43E+01**	**2.16E+01**
Y 89	2.86E-01	4.44E-01	6.60E-01	5.92E-01	4.63E-01	6.38E-01	4.24E-01	2.85E-01	6.30E-01	4.51E-01	6.60E-01
Y 90	7.08E-05	1.10E-04	1.63E-04	1.41E-04	1.15E-04	1.60E-04	1.07E-04	6.71E-05	1.57E-04	1.14E-04	1.63E-04
Yttrium	**2.87E-01**	**4.45E-01**	**6.60E-01**	**5.92E-01**	**4.63E-01**	**6.38E-01**	**4.24E-01**	**2.86E-01**	**6.30E-01**	**4.52E-01**	**6.60E-01**
Zr 90	7.74E-02	1.25E-01	1.88E-01	4.04E-01	1.28E-01	1.80E-01	1.23E-01	9.34E-02	1.80E-01	1.34E-01	4.04E-01
Zr 91	3.56E-01	5.72E-01	8.98E-01	3.63E-01	6.00E-01	8.70E-01	6.25E-01	3.41E-01	8.47E-01	6.59E-01	8.98E-01
Zr 92	3.66E-01	6.34E-01	1.05E+00	1.78E+00	6.51E-01	1.00E+00	7.86E-01	3.79E-01	9.75E-01	8.36E-01	1.78E+00
Zr 93	2.50E-01	3.94E-01	7.04E-01	5.47E-02	4.33E-01	6.71E-01	5.31E-01	1.97E-01	6.31E-01	5.35E-01	7.04E-01
Zr 94	4.16E-01	8.40E-01	1.47E+00	2.93E+00	8.24E-01	1.37E+00	1.19E+00	4.67E-01	1.37E+00	1.31E+00	2.93E+00
Zr 96	4.02E-01	8.01E-01	1.50E+00	5.51E-01	8.16E-01	1.41E+00	1.29E+00	3.77E-01	1.37E+00	1.38E+00	1.50E+00
Zirconium	**1.87E+00**	**3.37E+00**	**5.82E+00**	**6.08E+00**	**3.45E+00**	**5.50E+00**	**4.55E+00**	**1.85E+00**	**5.38E+00**	**4.85E+00**	**6.08E+00**

As a result of the concern for volatilization of the radionuclide species listed in Table A.8 during melt-dilute treatment, the available vapor pressure data for the radionuclide species present in quantities greater than 10^{-3} grams has been compiled in Table A.9. Table A.9 provides the temperature dependence of the vapor pressure for only the elemental radionuclide species—no compound formation between radionuclides or other fuel species is included. However, Table A.10 displays the possible compounds formed between Al, U, Cs, Rb, Te, Ba, Sr, I, and Tritium.

Table A.9 Vapor Pressure in Atmospheres

Element	**Temperature, °C**					
	600	**700**	**800**	**900**	**Range**	**T (mp)**
Aluminum	2.20E-13	1.78E-11	6.35E-10	1.23E-08	660 to1800	660
Americium (sol)	1.28E-10	6.54E-09	1.59E-07	2.21E-06	298 to mp	994
Barium (liq)	4.53E-06	4.14E-05	2.51E-04	1.12E-03	mp to 1200	725
Cadmium	1.16E-01	5.02E-01	1.65E+00	4.42E+00	mp to 650	321
Cerium	2.12E-19	6.65E-17	7.13E-15	3.45E-13	mp to 2450	798
Cesium	6.00E-01	1.69E+00	3.94E+00	7.94E+00	mp to 550	28
Curium	1.86E-16	2.65E-14	1.50E-12	4.25E-11	mp to 2200	1340

Element	Temperature, °C					
	600	700	800	900	Range	T (mp)
Dysprosium (sol)	5.54E-12	3.14E-10	8.28E-09	1.24E-07	298 to mp	1412
Europium (sol)	9.45E-06	1.08E-04	7.77E-04	3.95E-03	298 to mp	822
Gadolinium (sol)	2.23E-17	4.27E-15	3.07E-13	1.07E-11	298 to mp	1313
Iron	8.42E-17	1.70E-14	1.27E-12	4.57E-11	mp to 2100	1535
Lanthanum	7.53E-20	2.82E-17	3.49E-15	1.90E-13	mp to 2450	918
Magnesium (sol)	1.29E-03	9.84E-03	5.09E-02	1.97E-01	298 to mp	649
Manganese (sol)	1.77E-10	8.74E-09	2.05E-07	2.77E-06	298 to mp	1244
Molybdenum	3.41E-32	3.60E-28	6.68E-25	3.40E-22	298 to 2500	2617
Neodymium	6.11E-14	4.46E-12	1.46E-10	2.64E-09	mp to 2000	1021
Neptunium	2.51E-21	1.23E-18	1.87E-16	1.20E-14	mp to 2500	640
Niobium (sol)	5.56E-36	1.53E-31	6.26E-28	6.18E-25	298 to 2500	2468
Palladium	8.38E-16	1.07E-13	5.56E-12	1.47E-10	mp to 2100	1554
Plutonium	3.84E-16	3.51E-14	1.38E-12	2.92E-11	mp to 2450	641
Rhodium	1.30E-24	1.85E-21	6.80E-19	9.15E-17	mp to 2500	1965
Samarium						1074
Selenium	3.11E-01	1.20E+00	3.62E+00	9.02E+00	mp to bp	217
Silicon	6.85E-14	6.32E-12	2.48E-10	5.18E-09	mp to 3000	1410
Silver (sol)	4.35E-11	2.33E-09	5.90E-08	8.56E-07	298 to mp	962
Silver	8.19E-11	3.48E-09	7.34E-08	9.21E-07	mp to 1600	962
Strontium (sol)	8.34E-26	8.34E-26	8.34E-26	8.34E-26	298 to mp	769
Uranium (sol)	3.35E-41	4.59E-38	1.60E-35	2.00E-33	298 to mp	1132
Uranium (liq)	5.32E-25	8.33E-22	3.18E-19	4.27E-17	mp to 2500	1132
Yttrium (sol)	4.21E-19	1.62E-16	2.03E-14	1.11E-12	298 to mp	1552
Yttrium (liq)	3.13E-18	7.75E-16	6.88E-14	2.84E-12	mp to 2300	1552
Zirconium (sol)	3.90E-29	1.84E-25	1.77E-22	5.27E-20	298 to mp	1852
Zirconium (liq)	1.27E-28	4.68E-25	3.73E-22	9.53E-20	mp tp 2500	1852

Table A.10 Compounds and Alloys of Various Offgas Species with Uranium and Aluminum

	Al	U	Cs	Rb	Te	H^3	Ba	Sr	I
Al		Various solubility of both elements (see phase diagram); Al_4U (ε); Al_3U (ζ); Al_2U (η)	Slight solubility of Cs in Al; no other phases	No phase diagram available but no compounds have been observed	Limited solubility of both elements; Al_5Te; Al_2Te_3	Limited (~ zero) solubility of H in Al; no other phases	Limited solubility of Ba in Al but 5.4 at% solubility of Al in Ba; Al_4Ba; Al_2Ba; AlBa; $AlBa_2$ phases	Limited solubility of both elements; Al_4Sr; Al_2Sr, Al_2Sr_3	No phase diagram available
U	See Al-U		No phase diagram available	No phase diagram available	See Te-U	See H^3-U	No phase diagram available	No phase diagram available	No phase diagram available
Cs	See Al-Cs	No phase diagram available		Complete immiscibility of both elements	Limited solubility of both elements; Cs_2Te; Cs_2Te_2; Cs_5Te_4; CsTe; Cs_2Te_3; Cs_2Te_5; $CsTe_5$	No phase diagram available; CsH is formed	See Ba-Cs	Complete immiscibility of both elements but no phase diagram given	Limited solubility of both elements; CsI; CsI_3; CsI_4
Rb	See Al-Rb	No phase diagram available	See Cs-Rb		Limited solubility of both elements; Rb_2Te; Rb_3Te_2; Rb_5Te_4; RbTe; Rb_2Te_3; Rb_2Te_5	See H^3-Rb	See Ba-Rb	Complete immiscibility of both elements but no phase diagram given	See I-Rb
Te	See Al-Te	Limited solubility of both elements; UTe; U_3Te_4; U_3Te_5; UTe_2; U_3Te_7; U_2Te_3; UTe_3; UTe_5	See Cs-Te	See Rb-Te		No phase diagram available	See Ba-Te	See Sr-Te	See I-Te
H^3	See Al-H^3	Limited (~0 to 28 wppm) solubility of H in various U allotropes; α, β, δ, ε - UH_3	See Cs-H^3	No phase diagram available; RbH is formed	No phase diagram available		See Ba-H^3	43.2 at% solubility of H in β-Sr; 4.3 at.% solubility of H in α-Sr; α and β-SrH_2	No phase diagram available; HI may be possible but no reference has been found
Ba	See Al-Ba	No phase diagram available	Complete immiscibility of both elements but no phase diagram given	Complete immiscibility of both elements but no phase diagram given	Limited solubility of both elements; BaTe; Ba_2Te_3; $BaTe_2$	Large solubility of H in Ba (57 at.% at 950°C); α-BaH_2; β-BaH_2		Two solid solutions formed; no other phases	Limited solubility of both elements; BaI_2
Sr	See Al-Sr	No phase diagram available but no compounds have been observed	See Cs-Sr	See Rb-Sr	Limited solubility of both elements; SrTe; Sr_2Te_3; $SrTe_2$	See H^3-Sr	See Ba-Sr		See I-Sr
I	No phase diagram available	No phase diagram available	See Cs-I	Limited solubility of both elements; RbI; RbI_3	Limited solubility of both elements; TeI; TeI_4	See H^3-I	See Ba-I	Limited solubility of both elements; SrI_2	

A.5 References

[1] Duguid, J. O., McNeish, J. A., Vallikat, V., Cresap, D., and Erb, N. J.. ***"Total System Performance Assessment Sensitivity Studies of U.S. Department of Energy Spent Nuclear Fuel,"*** DI A00000000-01717-5705-00017, Rev. 01 (September 30, 1997).

[2] **Final Programmatic Spent Nuclear Fuel Management and Idaho National Engineering Environmental Restoration and Waste Management Programs Environmental Impact Statement,** DOE (U.S. Department of Energy), DOE/EIS-0203, Idaho Operations Office, Idaho Falls, Idaho (1995).

[3] Brooks, H. M. and Sindelar R. L., ***"Characterization of FRR SNF in Basin and Dry Storage Systems,"*** Third Topical Meeting on DOE Spent Nuclear Fuel and Fissile Material Management, Charleston, SC, American Nuclear Society (September 1998).

[4] Burke, S. D. to Skwarek, R. J., interoffice memorandum, ***"Proposed New Criteria for Acceptance of Al-SNF for SRS Basin Storage (U),"*** SRS-RSE-970167 (February 11, 1998).

This Page Intentionally Left Blank

WESTINGHOUSE SAVANNAH RIVER CO. REPORT WSRC-TR-2002-00128

DISTRIBUTION

SAVANNAH RIVER SITE

W. A. Condon, 703-F
C. E. Armitage, 703-F
C. G. Nickell, 703-F
W. F. Swift, 707-C
D. W. Bickley, 707-C
R. R. Reichel, 707-C
T. M. Bolen, 707-C
H. M. Brooks, 707-C
E. R. Conatser, 704-C
C. R. Wolfe, 773-A
N. C. Iyer, 773-41A
M. R. Louthan, Jr., 773-A
R. L. Sindelar, 773-41A
G. T. Chandler, 773-A
D. W. Vinson, 773-41A
A. J. Duncan, 773-41A
T. M. Adams, 773-41A
S. Y. Lee, 773-42A
H. B. Peacock, 773-A
Site Records, 773-52A